Medical Sample Classifier Design Using Fuzzy Cerebellar Model Neural Networks

Hsin-Yi Li[1], Rong-Guan Yeh[2], Yu-Che Lin[3], Lo-Yi Lin[4], Jing Zhao[5], Chih-Min Lin[6,*], Imre J. Rudas[7]

[1] Information and Communications Research Division, National Chung-Shan Institute of Science & Technology, Taoyuan 320, Taiwan, s988506@mail.yzu.edu.tw

[2] School of Mechanical & Electronic Engineering, Sanming University, Sanming 365004, China, styeh@saturn.yzu.edu.tw

[3] Information and Communications Research Division, National Chung-Shan Institute of Science & Technology, Taoyuan 320, Taiwan, s1004603@mail.yzu.edu.tw

[4] School of Medicine, Taipei Medical University, Taipei 100, Taiwan, zoelin56@hotmail.com

[5] School of Electrical Engineering & Automation, Xiamen University of Technology, Xiamen 361000, China; and Department of Electrical Engineering, Yuan Ze University, Tao-Yuan 320, Taiwan, jzhao@xmut.edu.cn

[6*] Corresponding author, Department of Electrical Engineering, Yuan Ze University, Chung-Li, Taoyuan 320, Taiwan; and School of Information Science and Engineering, Xiamen University, Xiamen 361000, China, cml@saturn.yzu.edu.tw

[7] Óbuda University, Bécsi út 96/b, H-1034 Budapest, Hungary, e-mail: rudas@uni-obuda.hu

Abstract: This study designs a stable and convergent adaptive fuzzy cerebellar model articulation classifier for the identification of medical samples. Research on medical diagnosis is important and complex. Uncertainty is unavoidable in medical diagnosis. The symptoms are one of the uncertainties of an illness and may or may not occur as a result of the disease. There is an uncertain relationship between symptoms and disease. Diagnostic accuracy can be improved using data forecasting techniques. This study proposes a generalized fuzzy neural network, called a fuzzy cerebellar model articulation controller (FCMAC). It is an expansion of a fuzzy neural network and it will be shown that the traditional fuzzy neural network controller is a special case of this FCMAC. This expansion type fuzzy neural network has a greater ability to be generalized, has greater learning

ability and a greater capacity to approximate than a traditional fuzzy neural network. The steepest descent method has a fast convergent characteristic, so it is used to derive the adaptive law for the adaptive fuzzy cerebellar model classifier. The optimal learning rate is also derived to achieve the fastest convergence for the FCMAC, in order to allow fast and accurate identification. The simulation results demonstrate the effectiveness of the proposed FCMAC classifier.

Keywords: cerebellar model articulation controller; fuzzy rule; classifier; diseases diagnosis

1 Introduction

Recently, neural networks have been widely used for system identification and control problems [1-4]. The most prominent feature of a neural network is its ability to approximate.

The Cerebellar Model Articulation Controller (CMAC), was first proposed by Marr [5] in 1969. In 1975, Albus published two articles on the CMAC, based on the cerebellar cortex model of Marr [6, 7], including the mathematical algorithms and memory storage methods for a CMAC. A CMAC is a neural network that behaves similarly to the human cerebellum. It is classified as a non-fully connected perceptual machine type network. A CMAC can be used to imitate an object. The imitating process can be divided into the learning and recalling processes. The CMAC can repeat the learning process and correct the memory data until the desired results are achieved. In contrast with other neural networks, the CMAC does not use abstruse mathematical calculation. It has the advantage of a simple structure, easy operation, fast learning convergence speed, an ability to classify regions and it is easy to implement, so it is suitable for application to online learning systems.

Previously, CMACs have been the subject of many studies by researchers in various fields and many studies have verified that CMACs perform better than neural networks in many applications [8, 9]. CMACs are not limited in control problems and also can perform as a full regional approximation controller. In a traditional CMAC, the output value from each hypercube is a constant binary value and it lacks systematic stability analysis for the applications of a CMAC. Some studies have proposed the differential basis function as a replacement for the original constant value of the hypercube's output, in order to obtain the output and input variables' differential message. In 1992, Lane et al. proposed a method that combines a CMAC with a B-spline function, so that a CMAC can learn and store differential information [10]. In 1995, Chiang and Lin proposed a combination of a CMAC and a general basis function (GBF) to develop a new type of cerebellar model articulation controller (CMAC_GBF). The ability of the

CMAC to learning is improved with differential information [11]. In 1997, Lin and Chiang proved that the learning result for a CMAC_GBF is guaranteed to converge to the best state with the minimum root mean square error [12]. In 2004, Lin and Peng provided a complete stability analysis of a CMAC [13]. Recently, Lin and Li introduced a new Petri fuzzy CMAC [14].

Classification problems are important because, the classification of everything is inherent, in human cognition. Classification uses existing categories to define features, to learn rules by training and to establish the model of the classifier. Therefore, a classifier can be used to determine a new information category [15]. Current classification methods have been widely applied to various problems, such as diseases, bacteria, viruses, RADAR signals and missile detection, etc. Research on medical diagnosis is important and complex. Uncertainty is unavoidable in medical diagnosis [16-18]. The symptoms are one of the uncertainties for an illness. They may or may not occur, or occur as a result of a disease. There is an uncertain relationship between symptoms and disease. Addressing uncertainty allows more accurate decisions to be made. In the past, physicians have given medical diagnoses that mostly rely on past experience, but disease factors have become more diverse. Using techniques for data prediction allows medical practitioners to improve diagnostic accuracy.

2 The FCMAC Neural Network Architecture

This paper proposes a generalized fuzzy neural network, which is called a FCMAC. It is an expansion-type fuzzy neural network. A traditional fuzzy neural network can be viewed as a special case of this FCMAC.

2.1 FCMAC Architecture

A multi-input, multi-output, FCMAC neural network architecture, is shown in Fig. 1.

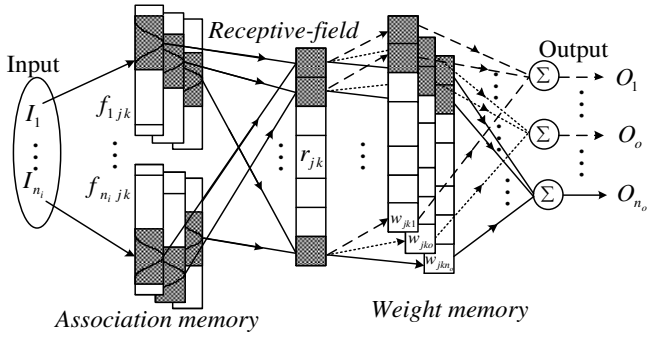

Figure 1
The architecture of a FCMAC

Its fuzzy inference rules are expressed as

$$R^{\lambda}: If\ I_1\ is\ f_{1jk}, I_2\ is\ f_{2jk},,\cdots, I_{n_i}\ is\ f_{n_i jk}, then$$
$$o_o = w_{jko}\quad for\ j = 1, 2, \cdots, n_j,\quad k = 1, 2, \cdots, n_k, \tag{1}$$
$$\lambda = 1, 2, \cdots, n_l,\ and\quad o = 1, 2, \cdots, n_o$$

where, λ is the λ-th fuzzy rule, j is the j-th layer and k is the k-th segment. The difference between this FCMAC and a traditional fuzzy neural network is that it uses the concept of layers and segments, as shown in Fig. 1. If this FCMAC is reduced to only one layer and each segment only contains one neuron, then it is reduced to a traditional fuzzy neural network. Therefore, this FCMAC can be viewed as a generalization of a fuzzy neural network and it learns, recalls and approximates better than a fuzzy neural network. Its signal transmissions and field functions are described below.

a) The Input : For the input space $\boldsymbol{I} = [I_1, \cdots, I_i, \cdots, I_{n_i}]^T \in \Re^{n_i}$, every state variable I_i is divided into n_e discrete regions, called elements or neurons.

b) The Association Memory : Several elements are accumulated in a segment. Each input, I_i, has n_j layers and each layer has n_k segments. In this field, each segment uses a Gaussian function as its basis function and is expressed as:

$$f_{ijk} = \exp\left[\frac{-(I_i - m_{ijk})^2}{v_{ijk}^2}\right], \text{for } i = 1, 2, \cdots, n_i, \tag{2}$$
$$j = 1, 2, \cdots, n_j, \text{ and } k = 1, 2, \cdots, n_k$$

where m_{ijk} and v_{ijk} represent the i-th input corresponds to the j-th layer and the k-th segment center value and the variance of the Gaussian function, respectively.

c) The receptive-field : In this field, the hypercube quantity, n_l, is equal to the product of n_j and n_k. The receptive-field can be represented as

$$r_{jk} = \prod_{i=1}^{n_i} f_{ijk} = \prod_{i=1}^{n_i} \exp\left[\frac{-(I_i - m_{ijk})^2}{v_{ijk}^2}\right] \tag{3}$$

for $j = 1,2,\cdots,n_j$, and $k = 1,2,\cdots,n_k$

where r_{jk} is the j-th layer and the k-th segment of the hypercube. Therefore, the multi-dimensional receptive-field basis function can be expressed as a vector:

$$\boldsymbol{r} = [r_{11},\cdots, r_{1n_k}, r_{21},\cdots, r_{2n_k},\cdots, r_{n_j1},\cdots, r_{n_jn_k}]^T \in \Re^{n_jn_k} \tag{4}$$

d) The weight memory : The memory contents value that corresponds to the hypercube is expressed as:

$$\begin{aligned}\boldsymbol{w}_o = [&w_{11o},\cdots, w_{1n_ko}, w_{21o},\cdots, w_{2n_ko},\cdots, w_{n_j1o},\\ &\cdots, w_{n_jn_ko}]^T \in \Re^{n_jn_k} \quad, o = 1,2,\cdots,n_0\end{aligned} \tag{5}$$

where w_{jko} is the o-th output that corresponds to value of the weight of the j-th layer and the k-th segment.

e) The Output : The o-th output of FCMAC is represented as:

$$y_o = \boldsymbol{w}_o^T \boldsymbol{r} = \sum_{j=1}^{n_j}\sum_{k=1}^{n_k} w_{jko} r_{jk}, o = 1,\cdots,n_o \tag{6}$$

2.2 The Design of the Adaptive FCMAC Classifier

In this study, this FCMAC neural network is used as an intelligent classifier and is used to identify and classify biomedical bacteria. The literature survey shows that the normalized steepest descent method has fast convergence properties so this method is used to derive the parameters for the learning rules for the adaptive FCMAC classifier. The optimal learning rate for the adjustment rule is also derived so that the FCMAC achieves the fastest convergence. The entire learning algorithm is summarized as follows:

First, we define the energy function:

$$E(k) = \frac{1}{2}\sum_{o=1}^{n_o}(d_o(k) - y_o(k))^2 = \frac{1}{2}\sum_{o=1}^{n_o} e_o^2(k) \tag{7}$$

where $e_o(k)$=$d_o(k)$-$y_o(k)$ is the output error for the FCMAC classifier and $d_o(k)$ and $y_o(k)$ are the o-th objective and the real output, respectively. Therefore, the FCMAC classifier adjustment rule for weight is described by the following equation:

$$\begin{aligned}\Delta w_{jko} &= -\eta_w \frac{\partial E}{\partial w_{jko}} = -\eta_w \frac{\partial E}{\partial y_o}\frac{\partial y_o}{\partial w_{jko}} \\ &= -\eta_w \frac{\partial}{\partial y_o}\frac{1}{2}\sum_{o=1}^{n_o}(d_o - y_o)^2 \frac{\partial}{\partial w_{jko}} w_{jko} r_{jk} \\ &= \eta_w \sum_{o=1}^{n_o} e_o r_{jk}\end{aligned} \tag{8}$$

where η_w is the learning rate for weight. The new weight value for the FCMAC classifier is updated as:

$$w_{jko}(k+1) = w_{jko}(k) + \Delta w_{jko}(k) \tag{9}$$

The center value and the variance of the receptive-field basis function for the FCMAC is adjusted as:

$$\begin{aligned}\Delta m_{ijk} &= -\eta_m \sum_{o=1}^{n_o} \frac{\partial E(k)}{\partial m_{ijk}} = -\eta_m \sum_{o=1}^{n_o} \frac{\partial E}{\partial y_o}\frac{\partial y_o}{\partial r_{jk}}\frac{\partial r_{jk}}{\partial m_{ijk}} \\ &= -\eta_m \sum_{o=1}^{n_0} \frac{\partial}{\partial y_o}\frac{1}{2}(d_o - y_o)^2 \frac{\partial}{\partial r_{jk}} w_{jko} r_{jk} \frac{\partial}{\partial m_{ijk}} \exp\left(\frac{-(I_i - m_{ijk})^2}{v_{ijk}^{\ 2}}\right) \\ &= -\eta_m \sum_{o=1}^{n_0} -(d_o - y_o) w_{jko} \exp\left(\frac{-(I_i - m_{ijk})^2}{v_{ijk}^{\ 2}}\right) 2(I_i - m_{ijk}) v_{ijk}^{\ -2} \\ &= \eta_m \sum_{o=1}^{n_0} e_o w_{jko} r_{jk} 2(I_i - m_{ijk}) v_{ijk}^{\ -2}\end{aligned} \tag{10}$$

$$\begin{aligned}\Delta v_{ijk} &= -\eta_v \sum_{o=1}^{n_o} \frac{\partial E(k)}{\partial v_{ijk}} = -\eta_v \sum_{o=1}^{n_o} \frac{\partial E}{\partial y_o}\frac{\partial y_o}{\partial r_{jk}}\frac{\partial r_{jk}}{\partial v_{ijk}} \\ &= -\eta_v \sum_{o=1}^{n_0} \frac{\partial}{\partial y_o}\frac{1}{2}(d_o - y_o)^2 \frac{\partial}{\partial r_{jk}} w_{jko} r_{jk} \frac{\partial}{\partial v_{ijk}} \exp\left(\frac{-(I_i - m_{ijk})^2}{v_{ijk}^{\ 2}}\right) \\ &= -\eta_v \sum_{o=1}^{n_0} -(d_o - y_o) w_{jko} \exp\left(\frac{-(I_i - m_{ijk})^2}{v_{ijk}^{\ 2}}\right) 2(I_i - m_{ijk})^2 v_{ijk}^{\ -3} \\ &= \eta_v \sum_{o=1}^{n_0} e_o w_{jko} r_{jk} 2(I_i - m_{ijk})^2 v_{ijk}^{\ -3}\end{aligned} \tag{11}$$

where η_m and η_v are the learning rate for the center value and the variance of the receptive-field basis function, respectively. The new center value and the variance of the receptive-field basis function are updated as:

$$m_{ijk}(k+1) = m_{ijk}(k) + \Delta m_{ijk}(k) \tag{12}$$

$$v_{ijk}(k+1) = v_{ijk}(k) + \Delta v_{ijk}(k) \tag{13}$$

Although small values for the learning rate guarantee the convergence of FCMCA classifier, the learning process is slow. Large values for the learning rates allow a faster learning speed, but the classifier is less stable. In order to more effectively train the parameters for the FCMAC classifier, the Lyapunov theorem is used to derive variable learning rates that allow the fastest convergence for the output error of the FCMAC classifier.

First, define the gradient operator as $P_z(k) = \frac{\partial y_o}{\partial z}$, where z is w, m or v.

Second, define the Lyapunov function as:

$$V(k) = \frac{1}{2}\sum_{o=1}^{n_o} e_o^2(k) \tag{14}$$

The variation in $V(k)$ is expressed as:

$$\Delta V(k) = V(k+1) - V(k) = \frac{1}{2}\sum_{o=1}^{n_o} [e_o^2(k+1) - e_o^2(k)] \tag{15}$$

The o-th output error for the k+1 time is

$$e_o(k+I) = e_o(k) + \Delta e_o(k) = e_o(k) + [\frac{\partial e_o(k)}{\partial z}]^T \Delta z \tag{16}$$

Using the chain rule, it can be calculated that

$$\frac{\partial e_o(k)}{\partial z} = \frac{\partial e_o(k)}{\partial y_o(k)} \frac{\partial y_o(k)}{\partial z} = -P_z(k) \tag{17}$$

Substituting (17) into (16) gives

$$\begin{aligned} e_o(k+1) &= e_o(k) - [P_z(k)]^T \eta_z e_o(k) P_z(k) \\ &= e_o(k)[1 - \eta_z \left\| P_z(k) \right\|^2] \end{aligned} \tag{18}$$

Substituting (18) into (15) and through simplification:

$$\Delta V(k) = \frac{1}{2}\eta_z e^2(k) \left\| P_z(k) \right\|^2 [\eta_z \left\| P_z(k) \right\|^2 - 2] \tag{19}$$

The value for η_z is chosen to be in the $0 < \eta_z < \frac{2}{\left\| P_z(k) \right\|^2}$ region, so $V > 0$ and $\Delta V < 0$ and the Lyapunov stability is guaranteed. When $k \to \infty$, the convergence of the FCMAC classifier output error $e_o(k)$ is guaranteed. The optimal learning-rates, η_z^*, are selected to achieve the fastest convergence by letting $2\eta_z^* \left\| P_z(k) \right\|^2 - 2 = 0$, which results from the derivative of (19) with respect to η_z and equals to zero. The optimal learning rates are then:

$$\eta_z^* = \frac{1}{\left\| P_z(k) \right\|^2} \tag{20}$$

In conclusion, the adaptive FCMAC classifier output is defined in (6). Its parameter learning rules are derived by using the normalized steepest descent method. Equations (9), (12) and (13) are used to adjust the output space weights, the center value and the variance of the receptive-field. The optimal learning-rates are defined by (20) and the convergence of FCMAC classifier is guaranteed.

3 Experimental Results

As stated earlier, uncertainty is a problem for medical diagnosis. The detection of intestinal bacteria, such as Salmonella or E. coli, allows practitioners to judge whether typhoid or gastrointestinal diseases cause physical discomfort. Using pre-defined disease feature categories, the detected bacteria are compared with most similar feature to enable a medical diagnosis. The training data (from [19] for Case 1 and from [20] for Case 2) are applied to the FCMAC classifier, presented in Section 2, for learning process with 1000 iterations. When the learning process is completed, the test data are fed into the FCMAC for classification. Then this classifier can classify the samples to allow a medical diagnosis.

3.1 Medical Sample

a) Case 1: Bacteria

The bacterial cells are classified as shown in Fig. 2 [19]. Four bacterial cell characteristic values are shown in Table 1 [19]. F and V represent bacterial feature sets and species, respectively. The information about the bacterial samples includes F = {Domical shape, Single microscopic shape, Double microscopic shape, Flagellum} and V = {Bacillus coli, Shigella, Salmonella, Klebsiella}. The samples for classification are shown in Table 2 [19].

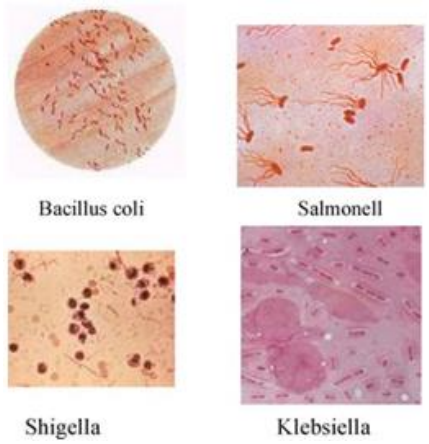

Figure 2
Different types of bacterial cell samples [19]

Table 1
The features' values in the studied bacteria classes (base patterns)

Bacteria	Features			
	F1	F2	F3	F4
V1	<0.850,0.050>	<0.870,0.010>	<0.020,0.970>	<0.920,0.060>
V2	<0.830,0.080>	<0.920,0.050>	<0.050,0.920>	<0.080,0.910>
V3	<0.790,0.120>	<0.780,0.110>	<0.110,0.850>	<0.870,0.010>
V4	<0.820,0.150>	<0.720,0.150>	<0.220,0.750>	<0.120,0.850>

Table 2
The features' values of the samples detection

Samples	Features			
	F1	F2	F3	F4
S1	<0.873,0.133>	<0.718,0.159>	<0.064,0.897>	<0.021,0.806>
S2	<0.911,0.029>	<0.831,0.031>	<0.028,0.894>	<0.952,0.036>
S3	<0.929,0.037>	<0.812,0.033>	<0.021,0.926>	<0.054,0.922>
S4	<0.815,0.091>	<0.949,0.048>	<0.020,0.880>	<0.833,0.042>
S5	<0.864,0.020>	<0.610,0.230>	<0.243,0.624>	<0.000,0.964>
S6	<0.905,0.016>	<0.878,0.015>	<0.072,0.917>	<0.789,0.114>

b) Case 2: Disease

The symptomatic characteristics of the target sample are shown in Table 3 [20]. There are five diseases: viral fever, malaria, typhoid, stomach problems and chest problems. Each disease has five features: temperature, headache, stomach pain, coughs and chest pain. Four disease samples classified are shown in Table 4 [20].

Table 3
Symptoms feature of five diseases

	Temperature	Headache	Stomach pain	Cough	Chest pain
Viral fever	(0.4,0.0,0.6)	(0.3,0.5,0.2)	(0.1,0.7,0.2)	(0.4,0.3,0.3)	(0.1,0.7,0.2)
Malaria	(0.7,0.0,0.3)	(0.2,0.6,0.2)	(0.0,0.9,0.1)	(0.7,0.0,0.3)	(0.1,0.8,0.1)
Typhoid	(0.3,0.3,0.4)	(0.6,0.1,0.3)	(0.2,0.7,0.1)	(0.2,0.6,0.2)	(0.1,0.9,0.0)
Stomach problem	(0.1,0.7,0.2)	(0.2,0.4,0.4)	(0.8,0.0,0.2)	(0.2,0.7,0.1)	(0.5,0.7,0.1)
Chest problem	(0.1,0.8,0.1)	(0.0,0.8,0.0)	(0.2,0.8,0.0)	(0.2,0.8,0.0)	(0.8,0.1,0.1)

Table 4
Symptoms feature of four people disease samples

	Temperature	Headache	Stomach pain	Cough	Chest pain
Al	(0.8,0.1,0.1)	(0.6,0.1,0.3)	(0.2,0.8,0.0)	(0.6,0.1,0.3)	(0.1,0.6,0.3)
Bob	(0.0,0.8,0.2)	(0.4,0.4,0.2)	(0.6,0.1,0.3)	(0.1,0.7,0.2)	(0.1,0.8,0.1)
Joe	(0.8,0.1,0.1)	(0.8,0.1,0.1)	(0.0,0.6,0.4)	(0.2,0.7,0.1)	(0.0,0.5,0.5)
Ted	(0.6,0.1,0.3)	(0.5,0.4,0.1)	(0.3,0.4,0.3)	(0.7,0.2,0.1)	(0.3,0.4,0.3)

3.2 Results

a) Case 1: Bacteria

The concept of clustering is used to determine the similarity between each known bacteria and unknown sample features. Four information features of known bacteria and unknown samples are used for a pairwise comparison. For example, each known bacterial first feature value combination of F1 and F2 is compared with the same feature value combination for each unknown sample and each known bacterial first feature value combination of F1 and F3 is compared with the same feature value combination for each unknown sample. The six reference figures, Fig. 3 to Fig. 8, show the results.

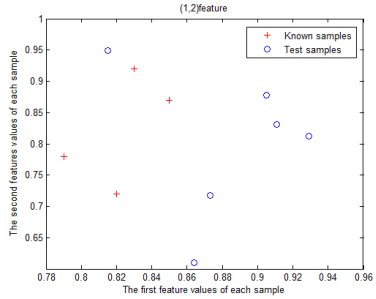

Figure 3
(1,2) feature distribution

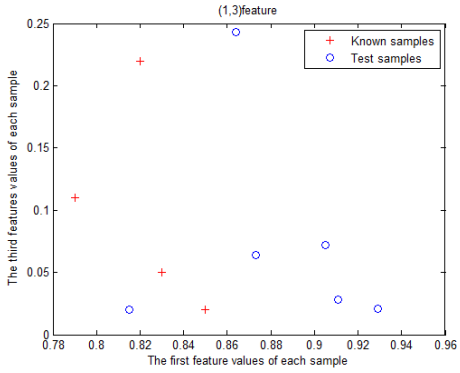

Figure 4
(1,3) feature distribution

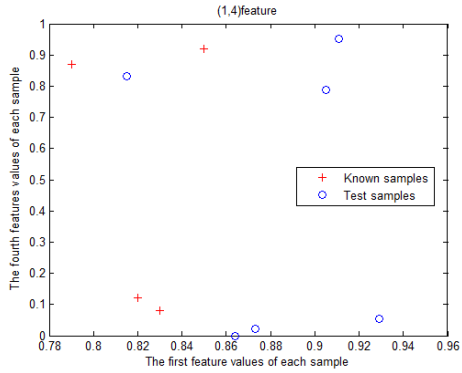

Figure 5
(1,4) feature distribution

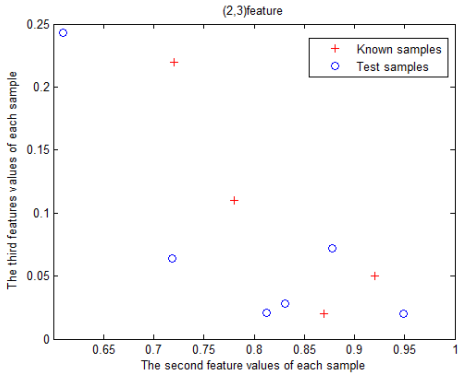

Figure 6
(2,3) feature distribution

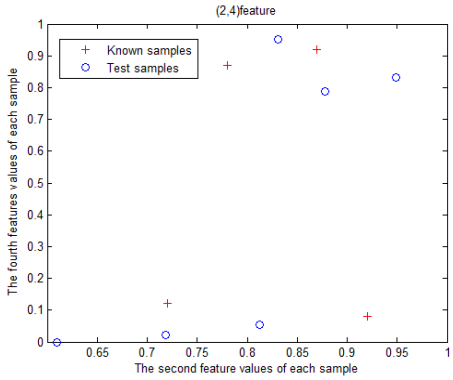

Figure 7
(2,4) feature distribution

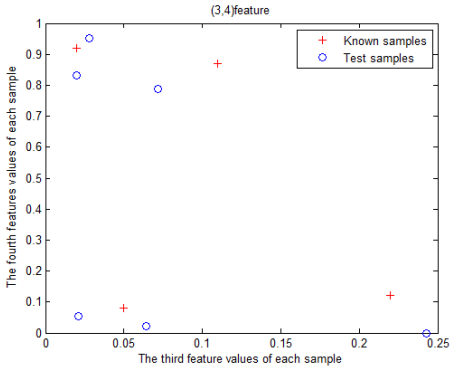

Figure 8
(3,4) feature distribution

The proposed FCMAC classifier identifies the bacterial samples.

The bacterial sample data is

$$m = \begin{bmatrix} 0.85 & 0.87 & 0.02 & 0.92 \\ 0.83 & 0.92 & 0.05 & 0.08 \\ 0.79 & 0.78 & 0.11 & 0.87 \\ 0.82 & 0.72 & 0.22 & 0.12 \end{bmatrix}$$

Table 5 shows the classification results for the intuitive fuzzy set (IFS) method [20] and the proposed FCMAC. The correct recognition rate shows that the proposed FCMAC classifier performs better than the IFS classifier.

Table 5
IFS and FCMAC classification results

Identification method	Correct recognition rate	Error recognition rate
IFS	95.27%	4.73%
FCMAC	97.55%	2.45%

b) Case 2: Disease

Using Table 3 and Table 4, the ten reference figures, Fig. 9 to Fig. 18, show the degree of difficulty of classification. Table 6 shows that the FCMAC classifier can achieve exact classification and produce good recognition results. The proposed classifier will allow medical practitioners to improve diagnostic accuracy.

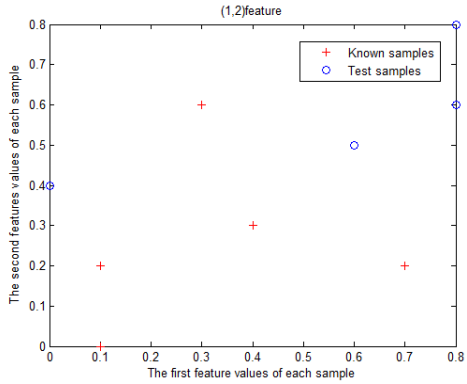

Figure 9
(1,2) feature distribution

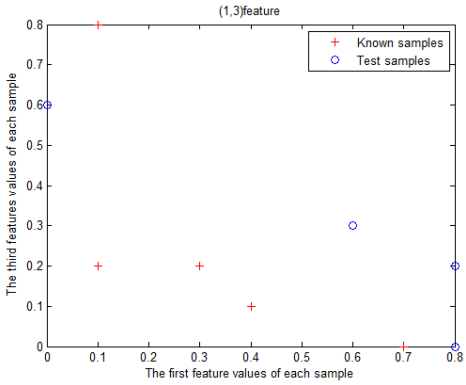

Figure 10
(1,3) feature distribution

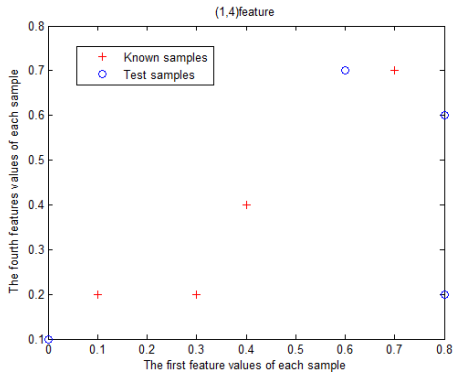

Figure 11
(1,4) feature distribution

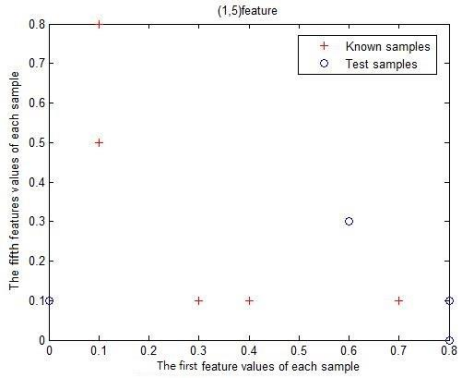

Figure 12
(1,5) feature distribution

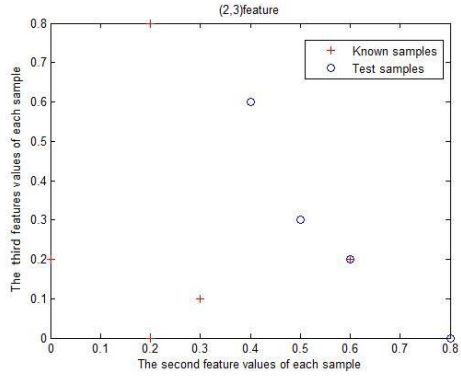

Figure 13
(2,3) feature distribution

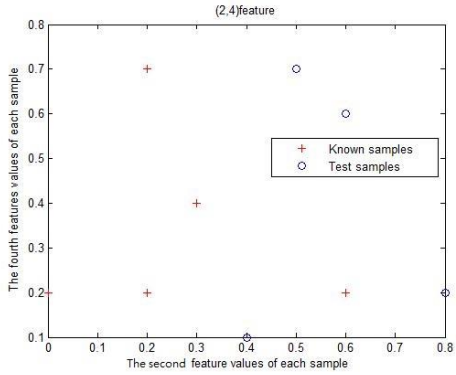

Figure 14
(2,4) feature distribution

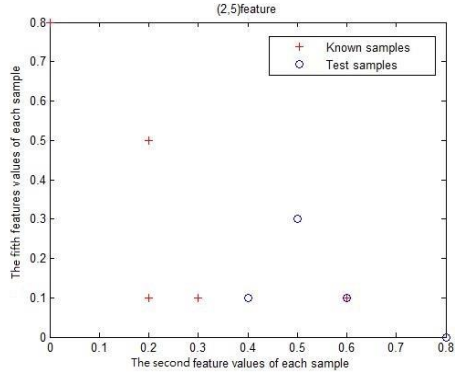

Figure 15
(2,5) feature distribution

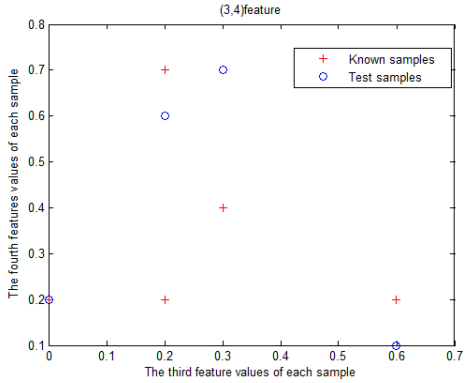

Figure 16
(3,4) feature distribution

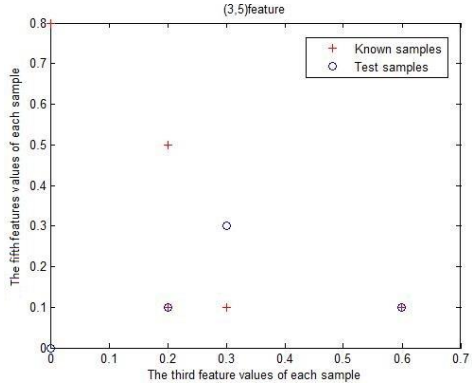

Figure 17
(3,5) feature distribution

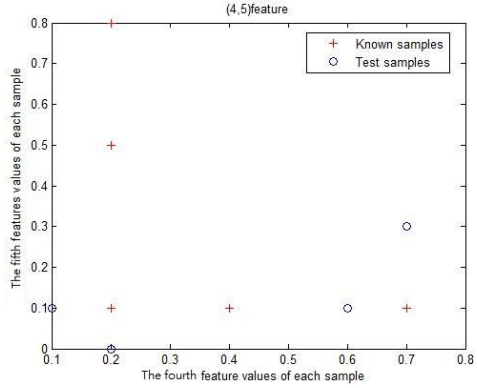

Figure 18
(4,5) feature distribution

Table 6
FCMAC classification results

	Viral fever	Malaria	Typhoid	Stomach problem	Chest problem
Al	**1**	0	0	0	0
Bob	0	0	0	**1**	0
Joe	**1**	0	0	0	0
Ted	**1**	0	0	0	0

Conclusions

This paper proposes a generalized fuzzy neural network, called a fuzzy CMAC (FCMAC), which combines fuzzy rules and CMAC. This network is used as an adaptive FCMAC classifier that allows stable classification and a fast convergence.

The developed network is an expansion-type fuzzy neural network. A traditional fuzzy neural network can be viewed as a special case of this network.

This expansion-type fuzzy neural network allows better generalization, learning and approximation than a traditional fuzzy neural network so it greatly increases the effectiveness of a neural network classifier. The Lyapunov stability theory is used to develop the learning rule, for classifier parameters, in order to allow online self-adjustment. Therefore, the convergence of the design classifier is guaranteed.

This study successfully extends the application of the proposed adaptive FCMAC neural network to the classification of medical samples. The effectiveness of the expansion-type FCMAC neural network is verified by the simulation results.

Acknowledgement

The authors appreciate the financial support in part from the Nation Science Council of Republic of China under grant NSC 101-2221-E-155-026-MY3.

References

[1] S. S. Ge, C. C. Hang, and T. Zhang, "Adaptive Neural Network Control of Nonlinear Systems by State and Output Feedback," *IEEE Trans. Syst., Man, Cybern., B,* Vol. 29, No. 6, pp. 818-828, 1999

[2] S. K. Oh, W. D. Kim, W. Pedrycz and B. J. Park, "Polynomial-based Radial Basis Function Neural Networks (P-RBF NNs) Realized with the Aid of Particle Swarm Optimization," *Fuzzy Sets and Systems*, Vol. 163, No. 1, pp. 54-77, 2011

[3] C. M. Lin, A. B. Ting, C. F. Hsu and C. M. Chung, "Adaptive Control for MIMO Uncertain Nonlinear Systems Using Recurrent Wavelet Neural Network," *International Journal of Neural Systems*, Vol. 22, No. 1, pp. 37-50, 2012

[4] C. F. Hsu, C. M. Lin and R. G. Yeh, "Supervisory Adaptive Dynamic RBF-based Neural-Fuzzy Control System Design for Unknown Nonlinear Systems," *Applied Soft Computing,* Vol. 13, No. 4, pp. 1620-1626, 2013

[5] D. Marr, "A Theory of Cerebellar Cortex," *J. Physiol.*, Vol. 202, pp. 437-470, 1969

[6] J. S. Albus, "A New Approach to Manipulator Control: the Cerebellar Model Articulation Controller (CMAC)," *ASME, J. Dynam., Syst., Meas., Contr.,* Vol. 97, No. 3, pp. 220-227, 1975

[7] J. S. Albus, "Data Storage in the Cerebellar Model Articulation Controller (CMAC)," *ASME, J. Dynam., Syst., Meas., Contr.*, Vol. 97, No. 3, pp. 228-233, 1975

[8] W. T. Miller, F. H. Glanz, and L. G. Kraft, "CMAC: an Associative Neural Network Alternative to Backpropagation," *Proc. of the IEEE*, Vol. 78, No. 10, pp. 1561-1567, 1990

[9] R. J. Wai, C. M. Lin, and Y. F. Peng, "Robust CMAC Neural Network Control for LLCC Resonant Driving Linear Piezoelectric Ceramic Motor," *IEE Proc., Cont. Theory, Applic.*, Vol. 150, No. 3, pp. 221-232, 2003

[10] S. H. Lane, D. A. Handelman, J. J. Gelfand, "Theory and Development of Higher-Order CMAC Neural Network", *IEEE Control Systems Magazine*, Vol. 12, No. 2, pp. 23-30, 1992

[11] C. T. Chang and C. S. Lin, "CMAC with General Basis Functions," *Neural Network*, Vol. 9, No. 7, pp. 1199-1211, 1996

[12] C. S. Lin and C. T. Chiang, "Learning Convergence of CMAC Technique," *IEEE Trans. Neural Networks*, Vol. 8, No. 6, pp. 1281-1292, 1997

[13] C. M. Lin and Y. F. Peng, "Adaptive CMAC-based Supervisory Control for Uncertain Nonlinear Systems," *IEEE Trans. System, Man, and Cybernetics Part B*, Vol. 34, No. 2, pp. 1248-1260, 2004

[14] C. M. Lin and H. Y. Li, "Dynamic Petri Fuzzy Cerebellar Model Articulation Control System Design for Magnetic Levitation System," *IEEE Control Systems Technology*, Vol. 23, No. 2, pp. 693-699, 2015

[15] G. Gosztolya and L. Szilagyi, "Application of Fuzzy and Possibilistic c-means Clustering Models in Blind Speaker Clustering," *Acta Polytechnica Hungarica*, Vol. 12, No. 7, pp. 41-56, 2015

[16] J. Zheng, W. Zhuang,, N. Yan, G. Kou, H. Peng, C. McNally, D. Erichsen, A. Cheloha, S. Herek, C. Shi, Y. Shi, " Classification of HIV-I-mediated Neuronal Dendritic and Synaptic Damage using Multiple Criteria Linear Programming, Neuroinformatics, Vol. 2, No. 3, pp. 303-326, 2004

[17] E. Straszecka, "Combining Uncertainty and Imprecision in Models of Medical Diagnosis," *Information Sciences*, Vol. 176, No. 20, pp. 3026-3059, 2006

[18] J. W. Han and M. Kamber, *Data mining: concepts and techniques*. Morgan, San Mateo, CA, 2006.

[19] V. Khatibi and G. A Montazer, "Intuitionistic Fuzzy Set vs. Fuzzy Set Application in Medical Pattern Recognition," *Artificial Intelligence in Medicine*, Vol. 47, pp. 43- 52, 2009

[20] K. C. Hung, "Medical Pattern Recognition: Applying an Improved Intuitionistic Fuzzy Cross-Entropy Approach," *Advances in Fuzzy Systems*, Published on line, Vol. 2012, Article ID 863549, 6 pages, 2012

Service-oriented Architecture and Cloud Manufacturing

Tomáš Lojka, Marek Bundzel, Iveta Zolotová

Department of Cybernetics and Artificial Intelligence, Faculty of Electrical Engineering and Informatics, Technical University of Košice, Letná 9/B, 042 00 Košice, Slovakia, e-mails: {tomas.lojka, marek.bundzel, iveta.zolotova}@tuke.sk

Abstract: This paper deals with service oriented architecture (SOA) and cloud technologies in the industry. SOA and cloud technologies have considerable potential to improve industrial production and control. This paper analyzes those systems and proposes an architecture for device integration, data acquisition, data processing and remote control. We designed and implemented SOA for industrial technological routers, allowing device integration in the designed architecture and cloud interoperability. We used a private cloud and designed atomic and composite services. These services empower the architecture with data acquisition, processing and data analytics. The architecture offers a solution for connecting to an industrial network with a remote HMI client and a cloud MES application. We used greenhouse and assembly lines models, a PLC, an eWON, an eFive, a private cloud (Windows Azure Pack), Android, Windows tablet applications, smartphones and desktop computers. We designed and implemented a multi-tenant cloud architecture. In our experiments, we verified our architecture in two simulated plant divisions. Each of them has their own implementation. Our architecture offers better interactivity with suppliers, cooperation with internal systems and can be easily adapted to other extensions of the processes of a plant.

Keywords: Industrial cloud; IoT; SCADA; SOA; MES, Windows Azure

1 Introduction

Control systems dynamically improve and attempt to meet industrial requirements, such as the need for real-time online analysis, realistic representation of industrial processes or obtaining accurate information to control the industrial processes. These requirements raise questions on how to improve the following:

- Integration of devices and data in a plant.
- Implementation of real-time data acquisition and analysis,
- Highly available data.

Flexibility and integration appear to be the main issues. For example, a large number of interconnected monitoring and data processing appliances can cause flexibility and integration problems. For this reason, it is necessary to design an architecture that will solve these problems. Nowadays, the trend for information and control systems (ICS) is to become more agile, heterogeneous, interoperable, open and dynamic [1], [2], [3], [4]. A design and an implementation that ensure the stability of the systems and their functionality in real time appear to be a robust solution. Such a solution should be stable during the current expansion of data flows and, during the expansion of the infrastructure of an entire plant and mainly during the expansion of the number of interconnected devices in it. Service oriented architecture (SOA), the Cloud and the Internet of Things (IoT) can meet the industrial requirements. SOA extends the solution with atomic, device, composite and deployment services. These services support cooperation, offer agility, and operate in a heterogeneous environment [5]. The IoT supports interconnection and the Cloud offers stability and integration. The Cloud can host the representation of the environment where the services are hosted.

In this paper, we focus on the design, implementation and verification of our future solution of an industrial architecture that satisfies the agility, stability and interoperability criteria and works in heterogeneous environments. The architecture consists of Cyber-physical systems, IoT, SOA and the Cloud.

This paper is organized into three main chapters. The first chapter describes the increase in the Supervisory Control and Data Acquisition (SCADA) and Manufacturing Execution System (MES) performance and deals with the SOA. The second chapter deals with the concept definition of the future cloud SCADA and MES architectures. The last chapter presents an evaluation of two use cases.

1.1 Increasing the SCADA and MES Performance

Nowadays, SCADA and MES are parts of the ISA-95 standard. Many industrial information and control systems are based on this standard. The standard has five levels and each level only communicates with the adjacent levels (the pyramid in Figure 1). Level 0 represents physical production processes. Sensors and actuators are a part of the next level that is responsible for monitoring and affecting physical processes. The Control/Interlocking level controls physical processes and it is also labeled as Level 1. The SCADA level is responsible for data acquisition and supervision control. SCADA is also labeled as a system for a remote control and monitoring. It collects data and stores them into databases, offers viewing the current and historical trends, triggers alarms and does statistical data processing. MES is the next layer in the standard and controls the workflow to reach the desired product. It operates with the data stored in the databases and helps make decisions, understand the current situation in the production processes and manage the transformation of materials to the final product. The top layer is Enterprise resource planning (ERP). It covers business activities and deals with an enterprise organization [4].

New IT technologies lead to new approaches in SCADA systems and MES. Cloud computing and services emerged in the last few years. The Cloud offers enough resources and offers robust services for aggregating, processing and analyzing data. It is accessible for collecting and offering data or services anytime and anywhere. It also improves SCADA and MES and other layers with features described by NIST (National Institute of Standards and Technology) [1], [6], [7].

There is some research and implementations of SCADA and MES in the Cloud that use SOA. For example, WebSCADA offers solutions that reallocates SCADA into the Cloud and uses SOA [8]. The ICM-AESOP is a project that reallocates even more than WebSCADA does [4]. It reallocates control, SCADA, MES and ERP into the Cloud and benefits from SOA [4]. Project SOCRADES uses SOA in an embedded device. In general, these solutions and projects focus on SOA-based embedded devices and the reallocation of some ISA-95 levels into the Cloud. The missing part here is a gateway that implements SOA into the existing process level, aggregates data and creates universal access to the Cloud. The SOA gateway can then create a consistent system by offering atomic services for composite services in cloud modules.

With the increasing number of devices, the amount of data grows. This causes problems in human-machine interaction, SCADA and MES. One of the approaches is Machine-to-Machine (M2M) communication, which reduces the human-machine interaction [3], [9]. Another approach is data pre-processing [10]. However, SCADA is supposed to work with larger amounts of data that increase quickly. Nowadays, thousands of industrial devices and appliances can use network communication to transmit data. Therefore, SCADA should change the way of processing such an amount of distributed data and information [1], [2]. MES has the information about the current situation on the plant floor and helps optimize processes on it.

1.1.1 Flat and Information-based Architecture

SCADA, MES and basically all ICS seem to be headed towards using SOA services in the future. Therefore, it is important to find the optimal distribution of functionalities between the users, the computing systems and the Cloud solutions. In the next generation of ICS (some functionalities are relocated to a cloud-based side. The traditional ISA-95 standard is oriented to a hierarchical model, whereas the next generation of industrial applications is oriented to use the services exposed by cyber-physical systems or cloud services (Figure 1). The architecture changes into a flat, information-based architecture composed of services. These services are represented as modules, which improves the flexibility of information-based architectures. These changes were defined in the ICM-AESOP project [4].

1.1.2 Services in the Information-based Architecture

The services can divide the architecture into domains with a better interaction and modularity. Another important aspect of ICS based on SOA is robustness and the reinforcement and automation of industrial activities [3].

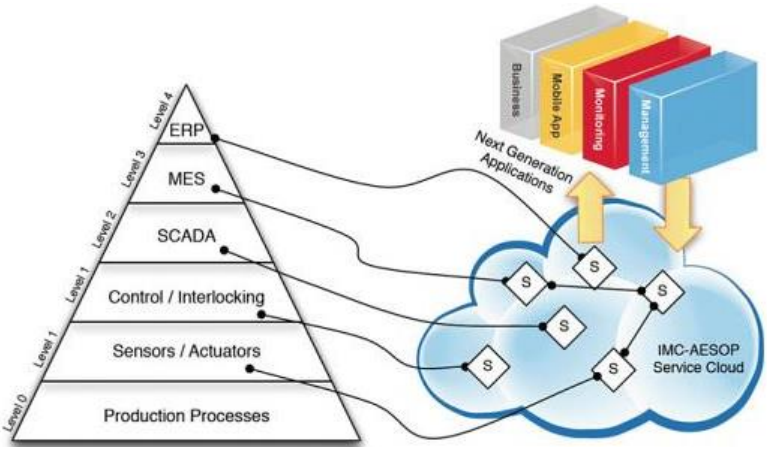

Figure 1

The evolution of ICS - Traditional ISA-95 standard with a flat information-based architecture [4]

We focus on the application of SOA and cloud technologies in ICS, particularly in SCADA and MES parts of ICS. The services increase the functionality and interoperability with devices [11], [12]. We designed, implemented and tested our architecture which makes use of SOA, an industrial gateway/mediator and the Cloud. We created our architecture for service-oriented SCADA systems and MES. This service-based system will support horizontal and vertical connections, such as communication between enterprise systems, plant-floor devices or controllers. This communication is an important part of the Industry 4.0 key paradigms: smart products, smart machines, smart planners, and smart operators [6].

1.2 Service-oriented Architecture in SCADA and MES

SOA enables to improve and automate plant functionalities, and to design, implement and aggregate services. A service represents a primal functional side of the implemented SOA [13]. The plant uses a set of services that communicate with clients or with other services [14].

The reason for using SOA in a plant reflects the base features of SOA [15]:

1. Autonomy
2. Interoperability
3. Weak dependencies

4. Independent implementation
5. Flexibility

A SOA-based industrial solution may consist of components like SCADA, Enterprise Resource Planning (ERP), Customer Relationship Management (CRM), Programmable logic controller (PLC), Distributed control system (DCS), MES, devices, and cloud service integration (Figure 2) [6], [16], [19]. These components represent atomic or composite services which can interact with each other. Devices communicate with highly accessible resources. The services can be implemented in the Cloud. These services enable data analysis and encourage making decisions over larger amounts of data and offer the control and visualization of the data to clients.

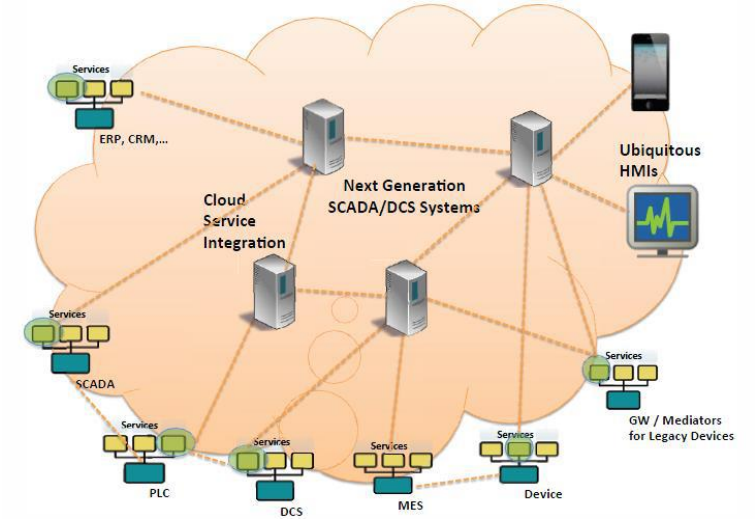

Figure 2

The architecture for SOA in the industry. ERP, CRM, SCADA, PLC, etc. with implemented services. The services communicate with the cloud Service Integration. The Cloud enables communication with HMI clients [3]

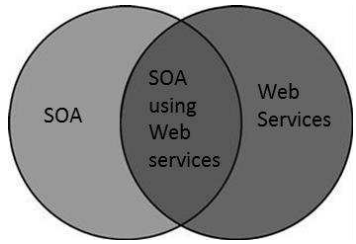

Figure 3

The relation of SOA and Web services [3]

Communication is required in almost all cases. The services are mainly web-based [13]. The relation between SOA and Web Services is described in Figure 3.

Web services enable interactivity among the processes and the machines in the plant. The communication transmits distributed data and information between the plant devices, appliances or software via the web services [18], [19].

SOA is one of the main focus points of this paper because of its autonomy, interoperability, easy integration and the flexibility of configuration. The services may be used in various ways, thus increasing their reusability. There are two types of services: atomic and composite. Atomic services are well defined and independent of the state of other services. Composite services are a set of atomic or other composite services. These depend on the status of other services comprising the service in question. One of the best service implementations is via web services, which have huge potential in remote control. In our work, we implemented the web services on a traditional, easily programmable eWON industrial router, thus extending its basic-features. We satisfied-the interoperability criteria with atomic and composite services.

In other words, the services represent a solution for interactive communication between machines or systems. The following list briefly describes the reasons why service-based SCADA systems and MES can increase the efficiency of manufacturing processes:

- **Cooperation** with mobile devices, sensors and actuators, smartphones and tablets.
- Easy **interoperability** with devices, machines or systems with special human interaction, for example using an intuitive **multi-touch control** on a touch screen tablet or a smartphone.
- **Open integration** with devices, and cloud and third-party applications.

The services have additional features such as security, discovery of other services, data encryption, data management and communication reduction tools. Generally, the services in SCADA and MES can be grouped based on what they do: alarms, control, data management, discovery, Human-Machine Interaction (HMI), life cycle management, diagnostic, safety and process monitoring, resource management, scheduling and performance analysis [4]. However, we mainly focus on data acquisition, alarms, remote control, visualization and performance analysis in this paper.

According to the mentioned problems, we aim to develop a SCADA solution, addressing:

- The use of standards for integration with industrial devices from different vendors and satisfying M2M communication.
- The increase of performance of SCADA systems.

- The implementation of security in SCADA systems.
- The Cloud and SCADA interoperation.

MES provide correct information about the current situation on the plant floor. On top of that, they also offer information on optimization. In this paper, we focus on MES, too. However, we deal with a developed cloud service representation of simple MES functionalities like Overall Equipment Effectiveness (OEE).

2 Concept Definition of the Future Cloud SCADA and MES Architecture

Our concept was developed in two steps and consists of SOA, industrial devices and a private cloud. In the first step, we identified and designed services before designing the architecture. We designed atomic services that:

- Help create composite services.
- Allow for easy maintenance.
- Possess the SCADA functionality with better interaction and robustness.
- Simplify the expansion of the system.

Our concept features services with two types of implementation. The services can be implemented directly on the plant-floor devices and the gateway/mediator, or in the Cloud. According to [4], we specified services and groups for our concept (Table 1). There are many more services described in [4] but we did not use all of them.

Table 1
Services in architecture's concept definition

Service Group	Service role	Description
Alarm	Alarm processing, Alarm configuration	Processes the alarm and creates alarm events for the HMI, and the Control and data management Service groups.
Control	Control	Executes control based on input data and produces control values.
Data management	Data acquisition Data output Logging	Transfers data between sensors, actuators and databases.
Data processing	Filtering/Normalizing Data analytics Event management	Data preprocessing and processing; creates events for the Alarm, Control and Data management groups.
HMI	Human-Machine interaction	Creates a HMI interface for PC and mobile service clients.

Model	Model Model management	Information model for control or optimization of processes.
OEE	Overall Equipment Effectiveness	Counting OEE for a selected production line.

In the next step, we designed an architecture that can improve data acquisition, alarms, remote control and visualization and we also designed a general representation of the architecture (Figure 4). The concept definition of the architecture consists of:

- Cyber-physical systems – representing the technological layer of a plant.
- Internet of Things – representing the interconnection between the Cloud and the Cyber-physical systems.
- The Cloud – representing composite and atomic services, implementing communication, database, SCADA, MES, ERP and Business intelligence services.
- Clients – representing the devices that use the cloud services in the Human-Machine Interaction (HMI).

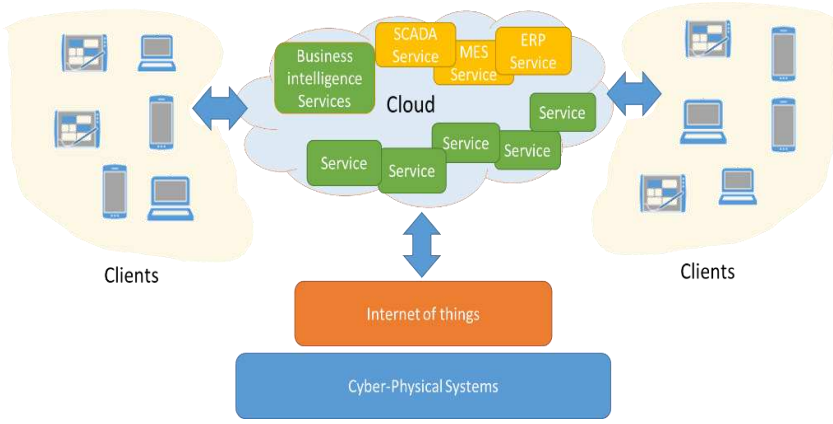

Figure 4

The concept definition of the proposed architecture

We defined the hardware and software resources needed to implement our concept definition of the architecture. The concept consists of a technological layer implemented in the laboratory, a CompactLogix PLC from Allen-Bradley, an eWON industrial router, an eFive industrial firewall, mobile devices, Windows Azure and Google servers. We used a virtual production line model and a greenhouse model to simulate the technological layer. The communication, interoperability and security with Cyber-physical systems are based on a programmable eWON industrial router and an eFive. We extended the eWON with SOA and used the eFive industrial firewall to create a modular and interoperable SOA environment secured by a VPN server. We chose the Windows

Azure cloud platform for the cloud implementation, where we designed and developed the services for connectivity, web services, HMI, simple MES, control, data processing and management, alarms and models.

2.1 Designing an Architecture for SCADA and MES

The architecture is based on SOA and the Cloud. Therefore, we used services described in Table 1. The architecture has the cooperation, interoperability and open integration features from subchapter 1.2. According to the defined concept (Figure 4), we focused on data acquisition, alarms, remote control and visualization. Therefore, we used the Cloud, SOA, the IoT idea and a client application in the design process of the architecture for SCADA and MES. In the proposed architecture (Figure 6), the PLC contains the control logic for assembly lines and greenhouse models. Mobile devices enable remote control and visualization of the technological process. A remote secure connection is made via the industrial VPN server. The mobile clients are smart phones, computers and tablets. The gateway/mediator we used has our own implementation of SOA described in Table 1. The architecture consists of the private cloud and a connection to a public cloud server. The main parts are the gateway/mediator and the private cloud. The implementation of the proposed architecture is in Figure 5.

Figure 5

Our designed architecture that consists of the technological layer of ICS, an industrial router eWON, Windows Azure as a cloud solution, a SOA service, an SQL database, a Google server, and mobile Android and Windows clients

2.2 Gateway/Mediator Services in the Designed Architecture

The industrial router does not offer any services in its standard implementation. Our intention was to build the means for a flexible interaction with various industrial devices from various vendors such as Rockwell, Siemens, Omron and others based on SOA. We built a software communication interface with a standardized protocol allowing every device in the factory to be a part of SOA and to be connected to the Cloud (Figure 2). This communication interface can be deployed on devices and it is based on a standardized protocol that is normally used in the Cloud, but not in industrial devices. The interface also improves the connectivity with various clients. Protocols such as HTTP are supported in many development frameworks and even in the most basic frameworks. HTTPS can be used as well, but we did not use it in our experiments because the router has a basic access authentication and we used a VPN tunnel for the connectivity. Another point of our concept definition was to define the format of the messages. The messages should be easily and quickly serializable and should be able to be represented as objects. Suitable formats include XML, JSON, YAML or a new format implementation. XML, JSON and YAML are standardized and can easily be parsed into objects. We decided to use JSON, because of its common popularity in the development community.

We defined a JSON communication protocol and a message format. Then we created a hash table for ID and request recording. We designed and implemented the following services for the hash table:

- Connection test - a simple echo from the service.
- Getting the value of a tag - returns a tag with the structure and the values from the addressed PLC or returns tags directly from the router.
- Setting the value of a tag – sets a value of the addressed tag.
- ACK of alarm – acknowledgement of the alarms.
- Getting the complete state information and the error bits collection.
- Getting the historical data from a specified interval.
- Getting all alarms values.
- Refresh of all tags in the defined tag collection.
- Getting a collection of values from the defined collection.

Every service replies with a response message containing the data for the client, and acknowledgement information or execution errors.

In conclusion, we designed gateway/mediator services and cloud services. The services are atomic and composite. We implemented the services with SCADA, HMI and MES functionalities, but we intend to consider extending them in the future.

2.3 Cloud Services in the Designed Architecture

We created atomic and composite services in a private Windows Azure cloud. The services save data into databases, communicate with our mediator/gateway services and communicate with the Google calendar service. The services can communicate with the gateway/mediator, directly with the PLC, with applications on mobile devices, with desktop application too. We also created atomic MES services and HMI services.

We developed the services in Microsoft Visual Studio and deployed them to the private Cloud. We used a MSSQL service to store the data from the technological layer and developed an OEE service working with the MSSQL service.

Based on Table 1, we implemented the Alarm Control, Data management and processing, HMI and OEE services. The private Cloud is important to form a robust architecture for ICS capable of implementing a commercial ICS solution but also a private or an open ICS solution.

Real-time communication is an important issue in the context of cloud computing [20]. There are approaches using predictive and deterministic behavior of devices that achieve real-time monitoring [4]. Real-time data processing and acquisition are important for control and we addressed this too. Based on our previous research in online data processing, we created specific events that reduce the load on the network and reduce the power consumption of the devices on the network [19]. Event processing will empower future architectures, too [4].

Data are originated in the technological layer or they are produced by the clients in our solution. Data exchange is done by an event-based communication. This way, only important data are sent to the Cloud, thus decreasing the amount of communication calls, communication cost and increasing the bandwidth of the network. We select the relevant information during data processing and information discovery from the raw sensor data. The discovered information is then classified based on the communication topic. According to the topic, an event is created containing factual information, the priority and statistical information derived from the sensor data. We used Tsallis entropy to process statistical information. The results of the statistical process are then classified into topic and event priority classes. New classification results trigger events. This processing is implemented on technological devices such as our gateway/mediator where we implemented SOA.

The cloud connectivity is based on services while a service is a client for other services. This helps create a modular system consisting of atomic and composite services. The device algorithm runs in the background, monitors data and decides when to create events. Event handlers process data and decrease the communication cost thanks to the used algorithm which reduces the number of messages with insufficient information value by 49. We created two cases to demonstrate the Cloud connectivity. In the first case, the Cloud is directly

connected to the PLC via the cloud service. In the second case, the Cloud is connected to the PLC via our SOA solution implemented on the gateway/mediator.

2.4 Description of the Devices and Technologies Used

The most important technological parts are the eWON and Microsoft Azure.

An **eWON** router is a specialized programmable industrial router containing integrated protocols for communication with PLCs from Rockwell, Schneider, Siemens, OMRON, etc. This router can also be connected to the eFive VPN server and can use the public connectivity service Talk2M hosted in the Cloud for remote management. We chose eWon because it is programable and offers connectors to industrial networks. It is a suitable hardware device for our designed architecture, because it is built for the industry. However, we created our own private remote management solution without using Talk2M. The router has other features like HTML visualization, sending alarms via SMS messages and e-mails, monitoring and controlling production processes, storing historical values and defined tags as well as setting thresholds to trigger the alarm status of these tags and other features. The main feature is a web server with HMI applications. This feature is common in the solution described in [17]. The most important features are the ability to be integrated with various vendors and the ability for its functionality to be extended with JAVA.

An **eFive VPN server** provides a VPN tunnel to a corporate network. The combination of an eFive and an eWON allows a central SCADA system to be created on the internet network and even the geographic locations of the individual components are insignificant. The server contains a native embedded firewall and can manage the routing of the internal corporate network. It also provides data logging in case of failure or communication issues. The eFive was designed to work with eWON routers, which is why we decided to use an eFive to guarantee secure access to our services implemented on an eWON.

Microsoft Azure Pack lets its users build a private cloud infrastructure. It supports web services and SQL databases. The Azure Pack is comparable to Microsoft Azure, but has fewer features (Figure 6). However, the Azure Pack has public “self-service” and “multi-tenant” features and our intention is to use the “multi-tenant” feature. The plant’s IT support can create its own Azure subscription for each division of the plant. Each division is a client and can have sufficient resources easily manageable by their IT support (“self-service”). This solution has huge potential for the plants where the possession of their own private cloud and internal management of data, software and hardware is required. We chose Azure because many automation projects design their software for Microsoft products.

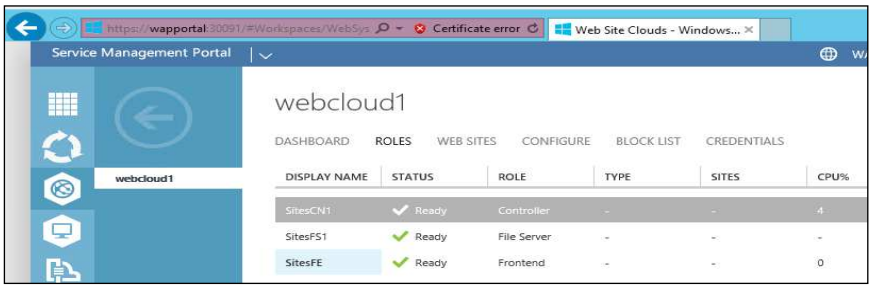

Figure 6

The Windows Azure pack portal of a private cloud

2.5 Implementation of the Designed Architecture

We deployed the Windows Azure Pack across seven virtual machine instances using HyperV, which was the minimal configuration. The Windows Azure private cloud offered a flexible database and SOA collecting data from the PLC via the technological router. The router has limited storage for historical data. Therefore, we used the cloud database for data storage.

The integration with Google servers is another feature of the designed architecture. We designed and developed a private cloud service to write important data to the Google server. After that, these data are accessible to other users such as plant suppliers. In our solution, we used Google cloud to simulate the interactivity with some cooperating industrial companies outside of the plant's private zone.

In the Cloud, we implemented a service for mobile devices. The service supports the tag management of the simulated assembly lines controlled by the PLC, and it also collects, stores and processes data from the PLC. It is accessible to mobile devices via an interface we designed for them that allows them to interact with the service and gives them the ability to send information on production quality, alarms or tag values.

The communication with the eWON was designed with a secure communication channel using OpenSSL. This security feature ensures a secure communication with the PLC-controlled technological processes. Our additional contribution is an implementation of SOA in an eWon industrial programmable router which does not come with any SOA functionality. Therefore, we have designed and implemented the SOA functionality at the beginning. Having done that, the eWON can be easily integrated and its services can be used by applications running on mobile devices, Android applications behind the VPN server and outside of the plant's private zone.

The last important part of the designed architecture is the PLC. We implemented a PLC program to control a greenhouse and simulate production lines. We control

the greenhouse temperature, lighting and humidity. The Rockwell PLC is connected to the eWON industrial router via Ethernet and uses the ABLogix protocol to communicate with it.

2.6 MES and HMI Mobile Clients

We created two types of clients. These client applications are consumers of the cloud services or consumers of the gateway/mediator services:

- An Android HMI SOA client application that monitors and controls the greenhouse model. The client uses the gateway/propagator services (implemented SOA in an eWON) to communicate with the PLC.
- A Windows tablet client that monitors the performance of assembly lines. This application is a MES client application and uses services implemented in the Azure Cloud.

The Android mobile device and the HMI Android application are shown in Figure 7. The tested controlled environment represents the green house controlled by the PLC.

Figure 7

Data from the eWON technological router. Data were sent to the mobile device via a VPN and a SOA service implemented on the eWON industrial router

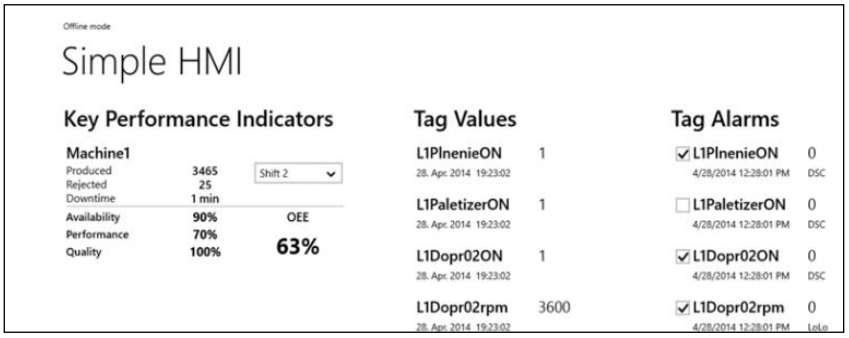

Figure 8

The main screen of the Machine1 of the production line. Data were delivered to the tablet MES Windows store application via the composite MES service

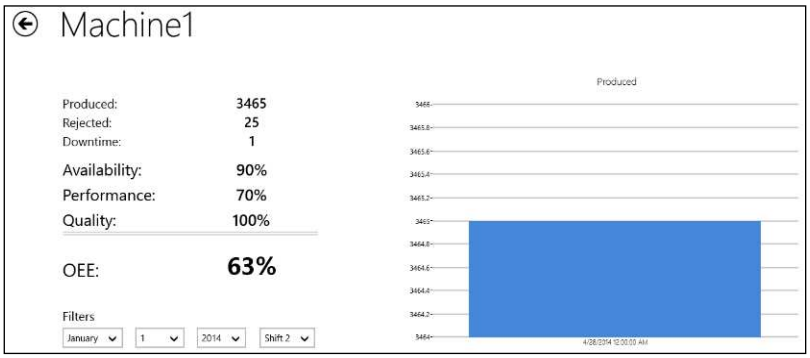

Figure 9

The Machine1's detailed view of the production line. Data were delivered to the Windows store application via the composite MES service

We developed the Windows client application as a Windows store application, too. The application enables managers to monitor the assembly lines, to set the KPI or the OEE. The application screens are shown in Figure 8 and Figure 9.

3 Testing and Evaluation of the Designed Architecture

We implemented our proposed architecture in laboratory conditions already. In the future, we plan to cooperate with an industrial company to implement and test this solution in real-world conditions. We took measurements in the case studies performed in our laboratory.

We verified our architecture in two case studies (Figure 10). Each case represents one division of a plant. The first is responsible for the greenhouse and the second for the assembly lines. Both divisions use PLCs, the Cloud and SOA.

The greenhouse uses a PLC and is directly connected to the Windows Azure Pack. The assembly lines use an eWON router to integrate the data from their PLC and to communicate using SOA. We created the services in Azure. The Windows Azure Pack enables communication with the services on the eWON router and interoperability with the Google server.

Firstly, we performed a qualitative comparison of the divisions using the attributes described in Table 2.

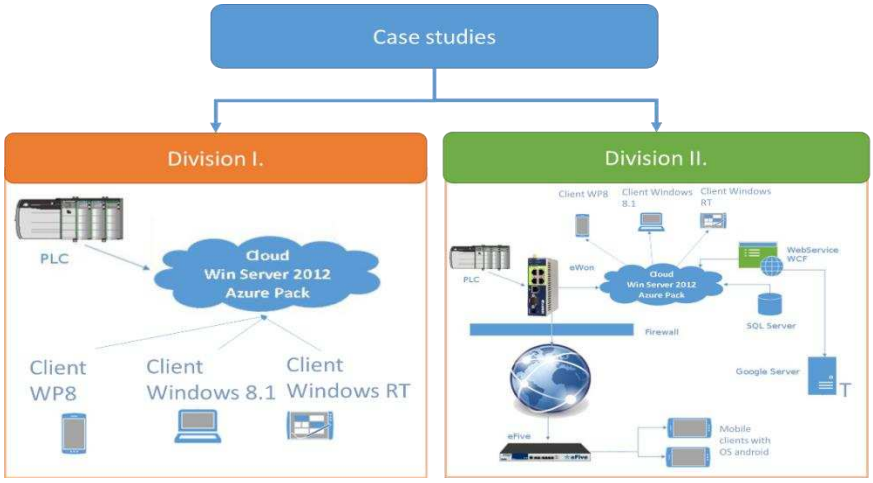

Figure 10

Two case studies used to test our architecture

Table 2

Comparison of the designed architecture implemented by two divisions

Attribute	**Division I**	**Division II**	**Comment**
Data accessibility	Periodic data reading (every 250 ms).	eWON enabled better accessibility with SOA.	SOA interacted with the cloud service only when data was changed.
Client interaction	The private cloud stored production data and had no public connection.	The SOA in the eWON interacts with local SOA clients and with remote clients through the firewall.	SOA enabled connection to the data accessible to the VPN client and did not allow connection to the sensitive data stored in the cloud.
HMI/MES	Direct connection to the PLC, efficiently reads/writes data, problem to integrate another device.	SOA makes it easier to interact with various industrial devices.	The Cloud and SOA provide great device and data integration for data acquisition and control.
Integration	Important to implement protocols for every special industrial device.	Thanks to the eWON and SOA, the cloud has access to the industrial devices of different types using various protocols.	The implementation of SOA-based gateways is a great advancement.
Interaction with third party companies/suppliers	The Cloud can integrate and analyze data faster, provides data to the local clients.	With the help of a shared Google calendar, and a VPN and SOA connection directly to the devices, the suppliers can immediately use the services, etc.	SOA increased the interoperability with third party companies and suppliers.

According to Table 2, the conclusion is that Division I. has faster data processing and reaction with the designed attributes. However, Division II offers easier integration of plant-floor devices and better scalability and modularity in lower levels. Therefore, Division II has bigger potential as a future modular, cooperative, agile, and heterogeneous plant architecture.

We defined our desired improvements in chapter 1.2. According to them, we created an open and an easily-integradable architecture. We chose the programmable router to satisfy any further requirements for the M2M communication. The better integrability of our infrastructure increased the SCADA performance. The common industry solution uses a local OPC or an aggregating point that resends data to the Cloud. This solution requires specialized implementation in various operating system too. In our architecture, the integration was improved because of our composite cloud services that uses atomic services from the field level. From another point of the view, SCADA and MES inherit beneficial features from the Cloud and SOA such as data availability, fault tolerance, disaster recovery and security.

3.1 Evaluation of Quality of Services

To evaluate our architecture, we defined the quality of services and their usability as the evaluation of the architecture in our experimental part. In our realized divisions, we measured the number of requests and their response time. We wanted to evaluate the quality and reusability of the services. Therefore, we designed an evaluation rule (1) which defines the quality of services. We used our own evaluation rule, which only dependents on the response time of the services, general errors and internal errors of the services.

$$\theta = \frac{\sum_{i=0}^{N} K_i}{(N*(t_T - t_0))} * \frac{n_r}{(n_r + n_e + n_0)} \tag{1}$$

We defined K as the load factor for atomic services. We identified it as the reciprocal value of the time between accepting the client's call and the service's response to it. N represents the number of called services that are executed in the sample interval set by the user. The $t_T - t_0$ represents the selected time interval, and n_r represents the number of the executed services that finished with an OK state, n_e is the count of requests that resulted in an error state, and n_0 represents the number of services which were not executed due to service errors.

We used the formula for measuring the quality of our implemented services in a simulation to empirically evaluate the solutions in Division I. and Division II. We were not able to simulate every situation in the laboratory, therefore we created a simulation process. This process consists of 8 requests that may receive three types of answers: 0 - Error with the information about the error, 1- OK, 2 - The

service did not answer within 1000 ms. The tests consisted of ten cases and each case consisted of eight calls.

The quality of the services is large in cases 3, 5 and 10 (Figure 11). The time of the response was low in these three cases and the states 0 (error) or 2 (the service did not answer within 1000 ms) did not occur. There was one state 0 and state 2 in case 9. Therefore, the quality value is the lowest.

The quality value of services in Division II. is improved when states 0 and 2 do not appear (case 5). However, if state 0 appears at least once in Division II, then the quality value of Division I is superior (case 6) because of its better error recovery. The after-error recovery will be addressed in further research.

This situation was only simulated in our laboratory implementation and may behave differently in real-world implementations.

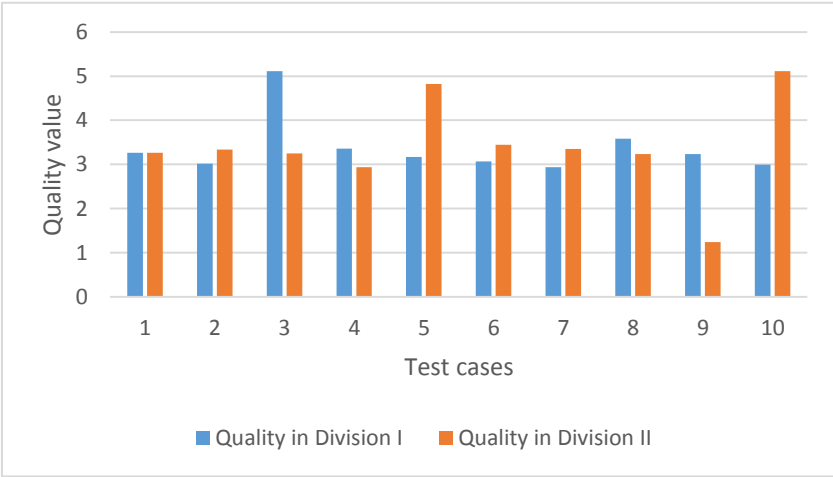

Figure 11

The test results of the quality of our services (Eq. (1))

A different behavior of the systems in the simulated environment is noticeable. However, we cannot yet strictly decide which division represents a better solution for real-world conditions. Both solutions are stable for industrial divisions and can improve the interoperability, data processing, HMI and control in the industry. However, there is still room for further research and safety tests should be done to verify our solution in real-world conditions.

Conclusions

We proposed an architecture that improves the data accessibility, integration and interoperability in the industry. One of our goals was to improve the SCADA and HMI interoperability. The architecture we designed and tested makes use of a private cloud and SOA. We implemented our own design of SOA on an eWON

industrial router that improves the interactivity with the integrated industrial devices, the clients and the Cloud. We also created atomic and component services to improve the SCADA and HMI interactivity. In the Cloud, we also implemented atomic services for MES clients working with data stored by another service in the cloud database. Thanks to the Windows Azure Pack, our architecture offers multi-tenancy for individual plant divisions. We tested two architectures and analyzed the results. The tests were performed on two plant divisions. According to the obtained results, we confirmed that using SOA for integration is more suitable than using a simple cloud solution without the service we designed and implemented on the eWON industrial router. The final architecture creates a universal access to the Cloud and benefits from an easy connection to the existing process level. The SOA gateway creates a consistent system by offering atomic services for our composite services in the Cloud modules.

Acknowledgement

This research was funded by the FEI Grants 2015 FEI-2015-10 project (70%) and KEGA - 001TUKE-4/2015 (30%). This project was carried out with the help of Jozef Sroka and Ladislav Pataki.

References

[1] J. Rhoton, *Cloud Computing Explained: Implementation Handbook for Enterprises*, London: Recursive Press, ISBN 0-9563556-0-9, 2010

[2] P. Mell, T. Grance, *The NIST Definition of Cloud Computing*, Gaithersburg: National Institute of Standards and Technology, 2011

[3] S. Karnouskos, A. W. Colombo, "Architecting the Next Generation of Service-based SCADA/DCS System of Systems", *IECON 2011 - 37th Annual Conference on IE EE Industrial Electronics Society*, Melbourne: IEEE, 2011, ISBN 978- 1 - 61284- 969 – 0, 2011, pp. 359-364

[4] A. W. Colombo, et al., "Industrial Cloud-based Cyber-Physical Systems", *The IMC-AESOP Approach*, 2014

[5] B. Dániel, P. Korondi, G. Sziebig, T. Thomessen, "Evaluation of Flexible Graphical User Interface for Intuitive Human Robot Interactions". *Acta Polytechnica Hungarica*, 11(1), 2014, pp. 135-151

[6] B. Lydon, "The 4th Industrial Revolution, Industry 4.0", *Unfolding at Hannover Messe 2014*, Automation.com, 2014

[7] W. Stolarz, M. Woda, "A Tenant-based Resource Allocation Model Application in a Public Cloud", *Acta Polytechnica Hungarica* 12.7 (2015)

[8] A. Soetedjo, et al. Web-SCADA for Monitoring and Controlling Hybrid Wind-PV Power System. TELKOMNIKA (Telecommunication Computing Electronics and Control), [S.l.], Vol. 12, No. 2, pp. 305-314, Jun. 2014, ISSN 2302-9293

[9] K. Breiner, D. Görlich, O. Maschino, G. Meixner, D. Zühlke, "Run-Time Adaptation of a Universal User Interface for Ambient Intelligent Production Environments", *Human-Computer Interaction. Interacting in Various Application Domains*, Springer Berlin Heidelberg, 2009, pp. 663-672

[10] A. Kovarova, M. Konopka, L. Sekerak, P. Navrat, "Visualising Software Developers' Activity Logs to Facilitate Explorative Analysis", *Acta Polytechnica Hungarica*, 13.2, 2016, pp. 159-178

[11] T. Lojka, M. Bundzel, I. Zolotová, "Industrial Gateway for Data Acquisition and Remote Control", *Acta Electrotechnica et Informatica*. Vol. 15/2 (2015), s. 43-48. - ISSN 1335-8243, 2015

[12] S. Weerawarana, et al., *Web Services Platform Architecture: SOAP, WSDL, WS-policy, WS-addressing, WS-BPEL, WS-reliable messaging and more*. Prentice Hall PTR, 2005

[13] D. K. Barry, D. Dick, *Web Services, Service - Oriented Architectures, and Cloud Computing*. Morgan Kaufmann, ISBN 978 - 0-12398 - 357 – 2, 2013, p. 248

[14] P. Spiess, et al., "SOA-based Integration of the Internet of Things in Enterprise Services", *Web Services*, 2009. ICWS 2009. IEEE International Conference, IEEE (2009, 2009), pp. 968-975

[15] D. Booth, et al., *Web Services Architecture*, W3C® (MIT, ERCIM, Keio) 2004

[16] I. Zolotová, M. Bundzel, T. Lojka, "Industry IoT Gateway for Cloud Connectivity", *Advances in Production Management Systems: Innovative Production Management Towards Sustainable Growth*, Springer International Publishing, 2015, pp. 59-66

[17] O. Bingol, et al. "Web-based Smart Home Automation", PLC-controlled Implementation. *Acta Polytechnica Hungarica* 11.3, 2014, pp. 51-63

[18] B. Kulvatunyou, H. Cho and Y. J. Son, "A Semantic Web Service Framework to Support Intelligent Distributed Manufacturing", *International Journal of Knowledge-based and Intelligent Engineering Systems 9.2 (2005)*, ISSN: 1327-2314, 2005, pp. 107-127

[19] T. Lojka, I. Zolotová, "Online Data Stream Mining in Distributed Sensor Network", *WSEAS Transactions on Circuits and Systems*. Vol. 13 (2014), ISSN 1109-2734, 2014, pp. 412-421

[20] J. Lee, B. Bagheri, H. A. Kao, "A Cyber-Physical Systems Architecture for Industry 4.0-based Manufacturing Systems", *Manuf Lett*, 2015, pp. 18-23

[21] L. Wang, X. Xu, "Advances and Challenges in Cloud Manufacturing", Journal *of Manufacturing Science and Engineering*, 137 (4), 2015

On Some Properties of Pseudo-Semiregular Graphs

Tamás Réti

Bánki Donát Faculty of Mechanical and Safety Engineering, Óbuda University
Népszínház u. 8, H-1081 Budapest, Hungary
reti.tamas@bgk.uni-obuda.hu

Imre Felde

John von Neumann Faculty of Informatics, Óbuda University
Bécsi út 96/b, H-1034 Budapest, Hungary
felde.imre@nik.uni-obuda.hu

Abstract: The application of the bipartite pseudo-semiregular graphs (BPS graphs) has recently had a growing importance in mathematical chemistry, mainly for QSAR (quantitative structure-activity relations) and QSPR (quantitative structure-property relations) studies. The aim of the research presented herein, is to give a systematic survey on the fundamental characteristics of BPS graphs and summarize some novel results concerning their structural-topological properties. We propose some practical methods for the construction of BPS graphs from various parent graphs. Moreover, a simple procedure is outlined by which a finite set of BPS graphs possessing the same spectral radius or the same second Zagreb index can be generated. Additionally, as a result of our investigations, it is verified that there is a strong correspondence between BPS graphs and balanced tree graphs of diameter 4.

Keywords: mathematical chemistry; strongly balanced tree graphs; Zagreb indices

1 Introduction

We consider only simple connected graphs. For a graph G with n vertices and m edges, V(G) and E(G) denote the set of vertices and edges, respectively. In this work our graph theoretical notation is standard and taken from [1].

An edge of G connecting vertices u and v is denoted by uv. The degree d(v) of a vertex v is the number of edges incident to v. The finite set of vertex degrees of a graph G is denoted by DS(G). As usual, the cyclomatic number of a connected

graph with n vertices and m edges is defined as Cy(G)= m – n +1. A connected graph G having Cy(G)=k ≥1 cycles is said to be a k-cyclic graph. As a particular case, if k=0, the corresponding acyclic graph is called a tree graph. A tree with n vertices has exactly n-1 edges.

We denote by $\Delta=\Delta(G)$ and $\delta=\delta(G)$ the maximum and the minimum degrees of vertices of G, and by $m_{r,s}$ the total number of edges in G with end-vertex degrees r and s, where we do not distinguish $m_{r,s}$ and $m_{s,r}$. For two different vertices u and w, the distance d(u,w) between u and w is the number of edges in a shortest path connecting them. The diameter of a connected graph G denoted by diam(G) is the maximum distance between any two vertices of G.

Using the standard terminology [1], the path, cycle and star with n vertices are denoted by P_n, C_n and $K_{1,n-1}$, respectively. Let A=A(G) be the adjacency matrix of G. The set of eigenvalues of A(G) is the spectrum of graph G, and the largest eigenvalue of A(G) denoted by ρ(G) is called the spectral radius of G.

An *integral graph* is a graph with integral eigenvalues. A graph is *R-regular* if all its vertices have the same degree R. A connected graph G is said to be *bidegreed* with degrees Δ and δ if at least one vertex of G has degree Δ and at least one vertex has degree δ, and if no vertex of G has a degree different from Δ or δ.

A connected bidegreed bipartite graph is called *semiregular* if each vertex in the same part of bipartition has the same degree. A connected graph G is said to be *harmonic* (pseudo-regular) [2, 3, 4] if there exists a positive constant p(G) such that each vertex u of G has the same average neighbor degree number [2, 3] identical with p(G). The spectral radius of a harmonic graph G is equal to p(G). It is obvious [2] that any connected R-regular graph G_R is a harmonic graph with $p(G_R)= \rho(G_R)=R$. A connected bipartite graph is called *pseudo-semiregular* [2, 5] if each vertex in the same part of bipartition has the same average degree. It is known among bipartite pseudo-semiregular graphs (BPS graphs) there exist connected graphs which are harmonic and pseudo-semiregular simultaneously.

By definition, a tree graph is called a *balanced tree*, if it has precisely one center vertex u for which $\Delta \geq d(u) \geq 2$ holds, and their vertices at the same distance j (at j^{th} level with j=1,2,.., k) from the center have the same degree [6]. The simplest types of balanced trees are the n-vertex stars $K_{1,n-1}$ having diameter 2.

Define the first and second Zagreb indices (M_1 and M_2) of a graph G as usual:

$$M_1 = M_1(G) = \sum_{u \in V} d^2(u) \qquad M_2 = M_2(G) = \sum_{uv \in E} d(u)d(v) \,.$$

The Zagreb indices belong to the family of global topological graph invariants which are widely used in the mathematical chemistry. For more detailed information on Zagreb indices, we refer the reader to surveys [7-16]. A connected

graph G for which identity $\rho(G) = \sqrt{M_2(G)/m}$ holds is called a Z_2 *graph*, because it is defined on the basis of the second Zagreb index [16].

The paper is organized as follows. In Section 2, the fundamental features of Z_2 graphs are reported. In Section 3, we summarize old and new results demonstrating some relevant properties of BPS graphs. Practical procedures for generating cyclic BPS graphs are presented in Section 4, where we also outline a method for the construction of an infinite set of BPS graphs with an identical spectral radius and/or a second Zagreb index. In Section 5, starting with the discussion of the spectral properties of tree graphs, we introduce the term of strongly balanced trees characterized by diameter 4, and we demonstrate that it is possible to construct infinitely many strongly balanced trees with integer spectral radii.

2 Some Properties of Z_2 Graphs

It is important to note that if G is an m-edge Z_2 graph then $\rho^2(G)=M_2(G)/m$ is a positive integer. The harmonic and bipartite pseudo-semiregular graphs form a subset of Z_2 graphs [17]. Until now, the types of Z_2 graphs have not exactly been identified and characterized. All regular graphs are Z_2 graphs.

Denote by **j** the n-component all-one vector. It is known that all semi-harmonic graphs for which $A^3\mathbf{j} = \rho^2 A\mathbf{j}$ holds, belong to the family of Z_2 graphs [16, 17, 18]. Consequently, the regular, semiregular, harmonic and bipartite pseudo-semiregular graphs are the subsets of semi-harmonic graphs [16, 18].

In Fig. 1 various types of Z_2 graphs with diameter 4 and integer spectral radius are depicted.

- Graph G_A is a pseudo-semiregular, non-harmonic graph with $\rho(G_A)=3$, $DS(G_A)= \{1,2,4,5\}$ and $Cy(G_A)=2$
- Graph G_B is a harmonic, non-pseudo-semiregular graph with $\rho(G_B)=4$, $DS(G_B) = \{1,4,7\}$, $Cy(G_B)=7$ [2]
- Graph G_C is a harmonic, pseudo-semiregular graph with $\rho(G_C)=3$, $DS(G_C) = \{1,2,3,6\}$, $Cy(G_C)=3$ [4]
- Graph G_D is a harmonic, bipartite pseudo-semiregular, and balanced tree graph with $\rho(G_D) =3$, $DS(G_D) = \{1, 3,7\}$ and $Cy(G_D)=0$ [19]

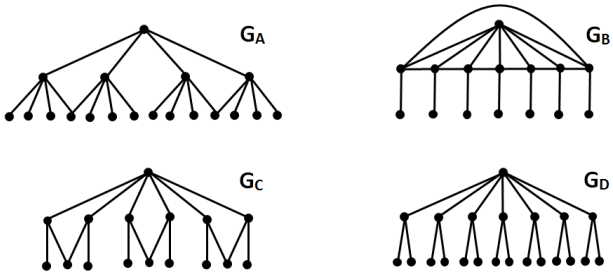

Figure 1
Four graphs with diameter 4 and integer spectral radius

However, there exist "sporadic" Z_2 graphs, not belonging to the graph families mentioned above. (They are neither harmonic nor bipartite pseudo-semiregular graphs.) The occurrence of such sporadic Z_2 graphs is a mysterious phenomenon.

As an example, a bipartite and a non-bipartite sporadic graph belonging to set Z_2 are depicted in Fig. 2. For these graphs the corresponding spectral radii are: $\rho(J_A)=\sqrt{5}$ and $\rho(J_B)=3$.

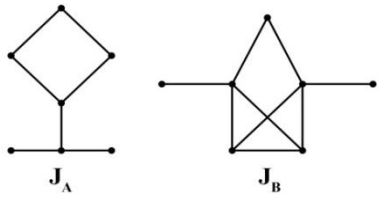

Figure 2
A bipartite graph (J_A) and a non-bipartite graph (J_B) belonging to set of Z_2 graphs

3 On the Characterization of BPS Graphs

The term of BPS graphs representing a subset of Z_2 graphs was introduced by Yu et al. in 2004 (see Ref. [2]). Until now, only some elementary properties of Z_2 graphs and BPS graphs have been established, and for their structural characterization, except in very few studies [2, 5, 16, 17], only limited attempts have been made.

As we have already mentioned, a pseudo-semiregular graph G is bipartite, consequently, the vertices of G can be partitioned as $V= V_1 \cup V_2$. Denoted by $p_1=p_1(V_1)$ and $p_2=p_2(V_2)$ as the corresponding average degrees of vertices in V_1 and V_2, respectively, the spectral radius of G can be calculated as $\rho(G)=\sqrt{p_1 p_2}$ [2]. Because for a semiregular graph the equality $p_1(V_1)=p_2(V_2)$ holds, this implies

that any semiregular graph is a bipartite pseudo-semiregular graph. It is conjectured that the maximal cardinality of the degree sets of BPS graphs is not larger than 4. (See graphs G_A and G_C in Fig. 1.)

It is easy to construct planar acyclic BPS graphs with diameter 4.

Proposition 1 For any $k \geq 2$ integer there exist k-cyclic BPS graphs with diameters not larger than 4. The maximum vertex degree Δ of these cyclic graphs can be arbitrary large. This implies that their corresponding spectral radii can be arbitrary large, as well.

Proof. In Figs. 3-5 it is demonstrated that for any $k \geq 2$ integer there exist k-cyclic pseudo-semiregular planar graphs composed only of quadrilaterals. ■

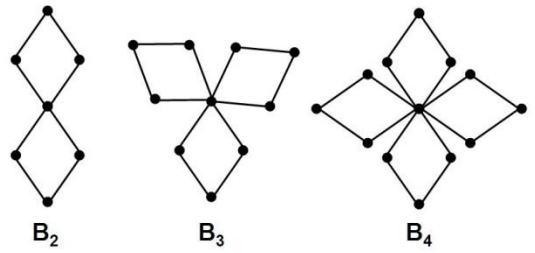

Figure 3
Bidegreed cyclic pseudo-semiregular graphs B_k including k=2, 3, 4 cycles

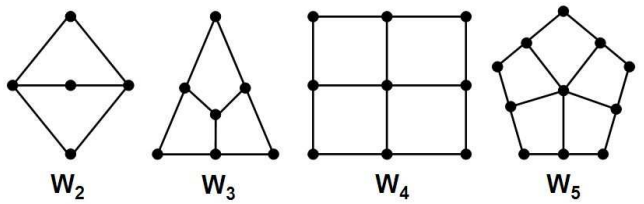

Figure 4
Cyclic pseudo-semiregular graphs W_k including k=2, 3, 4, 5 cycles

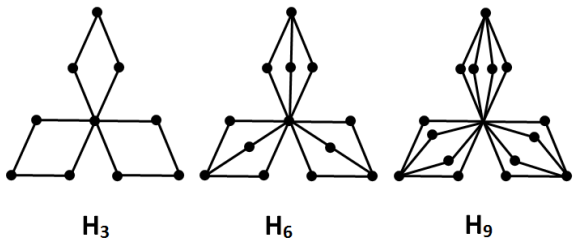

Figure 5
Cyclic pseudo-semiregular graphs H_k including k= 3, 6 and 9 cycles

A common property of planar BPS graphs B_k, W_k and H_k , depicted in Figs. 3-5, is that they include k quadrilaterals. Graphs W_2 and W_3 are characterized by diameter 2 and 3, respectively, while the others have diameter 4. Moreover, it is easy to show that depending on the appropriate choice of parameter k we can construct graphs BPS, with integer spectral radii, for example, $\rho(B_7)=4$, $\rho(W_5)=3$ and $\rho(H_9)=4$.

It is worth noting that there exist BPS graphs characterized by extremal relations between the spectral radius and graph diameter. It is easy to show that path P_5 is a BPS graph, and among all connected graphs with vertex number 5, the path P_5 has the minimal spectral radius. Moreover, it has been shown in [20] that among all connected graphs on 11 vertices and diameter 4, the bicyclic BPS graph denoted by $Q_{4,4,4}$ has the minimal spectral radius $\rho(Q_{4,4,4})=2.236068$. The bidegreed planar BPS graph $Q_{4,4,4}$ is depicted in Fig. 6.

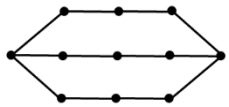

Figure 6
Extremal graph $Q_{4,4,4}$ with minimal spectral radius

4 Construction of BPS Graphs

A general method to construct BPS graphs is based on the use of edge-subdivision operations performed on connected graphs. By definition, an edge-subdivision of a graph G results from inserting a new vertex in every edge of G. For a connected graph G, the corresponding subdivision graph is denoted by S(G).

4.1 Construction of BPS Graphs from Semi-regular Graphs

Pseudo-semiregular graphs can be easily constructed from semiregular graphs by using a subdivision graph operation. Let $G(\Delta,\delta)$ be a semiregular graph. Performing a subdivision on $G(\Delta,\delta)$ we get a pseudo-semiregular graph $S(G(\Delta,\delta))$ with spectral radius $\rho(S(G(\Delta,\delta))) = \sqrt{\Delta+\delta}$.

Example 1: Using an edge-subdivision operation on the star $K_{1,n-1}$, one obtains the tridegreed pseudo-semiregular tree $S(K_{1,n-1})$ with diameter 4 and spectral radius $\rho(S(K_{1,n-1})) = \sqrt{\Delta+1} = \sqrt{n}$.

Example 2: Consider the semi-regular polyhedral graph J(4,3) with maximum degree 4 and minimum degree 3. The bidegreed graph J(4,3) with diameter 4 is the edge graph of the rhombic dodecahedron (See. Fig. 7). As a result of

subdivision, from J(4,3) we obtain a tridegreed pseudo-semiregular graph S(J(4,3)) with diameter 8. It is composed of octagons only and its spectral radius is $\rho(S(J(4,3))) = \sqrt{4+3} = \sqrt{7}$.

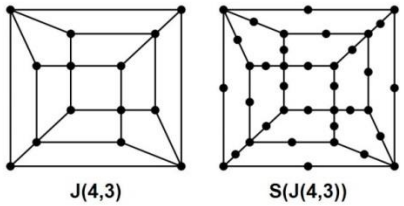

Figure 7
Construction of a tridegreed pseudo-semiregular graph using a single subdividing operation on the rhombic dodecahedron graph

4.2 Construction of BPS Graphs from Connected R≥3 Regular Graphs

Let G_R be an R≥3 regular connected graph. Performing on G a double edge-subdividing we get the bidegreed pseudo-semiregular graph $S(S(G_R))$. The spectral radius of resulting pseudo-semiregular graph will be $\rho(S(S(G_R)))=\sqrt{R+2}$. This implies that the spectral radius of graph $S(S(G_R))$ will be integer if (2+R) is a perfect square.

4.3 Construction of BPS Graphs with Identical Spectral Radii or Second Zagreb Indices

For unicyclic pseudo-semiregular graphs the following proposition can be verified:

Proposition 2 There exist unicyclic BPS graphs with arbitrary large spectral radii and arbitrary large diameters.

Proof. Consider the thorn-like graph $G_{t,q}$ depicted in Fig. 8. It is constructed from a cycle C_{2q} of length 2q by attaching t ≥1 terminal vertices (pendant edges) to every second vertices of the cycle.

The number of pendant vertices is $n_1 = tq$, the number of vertices with degree 2 is $n_2 = q$, and the number of vertices of maximal degree is $n_{t+2} = q$. This implies that the total number of vertices will be n=q(2+t). It is easy to see that for the edge parameters we have: $m_{1,t+2}=qt$, $m_{2,t+2}=2q$, consequently, $m(G_{t,q})=n(G_{t,q}) = q(2+t)$.

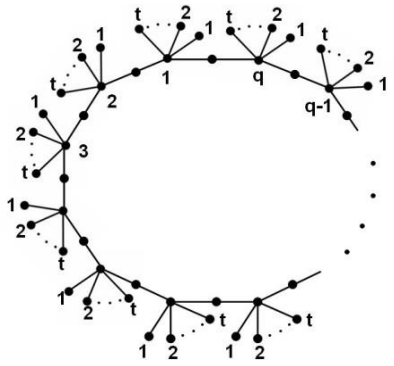

Figure 8
A tridegreed, unicyclic pseudo-semiregular graph, $G_{t,q}$

Because the graph $G_{t,q}$ is pseudo-semiregular, the corresponding first and the second Zagreb indices are: $M_1(G_{t,q}) = q\left(t^2 + 5t + 8\right)$ and $M_2(G_{t,q}) = q(t+2)(t+4)$, the maximum vertex degree $\Delta(G_{t,q}) = t+2$.

Moreover, $G_{t,q}$ is a Z_2 graph, this implies that its spectral radius is

$$\rho(G_{t,q}) = \sqrt{\frac{M_2(G_{t,q})}{m(G_{t,q})}} = \sqrt{t+4} = \sqrt{\Delta + 2}$$

■

From the above results the following conclusions can be drawn:

(i) For any fixed parameter $q \geq 2$, if t tends to infinity, then the maximum vertex degree $\Delta(G_{t,q}) = t+2$ and the spectral radius $\rho(G_{t,q})$ tend to infinity.

(ii) For a fixed parameter $t \geq 1$, if q tends to infinity, then the diameter $diam(G_{t,q})$ tends to infinity.

(iii) The spectral radius $\rho(G_{t,q})$ depends only on the parameter t. If the sum t+4 is a perfect square then the spectral radius will be a positive integer.

Based on the previous considerations, it is easy to construct non-isomorphic pseudo-semiregular graphs with identical spectral radius or second Zagreb index.

4.4 Construction of an Infinite Set of $G_{t,q}$ Graphs with an Identical Spectral Radius

A simple method which can be used for generating an infinite family of $G_{t,q}$ graphs with identical spectral radius is demonstrated in the following example: Let t=5. In this case, for any graph $G_{5,q}$ the spectral radius will be the same integer, $\rho(G_{5,q})=3$ for arbitrary $q \geq 2$. Then for given parameter pairs (t=5, $q \geq 2$) the corresponding edge numbers and second Zagreb indices of graphs $G_{5,q}$ can be simply determined. The computed results are given in Table 1.

Table 1
Computed topological parameters for graphs $G_{t,q}$ having an identical spectral radius

Graph	t	q	ρ	m=q(2+t)	$M_2=m\rho^2$	$M_1=q(t^2+5t+8)$	$Z=M_2/m-M_1/n=t/(2+t)$
$G_{5,2}$	5	2	3	14	126	116	5/7
$G_{5,3}$	5	3	3	21	189	174	5/7
$G_{5,4}$	5	4	3	28	252	232	5/7
$G_{5,5}$	5	5	3	35	315	290	5/7
$G_{5,6}$	5	6	3	42	378	348	5/7
$G_{5,7}$	5	7	3	49	441	406	5/7
$G_{5,8}$	5	8	3	56	504	464	5/7
$G_{5,9}$	5	9	3	63	567	522	5/7
$G_{5,10}$	5	10	3	70	630	580	5/7

Because graphs $G_{t,q}$ are Z_2 graphs, their spectral radius is equal to $\rho(G_{5,q})=\sqrt{M_2(G_{5,q})/m(G_{5,q})}=3$ for any $q \geq 2$. Additionally, in the last column of Table 1, the quantity denoted by Z is given. Topological parameter Z=Z(G) characterizes the structure of a graph G [17]. It is interesting to note that for all graphs included in Table 1 the values of Z are identical.

4.5 Construction of $G_{t,q}$ Graphs with an Identical Second Zagreb Index

The concept outlined previously, is applicable for generating $G_{t,q}$ graphs with an identical second Zagreb index. Let $t=q \geq 2$ be an arbitrary positive integer. As a first step, for graph $G_{t,t}$, we calculate its second Zagreb index given as $M_2(G_{t,t})=t(t+2)(t+4)$. As a second step, by using a computer search, we identify all graphs $G_{t,q}$ which satisfy the equality represented by $m=M_2(G_{t,t})/\rho^2(G_{t,q})=q(t+2)$, where t and q are positive integers. It can be expected that there exists a finite set of graphs $G_{t,q}$ with different (t,q) parameters for which the above equality holds. The method based on a simple computer search is demonstrated in the following example. Let t=q=10. In this case, $M_2(G_{10,10})=1680$ and there are exactly 8 non-isomorphic $G_{t,q}$ graphs satisfying the requirements of computer search. All of them have the same second Zagreb index 1680. The computed results are summarized in Table 2.

As can be seen, among $G_{t,q}$ graphs there exist graph pairs having equal first and second Zagreb indices as well. Namely, for such graphs the equalities $M_1(G_{1,112}) = M_1(G_{8,14}) = 1568$ and $M_1(G_{2,70}) = M_1(G_{4,35}) = 1540$ are fulfilled.

Table 2
Computed topological parameters for graphs $G_{t,q}$ having identical second Zagreb index

Graph	**t**	**q**	**m=q(2+t)**	**ρ^2=4+t**	**M_2=mρ^2**	**M_1=q(t^2 + 5t +8)**	**Z=M_2/m – M_1/n**
$G_{1,112}$	1	112	336	5	1680	1568	1/3
$G_{2,70}$	2	70	280	6	1680	1540	1/2
$G_{3,48}$	3	48	240	7	1680	1536	3/5
$G_{4,35}$	4	35	210	8	1680	1540	2/3
$G_{6,21}$	6	21	168	10	1680	1554	3/4
$G_{8,14}$	8	14	140	12	1680	1568	4/5
$G_{10,10}$	10	10	120	14	1680	1580	5/6
$G_{26,2}$	26	2	56	30	1680	1628	13/14

5 On the Spectral Properties of Tree Graphs

In 1974, Harary and Schwenk initiated the problem of finding connected graphs having integral spectrum [21]. During the past few decades, for certain families of integral graphs, many novel results have been obtained [4, 6, 21-29]. For the construction of integral trees, some efficient methods have been developed [6, 22, 25-29]. Among others, it was proved [6] that integral balanced trees with diameter 5, 7 and 9 do not exist, just like integral balanced trees with diameter 4k+1 (k is an arbitrary integer). Recently, it has been verified that there exist integral trees of arbitrary large diameters. Csikvári has constructed integral trees with arbitrary large even diameters [28], and Ghorbani et al. have settled the odd-diameter case [29]. It is worth noting that there exist integral trees with diameter 5 which belong to the family of Z_2 graphs. The 25-vertex graph T_{25} depicted in Fig.9 is the smallest integral tree of diameter 5 with the spectrum $\{3, 2^3, 1^3, 0^{11}, -1^3, -2^3, -3\}$ [26]. Tree T_{25} is a sporadic Z_2 graph because it does not belong to the sets of either harmonic or pseudo-semiregular graphs.

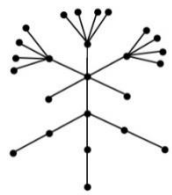

Figure 9
A “sporadic” integral tree belonging to the family of Z_2 graphs [26]

Currently, the search for non-integral tree graphs characterized by integer spectral radius has gained raising interest [30, 31]. Patuzzi et al. [31] investigated non-integral trees, namely star-like trees and double brooms. For each class, they determined conditions for the spectral radius to be integer. Moreover, it was concluded that among trees of diameter 4, there are infinitely many non-integral trees with integer spectral radius [30].

In the last decade, several authors have studied the spectral radius of connected graphs as a function of given graph invariants (fixed diameter diam(G) and largest vertex degree Δ).

Van Dam [32] determined the graphs with maximal spectral radius among all graphs on n vertices with diam(G) $\geq$ 2. It is important to note that Hansen and Stevanović obtained the same result using a completely different approach [33]. This complements the results published in [20] on connected graphs with minimal spectral radius for a given number of vertices and diameter. Yuan et al. [34] determined the graphs having the minimal spectral radius among all the graphs on n vertices with diam(G) = n – 4. The relevant results in this topic are summarized in [18]. Some of them will be used in our subsequent investigations.

Lovász and Pelikán [35] verified that among n-vertex trees the path P_n has the minimal spectral radius and the star $K_{1,n-1}$ has the maximal spectral radius. In [36] Simić and Tošić identified the n-vertex trees $T_{n,\Delta,}$ whose spectral radius has the maximal value among all trees with a fixed maximal degree Δ. As an example, in Fig. 10 four trees are depicted. These 7-vertex trees are extremal graphs in a certain sense.

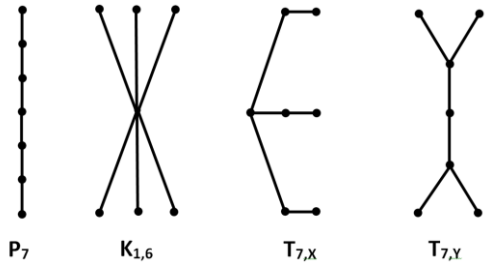

Figure 10
Extremal 7-vertex trees having maximal or minimal spectral radius

Except path P_7, all of them are BPS graphs. Path P_7 is has the minimal spectral radius, and star $K_{1,6}$ has the maximal spectral radius. Later on, it will be shown that $T_{7,X}$ and $T_{7,Y}$ represent the extremal trees which have identical minimal spectral radius among 7-vertex trees of diameter 4 ($\rho(T_{7,X})=\rho(T_{7,Y})=2$). Moreover, their second Zagreb indices are also equal: $M_2(T_{7,X})= M_2(T_{7,Y})=24$.

Stevanović proved [37] that for the spectral radius of a tree T the general inequality $\rho(T) \leq 2\sqrt{\Delta - 1}$ holds where Δ is the maximal degree of T. In the most

recent years the upper bound represented by the this inequality has been extensively studied and improved for some particular cases [18, 30, 38-42].

Chang and Huang [39] elaborated new ordering systems for n-vertex trees according to their spectral radius and diameter, and identified the tree types with maximal spectral radius. In [38] and [40] sharp upper bounds are given for the spectral radius of trees with diameter not larger than 4.

Rojo and Robinho [41] studied the spectrum of Bethe trees. By definition, a *Bethe tree* denoted by $B_{\Delta,k}$ is a rooted tree of k levels in which the root vertex has a degree equal to Δ - 1, the vertices in level j ($2 \le j \le k-1$) have degree equal to Δ and the vertices in level k have degrees equal to 1. They derived an explicit formula by which the nonzero eigenvalues of Bethe trees can be calculated [41]. The spectral radius $\rho(B_{\Delta,k})$ of a Bethe tree of k levels is

$$\rho(B_{\Delta,k}) = 2\sqrt{\Delta - 1}\cos\left(\frac{\pi}{k+1}\right)$$

By introducing the term of the completely full-degree tree, Song et al. [38] obtained a new upper bound on the spectral radius of trees which are neither a path nor a star. By definition, an n-vertex balanced tree $T_{\Delta,k}$ with maximum degree Δ is called a *completely full-degree tree* if the degrees of all the vertices of $T_{\Delta,k}$ are equal to Δ, except the vertices in the last level k, where each degree is equal to 1. They verified [38] that if T is a n-vertex tree with maximum degree Δ, for which $2\Delta < n \le \Delta^2 + 1$ is fulfilled, then $\rho(T) \le \sqrt{2\Delta - 1}$ with equality if and only if T is a completely full-degree tree of diameter 4. As an example, a Bethe tree and a completely full-degree tree are shown in Fig. 11.

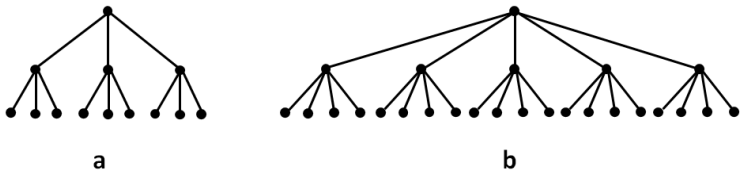

Figure 11
Bethe tree $B_{4,3}$ (a) and the completely full-degree tree $T_{5,3}$ with diameter four (b)

5.1 On the Construction of Balanced Tree Graphs

It is known that the diameter of a balanced tree having only one central vertex is even. Consequently, there are no balanced trees of diameter 3. The smallest balanced trees are the star $K_{1,2}$ with diameter 2, and the path P_5 with diameter 4. Both of them are BPS graphs.

Consider the Smith graphs G(n) with n≥7 vertices [43]. (See Fig. 12.) A fundamental property of trees G(n) is that they have an identical integer spectral radius equal to 2. If n≥8, the corresponding Smith graphs G(n) represent an infinite class of sporadic Z_2 trees with arbitrary large diameter. If n≥7 is an odd integer, then graphs G(n) are balanced trees. Moreover, it is easy to see that if n=7, then tree G(7) is a balanced BPS graph which is isomorphic to tree $T_{7,Y}$ depicted in Fig. 10.

Figure 12
Smith graphs G(n) with n≥7 vertices [43]

Using a subdivision operation on G(n) graphs we can generate novel balanced trees. If n≥7, then the corresponding subdivision graph S(G(n)) will be a balanced tree. The subdivision transformation can be repeated several times. Consequently, performing the subdivision transformation on S(G(n)), we obtain the balanced tree S(S(G(n))). From this observation the following general conclusion can be drawn: The subdivision graph $S(T_b)$ of a balanced tree T_b is a balanced tree.

The general topological structure of trees with diameter 4 is demonstrated in Fig. 13. As can be seen, their possible structure is determined by a large set of parameters denoted by (b, r, a_1, a_2,…,a_r).

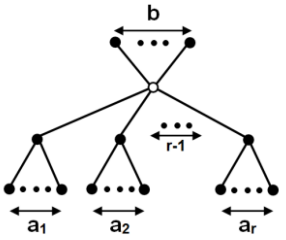

Figure 13
Tree T(b, r, a_1, a_2,…,a_r) of diameter 4 [30]

There are some interesting types of n-vertex trees which form particular subsets of balanced trees with diameter 4. Such graphs are the Bethe trees $B_{\Delta,3}$ and completely full-degree trees $T_{\Delta,3}$. Patuzzi et al. [30] have proven that for the spectral radius of the tree T(b, r, a_1, a_2,…,a_r) with diameter 4, the following sharp upper bound can be formulated:

$$\rho(T(b,r,a_1,a_2,...,a_r) \le \sqrt{2\Delta - 1}$$

In the above formula equality holds if and only if b=0, a_i=a for $1 \leq i \leq r$ and Δ=a+1=r.

It is easy to show that there is a strong correspondence between bipartite pseudo-semiregular graphs and balanced tree graphs. In what follows we restrict our attention primarily to the relations between the BPS graphs and balanced tree graphs having diameter four.

5.2 A New Class of Balanced BPS Trees with Diameter 4

We define a particular class Ω_4 of balanced trees with diameter 4 as follows: Let $d_A \geq 2$ and $d_B \geq 2$ be positive integers. By definition, a balanced tree $T(d_A,d_B)$ of 3 levels belongs to graph family Ω_4 if the centrum vertex has degree d_A, the vertices at distance 1 from the centrum have degree d_B, and all vertices at distance 2 have degree 1. From the definition it follows that parameter pairs (d_A,d_B) determine unambiguously the adjacency matrix of tree $T(d_A,d_B)$. It is easy to see that the edge number of $T(d_A,d_B)$ is equal to $m=m(T(d_A,d_B))=d_Ad_B$. For simplicity, graphs $T(d_A,d_B)$ included in Ω_4 are called *strongly balanced trees*.

Example 3 In a particular case, if $d_A=d_B=2$ holds, then the corresponding strongly balanced tree T(2,2) with m=4 edges is isomorphic to the 5-vertex path P_5 of diameter 4.

Lemma 1 [15]: The strongly balanced tree $T(d_A,d_B)$ is a BPS graph.

Proof. The vertex set of the bipartite tree $T(d_A,d_B)$ can be partitioned as $V=V_1 \cup V_2$ where $p_1=p_1(V_1)$ and $p_2=p_2(V_2)$ are the corresponding average degrees of vertices in V_1 and V_2, respectively. It is easy to see that $p_1=d_B$ and $p_2=(d_A+d_B - 1)/d_B$. This implies that $T(d_A,d_B)$ is a bipartite pseudo-regular graph. Consequently, its corresponding spectral radius is $\rho(T(d_A,d_B)) = \sqrt{p_1p_2} = \sqrt{d_A + d_B - 1}$. Because $T(d_A,d_B)$ is a Z_2 graph, one obtains that

$$\rho(T(d_A,d_B)) = \sqrt{M_2(T(d_A,d_B))/m(T(d_A,d_B))}$$

Proposition 3 Let $d_A \geq 2$ and $d_B \geq 2$ be positive integers for which $d_A \neq d_B$ holds. Then there exist exactly two non-isomorphic balanced BPS trees $T(d_A,d_B)$ and $T(d_B,d_A)$, for which the following relations are fulfilled:

i. $m(T(d_A,d_B))= m(T(d_B,d_A))=d_Ad_B$

ii. $M_2(T(d_A,d_B))= M_2(T(d_B,d_A))= d_Ad_B(d_A + d_B -1)$

iii. $\rho(T(d_A,d_B))= \rho(T(d_B,d_A)) = \sqrt{d_A + d_B - 1}$.

Proof. Identity (i) is trivial. Considering the validity of Eq.(ii), it should be taken into consideration that $m_{1,d_B} = d_A(d_B - 1)$ and $m_{d_A,d_B} = d_A$. This implies that

$$M_2(T(d_A,d_B)) = d_A(d_B - 1)d_B + d_Bd_A^2 = m(d_A + d_B - 1) = M_2(T(d_B,d_A))$$

and $\sqrt{\frac{M_2(T(d_A,d_B))}{m}} = \sqrt{\frac{M_2(T(d_B,d_A))}{m}} = \sqrt{\frac{m(d_A+d_B-1)}{m}} = \sqrt{d_A+d_B-1}$

Because tree $T(d_A,d_B)$ is a BPS graph, the validity of Eq.(iii) follows directly from the Lemma 1. ■

If $d_A \neq d_B$ holds then the corresponding pair of strongly balanced trees $T(d_A,d_B)$ and $T(d_B,d_A)$ are called *strongly balanced twin-like trees*.

Remark 1 It can be easily shown that the first Zagreb index of strongly balanced trees can be computed by the following formula:

$$M_1(T(d_A,d_B)) = d_A^2 + d_A d_B^2 + d_A(d_B-1) = d_A(d_A-1) + m(d_B+1)$$

Remark 2 The existence of an m-edge strongly balanced tree depends on the value of m. For example, there is no 7-edge tree belonging to the family of strongly balanced trees.

Proposition 4 Let m be a positive integer. A strongly balanced tree T with $m(T) \geq 4$ edge number exists if m is not a prime number.

Proof. i) Let $m \geq 4$ be an even integer. Then there exist non-isomorphic strongly balanced trees T(2, m/2) and/or T(m/2,2) with an identical spectral radius and a second Zagreb index. ii) Let $m \geq 9$ be an odd integer which is not a prime number. In this case there exists at least one odd divisor q of m. Consequently, T(q, m/q) will be a strongly balanced tree. ■

Corollary 1 Let $m \geq 6$ be an even integer. Then there exist at least two non-isomorphic strongly balanced m-edge trees $T(d_A,d_B)$ and $T(d_B,d_A)$ having an equal spectral radius and a second Zagreb index.

Example 4 The smallest strongly balanced tree graph pair of such type are the 7-vertex T(3,2) and T(2,3) trees. It is important to note that 7-vertex graphs $T_{7,X}$ and $T_{7,Y}$ depicted in Fig. 10 are isomorphic to trees T(3,2) and T(2,3) with $\rho(T(3,2)) = \rho(T(2,3)) = 2$.

The spectra of these strongly balanced trees are: Spec(T(3,2)) = {2, 1, 1, 0, -1, -1-2} and Spec(T(2,3)) = {2, 1.4142, 0, 0, 0, -1.4142, -2}. As can be observed, T(3,2) is a harmonic integral graph, but tree T(2,3) is a non-integral graph.

It is easy to construct a finite set of strongly balanced tree graphs having the same spectral radius. The method used for constructing such trees is demonstrated in the following example.

Example 5 Let $d_A+d_B=50$. It is easy to see that the strongly balanced trees denoted by T(2,48), T(3,47),...,T(25,25),…,T(47,3) and T(48,2) have the same integer spectral radius $\rho = \sqrt{50-1} = 7$. As an example, trees T(10,40) and T(40,10) are depicted in Fig. 14.

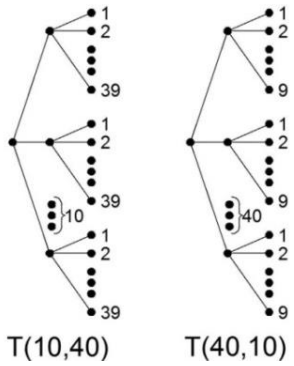

Figure 14
Twin-like trees TS(10,40) and TS(40,10) with 400 edges

Some computed results concerning Example 5 are summarized in Table 3.

Table 3
Computed topological parameters for strongly balanced trees

Graph	d_A	d_B	ρ	$m=d_Ad_B$	$M_2=m\rho^2$	$M_1=d_A(d_A-1)+m(d_B+1)$	$Z=M_2/m-M_1/n$
T(2,48)	2	48	7	96	4704	4706	0.4845
T(3,47)	3	47	7	141	6909	6774	1.2958
T(10,40)	10	40	7	400	19600	16490	7.8778
T(20,30)	20	30	7	600	29400	18980	18.3607
T(24,26)	24	26	7	624	30576	17400	21.1600
T(25,25)	25	25	7	625	30625	16850	22.0831
T(26,24)	26	24	7	624	30576	16250	23.0000
T(30,20)	30	20	7	600	29400	13470	26.5874
T(40,10)	40	10	7	400	19600	5960	34.1372
T(47,3)	47	3	7	141	6909	2726	29.8028
T(48,2)	48	2	7	96	4704	2544	22.7732

Based on the considerations outlined previously the following conclusions can be drawn:

i. The Bethe trees of 3 levels denoted by $B_{\Delta,3}$ and the completely full-degree trees of 3 levels denoted by $T_{\Delta,3}$ are strongly balanced trees.

ii. Let $C \geq 4$ be a positive integer. For strongly balanced trees T(2, C-2) the following equality holds: $M_2(T(2, C-2)) - M_1(T(2, C-2)) = - 2$.

iii. Let $C_1 \geq 4$ be an even positive integer. Among the strongly balanced trees the second Zagreb index has a maximum value if $d_A=d_B=C_1/2$ holds. This maximum value belongs to the strongly balanced tree $T(C_1/2, C_1/2)$.

iv. Let $C_2 \geq 5$ be an odd positive integer. Among the strongly balanced trees, there exist two non-isomorphic trees having an identical maximum second Zagreb index. These trees are: $T((C_2-1)/2, (C_2+1)/2))$ and $T((C_2+1)/2, (C_2-1)/2))$.

v. If $d_A+d_B - 1$ is a perfect square, then for trees $T(d_A,d_B))$ and $T(d_B,d_A))$ the corresponding spectral radius $\rho(T(d_A,d_B))=\rho(T(d_B,d_A))$ will be a positive integer.

Example 6 If $d_A=d_B =5$, then $d_A+d_B -1=9$ is a perfect square, consequently, the strongly balanced tree T(5,5) has an integer spectral radius $\rho(T(5,5)) = \sqrt{5+5-1)} = 3$. The completely full-degree tree $T_{5,3}$ depicted in Fig.11. is isomorphic to the strongly balanced tree T(5,5) which is an integral graph [22] with the spectrum $Spec(T(5,5))= \{3, 2^4, 0^{16}, -2^4, -3\}$. It is worth noting that among strongly balanced trees there are several integral graphs. For example, the smallest one is the 7-vertex tree $T_{7,X}=T(3,2)$ shown in Fig. 10.

Proposition 5 There exist infinitely many strongly balanced trees which are extremal graphs having a minimal spectral radius.

Proof. Belardo et al. [40, 18] considered the family of n-vertex trees with diameter 4. Among these trees, they identified those trees whose spectral radius is minimal. It has been proved [40] that for any $n \geq 5$, the minimum spectral radius among trees T(n,4) is attained only in two cases a) by a single tree $MT_{n,4}^{j}$ if $n \neq j^2+j+1$, and b) by tree pairs $MT_{n,4}^{j}$ and $MT_{n,4}^{j+1}$ if $n = j^2+j+1$ for arbitrary $j\geq 2$ integer.

It is easy to see that for even $m = n-1= j^2+ j$ $(j = 2, 3, 4,..)$ the corresponding extremal m-edge trees $MT_{n,4}^{j}$ and $MT_{n,4}^{j+1}$ are strongly balanced tree graphs having an identical spectral radius. For extremal tree pairs $MT_{n,4}^{j}$ and $MT_{n,4}^{j+1}$ the possible vertex numbers are n= 7, 13, 21, 31,… This implies that among 7-vertex trees of diameter 4 the strongly balanced trees $T_{7,X}=T(3,2)$ and $T_{7,Y}=T(2,3)$ depicted in Fig. 10 are extremal trees with identical minimal spectral radius $\rho(T_{7,X}) = \rho(T_{7,Y}) = \sqrt{3+2-1)} = 2$.■

Proposition 6 There exist infinitely many strongly balanced trees E(p) which are harmonic and pseudo-semiregular simultaneously and they have integer spectral radii.

Proof. Starting with the concept outlined in [19], consider the infinite sequence of balanced tree graphs $E(p)=T(d_A(p),d_B(p))$ constructed as follows: If $p\geq 2$, then trees E(p) can be obtained from $d_A(p)=p^2 – p +1$ disjoint stars $K_{1,p-1}$ by adding a vertex adjacent to the central vertex of each stars. It follows that the degree of central vertex is $d_A(p)=p^2 – p +1$ and $d_B(p)=p$. Moreover, the corresponding edge number is $m(E(p))=(p^2 – p +1)p$.

Trees E(p) are harmonic, pseudo-semiregular and strongly balanced simultaneously, their spectral radii is

$$\rho(E(p)) = \sqrt{d_A(p) + d_B(p) - 1} = \sqrt{p^2} = p$$

If p=2, tree E(2) is isomorphic to the 7-vertex graph $T_{7,X}$ depicted in Fig. 10. If p=3, as a particular case, tree E(3) is isomorphic to the 22-vertex tree graph G_D shown in Fig. 1. ■

Proposition 7 There exist infinitely many strongly balanced trees F(p) which are non-harmonic, pseudo-semiregular graphs having integer spectral radii.

Proof. The construction of balanced trees F(p) is based on the same concept presented previously in Proposition 6. Consider now the infinite sequence of strongly balanced trees defined as $F(p)=T(d_B(p),d_A(p))$. Because E(p) and F(p) are strongly balanced twin-like trees, this implies that they have similar properties: their spectral radii $\rho(E(p))=\rho(F(p))=p$ are positive integers. The only significant difference between them is that trees F(p) are not harmonic. If p=2, tree F(2) is isomorphic to the 7-vertex graph $T_{7,Y}$ depicted in Fig. 10. ■

It is an interesting observation that there exists a broad class of connected graphs with maximum degree $\Delta=\Delta(G)$ for which the equality $\rho(G) = \sqrt{\Delta + p}$ holds where p is a non-negative integer. These graphs can be classified into 3 disjoint subsets by considering the following relationships: $p < \Delta$, $p = \Delta$ and $p > \Delta$.

For parameter p a simple upper bound can be obtained. Because for the spectral radius of a graph G the inequality $\rho^2(G) \le \Delta^2$ holds, this implies that $\Delta+p = \rho^2(G) \le \Delta^2$ is fulfilled if $p \le \Delta(\Delta-1)$. The above inequality is sharp. Equality holds if G_R is an R-regular graph. Because $\rho(G_R)=R=\Delta$, it follows that $\rho(G_R) = \sqrt{\Delta + p}$ is fulfilled if p=R(R-1).

It is easy to check that equality $\rho(G) = \sqrt{\Delta + p}$ holds for any Z_2 graph, because $p=M_2/m - \Delta$ is a non-negative integer [16]. For example, equality with p=0 is valid for all n-vertex stars $K_{1,n-1}$.

Proposition 8 Let $p \ge 1$ be an arbitrary positive integer. Then for any parameter p there exists a strongly balanced tree K(p) for which $\rho(K(p)) = \sqrt{\Delta + p}$ is fulfilled.

Proof. The construction of such trees is based on the following considerations. Starting with graphs E(p), define the trees K(p) as follows: K(p)=E(p+1) for any positive integer p. Since E(p) is harmonic and strongly balanced, one obtains on the one hand

$$\rho(K(p)) = \rho(E(p+1)) = \sqrt{d_A(p+1) + d_B(p+1) - 1} =$$
$$\sqrt{((p+1)^2 - (p+1) + 1) + (p+1) - 1} = \sqrt{(p+1)^2} = p+1$$

On the other hand, because $\Delta(K(p))=\Delta(E(p+1))=d_A(p+1)=(p+1)^2 - (p+1) +1$ holds, we get

$$\sqrt{\Delta(K(p))+p}=\sqrt{\Delta(E(p+1))+p}=\sqrt{((p+1)^2-(p+1)+1)+p}=p+1. \blacksquare$$

Acknowledgement

We acknowledge the financial support of this work by the Mexican-Hungarian S&T bilateral project TÉT MX -1-2013-0001 and "Cooperative research on control of heat treatment stress and distortion for high value added machinery products" (2014DFG72020) projects.

References

[1] N. Biggs, *Algebraic Graph Theory,* Cambridge Univ. Press, Cambridge, 1974

[2] A. Yu, M. Lu, F. Tian, On the Spectral Radius of Graphs, Lin. Algebra Appl. 387 (2004) 41-49

[3] B. Borovićanin, S. Grünewald, I. Gutman, M. Petrović, Harmonic Graphs with a Small Number of Cycles, Discrete Math. 265 (2003) 31-44

[4] M. Petrović, B. Borovićanin, Z. Radosavljević, The Integral 3-Harmonic Graphs, Lin. Algebra Appl. 416 (2006) 298-312

[5] Y. Hou, Z. Teng, C. Woo, On the Spectral Radius, k-degree and the Upper Bound of Energy in a Graphs, MATCH Commun. Math. Comput. Chem. 57 (2007) 341-350

[6] P. Hik, R. Nadela, Balanced Integral Trees, Math. Slovaca 48 (1998) 429-445

[7] S. Nikolić, G. Kovačević, A. Miličević, N. Trinajstić, The Zagreb Indices 30 Years After, Croat. Chem. Acta, 76 (2003) 113-124

[8] I. Gutman, K. Ch. Das, The First Zagreb Index 30 Years after, MATCH Commun. Math. Comput. Chem. 50 (2004) 83-92

[9] B. Furtula, I. Gutman, S. Ediz, On difference of Zagreb indices, Discr. Appl. Math. 178 (2014) 83-88

[10] B. Zhou, Zagreb indices, MATCH Commun. Math. Comput. Chem. 52 (2004) 113-118

[11] D. Vukičević, I. Gutman, B. Furtula, V. Andova, D. Dimitrov, Some observations on comparing Zagreb indices, MATCH Commun. Math. Comput. Chem. 66 (2011) 627-645

[12] I. Gutman, Degree-based Topological Indices, Croat. Chem. Acta 86 (2013) 351-361

[13] B. Liu, Z. You, A Survey on Comparing Zagreb Indices, MATCH Commun. Math. Comput. Chem. 65 (2011) 581-593

[14] H. Abdo, D. Dimitrov, I. Gutman, On the Zagreb Indices Equality, Discr. Appl. Math. 160 (2012) 1-8

[15] A. Ilić, D. Stevanović, On Comparing Zagreb Indices, MATCH Commun. Math. Comput. Chem. 62 (2009) 681-687

[16] H. Abdo, D. Dimitrov, T. Reti, D. Stevanović, Estimation of the Spectral Radius of a Graph by the Second Zagreb Index, MATCH Commun. Math. Comput. Chem. 72 (2014) 741-751

[17] C. Elphick, T. Réti, On the Relations between the Zagreb Indices, Clique Numbers and Walks in Graphs, MATCH Commun. Math. Comput. Chem. 74 (2015) 19-34

[18] D. Stevanović, Spectral Radius of Graphs, Academic Press, Amsterdam, 2015

[19] P. Rowlinson, The Main Eigenvalues of a Graph: A Survey, Applicable Analysis and Discrete Mathematics, 1 (2007) 445-471

[20] E. R. van Dam, R. E. Krooij, The Minimal Spectral Radius of Graphs with a Given Diameter, Lin. Algebra Appl. 423 (2007) 408-419

[21] F. Harary, A.J. Schwenk, Which Graphs have Integral Spectra? In: R. Bari, F. Harary (Eds.), Graph and Combinatorics. Lecture Notes in Mathematics, 406, pp. 45-51. Springer, Berlin (1974)

[22] M. Watanabe, A.J. Schwenk, Integral Starlike Trees, J. Austral. Math. Soc. (Series A) 28 (1979) 120-128

[23] K. Balińska, D. Cvetković, Z. Radosavljević, S. Simić, D. Stevanović, A Survey on Integral Graphs, Univ. Beograd. Publ. Elektrotehn. Fak. Ser. Mat. 13 (2002) 42-65

[24] Z. Tang, Y. Hou, Integral Graphs with Index 3 and Exactly Two Main Eigenvalues, Lin. Algebra Appl. 433 (2010) 984-993

[25] Ligong Wang, Integral Trees and Integral Graphs, Ph.D. Thesis, University of Twente, 2005

[26] A. E. Brouwer, W. H. Haemers, The Integral Trees with Spectral Radius 3, Lin. Algebra Appl. 429 (2008) 2710-2718

[27] P. Hik, M. Pokorny, There are Integral Tees of Diameter 7, Univ. Beograd. Publ. Elektrotehn. Fak. Ser. Mat. 18 (2006) 59-63

[28] P. Csikvári, Integral Trees of Arbitrary Large Diameters, J. Algebr. Combin. 32 (2010) 371-377

[29] E. Ghorbani, A. Mohammadian, B.Tayfeh-Rezaie, Integral Trees of Odd Diameters, J. Graph Theory, 70 (2011) 332-338

[30] L. Patuzzi, M. A. A. de Freitas, R.R. Del Vecchio, Integer Index in Trees of Diameter 4, Filomat, 28:2 (2014) 241-248

[31] L. Patuzzi, M. A. A. de Freitas, R.R. Del Vecchio, Indices for Special Classes of Trees, Lin. Algebra Appl. 442 (2014) 106-114

[32] E. R. van Dam, Graphs with given Diameter Maximizing the Spectral Radius, Lin. Algebra Appl. 426 (2007) 454-457

[33] P. Hansen, D. Stevanović, On Bags and Bugs, Discrete Appl. Math. 156 (2008) 986-997

[34] X. Y. Yuan, J. Y. Shao, Y. Liu, The Minimal Spectral Radius of Graphs of Order n with Diameter n – 4, Lin. Algebra Appl. 428 (2008) 2840-2851

[35] L. Lovász, J. Pelikán, On the Eigenvalues of Trees, Periodica, Math. Hung. 3 (1973) 175-182

[36] S. Simić, D. V. Tošić, The Index of Trees with Specified Maximum Degree, MATCH Commun. Math. Comput. Chem. 54 (2005) 351-362

[37] D. Stevanović, Bounding the Largest Eigenvalue of Trees in Terms of the Largest Vertex Degree, Lin. Algebra Appl. 360 (2003) 35-42

[38] H. Song, Q. Wang, L. Tian, New Upper Bounds on the Spectral Radius of Trees with the Given Number of Vertices and Maximum Degree, Lin. Algebra Appl. 439 (2013) 2527-2541

[39] A. Chang, Q. Huang, Ordering Trees by their Largest Eigenvalues, Lin. Algebra Appl. 370 (2003) 174-184

[40] F. Belardo, EM. Li Marzi, S. Simić, Trees with Minimal Index and Diameter at most Four, Discrete Math. 310 (2010) 1708-1714

[41] O. Rojo, M. Robinho, An Explicit Formula for Eigenvalues of Bethe Trees and Upper Bounds on the Largest Eigenvalue of any Tree, Lin. Algebra Appl. 427 (2007) 138-150

[42] B. Wu, E. Xiao, Y. Hong, The Spectral Radius of Trees on k Pendant Vertices, Lin. Algebra Appl. 395 (2005) 343-349

[43] J. H. Smith, Some Properties of the Spectrum of a Graph, in: R. Guy, H. Hanani, N. Sauer, J. Schönheim (Eds.) Combinatorial Structures and Their Applications, Gordon and Breach, Science Publ. Inc., New York, London, Paris, 1970, 403-406

A Method for Comparing and Analyzing Wireless Security Situations in Two Capital Cities

Dalibor Dobrilovic[1], Zeljko Stojanov[1], Stefan Jäger[2], Zoltán Rajnai[3]

[1] University of Novi Sad / Technical Faculty "Mihajlo Pupin", Djure Djakovica bb, 23000 Zrenjanin, Serbia, dalibor.dobrilovic@uns.ac.rs; zeljko.stojanov@uns.ac.rs

[2] University of Jena/Department for Communication and Computer Engineering; IT-Security, Ernst-Abbe-Platz 1, 07743, Jena, Germany, m4jast@uni-jena.de

[3] Óbuda University/Doctoral School on Safety and Security Sciences, Népszínház u. 8, H-1081 Budapest, Hungary, rajnai.zoltan@bgk.uni-obuda.hu

Abstract: An increasing number of wireless Internet users and deployed wireless access points over the past several years and have raised the importance of wireless security issues. The absolute majority of wireless users are not IT professionals, but a population unaware of wireless security types, settings and importance. Wireless security assessment and analytics can help in raising the security awareness of users and in increasing their skills, leading to improvement of the entire security situation. In this paper a short overview of wireless security assessment and history is presented. The methodology and tools for a more accurate wireless security assessment, including data acquisition, processing and analysis, are offered. The proposed methodology and tools are used for processing wireless scan results for the two capital cities, Hungary (Budapest) and Serbia (Belgrade). The possibility of access point configuration changes and security improvement has also been investigated. The research results and potential improvements of wireless security situation are discussed.

Keywords: wireless network security; Wardriving; wireless security assessment;

1 Introduction

This paper focuses on wireless security issues. Motivation for this research rests in the fact, that in recent years, we have been witnesses of a rapid growth in the number of Internet users, who mainly use wireless technology. The advances in wireless technology, decline in the price of wireless equipment and ease of its

usage, have resulted in the deployment of a large number of wireless access points in most locations (homes, offices, public buildings, etc.). Although wireless access has become accessible to most everyone, the majority of wireless users are not skilled or educated in wireless security issues. This has led to the creation of the biggest security hole in computer systems since the beginning of the computing revolution. The importance of the assessment of wireless networks security, comes from the need to tackle the problem in order to identify the major causes of security faults and to find ways to prevent or minimize them.

This paper outlines the history of wireless security assessment, with examples from around the World, Europe and the regions where the research was conducted. The methodology and tools for data analysis are presented. Collected and processed data for two capital cities, Hungary (Budapest) and Serbia (Belgrade) are presented and compared. The possibility of access point configuration changes and security improvements are also investigated. Finally, the recommendations for further assessments are proposed.

2 Wireless Security and Wardriving

A widely accepted process for wireless security assessment is called "Wardriving" [1, 2]. This term comes from the term "wardialing" mentioned in the famous hacking movie "War Games" from 1983, where it was used for the process of calling a pool of telephone numbers in order to find a computer with a modem attached [1]. The Wardriving became world famous starting with Peter Shipley, a computer security consultant at Berkeley. He conducted a survey in Berkeley, California and reported the results at DefCon hacker conference in July 2001, aimed at raising the awareness of wireless security importance. The popularity of Wardriving continued to grow starting from 2002, when the first worldwide event called WWWD (World Wide War Drive) was held, with the total of 9,734 scanned access points. The participants in this event were from 6 countries and 2 continents. In the following events the number of participants and scanned access points increased: WWWD2 in September 2002 (24,958), WWWD3 in 2003 (88,122) and WWWD4 in 2004 with 228,537 discovered access points. Since these events, academy researchers, security experts and consultants have performed similar scans worldwide.

2.1 Research on Wireless Security

Since 2001, wardriving has become the activity practiced by enthusiasts, hobbyists, security experts and malicious hackers. This section presents only the Wardriving activities related to academic research [3, 4, 5]. The Wardriving has been widely accepted by academic researchers. It was performed all over the

world, e.g. in Malasya in 2005 [6], La Plata, Argentina in 2008 [7], Australia in 2011 [8, 9] and New Zealand in 2013 [10, 11]. This research field is also popular in the region, where recent and up to date statistical reports and analyses from Croatia in 2013 [12, 13], Romania in 2015 [14] and Serbia since 2010 [15, 16, 17, 18, 19] were published. The experiences from the presented research, acquisition tools and analysis techniques are used for shaping the methodology in this research work.

2.2 Wireless Security Settings

Basically, wireless network or access point (AP) security can be classified in five or seven categories. The five categories are: Open, WEP, WPA, WPA2 and mixed-mode networks. Mixed-mode networks support both WPA and WPA2. Those five categories can be expanded further by dividing the WPA and WPA2 categories to subcategories such as: WPA-Personal and WPA-Enterprise. The categories are defined by the encryption methods and by the authentication mechanism they use. The encryption methods and the authentication mechanisms will be explained in the following subsections.

Generally, WEP uses WEP encryption, WPA uses TKIP, and WPA2 uses CCMP. There is a possibility that WPA or WPA2 method uses both TKIP and CCMP due to the vendor's attempt to maintain legacy compatibility. The personal WPA and WPA2 use PSK (Pre-shared key) for local authentication and Enterprise WPA and WPA2 use 802.1x (EAP) and an external authentication server (RADIUS). All these methods will be explained in the following subsections.

Open network uses neither encryption nor authentication. In this research, with the used tools, open networks are identified as networks with the absence of encryption and authentication data, only with the data about the network type: [ESS] or extended service set (Table 1, item no. 7) for infrastructure networks and [IBSS] or independent basic service set for ad-hoc networks. In addition, they have an indicator whether WPS is used or not, with the presence or absence of [WPS] mark (see Table 1, item no. 15, in Research methodology section). Those networks do not have WEP, WPA, WPA2, TKIP, CCMP, EAP or PSK marks.

2.3 Wi-Fi Protected Setup (WPS)

WPS was designed by the Wi-Fi Alliance, to enable easy authentication despite the use of a complex password. The user-unfriendly typing of long and complex passwords is eliminated by the use of WPS. There are several variants of the use of WPS. From a security perspective, the PIN is to be regarded as critical [20].

Access Points which support this method have a WPS button. If this is pressed, the WPS PIN must be entered on the client device within a short period (usually 60 seconds). This PIN is usually found on a label on the access point. The problem

with this approach is the weak structure of the 8-digit PINs, which consist only of numbers. Thereby, brute force attacks can be performed very effectively within the allowed time frame. If there are no other security mechanisms for attacks against WPS, such attacks will be repeated within a few hours [21]. Since the WPS PIN does not change automatically, the attack can be interrupted and continued at a different time. Unlike attacks against WPA2, the attack must necessarily be directed against the Access Point.

There are several free tools specialized in this type of attack, for example, Reaver. The security mechanisms implemented in AP can block WPS mode in case there are too many PIN-tries, within a short time period. Reaver can circumvent these mechanisms and other safeguards. If the Reaver tool is successful, the Wi-Fi password will be returned as plain text.

In most Access Points, WPS is enabled by default in the PIN mode. Since most users assume that a strong WPA2 password is sufficient for a secure network, they often forget to turn off WPS. For safety considerations, the analyzed networks, therefore, must be checked for encryption on one side and for activation of WPS on the other.

2.4 Wireless Encryption Methods

Three encryption methods operating at Layer 2 of the OSI model are defined by 802.11-2007 standards. The three methods are: WEP, TKIP and CCMP. They are used to encrypt MAC Protocol Data Unit (MPDU) payload or the data contained in IP packets. All three methods use symmetric algorithms. WEP and TKIP use the RC4 cipher (stream cipher), while CCMP uses the AES (Advanced Encryption Standard) cipher (block cipher) [22]. The 802.11-2007 standards define WEP as a legacy encryption method, for pre–RSNA security, while TKIP and CCMP are considered to be compliant Robust Security Network (RSN) encryption protocols. The next difference between WEP on one side and TKIP and CCMP on the other side, is that WEP uses a preconfigured static key that is liable to attacks. Alternatively, TKIP and CCMP use encryption keys, dynamically generated by the 4-Way Handshake [22].

2.4.1 WEP

Wired Equivalent Privacy (WEP) is the simplest form of wireless security. It is a Layer 2 security protocol, that uses the Rivest Cipher 4 (RC4) streaming cipher [22]. It uses two variants of relatively small shared key: 64-bit and 128-bit. Standard 64-bit WEP uses a 40-bit key (also known as WEP-40), which is concatenated with a 24-bit initialization vector (IV) to form the RC4 key. This method of security is only a little bit more secure then clear-text passwords. The reason is the weakness in the WEP protocol. The WEP protection can be

compromised in several minutes, using free and widely available tools on the Internet [23]. If enough data packets are recorded, the password can be determined in any case. Because of this, the networks and Access Points using WEP will be considered extremely unprotected in this research.

2.4.2 WPA

WPA (Wi-Fi Protected Access) is based on the IEEE standard 802.11i. It was introduced in April 2003 by the Wi-Fi Alliance. The usage of TKIP encryption is defined within the standard as an enhancement of WEP aimed at overcoming its weaknesses. It uses Rivest Cipher 4 (RC4) streaming cipher for encryption and decryption processes. TKIP modifies WEP with longer 128-bit per-packet key that dynamically generates a 48-bit initialization vector (IV) with Message Integrity Check (MIC) for each new packet. MIC is designed for preventing active or passive man-in-the-middle attacks. Because WPA is designed as an interim short-term solution to enhance wireless security, it has its own weaknesses [24, 25]. WPA should only be used on legacy hardware that is not capable of supporting AES-CCMP. TKIP is mandatory when WPA is used [23].

2.4.3 WPA2

WPA2 is based on the IEEE 802.11i/WPA2 or IEEE 802.11i-2004 standard defined on June 24th, 2004 and it is a stronger version of WPA. It uses AES (Advanced Encryption Standard) cipher (block cipher) with Counter Mode with Cipher Block Chaining Message Authentication Code Protocol (CCMP). AES accepts keys with size of 128, 192, and 256 bits [24]. The usage of AES-CCMP is mandatory for WPA2. Still, in order to maintain compatibility with the legacy equipment, vendors allow TKIP to be used with the clients not supporting AES-CCMP.

2.5 Wireless Authentication

As described in the beginning of this section, both WPA and WPA2 support two methods of authentication: personal and enterprise. The personal method is local authentication, which is commonly used. The enterprise authentication is server based and much less present in access point configuration, because it requires a separate authentication server and it is designed primarily for companies.

2.5.1 Personal Networks

Personal WPA and WPA2 networks are intended to be used for ad-hoc configured access points and home networks. They use a pre-shared key (PSK) which is vulnerable to password/passphrase guessing using dictionary attacks [26]. PSK must start with the definition of passphrase at the access point (AP) which will be

used for generating encryption keys. In this operational mode, there is no authentication exchange and a single private key can be assigned to entire network or to one client. In order to create a secure passphrase, the recommendation is to compose a very complex one with more than 20 characters. The dictionary words should not be used and a passphrase must contain lower and upper case letters, numbers, and symbols. If the recommendations are not followed, networks are easier to crack [27, 28]. Personal networks will be identified in this research as [WPA-PSK.....] (Table I, column 2, first three rows).

2.5.2 Enterprise Networks

The enterprise authentication uses 802.1x and an external authentication server such as Remote Authentication Dial In User Service (RADIUS). Therefore, the three standards define this process: EAP, 802.1x, and RADIUS.

The Extensible Authentication Protocol (EAP) is a layer 2 process that allows a wireless client to authenticate to a network. There is a version of EAP that is used in LAN environments called EAP over LAN (EAPoL) and a version for wireless networks. EAP defines a standard way for encapsulating authentication information, such as a username and password or a digital certificate that the AP can use to authenticate the user. The authentication process is taking place beyond AP in communication with authentication server. EAP has several extensions: EAP-MD5, EAP-TLS, LEAP (Lightweight EAP), PEAP (Protected EAP), EAP-FAST and EAP-GTC [29].

802.1x and RADIUS define packets for EAP information, e.g. 802.1x standard defines transport from a client to a network access device (AP, switch, router, etc.). These data are passed using RADIUS protocol to an authentication server. The server will authenticate the user and allow his access to the network.

2.6 Wireless Security Assessment Tools

A numerous software tools can be used for performing Wardriving. The usage of tools also depends on hardware and software platforms. Only a small segment of Wardriving tools will be presented here, while a more detailed overview is given in [15]. In case of using PC or laptop computer and Windows operating system the possible tools are Vistumbler, InSSIDer, etc. In case of using Linux operating system, Kismet [30] presents almost de-facto standard. Great expansion of possible tools for Wardriving was influenced by the introduction of Android smart phone platform, which gave access to the variety of Wardriving tools such as: Wigle WiFi [31], War-drive, G-Mon, WiFi finder, WiFi tracker, etc. The iOS platform (available for iPhone and iPad) has the similar software tools, e.g. WiFiFoFum and WiFi Explorer.

The new minimized computer boards such as Raspberry Pi, Beagle Bone or Arduino Yun opened new horizons in building Wardriving platforms, as presented for Raspberry Pi in [32]. The added value is, inter alia, the fact that these mini computers combine the benefits of computers and smart phones. They can perform the tasks of computers, but they are as small and light, as a smart phone. Thus, these devices can not only, locate and scan networks, they can also perform security and penetration tests.

3 Research Methodology

The research methodology contains the following components: data acquisition tool, data processing tools and a method for data acquisition and analysis of results. Android application Wigle WiFi, designed for usage on smart phones, was used as the data acquisition tool.

The reason for using the Wigle application in this research is the positive experience of researchers in using this application in the long period in the past. Wigle application has a capability to export retrieved wireless access point (AP) or wireless networks data in KML (XML file format for geocoordinates) and CSV format. Basically, a wireless network and a wireless AP represent the same thing in this research. CSV format is used, in the following form:

```
AA:AA:AA:AA:AA:AA, BB, [WPA-PSK-TKIP][ESS], 6/20/2015 13:57,  6, -97,

44.8185463, 20.3735048, 0, 336, WIFI
```

The first column represents access point MAC address which is unique in the whole world for the corresponding device (used MAC address is fictional). The second column represents SSID (network name). The third column is the most important for this research, representing security type of the scanned AP. In this research, 86 different security types were identified in Belgrade and Budapest. The partial list of detailed security types is given in Table 1. The next data are date and time of scanning, channel or frequency used by the wireless network (1–13), RSSI or received signal strength in dBm, latitude, longitude, altitude, accuracy in meters and type of detected network (WIFI or GSM).

3.1 Data Processing Application

Data processing application called WDStat v2.0, is built with C#. This application allows import of Wigle CSV format, and some other formats as well (GPX). This software parses a Wardriving log downloaded from Android smart phones, aimed at creating a database. The additional data added to the database are locations of APs using the GPS coordinates from Wardriving logs, and determination of the

geographical location according to these coordinates. Description of a geographical location and association of the scanned network with the cities, towns, regions and countries is presented in [16].

Acquired data are further processed and statistically analyzed in order to make statistical reports. The reports summarize the following statistics: channel usage, SSID statistics, grouped security stats (e.g. Open, WEP, WPA, WPA2, and Mixed-mode), CCMP usage stats for WPA, WPA2 and Mixed-mode networks, WPS usage statistics, Ad-hoc or infrastructure network statistics, geographical locations statistics, detailed security statistics as described in Wigle CSV format and vendor statistics. The vendor statistics is built on MAC address allocation according to IEEE MAC address allocation list [33]. The results for Budapest 2015/2016, Belgrade 2015/16 and Belgrade 2013/2014 research scans for channels and security type usage are given in Fig. 1.

The application simplifies the security settings description, making security change analysis easier. The simplification is performed from security type description shown in Table 1, which is the original security type derived from Wigle WiFi scan log, to the simplified version shown in Table 8 and the most generalized one shown in Table 7.

For example, original security types, such as [WPA-PSK-TKIP+CCMP][WPA2-PSK-TKIP+CCMP][WPS][ESS] can be simplified as Mixed_TKIP_CCMP_ PSK_WPS and further simplified as Mixed and WPS security groups. The next example: [WPA2-EAP-CCMP][ESS] can be simplified as WPA2_CCMP_EAP_noWPS and further simplified as WPA2 and no_WPS security groups.

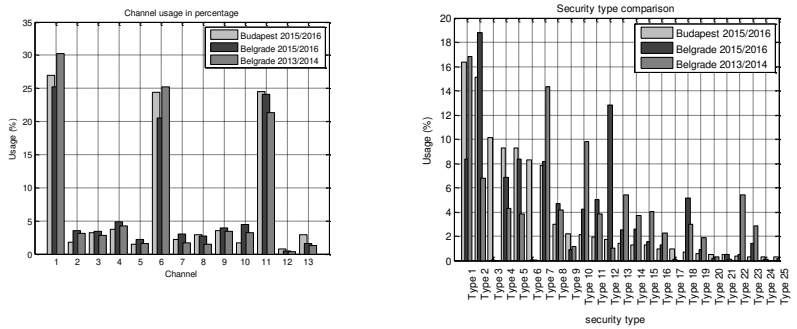

Figure 1

a) Wireless channel usage comparison b) The most used wireless security settings comparison

The top 25 detailed security analysis results are presented in Fig. 1 b) and in Table 1. The pair of columns represents the number of discovered access points and their percentage in accordance with the total discovered APs. The data are given for the Budapest 2015/2016, Belgrade 2015/2016 and Belgrade 2013/2014 scans, respectively.

Table 1
Comparison of the top 25 wireless security settings

Type No.	Security type / City	Budapest 2015/2016		Belgrade 2015/2016		Belgrade 2013/2014	
		No.	%	No.	%	No.	%
1	[WPA-PSK-CCMP+TKIP][WPA2-PSK-CCMP+TKIP][WPS][ESS]	2,336	16.35	1,513	8.37	4,926	16.84
2	[WPA-PSK-CCMP+TKIP][WPA2-PSK-CCMP+TKIP][ESS]	2,162	15.13	3,398	18.8	1,991	6.81
3	[WPA-EAP-CCMP+TKIP][WPA2-EAP-CCMP+TKIP][ESS]	1,449	10.14	2	0.01	0	0
4	[WPA2-PSK-CCMP][WPS][ESS]	1,330	9.31	1,243	6.88	1,253	4.28
5	[WPA2-PSK-CCMP][ESS]	1,328	9.3	1,507	8.34	1,253	3.81
6	[WPA2-EAP-CCMP+TKIP][ESS]	1,186	8.3	4	0.02	10	0.03
7	[ESS]	1,123	7.86	1,474	8.16	4,199	14.36
8	[WPA-PSK-CCMP][WPA2-PSK-CCMP][WPS][ESS]	427	2.99	842	4.66	1,225	4.19
9	[WPA2-PSK-CCMP+TKIP][ESS]	317	2.22	162	0.9	346	1.18
10	[WPA-PSK-TKIP][ESS]	304	2.13	768	4.25	2,860	9.78
11	[WPA-PSK-CCMP][WPA2-PSK-CCMP][ESS]	277	1.94	909	5.03	1,115	3.81
12	[WPA2-EAP-CCMP][ESS]	247	1.73	2,315	12.81	290	0.99
13	[WPA-PSK-CCMP+TKIP][WPA2-PSK-CCMP+TKIP-preauth][ESS]	202	1.41	461	2.55	1,592	5.44
14	[WPA2-PSK-CCMP+TKIP][WPS][ESS]	186	1.3	466	2.58	1,077	3.68
15	[WEP][ESS]	180	1.26	283	1.57	229	4.01
16	[WPA-PSK-TKIP][WPA2-PSK-TKIP][ESS]	139	0.97	228	1.26	658	2.25
17	[WPA-EAP-CCMP][WPA2-EAP-CCMP][ESS]	131	0.92	22	0.12	0	0
18	[WPA-PSK-CCMP][ESS]	102	0.71	929	5.14	867	2.96
19	[WPS][ESS]	76	0.53	158	0.87	545	1.86
20	[WPA-PSK-CCMP+TKIP][WPA2-PSK-CCMP+TKIP-preauth][WPS][ESS]	74	0.52	33	0.18	80	0.27
21	[WPA2-PSK-CCMP-preauth][ESS]	66	0.46	92	0.51	23	0.08
22	[WPA2-PSK-CCMP+TKIP-preauth][ESS]	50	0.35	89	0.49	1,592	5.44
23	[WPA2-PSK-TKIP][ESS]	46	0.32	251	1.39	843	2.88
24	[WPA2-PSK-CCMP][ESS][SEC80]	42	0.29	22	0.12	0	0
25	[WPA-PSK-TKIP][WPA2-PSK-CCMP+TKIP][ESS]	38	0.27	26	0.14	57	0.19

Note: The grouped security types are: Open = type 7 and type 19, WEP = type 15, WPA = type 18, WPA2 = type 4, type 5, type 6, etc., Mixed-mode = type 1, type 2, type 3, etc.

The grouped security statistics are given in Fig. 2 a) and WPS and CCMP statistics are given in Fig. 2 b).

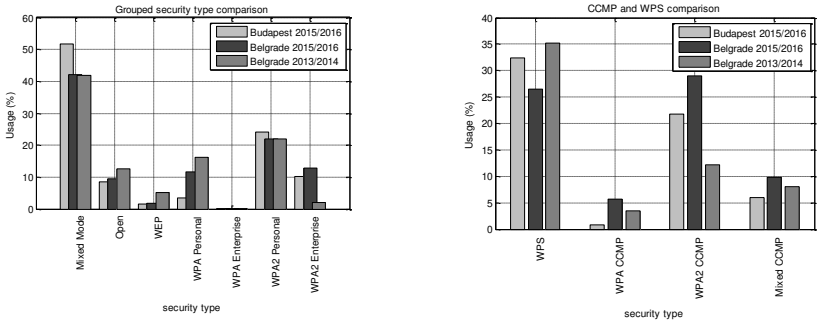

Figure 2
a) Security type comparison b) WPS and CCMP encryption usage comparison

3.2 Data Acquisition

Data acquisition was performed with several Android devices using different versions of the Wigle WiFi application. The Wardriving sessions were made in two separate periods. The first session was organized during 2013/2014 in larger parts of Serbia. The results of this Wardriving session were partially published in [15]. The second session was organized in Serbia in 2015/2016 and Hungary 2015/2016. The Hungarian session took place, mainly, in Budapest and the surrounding area.

For this research, the Hungarian 2015/2016 and Serbian 2015/2016 scans were used for analysis and comparison of wireless security situations in two capital cities. In order to determine the possibility, rate and quality of improvements of access point security through the changes during the usage period, the Serbian 2013/2014 session data for the city of Belgrade were used for comparison and determination of improvement rate of the wireless security of once configured access points. The quality of sample used for these analyses is justified with the number of scanned networks, number of appearances of the scanned networks and number of networks scanned in both research periods.

In this research the Wigle WiFi was used. Fig. 3 presents the part of the scanned wireless networks or access points with their locations in Budapest and Belgrade. Google maps are used for visualization. The part of scanned networks is presented in similar areas in Belgrade. The city center and its close surroundings are presented in these images. The profile of wireless users should be the same in these regions.

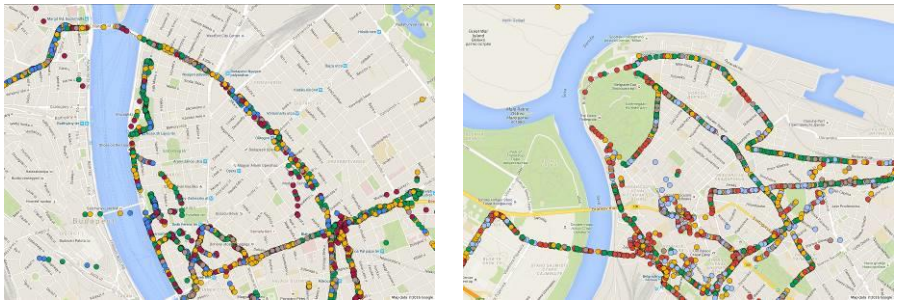

Figure 3

a) Part of scanned networks in Budapest 2015/2016 b) Part of scanned networks in Belgrade 2015/2016

3.3 Results

During both research sessions, 31,928 different networks were discovered. The networks were identified by their unique MAC addresses. After removing duplicates, 10,285 networks (APs) were discovered in both Wardriving sessions which can be used for security change analysis.

Table 2 presents the statistics of number of appearances of 10,285 networks scanned in two periods. It is important to point out that the 66.52% were scanned more than 5 times (first four rows in the table).

Table 2
The number of appearances of scanned access points in the 2013/2014 and 2015/2016 period

No. of appearances	No of APs	(%)
9	100	0.97
8	640	6.22
7	2,217	21.56
6	3,885	37.77
5	652	6.34
4	1,204	11.71
3	83	0.81
2	1,504	14.62
Total	**10,285**	**100.00**

Only 936 networks among 10,285 were detected to have changed their configuration compared to the initial scanning. The number of appearances of changed configuration networks is given in Table 3 in order to justify the quality of sample. Since 62.50% of networks were scanned 7 or more times (the first three columns in the Table) the sample can be qualified as good for analysis.

Table 3
The number of appearances of scanned access points in the 2013/2014 and 2015/2016 period

No. of appearances	No of APs	(%)
9	30	3.21
8	125	13.35
7	430	45.94
6	12	1.28
5	64	6.84
4	11	1.18
3	8	0.85
2	256	27.35
Total:	**936**	**100.00**

The number of changes is summarized and presented in Table 4. The majority of networks were changed only once – 916, which makes 97.86% of changed networks and only 8.91% of total networks. Only 20 networks were changed 2 or 3 times. These statistics clearly show that configuration changes are not likely to happen during the access point usage.

The configuration change analytics, together with the details of data acquisition, is given in the following section.

Table 4
The number of configuration changes per access point

No. of Changes per AP	No. of Aps	%	% (Total)
1	916	97.86	8.91
2	16	1.71	0.16
3	4	0.43	0.04
Total	**936**	**100.00**	**9.11**

4 Discussion

4.1 Comparison of Wireless Security in Two Capital Cities

The results presented in Fig 2 a) are summarized in Table 5. For researches in period 2015/2016, the same device and the same software have been used. According to the results presented in the table, the security situations in Budapest and Belgrade are similar. The percentage of Open and WEP security access points is similar. The only difference is that in Belgrade, there is a higher percentage of WPA-Personal networks, 7.97% more than in Budapest. On the contrary the percentage of Mixed-mode networks in Budapest is 9.61% higher than in Belgrade. This gives slightly better security result in favor of Budapest. The percentage of most secured networks (WPA2-Personal and WPA2-Enterpise) is similar for Budapest (34.5%) and Belgrade (34.83%).

Table 5
The grouped security types

City and period	Number	Open (%)	WEP (%)	WPA-Per (%)	WPA-Ent (%)	WPA2-Per (%)	WPA2-Ent (%)	Mixed Mode (%)
Budapest 2015/2016	14,287	8.62	1.45	3.56	0.06	24.18	10.32	51.81
Belgrade 2015/2016	18,070	9.49	1.9	11.53	0.03	21.96	12.87	42.22
Belgrade 2013/2014	13,621	12.71	5.14	16.2	0.12	21.91	2.06	41.86

Table 6 summarizes the results showed in Fig. 2 b) with the percentage of WPS enabled access points, and furthermore with the percentage of access points with the support for only CCMP encryption. The situation regarding the two security statistics is in favor of Belgrade, where the percentage of WPS-enabled networks is 5.91% lower. Considering the WPS vulnerabilities, the smaller percentage is better. The access points enabling only CCMP are also in favor of Belgrade, meaning that 15.97% networks in Belgrade are more secure since they use exclusively this encryption method.

Table 6
WPS and CCMP security statistics

City and period	Number	WPS (%)	WPA_CCMP (%)	WPA2_CCMP (%)	Mixed CCMP (%)
Budapest 2015/2016	14,287	32.44	0.8	21.78	5.91
Belgrade 2015/2016	18,070	26.53	5.63	28.97	9.86
Belgrade 2013/2014	13,621	36.74	3.19	14.27	8.71

4.2 Access Points Configuration Changes

Scanning of wireless networks considered for the configuration change analyses took place in Belgrade from November 2013 to February 2016. During this period 79,947 different scans were collected, among which 31,928 unique networks were identified. For this research it is important that 10,285 networks appear more than once in the retrieved data. These networks were scanned at least twice and up to 9 times. One to up to tree changes were detected on analyzed networks. The detailed overviews of appearances of scanned networks are given in Table 2 for the discovered networks in both research periods and in Table 3 for the networks with detected changes.

For this research, the grouping which is described later was made according to the first and the last change, so that the last change is considered as a final change of a configuration. For example, some networks were changed 3 times, meaning that the changes were tracked in the following format: Configuration1 → Configuration2 → Configuration3 → Configuration4. In this research, the change of configuration is made according to Configuration1 → Configuration4 format, i.e. only the first and the last configurations are considered for the transition.

All scanned data were sorted according to the date and time of data acquisition, before data analysis with the software tool built for that purpose. This was made in order to avoid confusion with the timeline of configuration changes and to avoid possible data inaccuracy. For example, if the collected data are not sorted according to timeline, the configuration change might be accidentally identified as a change from a higher to a lower level of configuration.

Among the scanned networks, there are several recorded cases where configuration transition is as follows: WPA2→Open, Mixed→Open, WPA→Open, WPA2→WEP, WPA→WEP, Mixed→WEP, WEP→WEP and Open→WEP. In all these cases, the settings which might be qualified as secure are changed to less secure settings, even using obsolete encryption type such as WEP. Since there is a little possibility to justify reconfigurations from WPA/WPA2 secured to Open networks, the explanation for transition from WPA/WPA2 secured to WEP networks is not possible, especially in the period between 2013 and 2016. Therefore, there is space for thinking that there might be an error in acquired data, sorting process or even in analyzing software itself. So far, the errors have not been identified and all statistical data can be considered accurate. If the errors

exist, the important thing is that they do not significantly affect the results and analysis since the number of listed cases is 62 or 0.6% of total networks. The other explanation is that AP was reset to factory settings and after this the provider or owner failed to configure AP again.

The software identified 936 networks with changed configurations, which makes only 9.1% of all analyzed networks. Furthermore, the analysis tried to identify if these changes were generally made for better, worse or similar security levels. In order to do these analyses, the three criteria are defined. One criterion divides a large number of security types shown in Table I and Fig. 2b) in 25 categories according to transition from one grouped security level such as: Open, WEP, WPA, WPA2 and Mixed. The number of 25 means that each of 5 groups can be changed to the same 5 groups, e.g. Open→Open, Open→WPA2 or WEP→WPA2. The presented transitions are given in Table 7.

Table 7

The types of security setting changes and their percent in analyzed networks

No.	Group change	No. of APs	(%)	Ch	No.	Group change	No. of APs	(%)	Ch
1	Mixed→Mixed	371	39.64	N	**14**	WPA→WPA	17	1.82	N
2	Mixed→WPA2	61	6.52	B	**15**	Mixed→Open	16	1.71	W
3	WPA2→Mixed	61	6.52	W	**16**	Open→Open	14	1.50	N
4	Open→Mixed	53	5.66	B	**17**	WEP→Mixed	14	1.50	B
5	Open→WPA2	49	5.24	B	**18**	WPA→Open	14	1.50	W
6	Mixed→WPA	48	5.13	W	**19**	WEP→Open	5	0.53	N
7	WPA2→WPA2	39	4.17	B	**20**	WPA2→WEP	4	0.43	W
8	WPA→WPA2	36	3.85	B	**21**	WPA→WEP	3	0.32	W
9	Open→WPA	31	3.31	B	**22**	Mixed→WEP	3	0.32	W
10	WPA→Mixed	30	3.21	N	**23**	WEP→WEP	2	0.20	N
11	WPA2→WPA	26	2.78	W	**24**	WEP→WPA	2	0.20	B
12	WPA2→Open	18	1.92	W	**25**	Open→WEP	2	0.20	N
13	WEP→WPA2	17	1.82	B		**Total**	**936**	**100**	

The first analysis shows that a total of 936 changes of configurations were made. Further analysis shows that only some changes can be qualified as improvements in configurations. For this research, those changes are defined as: Mixed→WPA2, Open→Mixed, Open→WPA2, WPA2→WPA2, WPA→WPA2, Open→WPA, WEP→WPA2, WEP→Mixed and WEP→WPA. According to this definition, only 302 access points have been configured to match better security level, which makes only 32.26% of changed APs, and only 2.94% of all analyzed access points (10,285). In Table 7 in the column Ch, changes qualified as changes to better are marked with B, changes to worse are marked with W and with neutral impact on higher security with N (none).

The second criterion is defined by considering changes to WPS configuration. Only 4 categories are defined here: noWPS→WPS, WPS→WPS, noWPS→noWPS, and WPS→noWPS. Again, the results are similar. Only 344 or 36.75% of the changed APs are scanned with improved settings, which is only 3.34% compared to the total number of analyzed APs. Only the transition from WPS to noWPS is considered as a transition to a higher security level.

The third criterion defines 228 different security groups. Those groups are more detailed compared to 5 groups given in Table 7. The most frequent changes between groups (15 in total) are presented in Table 8. As in Table 7, changes in Table 8 in column Ch are marked with B for changes qualified as better, with W for changes qualified as worse and with N for changes without improvement.

According to these analyses 652 detailed security groups were improved (a wide range of changes to betterment was considered, even the very small improvements), which makes only 69.66 % of changed APs, and only 6.34% of all scanned and analyzed networks.

Table 8
The detailed types of security setting changes and their percent in the total number of analyzed networks

No.	Detailed Security Group	No. of APs	(%)	Ch
1	Mixed_TKIP_CCMP_PSK_WPS→Mixed_TKIP_CCMP_PSK_noWPS	284	30.34	B
2	Mixed_CCMP_PSK_noWPS→WPA_CCMP_PSK_noWPS	18	1.92	W
3	Open_noWPS→WPA2_CCMP_PSK_noWPS	18	1.92	B
4	WPA_TKIP_PSK_noWPS→WPA2_TKIP_PSK_noWPS	16	1.71	B
5	Open_noWPS→WPA2_TKIP_PSK_noWPS	15	1.6	B
6	Open_noWPS→WPA_TKIP_PSK_noWPS	15	1.6	B
7	Mixed_TKIP_CCMP_PSK_noWPS→Mixed_TKIP_CCMP_PSK_WPS	14	1.5	W
8	Open_noWPS→Mixed_TKIP_CCMP_PSK_preauth_noWPS	12	1.28	B
9	Open_WPS→Mixed_TKIP_CCMP_PSK_WPS	12	1.28	B
10	WPA_TKIP_PSK_noWPS→Open_noWPS	11	1.18	W
11	Open_noWPS→WPA_CCMP_PSK_noWPS	11	1.18	B
12	Mixed_TKIP_CCMP_PSK_WPS→Mixed_CCMP_PSK_WPS	10	1.07	B
13	WPA2_CCMP_PSK_noWPS→WPA_CCMP_PSK_noWPS	10	1.07	W
14	Open_noWPS→Mixed_TKIP_PSK_noWPS	9	0.96	B
15	WPA2_CCMP_PSK_WPS→Mixed_CCMP_PSK_WPS	8	0.85	W

In all three cases, the percentage of changes to a higher level of security ranges from 2.94% to 6.34%. The percentage is given in comparison with all scanned networks discovered more than once for the period of 3 years. These results definitely confirm that, once the access point is installed and wireless network is configured, there is less than a 10% chance that the system will be configured again. The chances that the access point configuration will lead to better security settings are even smaller, since only 2.94 to 6.34 percent of configuration changes actually raise the security level.

4.3 Limitations of the Study

Certain limitations were identified during this study. The research lacks the second scan in the city of Budapest in the period after 1-2 years. This second scan will allow analysis of the configuration change rate for Budapest, as well as comparison of this wireless security aspect between Budapest and Belgrade.

Careful planning for the Wardriving routes is also missing in this research. For example, by distinguishing tourist, business and residential areas, this research can enable carrying out a more accurate and more productive analysis, allowing deeper understanding of problems and leading to more suitable solutions for specific areas of human living. The separate analytics of enlisted areas will also provide a good starting point for further analysis, and possible inclusion of sociologists, urban and economic experts in multidisciplinary research projects.

Conclusions

This paper presents the results of the wireless security circumstances in Budapest and Belgrade, by using a methodology based on Wardriving. The research was conducted from November 2013 to February 2016. The first part of the research is from 2015/2016 period and it is used for comparison of wireless security in Budapest and Belgrade. The total of 14,287 networks in Budapest and 18,070 networks in Belgrade were discovered during this period.

The wireless security situation in the cities of Budapest and Belgrade shows a lot of potential for improvement. The highest level of security (WPA2 with CCMP) is not present in a desired range. The situation in Belgrade is better regarding this parameter as 44.46% of the networks use CCMP in WPA, WPA2 or Mixed-mode, compared to 28.49% in Budapest. It still accounts for less than 50% of all networks and this should be improved. The situation in Belgrade is also better comparing the WPS features, since 26.53% networks in Belgrade and 32.44% networks in Budapest use this vulnerable feature. In both cities, the situation has to be significantly improved by reducing the number of WPS enabled access points.

The percentage of Open and WEP security access points is similar in both capital cities. The only difference is that in Belgrade there is a higher percentage of WPA-Personal networks, 7.97% higher than in Budapest. On the contrary, the percentage of Mixed-mode networks in Budapest is 9.61% higher than in Belgrade. This gives a slightly better security result in favor of Budapest while the total percentage of the most secured networks (WPA2-Personal and WPA2-Enterpise) is similar in Budapest (34.5%) and Belgrade (34.83%).

The second phase of research compared Belgrade Wardriving statistics for period 2013/2014 and period 2015/2016. Findings of this research clearly point out that the wireless security situation is not perfect, but it has changed through time. This conclusion can be made by comparing results in Belgrade in periods 2013/2014

and 2015/2016. The improvement in the security situation was made by deploying new and cost-effective access points over the time, where the newly deployed access points were configured with more expertise and attention. The configuration of once deployed access points changes very rarely (ranging from 2.94% to 6.34%).

The final conclusion is that the best way for raising the overall security of wireless networks is to raise the awareness of wireless users and wireless network providers regarding the threats, vulnerabilities and best methods for security settings.

In future work the presented methodology for security change analysis, can be improved, by making changes in the software for security analysis and reporting. For example, development of more detailed criteria for rating improvements of security changes can also be useful, leading to creation of better policies in deploying new APs, as well as, finding the main reasons for the less secure APs settings. In addition, the discussed limitations of the study open challenging directions for further research through considering different aspects of human living and composing multi-disciplinary research teams.

References

[1] Chris Hurley, Frank Thorton, Michael Puchol, Russ Rogers: WarDriving: Drive, Detect, Defend: A Guide to Wireless Security, Syngress Publishing, Inc., Rockland, USA, 2004

[2] Hira Sathu: Wardriving: technical and legal context. In Proceedings of the 5th WSEAS international conference on Telecommunications and informatics (TELE-INFO'06), Stevens Point, Wisconsin, USA, pp. 162-167, 2006

[3] Tsui, A. W. T.; Wei-Cheng Lin; Wei-Ju Chen; Polly Huang; Hao-Hua Chu: Accuracy Performance Analysis between War Driving and War Walking in Metropolitan Wi-Fi Localization, IEEE Transactions on Mobile Computing, Vol. 9, No. 11, pp. 1551-1562, Nov. 2010, doi: 10.1109/ TMC. 2010.121

[4] Sagers, G.; Hosack, B.; Rowley, R. J.; Twitchell, D.; Nagaraj, R.: Where's the Security in WiFi? An Argument for Industry Awareness, Proceedings of 48th Hawaii International Conference on System Sciences (HICSS), pp. 5453-5461, 5-8 January, 2015, doi: 10.1109/HICSS.2015.641

[5] Said, H.; Guimaraes, M.; Al Mutawa, N.; Al Awadhi, I.: Forensics and War-Driving on Unsecured Wireless Network, Proceedings of International Conference for Internet Technology and Secured Transactions (ICITST), pp. 19-24, 11-14 December 2011

[6] Issac, B.; Jacob, S. M.; Mohammed, L. A.: The Art of War Driving and Security Threats - a Malaysian Case Study, Networks, 2005. Jointly held with the 2005 IEEE 7th Malaysia International Conference on

Communication, 2005 13th IEEE International Conference on , Vol. 1, No., pp. 6-pp., 16-18 Nov. 2005

[7] Díaz, Javier F.; Robles, Matías; Venosa, Paula; Macía, Nicolás; Vodopivec, Germán: Wardriving: an Experience in the City of La Plata, Proceedings of XIV Congreso Argentino de Ciencias de la Computación CACIC 2008, October 8-10 2008

[8] Lucas Jacob, Damien Hutchinson, Jemal Abawajy: Wi-Fi Security: Wireless with Confidence, in Proceedings of the 4th Australian Security and Intelligence Conference, pp. 88-06, 5th-7th December, Perth, Australia, 2011

[9] Niloufer Selvadurai, Md. Rizwanul Islam, Peter Gillies: Unauthorised Access to Wireless Local Area Networks: The Limitations of the Present Australian laws, Computer Law & Security Review, Vol. 25, Issue 6, November 2009, pp. 536-542, ISSN 0267-3649, http://dx.doi.org/ 10.1016/j.clsr.2009.09.003

[10] Nisbet, A.: A Tale of Four Cities: Wireless Security & Growth in New Zealand, Proceedings of International Conference on Computing, Networking and Communications (ICNC), pp. 1167-1171, Jananuary 30 2012-February 2 2012, doi: 10.1109/ICCNC.2012.6167391

[11] Nisbet, A.: A 2013 Study of Wireless Network Security in New Zealand: Are We There Yet?‖, in the Proceedings of the 11th Australian Information Security Management Conference, Perth, Western Australia, 2nd-4th December, 2013

[12] Redzepagic, J.; Studen, D.; Gavranic, V.; Tekovic, A.,: Security of End User Wireless Networks in Zagreb Area, Proceedins of 38th International Convention on Information and Communication Technology, Electronics and Microelectronics (MIPRO), pp. 1613-1616, 25-29 May, 2015, doi: 10.1109/MIPRO.2015.7160529

[13] Davor Janić, Dragan Peraković, Vladimir Vukelić: An Analysis of Wireless Network Security in the Sity of Zagreb and Zagreb and Karlovac County, In Procedeengs of 7th International Conference on Ports and Waterways - POWA 2012, pp. 216-223

[14] Ionescu, V.; Smaranda, F.; Sima, I.; Diaconu, A.: Current Status of the Wireless Local Area Networks in Romania, Proceedings of 11th International Conference (RoEduNet) in Roedunet, pp. 1-4, 17-19 January 2013, doi: 10.1109/RoEduNet.2013.6511752

[15] Stefan Jäger, Dalibor Dobrilovic: Tools for WLAN IEEE 802.11 Security Assessment‖, In proceedings of 2nd International conference of Applied Internet and Information Technologies ICAIIT 2013, pp. 56-62, Zrenjanin, Serbia, 25th October, 2013

[16] Dalibor Dobrilovic, Borislav Odadzic, Zeljko Stojanov, Zlatko Covic: Approach in IEEE 802.11 Security Analytics and its Integration in

University Curricula, in Proceedings of the 3rd regional conference Mechatronics in Practice and Education – MECHEDU 2015, pp. 41-46, December 5-6, Subotica, Serbia, 2013

[17] Dušan Švenda, Miroslav Djordjević: Mapping of IEEE 802.11 Wireless Networks in Belgrade (In Serbian: Mapiranje IEEE 802.11 bežičnih mreža u Beogradu), 18. Telecommunication forum TELFOR 2010 Serbia, Belgrade, November 23-25, 2010

[18] Saša Adamović, Marko Šarac, Dalibor Radovanović: Wireless Network IEEE 802.11 Security Analysis on the area of city of Belgrade (In Serbian: Analiza sigurnosti bežičnih mreža IEEE 802.11 na teritoriji grada Beograda, INFOTEH-JAHORINA Vol. 10, Ref. B-III-1, pp. 191-194, Bosnia and Herzegovina, Martch 2011

[19] Dalibor Dobrilović, Borislav Odadžić: Comparative Indicators of Security of Wireless IEEE 802.11 Networks in Parts of Serbia in Comparison to the Region and the World (In Serbian), Informaciona bezbednost 2013, 5. June, Belgrade, Serbia 2013

[20] Durmus Ali Avci, Kemal Hajdarevic: Security of Wi-Fi Networks, In IBU Journal of Science and Technology, Vol. 2, No. 1, pp. 133-144, 25 Sep 2014

[21] Pranav S. Ambavkar, Pranit U. Patil, Dr.B.B.Meshram, Pamu Kumar Swamy: WPA Exploitation in The World of Wireless Network, In International Journal of Advanced Research in Computer Engineering & Technology, Vol. 1, Issue 4, June 2012

[22] David D. Coleman, David A. Westcott, Bryan E. Harkins, Shawn M. Jackman: CWSP® Certified Wireless Security Professional Official - Study Guide Study Guide, Wiley Publishing, Inc., Indianapolis, USA, 2010

[23] Gary A. Donahue: Network Warrior, O'Reilly Media, Inc., Sebastopol, USA, 2011

[24] Mark Ciampa: CWNA Guide to Wireless LANs, Course Technology, Cengage Learning, USA 2013

[25] Johnny Cache, Joshua Wright, Vincent Liu, Hacking exposed™ wireless: wireless security secrets & solutions, 2nd, The McGraw-Hill Companies, 2010

[26] Eric Cole, Ronald Krutz, James W. Conley: Network Security Bible, Wiley Publishing, Inc., Indiana, USA, 2005

[27] Randy Weaver, Dawn Weaver, Dean Farwood: Guide to Network Defense and Countermeasures, 3rd, Course Technology, Cengage Learning, USA, 2014

[28] Richard Deal: CCNA® Cisco® Certified Network Associate Study Guide (Exam 640-802), McGraw-Hill Companies, 2008

[29] C. Hurley, R. Rogers, F. Thompson, D. Connelly, B. Baker: WarDriving and Wireless Penetration Testing, Syngress Publishing, Inc. Rockland, USA, 2007

[30] Haines, B., Thornton, F.: Kismet Hacking, Syngress Publishing, 2008

[31] Wigle - http://www.wigle.net, seen on 2016.03.12

[32] Stefan Jäger: Wardriving – die unterschätzte Gefahr, FIfF-Kommunikation 4/15, "Cybercrime" (in German), 2015

[33] http://standards-oui.ieee.org/oui.txt, Public MAC-list of vendors, seen on 2016.03.12

Quality Improvement Based on a Process Management Approach, with a Focus on University Student Satisfaction

Bálint Bedzsula, János Kövesi

Department of Management and Corporate Economics, Faculty of Economic and Social Sciences, Budapest University of Technology and Economics
Magyar tudósok körútja 2, H-1117 Budapest, Hungary
kovesi@mvt.bme.hu, bedzsula@mvt.bme.hu

Abstract: Customer oriented conduct and process-based thinking have become quasi-vital pillars of long-lasting competitiveness, for the business world today. Following this approach should result in satisfied customers, decreased costs and efficient employees. However, the leadership in higher education is just starting to learn this way of thinking. The increasing focus on quality issues and the process-related approach to this is catalyzed by several factors. For this reason, we have decided to take the analysis of a novel approach in higher education as the main topic of this study. The focus of our analysis is the organizational process of preparing the Scientific Students' Associations (SSA) conference; this conference is an indispensable element in the effective nurturing of talent. We used a questionnaire-based survey – which provided an in-depth analysis of the different elements of the SSA activities – to make proposals related to possibilities for improvement that could increase the satisfaction of university students.

Keywords: higher education; talent nurturing; process management; university student satisfaction questionnaire; quality improvement

1 Introduction

The quality of higher education has received growing attention in Hungary over the last couple of decades. This is similar to the experience in other European countries: higher education has become a mass market service, characterized by a growing number of students and increasingly distinctive institutions [1].

Simultaneously, with the transformation in higher education in Hungary, State support, for University Students, in social sciences and economic studies basically ceased to exist, resulting in students having to pay for their education. These issues have increased quality-related demands regarding both the content and the

supporting processes of education. In the meantime, the competition between institutions for students has also grown [2].

For these reasons, constant measurement and increases in efficiencies in student satisfaction have gained more traction [3]. An institution in the current Hungarian higher education system can best gain new students and keep its current base by achieving a suitable level of student satisfaction and actively managing the results. Several ranking processes also support this argument, as they put significant focus on measuring and documenting student satisfaction.

It has been proven that process-based organizational development could be the best practical solution for the efficiency increase mentioned above. Our paper aims to illustrate and prove the significance of this approach.

2 Literature Review

2.1 The Interpretation of Quality in Higher Education

Higher education is a service based on a special technology: the object of the technology is the student, and the one who implements it is the professor. [4] The final result of an education process that lasts for several years is that qualified students become professionals. This fact means that it is not easy to define the customer, but, in accordance with the approach that is nowadays widely accepted, we regard the student as the primary customer [5]. It is therefore, important to consider student feedback concerning the quality of the service provided by the higher education institution [6].

With respect to this special 'technology', education quality is the key issue for higher education. Crombag [7] divides this expression into two aspects: the efficiency of education (the time- and cost-efficient implementation of knowledge transfer) and the quality of graduates (the amount, depth and usability of the knowledge students have when they enter the labor market). This approach clearly implies that further factors, such as supporting administrative processes and infrastructural features, also have a significant impact on the quality of education.

2.2 Process-based Thinking

In order for organizational processes to work continuously and efficiently, different organizational features (i.e. 'enablers') are required, which Hammer [8] classified into the following five categories: creating a process model, following up on the process with numerical measures, preparing the implementers of the process, providing a process infrastructure and assigning a process administrator.

To implement these features successfully, in the long run, a wide-scale, strategic approach is necessary, which requires organizational culture change as a main element [9]. The process-based approach and process management have both become so widespread nowadays that it is difficult to imagine any quality management system that does not use them. The crucial features of the approach are also described by some of the principles defined by Hammer [10]:

- All work can fit into a process
- Any process is better than not having one at all
- Even a good process can be made better

A well-defined and regulated process structure serves as a starting point for further management activities, irrespective of the process management approach or process improvement principle that we use. A detailed mapping of the processes is an unavoidable task, as this will help us to get to know and understand how the company/organization works.

Recording the processes within the organization can be very advantageous: process procedures do not have to be invented, the responsibilities are clear for everyone, and the tasks are carried out – if careful considerations are applied – in an optimized way. There is usually serious resistance to change within an organization, but involving the employees in the changes and the creation of new systems, can positively affect the issues [11].

The examples set by foreign higher education institutions and in related domestic and international studies, however, increase the need for an institutional quality and process management environment [12]. Most of these institutions started to establish their own systems on an ISO, TQM and EFQM or ENQA basis, with some success. It is important to highlight the fact that the system models mentioned above all expect a process-based approach (the management of processes).

With regard to the characteristic features of higher education institutions, it is our view that a comprehensive implementation of the process management approach is also possible without relying on the systems briefly discussed above, as a result of that, the demand for efficient organizational work, which is the result of a lack of financing; customer orientation, which is more popular as the market size decreases (and requires, for example, clear, transparent, and consistent administrative measures) and supporting information systems become more pervasive, as a result of institutional developments.

2.3 Structured Measurement System

The approach based on process management related to quality improvement starts with process identification and the creation of a structured measurement system

based on this. Identifying the key elements and mapping their essential quality-related features are essential elements at this stage. Afterwards, quality indicators can be determined, the necessary measurements can be carried out and the results can be evaluated in order to identify the possibilities for improvement.

A quality indicator is a measurement index that provides information about past and present events and circumstances in a numerical form, to allow the measurement and evaluation of quality. It has to signal the deviating values, so that certain areas can become highlighted, for which a more in-depth examination and/or analysis is required. Quality-based indicators related to several levels of the higher education process, are necessary, in order to analyze the concept of quality, which is, effectively, too complex and unmanageable [13].

There are three different levels of quality indicators. Institutional/faculty indicators assist the work of the senior management. Quality indicators support operational decision-making, with the aim of measuring institutions' internal operations directly, and creating a basis for key indicators. Finally, there are also measurement units that help to evaluate and improve processes, and support the decisions of process administrators [14].

When it comes to improving domestic higher education institutions, it is worth starting from two sources: the systematically collected, wide-ranging and abundant data stored in IT systems and the feedback from satisfaction-related questionnaires. By performing a systemization, selection and evaluation of these data, we can establish quality indicators that are suited to the system-related requirements. Regularly analyzing these, in the long run, can help to track performance and to reach objectives in system improvement, and a comparison with other systems can also be achieved.

3 Case Study

In parallel to the increased mass marketing of higher education, nurturing talent still continues to be a strategic task of every higher education institution. As this mass marketing continues, we are convinced that it is of great importance to manage the process of nurturing talent according to scientific standards. The importance of the traditional master–student relationship is not to be neglected, although mass education requires other types of relationships, processes and methodologies, as well.

Our case study analyzes the process by which a Scientific Students' Associations (SSA) Conference of the Faculty and Economics and Social Sciences (FESS) at the Budapest University of Technology and Economics (BUTE) is organized.

The SSA conference is an important tool and opportunity for students to learn about new and interesting research areas beyond their direct everyday study activities and to enrich their professional experience. In this way, the SSA conference is also a quality-increasing tool that contributes to the increase in student satisfaction and the university's reputation. For this reason, an analysis of how the system works and how motivated the students are assists with the quality improvement practices of the faculty [15].

The organizing process is composed of several elements and a system built on these elements, but of course, it is also closely related to other educational and education-organizing processes regarding the nurturing of talent. The SSA itself is not suited to studying and supporting talent; for this, quality-oriented management of the whole educational-training process is necessary. The SSA activity is organized and managed by a faculty committee, at BME. We have collected their experiences in the field, after worked for several years within the faculty committee leadership.

3.1 Determining the Process

Drawing a flowchart is an excellent way of making a visual representation of a process and understanding its actions, activities and steps. By making the connecting points of each step in the process transparent, the flowchart can enable a flawless operation. For a flawless performance, an understanding and overview of the administrative processes that support education and the nurturing of talent in the mass market of higher education is essential.

For the University, the organization of an SSA conference is part of the basic research process, although it also contains several administrative elements. The process we analyzed was made up of a chain of events, starting from the first announcement of the conference and ending with the concluding steps after the award ceremony. We did not consider the connecting points to other processes, as we do not deal with these within this paper. The process is not logically complicated, and it is linear in terms of the structure. We considered the SSA Committee's decision about the date of the conference as the primary step. The core part of the process falls into a period of the first three months of the autumn semester. The main activities are the following:

- Spreading the call for the conference, advertising – organizers
- Registration the students (intention of participation, recording basic data and a summary, starting on 1st September) - organizers
- Preparing and submitting the papers - students
- Grouping the papers into sections, setting up commissions – organizers
- Preparing a program booklet – organizers

- Preparing for the presentation – students
- Organizing the conference and participating in the conference – students and organizers (typically organized in the middle of November)
- Administration concerning the results, data provision – organizers

The activities of students and institutional participants usually succeed each other during the organizing process, and the SSA secretary has a key role in these steps. A complex process diagram that contains all the tasks of everyone involved is too composite: it helps with an overview, but it is not particularly useful for clarifying personal roles. Thus, the responsibility circles are represented with pools and swimming lanes on the complex process diagram. Student satisfaction is the focus of our improvement, and the process has a significantly large number of participants in student-related roles. Therefore, we have prepared a simplified exhibit which only represents students' activities, thus keeping the connection points and putting the focus on the student 'lane'. The deadline for the activities was added on top of these, as that is the most critical element of the organization. For the preparation of the process diagram, we used a simplified version of the rules of BPMN (Business Process Model and Notation). Figure 1 shows a part of the process, prepared in ARIS Express.

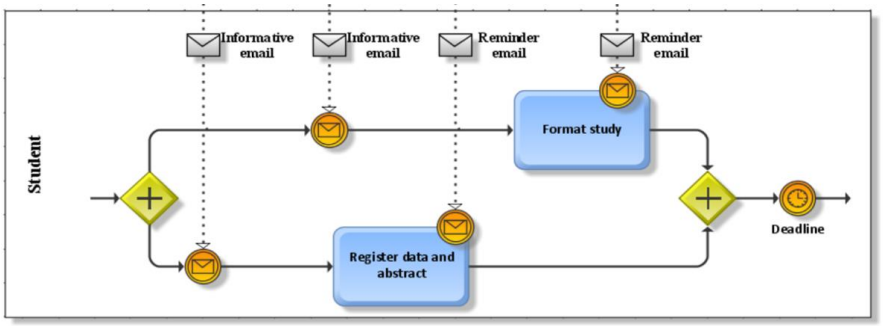

Figure 1
Part of the process diagram focusing on students

Information provision and deadline-related risks may arise at the level of the process steps. Transparent, detailed guides were prepared about certain tasks to mitigate these risks, and these were sent to the students in an email, as part of the steps for organizing the process. Additionally, as deadlines drew close, reminder emails draw the students' attention to carrying out tasks as soon as possible.

Further studies and research are possible in our view with the method of strategic technology road-mapping. This form of the method [16] could support both the process development in strategic analytical and marketing approach, and the visual systematization of the available information.

3.2 Identification of Measurement Indexes

Regarding the critical elements of the process, quality is a decisive factor for both the student and the institution, and quality can be ensured by performing certain tasks properly during the execution phase, in accordance with the deadlines. Although some steps and the whole process itself can only be effectively assessed after the conference, this assessment can still ensure that there is adequate preparation for the next year.

The following process indicators are examined: number of papers; number of applications after the deadline; number of papers submitted after the deadline; number of application-related technical problems; number of students pulling out of the competition, in proportion to the number of applicants, and proportion of prizewinners to participants; average number of students per supervising professor; proportion of SSA-participants in the latter PhD education; number and performance of students who were delegates to the National SSA Conference; and student satisfaction with the organization, infrastructural resources, and evaluations.

Some of the indicators can be determined from data extracted from the relevant administrative system, while some are measured with the help of a student questionnaire that is sent to students after the conference.

By using a web-based administrative system, a wide range of indicators can be measured. As an example, we present how three of them have developed over the last few years (Figure 2).

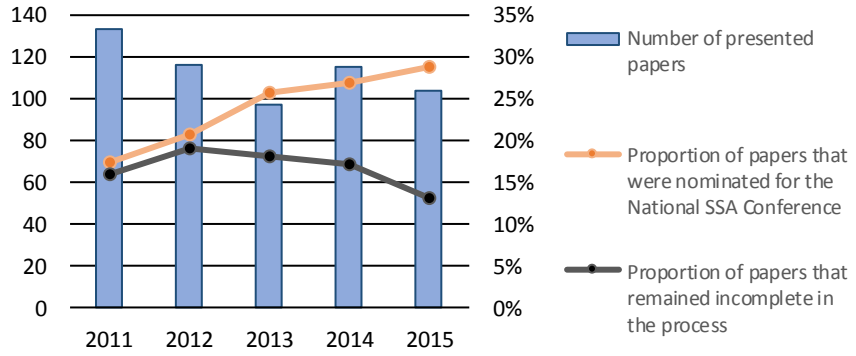

Figure 2
Development of measurement indexes in the last five years

A tendency can be observed in the decreasing number of papers. This is because the faculty has put a greater focus on the quality of the papers that can be submitted: authors have to come up with carefully composed work of their own.

During the conferences, we do our best to avoid using applicants who drop out during the preparatory period. To achieve this goal, we advise students to start their work in the semester prior to the conference, to plan their tasks and to make these tasks transparent. The number of papers submitted to the National SSA Conference has been constantly growing, over this period, as a result of a conscious decision to have as many faculty representatives and prizewinners there as possible.

We used the questionnaire method to collect information from the students involved. Our questionnaire (Figure 3) had the primary aims of assessing student satisfaction related to the important steps and to the significant actors in the process, collecting general feedback, and identifying improvement possibilities. As the process can be interpreted as a service provision, we used the ten service dimensions of Berry et al. [17] and the groups represented by the SERVQUAL model [18], to set up a list of questions for our questionnaire. Questions Q1-Q18 are all closed, process-related questions with positive content, which students evaluated using a four-level (1 – absolutely not, 4 – completely) scale. To inquire about the composite reputation of the conference, we applied the Net Promoter Score (NPS) method (Q19), which is also used in various service sectors to measure customer satisfaction. In practice, this means the evaluation of one simple question… 'What is the likelihood of you recommending the organization/service to your friends or colleagues?', on an 11-point scale [19]. We consider students' informal 'recommendations' of the SSA conference as a facultative program of great importance, and thus the method is worth applying. We also included three open questions (Q20-Q22) in the questionnaire, in order to make room for the formulation of individual and borderless opinions, and these questions covered the following: strengths, fields in need of improvement and additional feedback. It is an important goal at our faculty to include as many students as possible in the talent nurturing process of the SSAs, and therefore we also added some questions about student motivation and application circumstances (Q23-Q27): time of and reason for application [20], number of working hours spent on the SSA, relationship with the topic, and contact with the supervisor. We concluded the questionnaire with questions about the participants: their level of education and the faculty at which they were studying (Q28-Q29). In addition to the replies given to all these questions, we recorded one further piece of information about the responding students: the place they achieved at the conference (1st, 2nd, 3rd place, laude (4) or no place achieved (5)). They did not have to provide us with this information, as the questionnaires were sent out separately, in accordance with the five possible cases.

All the students who participated in the conference received a hyperlink to their contact email address directing them to the electronic questionnaire. One week was provided to fill it out.

To what extent do you agree with the following statements? (1 – absolutely not, 4 – completely)

1. Tasks and expectations related to the SSA conference were clear and easily understood.
2. The timing of the SSA conference was transparent and easy to plan against.
3. Tasks related to the SSA conference could be completed without any serious problem.
4. Instructions on the tasks to be completed and upcoming events were appropriate.
5. My supervisor was informed about the SSA to a necessary extent (general proceedings, some important information)
6. The faculty SSA's secretary was helpful and attentive.
7. Contact with the faculty SSA's secretary was appropriate (I could reach or could have easily reached him if needed)
8. The web portal gave effective help in the application process.
9. The program booklet contained all the essential and relevant information.
10. Presentational tools (e.g. laptops, projectors) were of appropriate quality and worked without any problems in our section.
11. I am satisfied with the venue (e.g. size, formation, location) for my section.
12. The commission for my section was well-prepared professionally and in how it dealt with the papers.
13. The commission for my section was objective and consistent in its work.
14. The final result and the prize-giving were professionally valid in my section.
15. The prize-giving ceremony was organized appropriately.
16. Overall, the conference was well-organized.
17. Participating in the conference was useful for me in a professional sense.
18. Participating in the conference was a positive experience for me.

NPS value (0 – absolutely not, 10 – I would recommend it absolutely)

19. On the whole, to what extent would you recommend the FESS SSA Conference to your fellow students?

Regarding the steps of the organizing process and the overall organization (open questions):

20. What did you like about the organization, the preliminary steps and the process of the conference?
21. What and how should we change to make the conference even better for next year?
22. What further comments or suggestions do you have about the conference?

Application-related questions (closed questions):

23. When did you decide to participate in the conference?
    1. One year prior to the conference, or earlier.
    2. In the spring semester just before the conference.
    3. In the summer directly before the conference.
    4. In the registration period of the conference.
24. How did you make contact with your supervisor regarding your SSA participation?
    1. You contacted a professor/supervisor, and it was your idea to participate.
    2. The professor/supervisor contacted you, and your participation was his idea.
    3. This cannot be clearly stated, as the idea and the getting in touch were mutual.
25. How was the decision for participation made?
    1. You chose to do research in a field that you were already acquainted with, using the help of a supervisor or professor that you had known from an earlier course.
    2. You chose to do research in a field that was completely new for you, using the help of a supervisor or professor that you had known from an earlier course.
    3. You chose to do research in a field that was already somewhat known to you, using the help of a new, unknown supervisor or professor.
    4. You chose to do research in a field that was completely new for you, using the help of a new, unknown supervisor or professor.
26. How much time did it take for you in total to write your paper?

27. To what extent were the following factors important for you when applying? (closed questions, on a four-point scale: 1 – absolutely not, 4 – completely)
    a presenting the results of academic work you had previously conducted
    b getting to know an interesting problem/field of science
    c enjoying the experience of conducting research
    d developing my presentation skills
    e preparing for my thesis or diploma project
    f earning bonus points to continue my education (for a Master's or PhD degree)
    g achieving professional success and recognition
    h earning bonus points for a scholarship (professional, international, university or faculty)
    i getting the financial reward related to prizes

Information about the responding student:

28. What is your level of education? (Bachelor or Master)
29. Which faculty are you studying at?
30. Your placement (1st, 2nd, 3rd, laude, no place achieved: each of them filled out different questionnaires)

Figure 3

The questions of the questionnaire

We have been collecting student feedback for years, after the end of each conference. The feasibility of this project has become more and more composite and complex over the years. In this study, we assess the results for the years 2014–2015, which are shown in Table 1.

Table 1

The data related to the satisfaction questionnaires in 2014 and 2015

	2014			**2015**		
Position	**Participants**	**No. of students who filled it out**	**Ratio**	**Participants**	**No. of students who filled it out**	**Ratio**
Winner	26	12	46%	20	10	50%
Runner-up	22	9	41%	22	14	64%
3rd place	20	10	50%	17	8	47%
Laude	19	9	47%	11	7	64%
No place achieved	40	15	38%	40	9	23%
Total	**127**	**55**	**43%**	**110**	**48**	**44%**

Using the data from the table, the totaled response rates of 43% (2014) and 44% (2015) show that the responses we collected enable us to make some deductions for quality improvement.

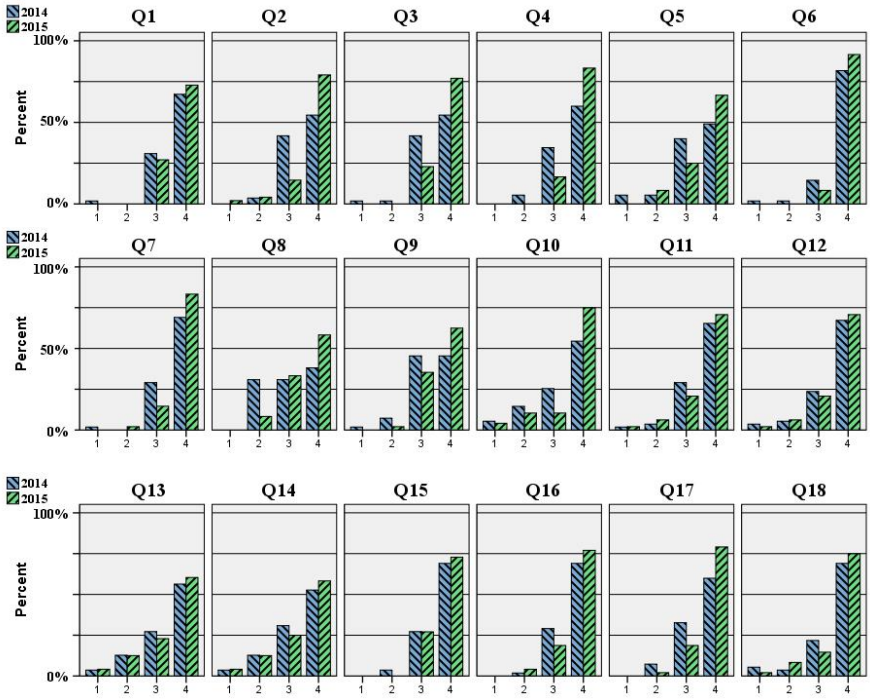

Figure 4
The results for questions Q1–Q18 in the two years that were assessed

Table 2
Aggregated results (2014 and 2015)

	Q1	Q2	Q3	Q4	Q5	Q6	Q7	Q8	Q9
Mean	3.73	3.71	3.77	3.81	3.58	3.92	3.83	3.50	3.60
Std. Deviation	0.449	0.651	0.425	0.377	0.647	0.279	0.445	0.652	0.536

	Q10	Q11	Q12	Q13	Q14	Q15	Q16	Q17	Q18
Mean	3.56	3.60	3.60	3.40	3.38	3.73	3.73	3.77	3.63
Std. Deviation	0.848	0.707	0.707	0.869	0.866	0.449	0.536	0.472	0.733

The histograms in Figure 4 and the statistical properties of Table 2 clearly show that the participants were basically satisfied with the process and the organization of the conference in both the years being examined. However, it can also be noted that areas of improvement can be identified with the help of this questionnaire and the ranking numbers related to it. Based on the numerical means for the results that were obtained from the ranking scales from the cumulative data for the two

years, Q6 (mean: 3.92) and Q7 (mean: 3.83) are exceptional fields, marking the distinctive role of the SSA Committee's secretary. Q4 is a field with a similarly high mean (3.81), signaling good results in communication and the provision of information. Q13 (mean: 3.40) and Q14 (mean: 3.38) clearly have some room for improvement, as their results demonstrate that the different commissions for each professional section make their decisions in a slightly different way, using evaluation and assessment criteria systems that are not very transparent for students. Examining the mean values mentioned above is also necessary because the deviations related to them are much smaller.

Above and beyond the descriptive statistical presentation, the questions regarding quality improvement can also be analyzed. As the histograms from the figures already show, there are some differences in the results for questions Q1–Q18 between 2014 and 2015. The homogeneity test can help describe these with mathematical-statistical tools. It is known that the Mann–Whitney test can be used as such a homogeneity test for the case of ranked numbers [21]. This test works with the hypothesis that two samples come from an identical population. If this can be proved, then there is no significant deviation for the results of the two years; otherwise, the results of the quality improvement can be clearly confirmed.

When making an individual analysis for each of the two years for the questionnaire questions related to conference organization, the Mann–Whitney test shows a significant improvement in the areas indicated in Table 3. This improvement is confirmed by the fact that the p values show an exceptionally low significance level, making the initial hypothesis unacceptable as there is a significant difference between the two populations.

Table 3

Questions showing differences for the two years (2014 and 2015)

Question	Q2	Q3	Q4	Q8	Q17
Mann-Whitney	$U = 1023.5$ $p = 0.018$	$U = 1011.5$ $p = 0.014$	$U = 1000.0$ $p = 0.007$	$U = 952.0$ $p = 0.008$	$U = 1058.0$ $p = 0.032$

The significant differences are not accidental. From the experience recorded in 2014, the SSA Committee of the faculty, its president and its secretary carried out important and conscious changes in the management of the application process, and also in the field of informative and reminder-related communication. The website of the conference was renewed to a significant extent for the whole university: important changes were made to it in regards to both its content and its structure. These results are essentially due to the successful identification of process elements that particularly contributed to an increase in student satisfaction.

As we have already indicated, the NPS method can be particularly helpful in analyzing the process of the SSA conference, as it is used to assess customer

satisfaction for several service-based processes. We therefore categorized the replies we received, using the NPS methodology, thus, based on the replies, differentiating between a category of detractors (those who would not recommend the conference) who gave values between 0 and 6, a passive category for those who gave values of 7 or 8 and a category of promoters (those who would recommend the conference) for those who gave 9 or 10. Calculating the final result is also simple: the percentage of detractors is subtracted from the percentage of promoters, which leads to the NPS index. [19] The NPS values, calculated from the results for the answers given to the question 'On the whole, to what extent would you recommend the FESS SSA Conference to your fellow students?' (Q19), confirm the positive reputation of the conference:

- NPS value in 2014: 44% (40%+15%-5%-2%-4%)
- NPS value in 2015: 67% (58%+17%-2%-6%)

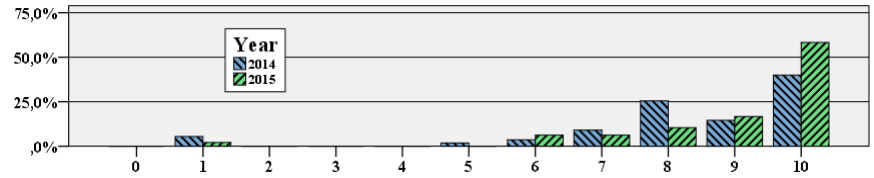

Figure 5
Results for question Q19

Based on the values from the two years, there is a clear improvement in the reputation of the conference. Along with the NPS methodology, the Mann–Whitney non-parametric test can also be used to assess the improvement related to question Q19. This test, comparing the ordinal values for the two years, again points out that the results cannot originate from the same population ($U = 1044$, $p = 0.051$).

The relations between certain questions can be analyzed using several different combinations, the results of which may then further perfect or slightly alter previous findings. In our case, it may make the most sense to examine whether there is any relationship between the position achieved and the cumulative evaluation of the conference (NPS). We carried out the analysis based on the cumulative data for 2014 and 2015. By using a cross-tabulation analysis, we examined both the position (Q30) and the cumulative evaluation (Q19) as ordinal variables. As the cross-tabulation based on the variables is asymmetric (5 categories for position, 11 categories for evaluation), the results for Kendall's tau-c measure, which is 0.235 in our case, are determinative. This indicates a weak relation with a reverse ratio, meaning that those who achieved a better position (those with a lower number) gave a better evaluation of the conference (a higher value).

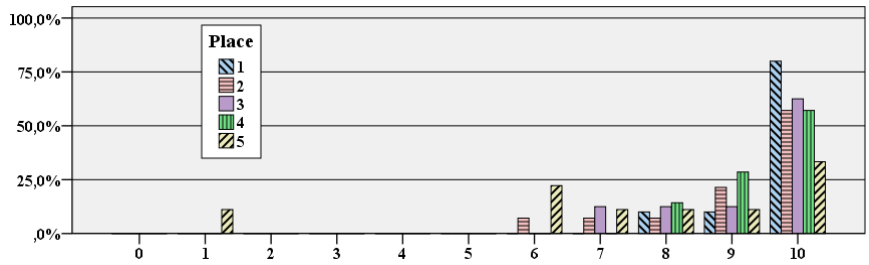

Figure 6
The relation between the cumulative evaluations (Q19) and the placement (Q30)

From the assessment of the achieved positions and certain questions it is worth highlighting the two with the worst results (Q13, Q14), which relate to the evaluation of the commission and the final result within the section. We carried out the analysis based on the cumulative data for 2014 and 2015, in a similar way to the process presented above: an asymmetric cross-tabulation was obtained from the variables (5 categories for position, 4 categories for evaluation), and the results of Kendall's tau-c measure, which are -0.260 for Q13 and -0.370 for Q14, are determinative. This indicates a moderate relation with a reverse ratio, so that those who achieved a better position (those with a lower number) gave a better evaluation for the relevant questions (they gave a higher value). This observation further supports our previous arguments: the work of commissions has to be made more transparent and clear for the students.

With the help of students' answers given to the open questions (Q20-Q22), we get an overview about the areas and features of the conference that can be identified as strengths or in need of improvement. This feedback is also important because solutions to the problems may also be recommended by the respondents. When analyzing the outcomes for previous periods, we can show that the results to the closed questions in the satisfaction assessment are supported by the answers to the open questions.

SSA conference is the significant way of nurturing talent in higher education and when considering its long-term possibilities for success, it is essential to assess how the students make contact with their professors and supervisors. It is for this reason, that we composed questions Q23, Q24 and Q25 in the questionnaire. The diagrams in Figure 8 show the cumulative results for two years. These diagrams clearly show further potential for improvement. The results for question Q23 (the diagram on the left) imply that almost 50% of the students only decided to participate in the conference (4 response options) a few weeks before the event. This demonstrates that student–professor links are missing for these students, when such links could guide the students much earlier and in a more conscious way in order to achieve better results. Question Q24 (the diagram in the middle) also shows similar results, as a significant number of the students indeed made

contact with their supervisors on their own, and it was not the professors who guided their students (the first response option). The results from question Q25 (the diagram on the right) clearly draw our attention to the fact that the talent nurturing process goes beyond the activities related to the SSA conference, as a clear majority of students decided to participate in the conference on the basis of their earlier study experience and their ties to professors (first response option).

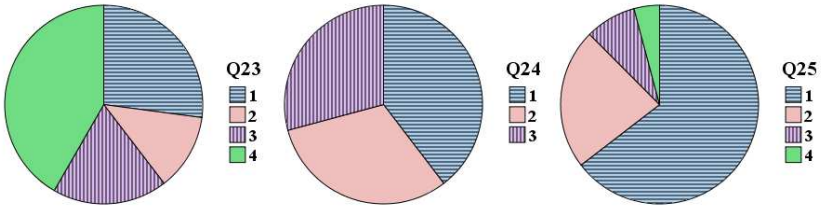

Figure 8
Results for questions Q23, Q24 and Q25

As we have already shown in previous examples, the correlation between the individual answers can also be assessed for this group of questions. We used the cumulative data from two years to analyze the relationship between questions Q23 and Q25, and we assessed both of them as nominal variables, with the help of cross-tabulation. The significance level of the Pearson Chi-Square is 0.028, and we therefore reject our hypothesis about the independence of the two variables, meaning that there is in fact a relation between the two variables. The Cramer V associative measurement index shows the strength of the correlation between two nominal variables, and this is a number lying between 0 and 1. In our case, it is 0.380, indicating a weak-moderate correlation. When analyzing the cells of the cross-tabulation we find that the applicants who applied in the registration period usually did so, on the basis, of an earlier topic and having a supervisor they had previously known.

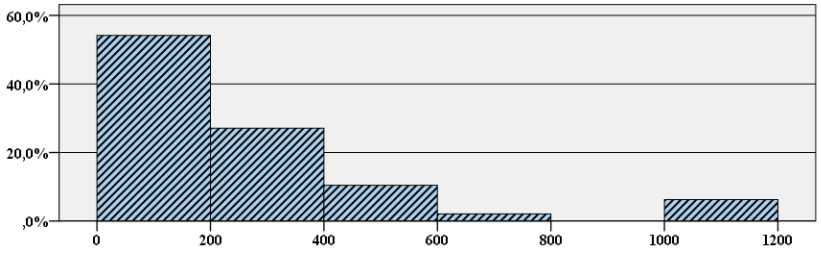

Figure 9
Results for question Q26

The results for question Q26, in the same way as before, also draw our attention to the fact that talent nurturing has great importance in all phases of the education

process. Figure 9 shows that the number of work hours spent on writing the paper is not significant for the majority of the students. It is our belief, and it also matches our previous findings, that this is not the real result, because a lot of students link their SSA conference preparations with their earlier and current tasks related to their project-based education. At our faculty, students spend a significant number of work hours carrying out different project tasks for external institutions, besides their SSA activities. These tasks also serve as a basis for theses or diploma plans later on. They are required to compose written reports and presentations about the tasks, and these can be effectively used when preparing the SSA conference paper. Tasks related to quality improvement for the future are also present in this area, as professors and supervisors of such project tasks need to realize this fact and be encouraged to combine project-based teaching and the SSA activities during their students' studies.

An interesting correlation is shown when analyzing the relationship between question Q26 and the position achieved. To assess this, we treat the self-admitted work hours as a (numerical) variable that can be measured on a ratio scale, while the position is regarded as an ordinal variable. Thus, we can analyze the relationship between the variables using one-way variance analysis (One-way ANOVA). Before doing this, it is worth checking whether the groups assigned by the ordinal variable have the same dispersion within the group. In our case, we proved this successfully, using the Levene test: $F=0.237$, $p=0.883$. According to the F-test of ANOVA, the null hypothesis, claiming that the group means assigned by the ordinal variable are equal, needs to be accepted ($p=0.883$), so the position achieved is independent of the admitted work hours. As for the results of our previous analyses, we believe this to be the reason for the latent talent nurturing already mentioned.

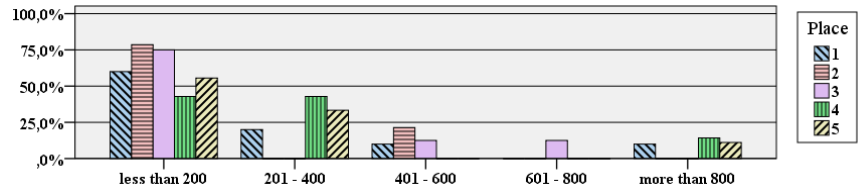

Figure 10

The correlation between the number of work hours (Q26) and position

Using our questionnaire, we can assess the situation relating to the evaluation of the SSA sections, which has been a problem ever since the introduction of multi-cycle education: if Bachelor and Master students who are competing against each other are evaluated in the same way, is it the Master students with more professional knowledge who win prizes more often? To assess this question, we again took the results from 2014 and 2015, as the basis. We analyzed the ordinal variables for position (Q30 – 5 categories) and level of education (Q28 – 2 categories: Bachelor and Master Students) with the help of a non-symmetrical

cross-tabulation method. The value of Kendall's tau-c measure is -0.305. This indicates a moderate relation with a reverse ratio, so those who achieved a better position (a category with a lower number) are more likely to be Master students (a category with a higher number). This result means a new task for quality improvement. Although it is a constantly emphasized expectation of the SSA Committee that each commission evaluates everyone equally, in accordance with the quality of their education, Figure 11 still shows that this is not so in reality. Therefore, if it remains impossible to organize separate sections for Bachelor and Master Students, we will have to keep up our strong efforts regarding the evaluations.

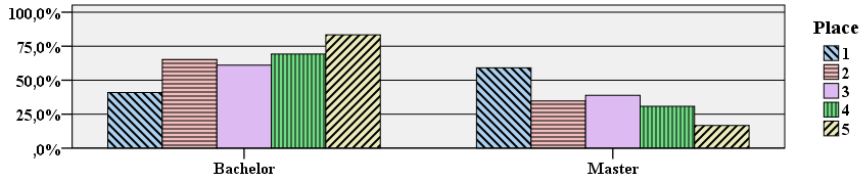

Figure 11
The correlation between the level of education (Q28) and position

Question Q27 analyses students' motivational viewpoints. Nine reply options (Q27a-Q27i) were identified, using student feedback from previous years. Figure 12 shows the cumulative results for the two years. Concerning the objectives of nurturing talent, the results are comforting, as the students are primarily motivated by enjoying the experience of conducting research (Q27c, mean: 3.39), getting to know an interesting problem/field of science (Q27b, mean: 3.37) and achieving professional success and recognition (Q27g, mean: 3.37), and they are not particularly motivated by the financial reward of the prizes (Q27i, mean: 1.87) or earning bonus points for a scholarship (professional, international, university or faculty) (Q27h, mean: 2.32). These results are similar to findings of Bérces' former studies [20].

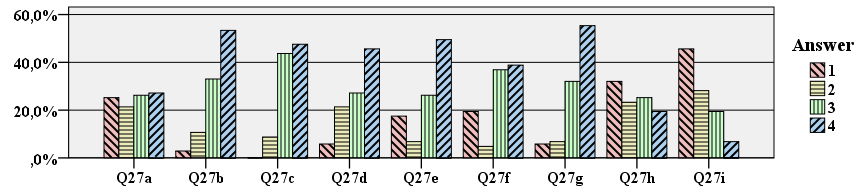

Figure 12
Students' motivational reasons (Q27)

Conclusions

Identifying processes and setting up a measurement system based on these processes makes it possible to carry out quality improvement using a process

management approach. This argument is supported in our case study, in which we analyzed the organizational process for the Students' Scientific Association Conference at the Faculty of Economic and Social Sciences of the Budapest University of Technology and Economics. Since student satisfaction was the focus of quality assessment, we identified the process based on this and we used the simplified rules of BPMN modeling and the ARIS Express software to prepare a flowchart. This step was followed by identifying measurement indexes and process indicators. Based on data from previous years, we provided numerous examples of how indicators, that were either available in the administrative systems or were retrieved from the results of the questionnaire, could be analyzed. The SPSS program was used for mathematical/statistical analyses.

Finally, we found that a process management approach and methodology can be an excellent choice, when it comes to quality improvement in higher education processes. Process identification, choosing indicators, completing related measurements and designating quality improvement actions, can all be applied in the case, of any fundamentally important, higher education process.

References

[1] Finna H., Erdei J. (2015): "Qualification as a Success Factor in the Labor-Market: The Faculty-Specific Attributes of the Employment of the Budapest University of Technology and Economics Recent Graduates", Acta Polytechnica Hungarica, Vol. 12, No. 8, pp. 135-154

[2] Tóth Zs. E., Jónás T. (2014): "Enhancing Student Satisfaction Based on Course Evaluations at the Budapest University of Technology and Economics", Acta Polytechnica Hungarica, Vol. 11, No. 6, pp. 95-112

[3] Helgesen, O., Nesset, E. (2007): "What Accounts for Students' Loyalty? Some Field Study Evidence", International Journal of Educational Management, Vol. 21, No. 2, pp. 126-143

[4] Veress, G. (1999): "A felsőoktatási intézmények minőségmenedzsmentje", (Quality Management in Higher Education Institutions) Budapest: Műszaki Könyvkiadó

[5] Munteanu, C., Ceobanu, C., Bobalca, C., Anton, O. (2010): "An Analysis of Customer Satisfaction in a Higher Education Context", International Journal of Public Sector Management, Vol. 23, No. 2, pp. 124-140

[6] Yusoff, M., McLeay, F., Woodruffe-Burton, H., (2015): "Dimensions Driving Business Student Satisfaction in Higher Education", Quality Assurance in Education, Vol. 23, Iss. 1, pp. 86-104

[7] Crombag, H. (1978): "On Defining Quality of Education", Higher Education, Vol. 7, No. 4, pp. 389-403

[8] Hammer, M. (2007): "The Process Audit", Harvard Business Review, Iss. 85, pp. 111-123

[9] Rosemann, M. & vom Brocke, J., (2010): "The Six Core Elements of Business Process Management", In: Brocke, J., Rosemann, M. (Eds): Handbook on Business Process Management 1. Heidelberg: Springer-Verlag, pp. 107-122

[10] Hammer, M., (2010): "What is Business Process Management?", In: Brocke, J., Rosemann, M. (Eds): Handbook on Business Process Management 1. Heidelberg: Springer, pp. 3-16

[11] Hung, R. Y. (2006): "Business Process Management as Competitive Advantage: A Review and Empirical Study", Total Quality Management, Vol. 17, pp. 21-40

[12] Csizmadia, T. (2006): "Quality Management in Hungarian Higher Education", Czech Republic: UNITISK

[13] Bedzsula, B., Dénes, R., Topár, J. (2015): "Mérőszámok szerepe a társadalmi szolgáltatások minőségfejlesztésében", In: Veresné Somosi Mariann, Lipták Katalin (Eds): "Balance and Challenges" IX. International Scientific Conference 2015, Miskolci Egyetem Gazdaságtudományi Kar, Miskolc, pp. 140-154

[14] Bedzsula, B., Topár, J. (2014): "Minőségmenedzsment szemlélet és eszközök szerepe a felsőoktatás fejlesztésében", Magyar Minőség, Vol. XXIII, No. 3, pp. 34-47

[15] Finna, H. (2012): "Enhancing Employment and Motivation Opportunities of Recent Graduates with the Help of Atypical Solutions", In: Topár J. (Ed): Relevant Issues in Engineering Management, Technical Publishing House Ltd., Budapest, pp. 243-259

[16] Bíró-Szigeti, Sz. (2014): Strategy Support of Residential Energy Saving Investments in Hungary with the Method of Technology Roadmapping. Acta Polytechnica Hungarica, Vol. 11, No. 5, pp. 167-186

[17] Berry, L., Parasuraman, A., Zeithaml, V. A. (1985): "A Conceptual Model of Service Quality and Its Implications for Future Research", Journal of Marketing, Vol. 49, No. 4, pp. 41-50

[18] Berry, L., Parasuraman, A., Zeithaml, V. A. (1988): "SERVQUAL: A Multiple-Item Scale for Measuring Consumer Perceptions of Service Quality", Journal of Retailing, Spring, Vol. 64, Iss. 1, pp. 12-40

[19] Reichheld, F. (2003): "The One Number you Need to Grow", Harvard Business Review, Vol. 81, No. 12, pp. 46-54

[20] Bérces, R. (2015): "The Improvement of Higher Education Quality and Talent-Nurturing with Scientific Students' Association (SSA) Commitment", Acta Polytechnica Hungarica, Vol. 12, No. 5, pp. 101-120

[21] McCrum-Gardner, E. (2008): "Which is the Correct Statistical Test to Use?", British Journal of Oral and Maxillofacial Surgery, Vol. 46, pp. 38-41

Exploring the Contribution of a Changing External and Internal Organizational Context to the Innovation of Large Organizations

Slavica Tomić, Maja Strugar Jelača, Agneš Boljević

University of Novi Sad, Faculty of Economics Subotica, Department of Management, Segedinski put 9-11, 24000 Subotica, Serbia

e-mail: tomics@ef.uns.ac.rs; m.strugar.jelaca@ef.uns.ac.rs; aboljevic@ef.uns.ac.rs

Abstract: The aim of this study is to establish the relationship between the degree of an organizations' innovation and external dimensions, taking into account the dynamics of fluctuations from the environment together with the characteristics of organizations, implemented incremental management innovations and realized business results. The object of the research is the analysis of a changeable contextual frame of innovation in large organization systems. While doing the research, we observed the performance of large organizational systems during 2012 and 2013, depending on the fluctuations of external and internal factors that influence innovation. A random sample of 50 large organizational systems, in the territory of the Republic of Serbia was used, which represents 5% of the base number and covers all regions and business sectors. During the testing of set hypotheses, we used the following statistical methods: ANOVA, MANOVA, and the Kruskal-Wallis tests. The research results indicate the existence of the difference in innovation degree, depending on consumers' preferences, as external dimension and number of employees, values of operating income and operating assets as internal dimension, as well as, a statistically significant correlation between entrepreneur-oriented managerial behavior as an aspect of management innovation and organizations' innovation.

Keywords: contextual perspective; institutional changes; entrepreneur-oriented managerial behavior; organization's innovation

1 Introduction

Innovation is of fundamental importance for improving organizational performance and the very survival of an organization [13, 42]. It also represents a necessary and natural part of modern business concept in order to make maximum

use of the positive changes that lead to progress and development at the level of organizations, state and society. The research focuses on the impact of turbulent developments, from the external environment, on the degree of organizations' innovation, as well as, the influence of changing internal organizations' context through characteristics of organizations and implemented incremental management innovation, such as, the application of entrepreneurial-oriented managers' behavior, at the level of observed organizations. Management innovation is the difference in the form, quality, or state over time of the management activities in an organization, where a change is a novel or unprecedented departure from the past [24, 49] of an organization or the whole business sector. Until now, this type of innovation was analyzed from different aspects [23, 29, 48], but it still represents an insufficiently analyzed empirical category [6, 39] which should not be neglected due to positive effects it has on business performance. Such poor attention of public research aimed at innovation in management is unjustifiable. Today, in the modern business environment faces a transition from a knowledge based economy, to an economy based on creativity. This raises the necessity of implementing novel innovations, to insure organizations can still be leaders in the market [11, p. 17]. As such, innovation in management is a significant driver of efficient and effective business based on the application of new ways of doing business which results in the growth of business performance [6, 23] and maintains a competitive advantage.

The orientation of the research is focused on identifying the external and internal context of major organizational innovation systems within the territory of the Republic of Serbia. The external context is analyzed through the impact of turbulent competitive developments, technological progress, changes concerning consumers and legislation. This is one of the possible classifications of external factors according to Bourgeois and Eisenhardt (1988). The internal context of innovation is seen through an implemented incremental management innovation, such as, entrepreneurial-oriented management behavior. With the proper institutional framework in place, the necessary incentives are created in order to foster productive entrepreneurial activity which, then, in general, serves as a catalyst to greater long-term growth [18, p. 73]. The difference between levels of innovation within organizations that belong to the sector of large organizations was also observed from the perspective of selected characteristics, such as: number of employees, the amount of operating income and operating assets.

Emphasis was placed on large organizational systems because theory and practice, in terms of business innovation, have at been given precedence, to small and medium-sized organizations and only more recently, to large business systems. Large organizational systems whose operations are geographically dislocated have global access to information and resources, which provides a basis for innovative ideas and enables usage of more modern equipment and greater expertise. On the basis of various theoretical points of view, some of the criteria in favor of greater innovation within large organizational systems [4, p. 134], [41, p. 213], [44, p. 3]

are: Investment into research and development activities in proportion to the growth of organization; as the organization grows, research and development productivity grows thus accordingly; higher return on investment within those organizations whose fixed costs of innovation are allocated to higher sales volumes; lower risk regarding the implementation of innovative activities; possibility of applying economies of scale and width during innovation production. However, some studies suggest a more frequent failure in attempting innovation implementation within large organizations, often leading to engagement of consulting organizations that carry out market analysis, identify new or unmet needs, generate promising ideas and transform them into working prototypes [2].

2 Literature Review

Innovation in a broader sense represents a profitable use of novelties in the form of new technologies, products and services, organizational, technical and socio-economic solutions [32, p. 6], as well as, challenges from the environment. That emphasizes the importance of the interaction of innovative activities of an organization within the environment, as the use of external sources leads to the implementation of new concepts of creativity and know-how in organizations [34, p. 528]. Lately, greater attention has been devoted to the role of management as a rational category in the implementation of innovation, because they lead to higher productivity, better quality of satisfaction of clients' needs [26, 37], growth efficiency, effectiveness, and achievement of sustainable performance, in order to achieve long-term competitive advantage. Therefore, we can introduce a new category of open management innovation that will enable systematic encouragement of research and a wide range of internal and external sources of innovation opportunities, integrating them with capabilities of the organization and widespread usage of these possibilities, using a number of communication channels [52, p. 377].

From the perspective of innovation, management activity can be seen as a process for creating innovation throughout the whole chain of operations at the micro and/or macro levels, which allows participants, individuals, entrepreneurs and organizations to produce specific and novel results [36, p. 6]. Coordinating creative and productive resources is necessary during this process, including financial resources, technological artifacts and human/social capital [17]. The goal is to create organizational systems that support cooperation and learning, to implement management practices focused on business processes based on continuous improvement of products, services, processes and employees' accomplishments, aiming at customer satisfaction and organizations' survival [3, p. 473].

Innovation in management can be defined as the process of generating and implementing management practices, processes, structures and techniques that are new and focused on improving organizational goals [6, p. 829]. Throughout the process of style transformation and the fundamental principles of contemporary business management, organizational changes are implemented into existing or new operational and production activities [31]. This leads to the formation of a new business model with the goal of successful conversion of existing input into the desired output while taking time, cost and quality into account. Within their management system, organizations can implement organizational changes of greater or lesser degree of innovation through implementing incremental innovation in order to keep the current vitality of an organization, and radical ones with the aim of achieving business vitality in the future [16]. Convergent changes lead to minimal changes in business management, similar to the way it was done in the past, while the revolutionary ones imply parallel changes in strategy, structure, systems and culture of the organization, leading to a radically new way of doing business [5, p. 4]. According to Lambić [30, p. 146] revolutionary changes in organizational activities can result in the introduction of new production processes and new ways of creating original technologies and products. The ultimate goal of these changes is the implementation of a new business model, which means finding new business logic and creating new value for stakeholders through income generation and eventually defining new propositions for consumers, suppliers and business partners [9, p. 464].

In order for organizations to survive in today's business environment, they must constantly innovate in their practices and business behaviors [38, p. 291] through the implementation of entrepreneurial management perspectives. This involves radical changes and demands innovation and creation, either bringing an entirely new market into existence or enhancing an existing market in a significant way [46, p. 160]. Organizations cannot be successful, in the long term, without people who possess the characteristics of entrepreneurs; also, organizations cannot be successful if individuals are entrepreneurial, but the conditions within the organizations are not established, to promote entrepreneurship or even hinders the entrepreneurial actions of employees [19, p. 128]. The main task of a manager is to establish a strong organizational culture for implementation of internal innovation, which is possible through promotion of continuous learning and establishing new views that encourage formal and informal collaboration of employees [15, p. 359]. Innovative organizational culture needs to encourage team spirit as well since organizing employees into teams enables them to widen their skills and perspectives, encourages the emergence of common ideas and common responsibility which leads to successful transformation of ideas into new products [8]. An entrepreneurial-minded manager needs to establish a sustainable work environment where employees can meet the obligations and objectives set by the principle of collaboration [1, 40, 45]. This is done for the sake of forming the information base by creating social networks that use successful information processing [28, p. 200] as a platform for making optimal decisions. Managers

need to make business decisions that are going to meet situational changes; they have to accept the contradictory forces of the environment and take them into consideration, which points to the compilation of a broad base of information. This database can be characterized as complex, as it includes a large number of quantitative, qualitative, financial and non-financial information [22, p. 470], which is mutually differentiated and may lead to different interactions, to new combinations that form alternative decisions. Thus, one has to choose sources carefully and know how to make optimal decisions that will include novelties in business management.

3 Research Methodology

The research was conducted by application of the questionnaire method. The questionnaire consisted of three sections with a total of 37 questions concerning fluctuations from the external environment, entrepreneurial-oriented behavior of managers and innovation within organizations. Within each part of the questionnaire, there were questions in the form of statements, to which the management was required to respond expressing the degree of agreement with the aforementioned statements, according to the Likert scale, from 1 to 5. The first part of the questionnaire is a set of customized questions about the analysis of turbulent external environment [7]. The second part includes a scale of the entrepreneurially oriented behavior of managers, which is structured on the basis of different authors on managers' innovative behavior [10, 25, 27, 47, 51]. The last part of the questionnaire includes a scale for the assessment of organizations' innovation, which was examined through a number of innovations that the organization accepted and produced [13, 21, 43]. Reliability of the statements was analyzed by the Cronbach's Alpha coefficient. The value of this coefficient for the questionnaire is 0.8, indicating the very good reliability of the scale, as well as the very good internal coherence of the statements in the questionnaire because the acceptable value of this ratio is above 0.7 [35].

In addition to using the information base created through the questionnaire method, the data from financial statements for 2012 and 2013 were compared in order to analyze the existence or non-existence of differences in the degree of innovation depending on the number of employees, values of operating incomes and operating assets, as well as the development trend of the mentioned variables.

We interviewed the management of organizations categorized as large legal entities in the Republic of Serbia. According to the Law in Accounting and Auditing (Official Gazette of RS, no. 46/2006, 111/2009, 99/2011, 062/2013), [50] large legal entities are considered to be the ones that meet at least two of the following criteria on the date of giving their financial statements: 1) the average number of employees in the year for which the report is submitted is over 250; 2)

the annual revenue exceeds 10,000,000 euros, equivalent in dinars; 3) the average value of operating assets is over 5,000,000 euros, equivalent in dinars.

The target group was managers of different levels, who we define as individuals on a formal position who are responsible for the work of other employees and the usage of resources, mainly financial [12, p. 264]. Questionnaires were distributed to the e-mail addresses of the management of 70 large legal entities in the Republic of Serbia and we obtained the responses from the management of 50 large organizations.

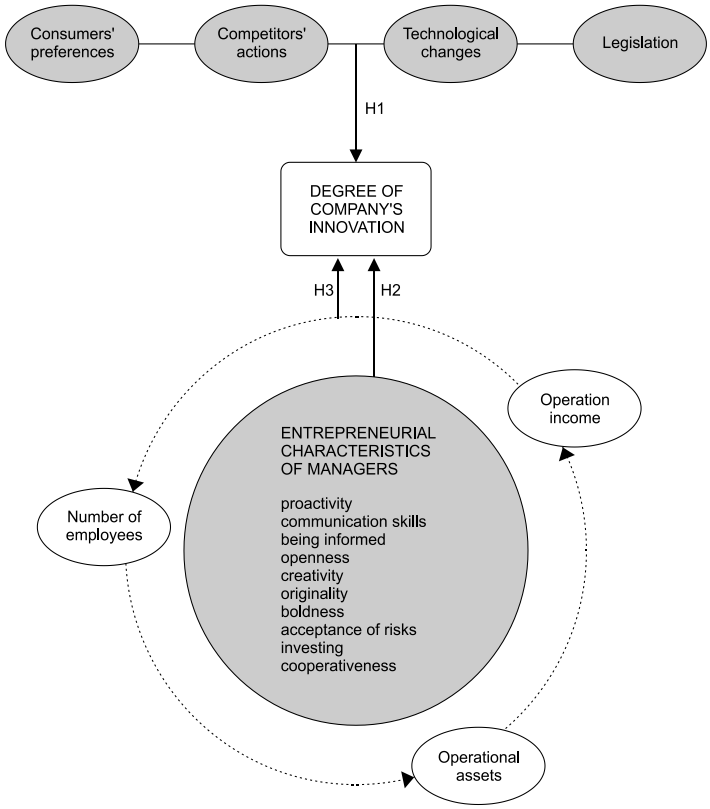

Figure 1
Conceptual framework

Based upon the ruling attitudes in this area and the research orientation that was set, a conceptual framework of the research was formed and these hypotheses:

H1: *There is a difference in the degree of innovation of large organizational systems depending on the fluctuations of external factors.*

H2: *Entrepreneurial nature of managing behavior positively affects the degree of innovation of large organizational systems.*

H3: *A higher degree of innovation is present in large organizational systems with a higher average number of employees and greater value of annual revenue and business property.*

Parametric and non-parametric statistical methods were used when testing the previously set hypothesis, using the software package, SPSS 20.0. The first hypothesis was tested by MANOVA. Testing of hypothesis H2, was conducted using the correlation analysis of Spearman coefficient of ranking. Finally, the last hypothesis was tested by a combination of ANOVA and the Mann-Whitney test.

4 Empirical Results

We carried out the analysis of turbulent changes in external factors that determine institutional business framework and influence organizations' innovation. The difference in innovation depending on the influence of external factors, both isolated instances and those interacting were analyzed by MANOVA.

Table 1
Multifactor analysis of variance

Fluctuations of external factors	Type III Sum of Squares	Df	Mean Square	F	Sig	Partial Eta Squared
Consumers often change their preferences within your line of work	16.637	3	5.546	2.893	0.124	0.591
Your consumers tend to constantly seek new products or services	28.667	2	14.333	7.478	**0.023**	0.714
Competitive environment is turbulent within your line of work	0.500	2	0.250	0.130	0.880	0.042
Technology changes in industry are significant	6.184	3	2.061	1.076	0.427	0.350
Within your line of work innovative activity is regulated by laws, which often change	9.955	3	3.318	1.731	0.260	0.464

Source: Authors' analysis

Individually observed, the impact of every external factor on the innovation of organizations has pointed out that statistically significant effects on innovation are caused only by the consumers who constantly strive to find new products and services (F=7.478, Sig.=0.023). The magnitude of the impact is measured by the Partial Eta Squared coefficient. According to the Cohen's criterion [20], the size of

the resulting coefficient speaks about the great influence of consumers who constantly strive to find new products and services on innovation (coefficient greater than 0.14, and is 0.714). Large organizational systems which cater for a group of consumers constantly strive to purchase new products and services do innovate more than the organizational system which serves consumers whose needs and wishes do not change very often. By introducing new products in accordance with unmet customer needs, the company is gaining customers' confidence, necessary for company's market success [14]. When conducting subsequent Tukey HSD test, surveyed large legal entities are divided into five groups, i.e. organizations which consider the claim that their customers tend to constantly find new products and services to be: true, partially true, neither true nor false, partly false and false.

Table 2

The Tukey HSD test

Dependent variable: Degree of company's innovation

Your consumers constantly strive to find new products and services		**Mean Difference**	**Std. Error**	**Sig**	**95% Confidence Interval**	
					Lower bound	**Upper bound**
1 (true)	2	-1.83	0.799	0.264	-4.83	1.16
	3	-2.67	0.715	0.051	-5.35	0.02
	4	-2.27	0.644	0.065	-4.68	0.15
	5	-3.67*	0.770	**0.017**	-6.56	-0.78
2 (partially true)	1	1.83	0.799	0.264	-1.16	4.83
	3	-0.83	0.715	0.770	-3.52	1.85
	4	-0.43	0.644	0.956	-2.85	1.58
	5	-1.83	0.770	0.239	-4.72	1.06
3 (neither true nor false)	1	2.67	0.715	0.051	-0.02	5.35
	2	0.83	0.715	0.770	-1.85	3.52
	4	0.40	0.536	0.937	-1.61	2.41
	5	-1.00	0.682	0.615	-3.56	1.56
4 (partly false)	1	2.27	0.644	0.065	-0.15	4.68
	2	0.43	0.644	0.956	-1.98	2.85
	3	-0.40	0.536	0.937	-2.41	1.61
	5	-1.40	0.608	0.261	-3.68	0.88
5 (false)	1	3.67*	0.770	0.017	0.78	6.56
	2	1.83	0.770	0.239	-1.06	4.72
	3	1.00	0.682	0.615	-1.56	3.56
	4	1.40	0.608	0.261	-0.88	3.68

*. The mean difference is significant at the 0.05 level.

Source: The authors' analysis

The results of subsequent tests support the conclusion that there is a difference in the level of innovation in organizational systems where consumers tend to constantly seek new products and services and those organizational systems where consumers do not tend to do that. Top management organizations that serve innovative intensive consumers, from the perspective of product innovation and service innovation, should continuously innovate all levels of business, in order to allow placement of the new products and services that comply with the changes in consumer demands.

In addition to the analysis of the external context, we also conducted an analysis of the internal context of an organization, from the angle of connection between the application of the novel entrepreneurial oriented managing behavior, as a form of management innovation and the degree of innovation of large organizational systems. For this purpose, we used the Spearman rank correlation whose results are shown in the following table.

Table 3

The Spearman rank correlation

Statements describing entrepreneurial behavior of managers		**Degree of company's innovation**
Statements describing entrepreneurial behavior of managers	ρ	**0.674****
Representing the organization to wider public in an innovative way	ρ	**0.560****
Implementing innovations into the business plan	ρ	**0.300***
Constantly spreading managers' social network	ρ	**0.288***
Frequent and good relations with business partners	ρ	**0.439****
Constant search for innovation ideas	ρ	**0.303***
Emphasizing their own originality and creativity together with realization of tangible results	ρ	-0.066
Application of bold and aggressive business attitude in order to use potentials to the maximum	ρ	**0.405****
Timely and successful conflict resolution among the employees and team members	ρ	**0.459****
Giving constructive solutions in case of a delay during project implementation	ρ	0.167
Allocating different kinds of resources to realization of business activities	ρ	**0.435****

*. Correlation is significant at the 0.05 level (2-tailed).

**. Correlation is significant at the 0.01 level (2-tailed). *Source: Authors' analysis*

The results indicate the existence of a strong and statistically significant relation between the managers who represent the organization in an innovative manner and the degree of innovation for the whole organization ($\rho = 0.674$; Sig. = 0.000). In addition to strong relation, statistically significant relation of the medium intensity has been isolated between innovation of organizations and the managers who:

- Constantly encourage implementation of innovation in business plans with the aim of increasing customer values, satisfaction of existing customers and attracting the new customers (ρ = 0.560; Sig. = 0.000)
- Use their own creative potential to the maximum with the constant search for ideas for innovation (ρ = 0.439; Sig. = 0.001)
- Consider themselves to be original and creative people (ρ = 0.303; Sig. = 0. 033)
- Successfully resolve conflicts between employees and team members (ρ = 0.405; Sig. = 0.004)
- Provide constructive solutions in the case of delay during project implementation (ρ = 0.459; Sig. = 0.001)
- Negotiate and encourage cooperation with business partners (ρ = 0.435; Sig. = 0.002)

Statistically, the significant relation of low intensity was confirmed between managers who constantly widen their social network of contacts (ρ = 0.280; Sig. = 0.049), have good relationships with customers and business partners (ρ = 0.288; Sig. = 0.043) and the degree of innovation within the organization.

Analysis of internal characteristics at the level of the whole organization was conducted through ANOVA and Mann-Whitney test. Depending on the isolated characteristics and performance of organizations, we conducted an analysis of the differences in innovation degrees in large organizational systems, as shown in the table below.

Table 4

Differences in innovation of an organization according to isolated characteristics and performance of companies

	Single factor analysis of variance			**M-V U test**		
	F.	**Sig.**		**U**	**Z**	**sig.**
Number of employees	55.146	**0.000**	The coefficient of fluctuation in the number of employees	200.500	-2.117	**0.034**
Value of operating revenue	53.628	**0.000**	Fluctuation of the operating revenue	210.500	-2.050	**0.040**
Value of operating assets	54.192	**0.000**	Fluctuation in the value of operating assets	242.500	-1.076	0.282

Source: The authors' analysis

One of the important criteria of business is personnel potential, both in qualitative and quantitative terms. Application of ANOVA showed the existence of differences in the innovation of organizations depending on the number of employees (F = 55.146, Sig. = 0.000). The project included detailed analysis using the Tukey HSD test since the sample consisted of large organizations whose number of employees ranged from 48 employees to 4,701. There was a difference in the level of innovation among organizations with 48 to 300 employees (M = 14.5263; SD = 2.52473), organizations employing 300 to 700 employees (M = 18.7143; SD = 0.91387), and those with over 700 employees (AS = 20.0000; SD = 0.00000). Organizations that have the highest number of employees also have the greatest opportunities for improving innovation by motivating their employees for creative thinking and more innovative implementation of business tasks. The trend in the number of employees and the influence of such developments on the existence of differences in the innovation of organizations is significant. Application of the Mann-Whitney test has shown the existence of differences (Mann-Whitney = 200.500; Asymp. Sig. = 0.034) when considering the level of organizations' innovation, depending on the changes in the number of employees. Based on median values of the organizations that had a growth in the number of employees or in which the number of employees remained unchanged (Median = 20.0000), those proved to be more innovative in comparison to the organizations which had a reduction in the number of employees (median = 17.0000). Those organizations that have modernized their human potential, both in qualitative and quantitative terms, record greater innovation than others that have reduced their staff potential through dismissal or employees' retirement.

By using ANOVA we determined the existence of differences in innovation in organizations when it comes to the value of operating income (F = 53.628; Sig. = 0.000). Results of the Tukey HSD test revealed a significant difference (Sig. = 0.000) between the degree of innovation of organizations with the value of operating income ranging from 3,489,183 to 26,168,876 euros (M = 14.3889; SD = 2.52374), organizations with medium business revenue of between 26,168,876 and 95,952,547 euros (M = 18.8947; SD = 1.04853) and organizations with the highest value of operating income, 95,952,547 to 558,269,364 euros (M = 20.0000; SD = 0.00000). The results indicate that organizations with a higher value of operating income have greater opportunities to invest in innovation. The dynamic category of operating income was also discussed, i.e. influence of its fluctuation on existence or non-existence of differences in innovation. Nonparametric Mann-Whitney test was conducted, which showed the existence of differences (Mann-Whitney = 210.500; Asymp. Sig. = 0.040) in the degree of innovation, depending on the fluctuations of operating income. The value of the median indicates that organizations that had a decline in the value of operating income (Median = 20.0000) are more innovative in comparison to the organizations which had growth of operating income (Median = 17.0000). Obtained results can be explained by the attitude of the management in organizations which have been declining in revenue and their ability to come up

with new ways of doing business, eliminate the negative trend and move forward in business. On the other hand, strong organizations that continuously generate revenue growth can become complacent due to their previous business success and therefore ignore innovation.

Application of ANOVA showed the existence of differences in innovation depending on the value of operating assets (F = 54.192; Sig. = 0.000). By applying the Tukey HSD test we found differences in innovation between organizations that have a minimum value of the operating assets, i.e. 5,233,775 to 26,168,876 euros (M = 14.5263, sd = 2.52473) and organizations that have medium value of operating assets, i.e. 26,168,876 to 200,628,053 euros (M = 18.8000; SD = 0.94112), as well as those organizations that have the highest value of operating assets ranging from 200,628,053 to 1,334,612,700 euros (M = 20.0000; SD = .00000). It can be concluded that organizations that have the greatest levels of operating assets are also the most innovative. In relation to the fluctuations of operating assets by applying the nonparametric Mann-Whitney test, it was established that there was no statistically significant difference in the innovation of organizations depending on the fluctuation of operating assets (Mann-Whitney = 242.500; Asymp. Sig. = 0.282).

Conclusions

The objective of the conducted research is focused on providing answers to the following question: How do external market trends, together with the internal characteristics of the organization and managing the behavior of managers, affect innovation in large organizational systems? Statistically significant and separated features of markets, management, and internal organization represent a potential list of incentive factors when innovating in the entire organization.

Depending on the fluctuation of competitive organizations, technological changes, consumer needs and preferences, as well as, legislation, the difference in innovation occurred only between those organizations that serve innovation oriented consumers and those that do not serve such customer groups. Therefore, the hypothesis H1, is only partially confirmed. The result is logical because in modern business environments consumers are among the most important external parties that influence long-term survival of the organization. Meeting their needs, according to the principle of offering the highest customer value, encourages innovation of business processes.

A key role in creation, transfer and implementation of all types of innovation lies in the business behavior of the top management and in the chosen management style. The results of empirical studies have indicated that such management that creates entrepreneurial organizational culture fosters a greater degree of innovation. The previous statement is supported by the economists who believe that organizations whose organizational context supports new thinking, freedom of internal change agents increase [6, p. 834] influencing creation of new ideas and their successful exploitation [33, p. 301], all for the sake of obtaining

innovation. Greater freedom of managers should be transferred to the employee's at all hierarchical levels, in order to ensure a broader base of potential ideas that will further be analyzed and filtered in accordance with the possibilities of an organization, time and market trends. This is confirmed by the hypothesis H2.

If we observe the value of the operating income, the results of the empirical research lead to the conclusion that large entities whose operating income value is over 95,952,547 euros are more innovative, because greater financial possibilities offer better opportunities in terms of innovation. Thus, they can maintain the current trend of growth or achieve sustainable competitive advantage. We obtained somewhat different results taking into account the aspect of fluctuations of the value of business revenue. These results showed that organizations that have met a decline of operational income are more innovative. The above-mentioned results have led to new conclusions – organizations which are faced with deteriorating business, invest more in the innovation of products, services and processes, in an effort to improve the deteriorating business processes. The more innovative organizations are those that employ more than 700 employees. The obtained result can be confirmed by some economists who believe that large legal entities are more innovative due to greater financial opportunities since those can facilitate greater personnel resources. Higher Personnel resources provide higher creative potential and better diversification of the risks related to the implementation of various innovations. The empirical findings confirm Schumpeter's traditional hypothesis, stating that large organizations are more innovative than smaller ones. Operation Asset values are one of the main criteria for doing business. This criterion indicates differences in innovation between organizations whose operating assets greater than 200,628,053 euros and those organizations that have lower operating assets value. A series of previously presented conclusions are confirmed by the hypothesis H3.

References

[1] Akhtar, S.: Human Capital Utilization through Effective HRM Practices, Middle-East Journal of Scientific Research, 8 (2) 2011, pp. 434-439

[2] Altringer, B.: A New Model of Innovation in Big Companies, Harward Business Review, https://hbr.org/2013/11/a-new-model-for-innovation-in-big-companies/, 2013

[3] Anderson, J. C., Rungtusanatham, M. and Schroeder, R. G.: A Theory of Quality Management Underlying the Deming Management Method, Academy of Management Review, 19 (3) 1994, pp. 472-509

[4] Aranda, D. A., Rata, B. M. and Duarte, A. R.: Innovation and Firm Size: an Empirical Study for Spanish Engineering Consulting Companies, European Journal of Innovation Management, 4 (3) 2001, pp. 133-142

[5] Balogun, J. and Hope Hailey, V.: Exploring Strategic Change, Prentice Hall, England, 2008

[6] Birkinshaw, J., Hamel, G. and Mol, M. J.: Management Innovation, Academy of Management Review, 33 (4) 2008, pp. 825–845

[7] Bourgeois, L. J., Eisenhardt, K. M.: Strategic Decision Processes in High Velocity Environments: Four Cases in the Microcomputer Industry, Management Science, 34, 1988, pp. 816-835

[8] Brown, T.: Change by Design: How Design Thinking Transforms Organizations and Inspires Innovation, HarperCollins Publisher, New York, 2009

[9] Casadesus-Masanell, R. and Zhu, F.: Business Model Innovation and Competitive Imitation: The Case of Sponsor-based Business Models. Strategic Management Journal, 34 (4) 2013, pp. 464-482

[10] Chakrabarti, A. K.: The Role of Champion in Product Innovation, California Management Review, 17 (2) 1974, pp. 58-62

[11] Chaniadi, F.: Innovative Management of Innovation Management, Manchester Bussines School, Manchester, 2014

[12] Coopey, J., Keegan, O. and Emler, N.: Managers' Innovations and the Structuration of Organizations, Journal of Management Studies, 35 (3) 1998, pp. 263-284

[13] Damanpour, F.: Organizational Innovation: A Meta Analysis of Effects of Determinants and Moderators, Academy of Management Journal, 34, 1991, pp. 555-590

[14] Dejanović, M. A., Nikolić, T. S. and Stanković, J.: Integral Model of Strategic Management: Identification of Potential Synergies, Acta Polytechnica Hungarica, 12 (8) 2015, pp. 115-133

[15] Denham, J. and Kaberon, R.: Culture Is King: How Culture Contributes to Innovation, Journal of Product Innovation Management, 29 (3) 2012, pp. 358-360

[16] Diaz Fernandez, M., Pasamar Reyes, S. and Valle Cabrera, R.: Are Ambidextrous Intellectual Capital and HRM Needed for an Ambidextrous Learning, Working paper Series BOM 12.01, http://www.upo.es/serv/bib/wpboam/wpboam1201.pdf, 2012

[17] Dodgson, M., Gann, D. and Salter, A.: The Management of Technological Innovation, Oxford University Press, USA, 2008

[18] Dove, J.: The effect of Judicial Independence on Entrepreneurship in the US States, Economic Systems, 39, 2015, pp. 72-96

[19] Dubravska, M., Mura, L., Kotulič, R. and Novotny, J: Internationalization of Entrepreneurship - Motivating Factors: Case Study of the Slovak Republic, Acta Polytechnica Hungarica, 12 (5) 2015, pp. 121-133

[20] Ellis, P. D.: The Essential Guide to Effect Sizes: An Introduction to Statistical Power, Meta-Analysis and the Interpretation of Research Results, Cambridge University Press, Cambridge, 2010

[21] Garcia, R., Calantone, R.: A Critical Look at Technological Innovation Typology and Innovativeness Terminology: a Literature Review, Journal of Product Innovation Management, 19 (2) 2002, pp. 110-132

[22] Hanh, T., Preuss, L., Pinkse, J. and Figge, F.: Cognitive Frames in Corporate Sustainability: Managerial Sensemaking with Paradoxical and business Case Frame, Academy of Management Review, 39 (4) 2014, pp. 463-487

[23] Hamel, G.: The Why, What, and How of Management Innovation (cover story), Harvard Business Review, 84 (2) 2006, pp. 72-84

[24] Hargrave, T. and Van de Ven, A.: A collective action model of institutional innovation, Academy of Management Review, 31, 2006, pp. 864-888

[25] Howell, J., Higgins, C.: Champions of Technological Innovation, Administrative Science Quarterly, 35, 1990, pp. 317-341

[26] Ichniowski, C., Shaw, K., Prennushi, G.: The Effects of Human Resource Management Practices on Productivity: a Study of Steel Finishing Lines, American Economic Review, 87 (3) 1997, pp. 291-313

[27] Keller, R. T., Holland, W. E.: Communicators and Innovators in Research and Development Organizations, Academy of Management Journal, 26 (4) 1983, pp. 66-74

[28] Kleinschmidt, E., Brentani, U. and Salomo, S.: Information Processing and Firm-Internal Environment Contingencies: Performance Impact on Global New Product Development, Creativity and Innovation Management, 19 (3) 2010, pp. 200-218

[29] Kossek, E. E.: The Acceptance of Human Resource Innovation by Multiple Constituencies. Personnel Psychology, 42, 1989, pp. 263-280

[30] Lambić, M.: Inženjerstvo i inovacije, Tehnički fakultet Mihajlo Pupin, Zrenjanin, 1996

[31] Mol, J. M., and Birkinshaw, J.: The Sources of Management Innovation: When Firms Introduce New Management Practices, Journal of Business Research, 62 (12) 2009, pp. 1269-1280

[32] Морозов, Ю., П.: Иновационный менеджмент, юнити-дана, Москва, 2000

[33] O'Regan, N. and Ghobadian, A.: Innovation in NTBFs: Does Leadership Really Matter?, International Entrepreneurship and Management Journal, 2 (2) 2006, pp. 299-314

[34] Ortt, J. R. and Van der Duin, A. P.: The Evolution of Innovation Management Towards Contextual Innovation, European Journal of Innovation Management, 11 (4) 2008, pp. 522-538

[35] Pallant, J.: SPSS priručnik za preživljavanje, 4 izdanje (prevod): Mikro knjiga, Beograd, 2011

[36] Pervaiz, K. A. and Charles, D. S.: Innovation Management: Context, Strategies, Systems and Processes. Pearson Education Limited, England, 2010

[37] Pil, F. K. and MacDuffie, J. P.: The Adoption of High Involvement Work Practices, Industrial Relations, 35 (3) 1996, pp. 423-455

[38] Potocan, V., Nedelko, Z. and Mulej, M.: Influence of Organizational Factors on Management Tools Usage in Slovenian Organizations. Inzinerine Ekonomika-Engineering Economics, 23 (3) 2012, pp. 291-300

[39] Radu, O. M.: Stimulating Firm Innovativeness: Probing the Interrelations between Managerial and Organizational Determinants, Erasmus University, Rotterdam, 2012

[40] Ramezani, Z. N., Khabiri, M., Alvani, S. M. and Tondnevis, F.: Use of Mintzberg's Model of Managerial Roles to Evaluate Sports Federations Managers of Iran, Middle-East Journal of Scientific Research, 10 (5) 2011, pp. 559-564

[41] Schilling, M. A.: Strategic Management of Technological Innovation, McGraw-Hill, New York, 2010

[42] Smith, K. G., Collins, C. J. and Clark, K. D.: Existing Knowledge, Knowledge Creation Capability, and the Rate of New Product in Production in High-technology Firms, Academy of Management Journal, 48, 2005, pp. 346-357

[43] Subramanian, A., Nilakanta, S.: Organizational Innovativeness: Exploring the Relationship between Organizational Determinants of Innovation, Types of Innovations, and Measures of Organizational Performance, Omega, 24 (6) 1996, pp. 631-647

[44] Symeonidis, G.: Innovation, Firm Size and Market Structure, OECD Economics Department Working Papers No. 161, http://dx.doi.org/10.1787/603802238336, 1996

[45] Tengblad, S.: Is there a New Managerial Work? A Comparison with Henry Mintzberg's Classic Study 30 Years Later, Journal of Management Studies, 43, 2006, pp. 1437-1461

[46] Troilo, M.: Legal Institutions and High-Growth Aspiration Entrepreneurship, Economic Systems, 35, 2011, pp. 158-175

[47] Tushman, M. L., Scanlan, T. J.: Characteristics and External Orientations of Boundary Spanning Individuals, Academy of Management Journal, 24 (1) 1981, pp. 83-98

[48] Vaccaro, G. I., Jansen, J. P .J., Van Den Bosch, A. J. F. and Volberda, W. H.: Management Innovation and Leadership: The Moderating Role of Organizational Size, Journal of Management Studies, 49 (1) 2012, pp. 28-51

[49] Vande Ven, A. H. and Poole, M. S.: Explaining Development and Change in Organizations, Academy of Management Review, 20, 1995, pp. 510-540

[50] Law on Accounting and Auditing, the Official Gazette of the Republic of Serbia no. 62/2013

[51] Walter, A., Parboteeah, K., Riesenhuber, F., Hoegl, M.: Championship Behaviors and Innovations Success: An Empirical Investigation of University Spin-Offs, Journal of Product Innovation Management, 28, 2011, pp. 586-598

[52] Wikhamn, R. B.: Two Different Perspectives on Open Innovation–Libre versus Control, Creativity and Innovation Management, 22 (4) 2013, pp. 375-389

Evaluation and Improvement of Parallel Discrete Event Simulation Performance Predictions: A Rough-Set-based Approach

László Muka, István Derka

Department of Telecommunications, Széchenyi István University
Egyetem tér 1, H-9026 Győr, Hungary; muka@sze.hu, steve@sze.hu

Abstract: Simulation performance prediction methods make possible the realization of performance improvement potentials of Parallel Discrete Event Simulation (PDES) methods, important in the analysis of complex systems and large-scale networks. Currently, high performance execution environments (emerging clusters and computing clouds) advance the development of quality/cost analysis capabilities of performance prediction methods. In this paper, for the evaluation and management of prediction correctness/cost, the efficacy, efficiency and effectiveness coefficients and improvement operations are defined for predictions. The performance coefficients and improvement operations are embedded in the rough-set-modeling and learning process and presented as an enhancement approach of the conventional Coupling Factor Method (CFM). A case study based on the CFM analysis of PDES of a closed queuing network model is presented. In the example, after rough-modeling and train-and-test analysis, the correctness/cost evaluation and effectiveness improvement operations are shown for series of predictions and the feedback connection to modeling refinement phase is demonstrated too.

Keywords: Parallel Discrete Event Simulation; simulation performance prediction; quality/cost analysis; Systems Performance Criteria; Rough Set Theory; Coupling Factor Method

1 Introduction

Over the last few years, various research efforts have been made regarding Parallel Discrete Event Simulation (PDES) modeling and execution methods [1, 2, 3, 4], since parallel execution turned out to be an appropriate approach to meet high computing capacity requirements of Discrete Event Simulation (DES) analysis of complex systems and large-scale networks [5, 6].

In the present paper, PDES is defined as the execution of a single DES model on some high performance computing platform which can be clusters of homogeneous or heterogeneous computers and other emerging execution environments (cloud, grid, etc.) too.

Development of simulation models having high runtime performance features in a PDES execution environment is not an easy task even today, mainly because it is hard to tell the parallel execution features of a model, for example, possible resource capacity bottlenecks, in the development phase [7]. The *simulation performance prediction* of PDES execution can help to realize higher performance by providing preliminary knowledge about the behavior of the simulation model in the parallel execution environment [7, 8, 9, 10, 11]. The PDES performance prediction methods can support the performance increase throughout the whole modeling and simulation process including model development support, simulation setup and evaluation phases and taking into account different simulation framework specifics too [7].

Nowadays, emerging simulation operation forms, like on-line, real-time modeling and simulation and especially cloud computing with on-demand network access and pay-per-use feature and the developing simulation as a service (Simulation Software-as-a-Service) in public clouds [3, 21] put an increasing emphasis on quality/cost analysis capability of performance prediction methods.

The *motivation* of the authors to make the research presented in the paper was the lack of methods which can manage together the correctness and cost of performance prediction for a model in parallel simulation execution environment and which can also provide an easy feedback to the modeling and setup phases in the simulation.

The authors have developed the *Enhanced Simulation Performance Prediction Method (ESPPM)*. ESPPM is enhancing the standard *Coupling Factor Method (CFM)* of PDES performance prediction [14] by a method of improvement allowing handle together correctness and cost in speedup predictions. The improvement approach based on *Rough Set Theory (RST)* [13] train-and-test analysis with embedded *Systems Performance Criteria (SPC)* [30] of *efficacy (E1), efficiency (E2)* and *effectiveness (E3)* for complex evaluation and quality/cost performance improvements steps.

In this work, the authors make the following key *contributions*:

- Definitions of performance improvement operations, based on definitions of cost measures and on definitions of performance coefficients of *efficacy (E1)*, *efficiency (E2)* and *effectiveness (E3)* are described for single predictions and for series of predictions.
- A case study of the work of ESPPM is introduced using the example of a CFM PDES performance prediction of a Closed Queuing Network (CQN) model. In the analysis, the RST model of CFM modeling and its train-and-test examination is presented, the E1, E2 and E3 rule and attribute dropping operations are shown and the discussion of analysis results of performance predictions with feedback to the CFM and RST model-identification and refinement phase.

The rest of paper is organized as follows: Section 2 summarizes the related work, estimates the simulation performance prediction methods and relevant RST applications. Section 3 describes the components of the new method (RST, SPC and CFM). Section 4 introduces prediction performance improvement operations based on cost and prediction performance coefficients SPC-type definitions which are embedded into the process of train-and-test RST analysis. In Section 4, the process of ESPPM algorithm is described too. Section 5 introduces an example case study to demonstrate the use of the new method for the prediction analysis. Section 6 discusses the results of analysis. Finally, the conclusions are presented.

2 Related Work

The related research is overviewed in following two points.

2.1 Simulation Performance Prediction Methods

The method introduced in [8] uses execution *event-trace data* of sequential and parallel, simulation runs, for creating the *execution graph model* and for the subsequent *critical path analysis* to predict parallel simulation performance. The method takes into account, in the prediction, the characteristics of the simulation hardware (with hardware parameters and mapping algorithms). The use of a wide variety of conservative and optimistic parallel simulation synchronization protocols is allowed by the method, which is an advantage. Unfortunately, the evaluation of prediction quality and the common evaluation with the cost of prediction are not treated in the method.

As an alternative to the conservative synchronization, the time driven version of *the statistical synchronization method (SSM-T)* with its loose synchronization [18, 19, 20] is a less well-known, but promising PDES synchronization method, that can be applied for the parallel simulation of certain types of systems such as communication networks. The increased performance can be predicted based on the *trace of frequency of statistics exchange between segments*. The frequency of statistics exchange can be used similarly to *lookahead* [15]. There is no performance model used in the method, thus, performance prediction requires time-consuming analysis of the simulation model operation.

The method described in [7], uses a *hybrid approach* to define the theoretical limit of the execution improvement for conservative synchronization protocol. In the *trace-based part*, the method analyses only a definite part of the sequence of events of the simulation model; while in an *analytical modeling part*, for the calculation of the lower bound on the runtime of the parallel simulation, a simplified scheduling problem model and the linear programming approach of is applied. An important advantage of this method is the definition of the

performance improvement limit for a model (or model version) but the method does not pay attention to the quality/cost analysis of predictions.

Paper [14] introduces the CFM (details are described in point 3.3), a simulation performance prediction approach, based on the *coupling factor PDES performance model*. The coupling factor helps to predict the *parallelization potential* of the simulation models and can be defined in sequential simulation model runs. The method is appropriate only for conservative null message-based algorithm. Unfortunately, CFM introduced in [14] does not predict the speedup value and does not support the quality/cost evaluation in predictions either.

2.2 Rough Set-based Performance Prediction

Paper [22] presents a rough set modeling and application runtime prediction method. The method is based on identifying and extracting properties defining runtime similarity of applications using available past data. The method does not include any consideration on prediction cost and on the improvement of prediction quality.

Paper [23] introduces a scheduling optimization approach for a dynamic remanufacturing situation with uncertain data. The proposed method is using linear programming and rough set evaluation and learning in an iterative process. Monte Carlo simulation is also involved to improve consistency of data. Unfortunately, complex evaluation, allowing quality/cost analysis in the learning process, is not included in the method.

3 Method Components

3.1 Rough Set Elements and the Rough Prediction Algorithm

The RST (Rough Set Theory) is a mathematical framework suitable for modeling and analysis of information systems with imprecise relations, with uncertain data [25, 26, 27, 28, 29].

A *rough set information system* with embedded knowledge consists of two sets: the set of *objects* called the *universe* and the set of *attributes*.

More formally, $I = (U, A, f, V)$ denotes an *information system* of RST, where set U is the universe, A is the set of attributes. Sets U and A are finite nonempty sets where ($U = \{x_1, x_2, \dots, x_{|U|}\}$ and $A = \{a_1, a_2, \dots, a_{|A|}\}$). The attributes define an *information function* $f: U \to V$ for U where the set V is the set of values of A ($V = V_{a_1} \cup V_{a_2} \cup \dots \cup V_{a_{|A|}}$). The set V_{a_i}– named also the *domain* of a_i – contains

the collection of values of a_i and $V_{a_i} = \left\{ v_{1_{a_i}}, v_{2_{a_i}}, \dots, v_{\left|V_{a_i}\right|_{a_i}} \right\}$ where $\left|V_{a_i}\right|$ is the size of the domain of a_i.

Discretization is the operation of mapping the primary values and ranges of all attributes to *selected* (possibly optimized) sets of discrete values: $f_{V'}: V' \to V$. The set V' stands for the values of a before discretization.

The *B-indiscernibility relation* $IND(B)$for a set of attributes $B \subseteq A$is defined in the following way:

$IND(B) = \{(x_i, x_j) \in U^2 | \forall (a \in B)(\, a(x_i) = a(x_j))\}$.

If $(x_i, x_j) \in IND(B)$, then the objects x_i and x_j are indiscernible from each other in B and the *equivalence classes* $[x]_{IND(B)}$ of $IND(B)$ are formed by the objects indiscernible in B.

Rough sets are defined by their lower approximation and upper approximation sets. The set $B^*(X)$ and the set $B_*(X)$ is the *B-lower* and *B-upper approximation* of the set X and defined as follows:

$B_*(X) = \bigcup_{x \in U} \{x | [x]_{IND(B)} \subseteq X\}$ and

$B^*(X) = \bigcup_{x \in U} \{x | [x]_{IND(B)} \cap X \neq \emptyset\}$.

The set $BN_B(X)$ defined by the equation $BN_B(X) = B^*(X) \setminus B_*(X)$ is the *B-boundary region* of X. If X is a crisp set then, $X = B_*(X)$ thus $BN_B(X) = \emptyset$ which means the boundary region is empty.

A *reduct* R_B is the minimal subset of attributes B that allows the same classification of objects of U as the set of attributes B. This feature of a reduct may be described by indiscernibility function as follows:

$IND_{\forall x (x \in U)}(R_B) = IND_{\forall x (x \in U)}(B), B \subseteq A$.

In general, the information system may take the form of $I = (U, A = C \cup D, f, V)$ which is a *decision information system (DIS)*. The set $C = \{c_1, c_2, \dots, c_{|C|}\}$ denotes the set of condition attributes and D is the set of decision attributes $D = \{d_1, d_2, \dots, d_{|D|}\}$. The information function $f: U \to V$ may be expressed by information functions $f_C: C \to V_C$ and $f_D: D \to V_D$, where $V = V_C \cup V_D$ ($V_C = V_{c_1} \cup V_{c_2} \cup V_{c_3} \cup, \dots, \cup V_{c_{|C|}}$ and $V_D = V_{d_1} \cup V_{d_2} \cup \dots \cup V_{d_{|D|}}$) and

$V_C = \bigcup_{i=1}^{|C|} V_{c_i}$ where $V_{c_i} = \left\{ v_{1_{c_i}}, v_{2_{c_i}}, \dots, v_{\left|V_{c_i}\right|_{c_i}} \right\}$ and $V_D = \bigcup_{i=1}^{|D|} V_{d_i}$. where $V_{d_i} = \left\{ v_{1_{d_i}}, v_{2_{d_i}}, \dots, v_{\left|V_{d_i}\right|_{d_i}} \right\}$.

In a *decision table*$I = (U, A = C \cup \{d\}, f, V)$ based on a DIS, d denotes the *distinguished decision attribute*. Furthermore, a decision information system having the form of $I = (U, C \cup D, f_{V'}, f, V', V)$ denotes a DIS with *discretization information functions* $f_{V_C'}: V_C' \rightarrow V_C$ and $f_{V_D'}: V_D' \rightarrow V_D$.

The *classification* may also be described by a *set decision rules* $S = \{s_1, s_2, \ldots, s_{|S|}\}$ in the form of implication $s_k = (\varphi_k \Rightarrow \kappa_k), (s_k \in S)$, where φ_k and κ_k are *logical expressions* of the condition and decision attributes respectively. The formulas φ_k and κ_k may also be quoted as *LHS (Left Hand Side)* and *RHS (Right Hand Side)* part of the rule. A decision rule s_k may be evaluated by its $Match_U(s_k)$ and $Supp_U(s_k)$ values, where $Match_U(s_k)$ is the number of objects in U the attribute values of which satisfy φ_k (*matching* with the *LHS* part of s_k), and $Supp_U(s_k)$ denotes the number of objects in decision table the attribute values of which satisfy both φ_k and κ_k (matching with both the *LHS* and *RHS* parts of s_k).

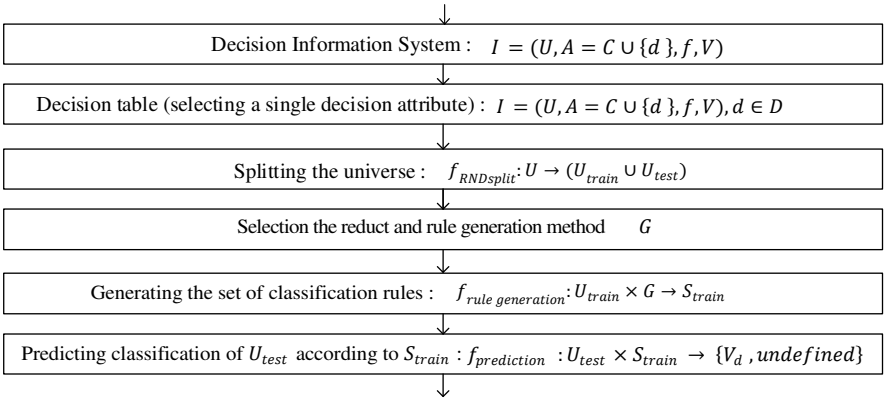

Figure 1

The Traditional Rough Set Theory (TRST) analysis algorithm for performance prediction

Figure 1 shows the process of the rough prediction algorithm. The essence of the algorithm is the random split of the universe into train and test partitions, generation a set of classification rules using the train partition and then generation classification predictions for the test partition using the generated rules.

3.2 Systems Performance Criteria

Efficacy (E1), *efficiency (E2)* and *effectiveness (E3)* are *Systems Performance Criteria (SPC)* [11, 30, 31]. E1, E2 and E3 coefficients are in a hierarchy-like relationship with each other. On the longer term, the performance of a system is checked by the effectiveness criterion, the efficacy criterion shows whether the performance is suitable at all, and the efficiency criterion characterizes the relation of the required output and the resources used to produce the output.

3.3 The Coupling Factor Method

Based on some theoretical considerations about the connectedness of PDES model segments, paper [14] describes a practical simulation performance prediction approach the *Coupling Factor Method (CFM)*. The method – using results of sequential simulation runs – predicts the *parallelization potential* of simulation models with conservative null message-based synchronization algorithm. The CFM performance model can be described by the formula:

$$\lambda = L * E/\tau * P$$

where L is the lookahead value characterizing the simulation model $[simsec]$ [6], E is the event density generated by the model $[event/simsec]$, τ is the latency of messages between logical processes (LPs) of the simulation model during the execution $[sec]$, and P is the event processing hardware performance $[event/sec]$. In this performance model, parameters L and Echaracterize the simulation model itself, parameters τ and P describe the execution environment. The performance model involves only four parameters for the performance prediction calculations that can be measured in simple *sequential simulation runs*. According to the method, the PDES speedup value cannot be predicted, but the high value of λ (λvalue is a couple of time 100 or higher [15]) shows the good potential for simulation model parallelization. For a separate process, the λ_N parallelization potential of a process is only a part of the whole potential:

$$\lambda_N = \lambda/N_{LP}$$

where N_{LP} the number of LPs [15]. (The four parameters of CFM formulates requirement on the simulation model and on how the parallelization potential can be exploited.)

The method has been validated by a series of simulation investigations for *homogeneous* and *heterogeneous* clusters of computers [15, 16, 17]. Example applications for telecommunication systems and for cloud computing systems have been introduced too in [16] and [32].

4 The Prediction Performance Enhancement

4.1 Defining Prediction Performance Coefficients

In a TRST simulation performance analysis, in a decision table $I = (U, A = C \cup \{d\}, f, V)$ the o*bjects* of the universe U are *computer simulation experiments.* Set of attributes (A) consists of independent (C) and dependent $\{d\}$ variables that are taken into account in performance evaluation and in classification prediction.

The classification of experiments in $U_{test(i)}$ ($U = U_{train(i)} \cup U_{test(i)}$) is *predicted* by $f_{prediction(i)}: U_{test(i)} \times S_{train(i)} \rightarrow \{V_d, undefined\}, (i = 1,2, \dots, \mathrm{n})$, using the set of rules $S_{train(i)} = \left\{s_1, s_2, \dots, s_{|S_{train(i)}|}\right\}, s_k = \varphi_k \Rightarrow \kappa_k$ that are generated according to function $f_{train}: U_{test} \times G \rightarrow S_{train}$ in TRST.

In the following the *E1*, *E2* and *E3* SPC will be defined in the form of *prediction performance coefficient*s: efficacy (E1) to measure prediction correctness, efficiency (E2) to assess correctness-to-cost relationship and effectiveness (E3) to take into account E1 and E2 for series of predictions. To calculate cost relationships *cost of experiments, attributes, rules and predictions* will be defined using the consumed computation time.

For the improvement of prediction performance, attribute and rule dropping operations are defined.

Definition 1. Efficacy (E1) of a prediction

$E1_{prediction}$ is calculated according to formula

$$E1_{prediction} = \frac{\sum_{l=1}^{|U_{test}|} p(x_l)}{|U_{test}|}$$

where $p(x_l)$ (*prediction correctness*) is equal to

$$p(x_l) = \begin{cases} 1, & |\langle d(x_l)_{predicted}\rangle = \langle d(x_l)_{observed}\rangle \\ 0 | otherwise \end{cases}$$ and where $d(x_l)_{predicted}$ is

$$d(x_l)_{predicted} = \begin{cases} v_d, \langle \kappa_k \rangle = v_d, v_d \in V_d \big| (Match_{U_{test}}(s_k) = 1 \\ undefined \ | otherwise \end{cases}$$ and

$(s_k \in S_{train})$, $\langle d(s_k)_{predicted}\rangle = v_{d_{(x_l, s_k)}}$.

The interval of $E1$ coefficient is $0 \leq E1 \leq 1$. If $E1_{prediction} \geq E1_{limit}$ is true then the prediction is *efficacious*. The $E1_{limit}$ denotes the lower limit of efficacy and the inequality $E1_{limit} > 0.5$ should be satisfied that is the efficacy of prediction is required to be better than random guess.

Definition 2. Cost of experiments, attributes, rules and predictions

For a decision table $I = (U, A = C \cup \{d\}, f, V)$ supposing that a homogeneous cluster of computers with equal cores is examined and supposing that all the cores are continuously working during the execution time, the *cost of a simulation experiment* $x_l (x_l \in U)$ is defined as: $K(x_l) = N_{cores} * execution\ time\ [sec]$.

Cost of a rule s_k is calculated as $K(s_k) = \sum_{l=1}^{|U|} K(x_l | Supp(s_k)) = 1)\ [sec]$.

Cost of a prediction $K(S_{prediction})$ is defined as $K(S_{train}) = \sum_{k=1}^{|S_{train}|} K(s_k)\ [sec]$, $(s_k \in S_{train})$.

Definition 3. Efficiency (E2) of a prediction

$E2_{prediction} = E1_{prediction}/K_{prediction}\ [\frac{1}{sec}]$

Definition 4. Effectiveness (E3) of a series of predictions

$E3_{series} = E3(S_{prediction}) = \overline{E2}_n|\overline{E1}_n$ where

$\overline{E1}_n = \frac{1}{n}\sum_{i=1}^{n} E1_{(i)}$ and $\overline{E2}_n = \frac{1}{n}\sum_{i=1}^{n} E1_{(i)}/\frac{1}{n}\sum_{i=1}^{n} K(S_{train(i)})\ [\frac{1}{sec}]$

and where i denotes the i-th prediction and n is the number of predictions in the series($n \geq 2$). For $n = 1$ $E3_{series}$ is *undefined* and for $\overline{E1}_n < E_{limit}$ $E3_{series}$ is *not effective*.

Definition 5. Rule and attribute dropping

Dropping of a rule s_k and dropping of an attribute c_j for the pair (S_{train}, U_{test}) are the replacement operations $S_{train} := S_{train} \setminus \{s_k\}$ and $C := C \setminus \{c_j\}$ respectively.

4.2 The Enhanced Simulation Performance Prediction Method

Figure 2 shows the process diagram of the *Enhanced Simulation Performance Prediction Method (ESPPM).*

The ESPPM process can be described as follows:

- The ESPPM input data are produced both in sequential (CFM parameter measurements) and parallel simulation model runs (PDES, CFM parameter measurements, runtime measurements for cost calculations are executed and other relevant (or possibly relevant) simulation modeling hardware and software environmental data are collected.
- The rough model is made for performance prediction (objects and attributes of DISs before and after discretization).
- The TRST train-and-test method is used in interactive manner for generation of predictions
- The E1, E2 and E3 coefficients (built in the TRST cycle) are used for evaluation and attribute and rule dropping operations are applied for improvement of correctness and cost of predictions.
- The method supports setting up feedback to identification and refinement phase of the simulation performance prediction models.

The method can be implemented by using the OMNet++ [12] and the Rosetta System [13] free software for DES modeling and RST examinations respectively.

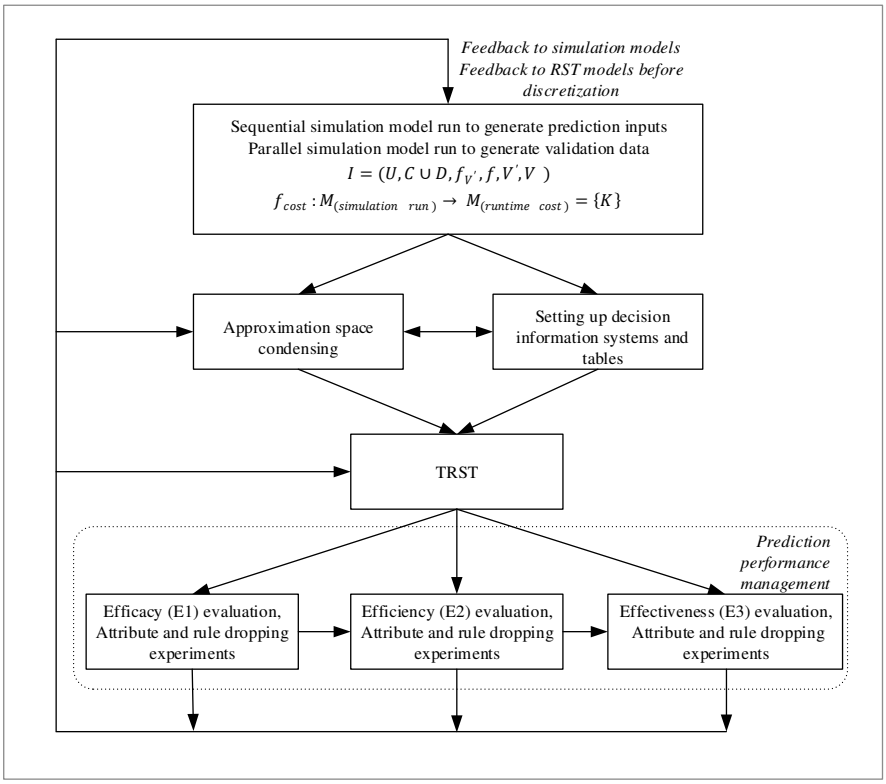

Figure 2
The process of the Enhanced Simulation Performance Prediction Method (ESPPM)

5 Prediction Performance Analysis Case Study

5.1 Simulation Performance Evaluation Example

The example analysis of the CFM approach described in [15] investigates the simulation runs of a CQN model with various configurations in a homogeneous cluster execution environment with different number of processors.

In Figure 3, the number of *tandem queues* in the CQN model is 24 ($Q_{1,\dots,24}$), the number of *simple queues* in a tandem queue is 50 ($q_{1,\dots,50}$). The switching between tandem queues is performed by *switches* ($sw_{1,\dots,24}$) according to *uniform probability distribution*. The delay of switching between tandem queues (shown by 2D arrow shapes, in Figure 3) will model the *lookahead* (L). The *lookahead delay* is the delay of *a job* before entering the next tandem queue and it is defined by the L value.

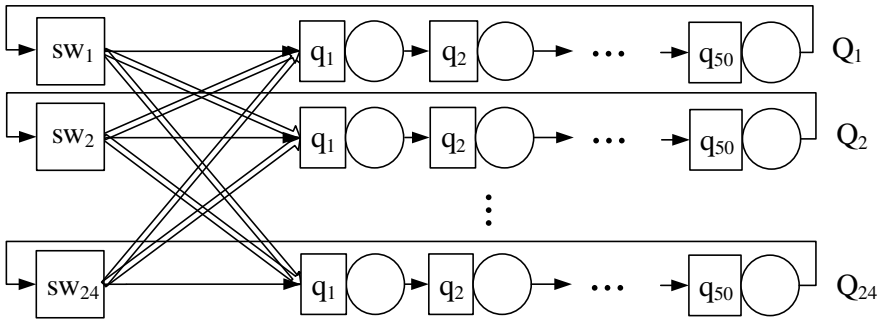

Figure 3
CQN model for PDES performance simulation

The starting number of jobs in every simple queue is 2 jobs, thus the *number of jobs in CQN* is 2400 and this value remains constant. Jobs have exponential *inter-arrival time* and exponential *service time* distributions with FCFS service discipline. The expected value for both the arrival and service time distributions is $10simsec$. The *delay* on links between *simple queues* is $1simsec$.

The *software environment* of simulation runs includes: *Linux (Debian) operating system, MPI, NFS, OMNet++ network simulator*. The *hardware environment* of simulation runs is a *homogeneous cluster* of 12 two-core host PCs. The communication latency of messages – measured by the OpenMPI PingPong benchmark and used as τ value – over MPI between the host PCs of the cluster is $25\mu sec$.

To calculate coupling factor λ the values of$E$ and P variableswere measured in *sequential simulation runs* on *one core* of a host PC (N_{cores}=1) with L =0.1, 1, 10, 100 and 1000 $simsec$ of lookahead values. The result of *sequential simulation* runs is summarized in Table 1 [15].

Table1
Coupling factor determination by sequential simulations

L [simsec]	0.1	1	10	100	1000
Execution time [sec]	524.18	521.36	523.09	516.54	415.73
P [ev/sec]	263502	264868	263465	261132	247653
E [ev/simsec]	159.86	159.83	159.51	156.12	119.16
Coupling factor λ	2.43	24.14	242.17	2391.39	19246.76

The *PDES experiments* were executed using equal number of cores and LPs: $N_{LP} = 2, 4, 6, 8, 12$ and 24 ($N_{cores} = N_{LP}$). The *relative speedup* results measured in *PDES executions* are summarized in Table 2.

The *simulated virtual time* both for sequential and PDES runs was $864000simsec$. The total number of execution runs for sequential simulation and for PDES were 55 and 330 respectively (11 runs with the same setup of an experiment).

Table 2
PDES relative speedup performance at different N_{cores} and L values

L [simsec]	0.1	1	10	100	1000
N_{cores}=2	0.43	0.78	0.85	0.99	0.99
N_{cores}=4	0.06	0.48	0.83	0.92	0.94
N_{cores}=6	0.03	0.28	0.76	0.91	0.94
N_{cores}=8	0.02	0.18	0.66	0.89	0.95
N_{cores}=12	0.01	0.09	0.48	0.86	0.94
N_{cores}=24	0.00	0.02	0.18	0.63	0.87

The *speedup* is defined as a proportion of the sequential and the PDES execution time of the simulation. The *relative speedup* is calculated as the proportion between the speedup values and the *number cores* used to achieve the speedup.

5.2 RST Modeling and Analysis

The *RST model of simulation performance prediction* is presented in the form of *decision information systems* and *decision tables:*

$I = (U, C \cup D, f_{V'}, f, V', V), I = (U, A = C \cup D, f, V),$

$I = (U, A = C \cup \{d\}, f, V,),\ d \in D.$

An extended but relevant list of elements of U, C and D sets are described below.

The *simulation experiments* are the *objects* of the universe $U = \{x_1, x_2, x_3, \dots, x_{30}\}$ where x_i denotes the object of the universe with index i.

An *extended set of condition attributes* may be defined as follows

$C = \{ P, E, L(c_{04}), \lambda(c_{01}), \lambda_N, N_{LP}, N_{cores}(c_{03}), \tau, simulated\ virtual\ time, \} \cup$

$\{conservative\ synchronisation\ protocol\ with\ null\ message\ algorithm\} \cup$

$\{ Q, q, number\ of\ jobs\ in\ CQN, inter\ arrival\ time,$

$service\ time, FCFS\ service\ discipline, switching\ time\ between\ tandems,$

$propagation\ delay\ between\ simple\ queues\ \} \cup$

$\{ OMNet++, MPI, Linux\ Debian \}.$

The set of *decision* attributes under consideration can be set as

$D = \{relative\ speedup(d_{01}), speedup(c_{02}, d_{02}), utilization\ of\ resources\}.$
(The variables in brackets (for example, c_{04}) shows the variables selected for the analysis.)

5.2.1 Generating Predictions and Costs

For the prediction performance analysis the following decision table after discretization and appropriate coding is used:

$I_{d_{01}} = (U, A = C \cup \{d_{01}\}, f, V)$, $U = \{x_1, x_2, \dots, x_{30}\}$, $C = \{c_{01}, c_{02}, c_{03}, c_{04}\}$,

$V_{c_{01}} = \{l, m, h, s, e\}$, $V_{c_{02}} = \{a, n\}$, $V_{c_{03}} = \{2,4,6,8,12,24\}$,

$V_{c_{04}} = \{f(v'_{c_{04}} = 0.1), g, h, o, t(v'_{c_{04}} = 1000)\}$, $V_{d_{01}} = \{L(0 \le v'_{d_{01}} < 0.6), H\}$.

(For the later analysis, some values are shown before coding too (for example, $v'_{c_{04}} = 0.1$))

The examination is performed in a form of *TRST train-and-test* analysis. For the *train-and-test* examination, based on our previous results presented in [24], the *Rosetta System* [13] is used with *G=Johnson's RSES (Rough Set Exploration System)* reduct and rule generation method and with the subsequent classification of objects. The algorithm of examination is as follows:

Input: $I_{d_{01}}$, simulation runtime and configuration data, TRST configuration setup data: $\left(U = U_{train(i)} \cup U_{test(i)}\right) \wedge ((U_{train(i)} \cap U_{test(i)}) = \emptyset) \wedge \left(\left|U_{train(i)}\right|/|U| = = \frac{15}{30}\right) \wedge (RND_{seed} = i) \wedge (G = Johnson's\ RSES)$

Output: approximation of classification prediction data, and SPC evaluation

begin

for i=1 **to** 8 **for** each prediction case **do**

//prediction cases = 0, 3, 4,

compute TRST

//for the series of computation use the same $(U_{train(i)}, U_{test(i)})$

//pairs $(i = 1,2, \dots, 8)$

return *classification prediction rules and classification prediction data, E1, E2 and E3 evaluation data*

end

Table 3 shows the *costs of simulation experiments* $K(x_i)$ $(x_i \in U, i = 1,2, \dots, 30)$.

Table 3
Cost of PDES simulation experiments $K(x_i)$ [ks]

N_{cores}	L=0.1simsec		L=1simsec		L=10simsec		L=100simsec		L=1000simsec	
	x_i	$K(x_i)$	x_i	$K(x_i)$	x_i	$K(x_i)$	x_i	$K(x_i)$	x_i	$K(x_i)$
N_{cores}=2	x_{01}	209.60	x_{07}	22.73	x_{13}	28.56	x_{19}	0.82	x_{25}	0.48
N_{cores}=4	x_{02}	52.40	x_{08}	56.88	x_{14}	10.92	x_{20}	0.60	x_{26}	0.44
N_{cores}=6	x_{03}	24.66	x_{09}	28.72	x_{15}	0.79	x_{21}	0.58	x_{27}	0.44
N_{cores}=8	x_{04}	16.55	x_{10}	18.48	x_{16}	0.69	x_{22}	0.56	x_{28}	0.44
N_{cores}=12	x_{05}	8.73	x_{11}	10.84	x_{17}	0.63	x_{23}	0.56	x_{29}	0.44
N_{cores}=24	x_{06}	1.23	x_{12}	0.67	x_{18}	0.62	x_{24}	0.58	x_{30}	0.42

In Table 4, values of c*ost of rules* $K(s_j)$ are shown in order of their occurrence in predictions ($s_j \in \bigcup_{i=1}^{8} S_{train(i)}, j = 1,2,\dots,24$).

Table 4
Cost of rules $K(s_j)$ [ks]

s_j	s_1	s_2	s_3	s_4	s_5	s_6	s_7	s_8
$K(s_j)$	313.17	3.70	2.67	2.87	1.85	2.90	0.79	2.29
s_j	s_9	s_{10}	s_{11}	s_{12}	s_{13}	s_{14}	s_{15}	s_{16}
$K(s_j)$	1.63	1.09	0.69	22.74	0.67	1.81	34.90	1.30
s_j	s_{17}	s_{18}	s_{19}	s_{20}	s_{21}	s_{22}	s_{23}	s_{24}
$K(s_j)$	0.79	0.63	2.87	1.09	1.10	1.70	6.68	5.68

In Table 5, *costs of predictions* $K(S_{train(i)})$ are shown together with the number of prediction rules $|S_{train(i)}|$ in the prediction ($i = 1,2,\dots,8$).

Table 5
Cost of predictions $K(S_{train(i)})$ [ks] and number of rules in $S_{train(i)}$

Prediction(i)	1	2	3	4	5	6	7	8
$K(S_{train(i)})$	331.85	322.97	351.79	357.85	329.67	364.82	336.05	357.99
$\lvert S_{train(i)} \rvert$	9	7	10	8	10	10	7	6

In the following points, based on simulation results and on RST modeling and train-and-test examination data, cases of single predictions and series of predictions, with and without dropping, are analyzed using *prediction performance coefficients*. The basic series of predictions (prediction case 0) is introduced in point 5.2.2. All the other prediction analysis examples (prediction case 1-5) introduced in the analysis are derived from prediction case 0. The efficacy minimum requirement for all prediction cases is $E1_{limit} \geq 60\%$.

5.2.2 Predictions with Full Set of Attributes and Rules

Prediction case 0: $\forall_{i=1}^{8} S_{prediction(i)} := S_{train(i)}$

Cost data and rule set sizes for the series of predictions are shown in Table 3, 4 and 5. The effectiveness coefficient of prediction series is

$E3_{series} = E3(S_{train}) = \overline{E2}_8 \left| \overline{E1}_8 \right.$ where

$\overline{E2}_8 = \frac{1}{8}\sum_{i=1}^{8} E1_i / \frac{1}{8}\sum_{i=1}^{8} K\left(S_{train(i)}\right) = 77\%/344.12ks = 0.224\frac{\%}{ks}$, and

$\overline{E1}_8 = \frac{1}{8}\sum_{i=1}^{8} E1(S_{train(i)}) = 77\% > (E1_{limit} = 60\%)$.

5.2.3 Dropping in Single Predictions: Efficacy and Efficiency Analysis

Prediction case 1: dropping $S_{prediction(1)} := S_{train(1)} \setminus \{s_3\}$

Set of prediction rules $S_{train(1)}$ consists of nine rules ($S_{train(1)} = \{s_1, s_2, \dots, s_9\}$). The limit $E1_{limit} \geq 0.6$ has been accepted, thus the rule $s_3 = (c_{04}(t) \Rightarrow d_{01}(H))$, $(s_3 \in S_{train(1)})$ can be dropped *efficaciously* since the effect of dropping on $E1$ is

$$\left(\left(\left(\sum_{l=1}^{15=|U_{test(1)}|} p(x_l)\right)_{S_{train(1)}} = 11\right) - \left(\left|Match_{U_{test(1)}}(s_3)\right| = 2\right) = 9\right) \geq$$
$$\left(E1_{limit} * \left|U_{test(1)}\right| = 0.6 * 15 = 9\right).$$

Decision rule $s_1 = (c_{04}(f) \Rightarrow d_{01}(L))$, $(s_1 \in S_{train(1)})$ *cannot* be dropped *efficaciously* because

$$\left(\left(\left(\sum_{l=1}^{15=|U_{test(1)}|} p(x_l)\right)_{S_{train(1)}} = 11\right) - \left(\left|Match_{U_{test(1)}}(s_1)\right| = 3\right) = 8\right) \not\geq$$
$$\left(E1_{limit} * \left|U_{test(1)}\right| = 0.6 * 15 = 9\right).$$

Cost of rule s_3 is $K(s_3) = 2.67ks$ thus after dropping s_3 $K\left(S_{train(1)} \setminus \{s_3\}\right) = 329.18ks$. The efficacy and efficiency coefficients after dropping are

$E1\left(S_{train(1)} \setminus \{s_3\}\right) = 60\%$, $E2\left(S_{train(1)} \setminus \{s_3\}\right) = 0.182\frac{\%}{ks}$ respectively. Comparing $E2_{limit} = E1_{limit}/\frac{1}{8}\sum_{i=1}^{8} K\left(S_{prediction}\right)$ for both before and after dropping cases, the next inequality has been got: $E2_{limit}\left(S_{train(1)}\right) = 0.181\frac{\%}{ks} <$

$< E2_{limit}\left(S_{train(1)} \setminus \{s_3\}\right) = 0.182\frac{\%}{ks}$, that is $S_{train(1)}$ is worse in effectiveness.

Prediction case 2: dropping $C_{prediction(1)} := C \setminus \{c_{03}\}$

Extending the previous case, the *attribute* c_{03} may be dropped *efficaciously* if the following set of *sufficient* conditions can be satisfied:

$$\exists S_{EF(1)}\left(S_{train(1)} = \left(S_{EF(1)} \cup S_{FE(1)}\right)\right) \wedge \left(\{c_{03}\} \notin C_{S_{EF(1)}}\right) \wedge E1\left(S_{EF(1)}\right) \geq$$

$\geq E1_{limit}$, where set $C_{S_{EF(1)}}$ denotes the set of condition attributes used by rules of set $S_{EF(1)}$. The partitioning $S_{train(1)} = (S_{EF(1)} = \{s_1, s_2, s_3\}) \cup S_{FE(1)} = \{s_4, s_5, s_6, s_7, s_8, s_9\}$, satisfies the conditions since $E1\left(S_{\mathrm{EF}(1)}\right) = 60\,\% = E1_{limit}$ and $\left(C_{S_{FE(1)}} \setminus C_{S_{EF(1)}}\right) = \{c_{03}, c_{04}\} \setminus \{c_{04}\} = \{c_{03}\}$.

The cost of prediction after dropping c_{03} is $K\left(S_{train(1)\setminus\{c_{03}\}}\right) = K\left(S_{EF(1)}\right) =$

$= 319.54ks$, thus the efficiency got is $E2\left(S_{train(1)\setminus\{c_{03}\}}\right) = 0.188\frac{\%}{ks}$.

5.2.4 Dropping in Series of Predictions: Effectiveness Analysis

Prediction case 3: dropping $\forall_{i=1}^{8} S_{prediction(i)} := S_{train(i)} \setminus \{s_1\}$

The effectiveness *after* dropping the *rule* s_1 is

$E3_{series} = E3(S_{train} \setminus \{s_1\}) = \overline{E2}_8 | \overline{E1}_8$ where

$\overline{E2}_8 = \frac{1}{8}\sum_{i=1}^{8} E1_{(i)} / \frac{1}{8}\sum_{i=1}^{8} K\,(S_{train(i)} \setminus \{s_1\}) = 1.680\frac{\%}{ks}$, and

$\overline{E1}_8 = \frac{1}{8}\sum_{i=1}^{8} E1(S_{train(i)} \setminus \{s_1\}) = 52\%$.

In this case, dropping s_1 is highly *efficient* (since $\overline{K}(S_{train}) = 344.12ks$ and $K(s_1) = 313.17ks$) but the dropping is not *efficacious* because $52\% < E1_{limit} = 60\%$ and thus the dropping is not *effective* too.

Prediction case 4: dropping $\forall_{i=1}^{8} S_{prediction(i)} := \{s_1, s_2, s_3\}$

For the case of this rule dropping effectiveness is

$E3_{series} = E3(\{s_1, s_2, s_3\}) = \overline{E2}_8 | \overline{E1}_8$ where

$\overline{E2}_8 = \frac{1}{8}\sum_{i=1}^{8} E1_i / \frac{1}{8}\sum_{i=1}^{8} K\,(S_{train(i)} = \{s_1, s_2, s_3\}) = 0.194\frac{\%}{ks}$, and

$\overline{E1}_8 = \frac{1}{8}\sum_{i=1}^{8} E1(S_{train(i)} = \{s_1, s_2, s_3\}) = 62\% > (E1_{limit} = 60\%)$.

Prediction case 5: dropping $\forall_{i=1}^{8} S_{prediction(i)} = S_{train(i)} | C := C \setminus \{c_{03}\}$

Attribute c_{03} could be dropped *efficaciously* for the series of predictions (continuing the analysis of prediction case 2) since the *sufficient* set of conditions,

$\bigvee_{i=1}^{8} \exists S_{EF(i)} \left(S_{train(\mathrm{i})} = \left(S_{EF(i)} \cup S_{FE(i)}\right)\right) \wedge (\{c_{03}\} \notin C_{S_{EF(i)}})) \wedge$

$\wedge \left(\left(\frac{1}{8}\sum_{i=1}^{8} E1\left(S_{EF(i)}\right)\right) \geq E1_{limit}\right)$, can be satisfied by simply taking $\bigvee_{i=1}^{8} S_{EF(i)} = \{s_1, s_2, s_3\}$ for this case too. Thus, the effectiveness evaluation gives the same numbers as for prediction case 4:

$E3_{series} = E3(S_{EF} | C \setminus \{c_{03}\}) = \overline{E2}_8 | \overline{E1}_8$ where

$\overline{E2}_8 = \frac{1}{8}\sum_{i=1}^{8} E1_i / \frac{1}{8}\sum_{i=1}^{8} K\,(S_{train(i)} = S_{EF(i)}) = 0.194\,\frac{\%}{ks}$, and

$\overline{E1}_8 = \frac{1}{8}\sum_{i=1}^{8} E1(S_{EF(i)}) = 62\% > (E1_{limit} = 60\%)$.

6 Comparison and Discussion of Predictions

Figure 4 compares three series of predictions $S_{prediction} = S_{train}$ (case 0), $S_{prediction} = \{s_1, s_2, s_3\}$ (case 4) and $S_{prediction} = S_{train} \setminus \{s_1\}$ (case 3). The diagram shows $E1$ and $E2$ coefficients for every single prediction and shows $\overline{E2}$ and $\overline{E1}$ values of $E3$ for the series of predictions too. To make the comparison of predictions easier, the efficiency coefficients are calculated such that $K\left(S_{prediction} = \{s_1, s_2, s_3\}\right) = 319.54ks = 100\%$.

For the single predictions of $S_{prediction} = S_{train}$, the relation $\forall_{i=1}^{8} E1_{(i)}\left(E1_{(i)} \geq \geq E1_{limit}\right)$ is hold, and the relative efficiency of the series $\overline{E2}$ is 72% ($\overline{E1}$= 77%).

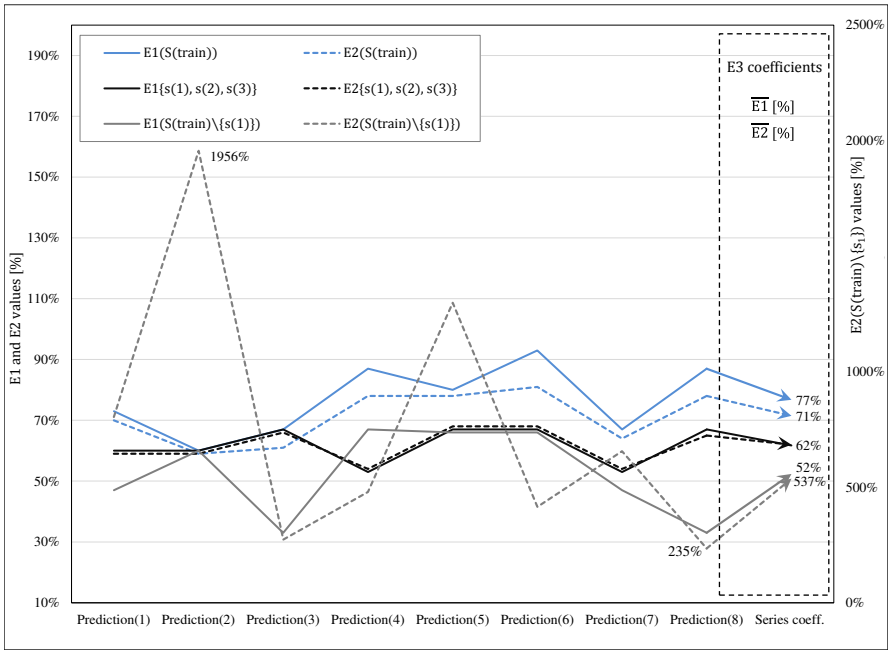

Figure 4
E1, E2 and E3 evaluation of predictions and droppings

For $S_{prediction} = \{s_1, s_2, s_3\}$, the relation $\forall_{i=1}^{8} E1_{(i)}(E1_{(i)} > 50\%)$ is true for every single prediction. Efficacy of series is $\overline{E1} = 62\%$, with a relative efficiency of $\overline{E2} = 62\%$ too. If $\overline{E1} = 60\% = E1_{limit}$ has been accepted then $S_{prediction} = \{s_1, s_2, s_3\}$ performs better: $\overline{E2}(\{s_1, s_2, s_3\})$ =60% and $\overline{E2}\left(S_{prediction} = S_{train}\right)$ = =56%.

Dropping s_1 ($S_{prediction} = S_{train} \setminus \{s_1\}$) leads to a significant decrease of $\overline{E1}$ (77% → 52%), and results in an *ineffective* series of predictions. All the single predictions of $E2(S_{train} \setminus \{s_1\})$ are in the range between 235% and 1956%. The efficiency of the series $\overline{E2}(S_{train} \setminus \{s_1\})$ is 537%. The rule with the highest cost s_1 has significant influence on efficacy and dominating influence on efficiency of predictions. (Rule s_1 is included in $S_{prediction} = \{s_1, s_2, s_3\}$ and its proportion in the cost of the whole set is 98% (Table 4).)

This evaluation indicates the need for the feedback to model identification phase.

The s_1 rule has the form $s_1 = (c_{04}(f) \Rightarrow d_{01}(L))$ where $c_{01}(f) = v'_{c_{04}} = 0.1$ and $d_{01}(L) = v'_{d_{01}} < 0.6$. The relation $Supp(s_1) = 1$ is true for the

$lookahead = 0.1$ column in Table 2. The cost of the rule $K(s_1) = \sum_{l=1}^{6} K(x_l) = 313.17ks$ is the sum of costs of 6 experiments of the universe $x_{01} - x_{06}$ in Table 3. It means that if objects $x_{01} - x_{06}$ are excluded from the model, then there is no need for the high cost s_1 rule.

This modification of the model allows decreasing prediction costs without losing the prediction power in ranges with higher potential speed increases.

Conclusions

In past years, numerous simulation performance prediction methods have been developed that support simulation model development for PDES, since PDES execution can significantly decrease model runtime and developing simulation models with high PDES runtime features have remained challenging tasks. The emerging execution platforms with on-demand access and charge-per-use services bring into focus, the importance of cost/quality evaluation in performance predictions. Here, we have defined prediction performance improvement operations, based on the system of performance coefficients of efficacy (E1), efficiency (E2), effectiveness (E3), characterizing prediction correctness, evaluating correctness to cost relationship and describing correctness cost behavior for a series of predictions, respectively. We included the evaluation and improvement steps in a traditional RST train-and-test algorithm and added it to a classic CFM to form an integrated prediction method. We presented the work of the improved prediction method on a case study of a Closed Queuing Network (CQN) model PDES CFM analysis. In the analysis of the CFM RST model and results of the train-and-test examination, we presented the use of E1, E2 and E3 coefficients for rule and attribute dropping operations and the feedback to the CFM and RST model-identification phase was shown. For the case study implementation, the OMNet++ DES framework and the Rosetta Rough Set Software System were used. Future research is planned to focus on the effectiveness evaluation of simulation model output data, preprocessing for rough modeling and on the application of the method, for methods other than CFM.

References

[1] Perumalla, K. S., (2010) μπ: a Scalable and Transparent System for Simulating MPI Programs, In Proceedings of the 3rd International ICST Conference on Simulation Tools and Techniques, ICST (Institute for Computer Sciences, Social-Informatics and Telecommunications Engineering), p. 62

[2] Perumalla, K. S., (2006) Parallel and Distributed Simulation: Traditional Techniques and Recent Advances, In Proceedings of the 38th Winter Simulation Conference, pp. 84-95

[3] D'Angelo, G., (2011) Parallel and Distributed Simulation from Many Cores to the Public Cloud (Extended Version), In: Proceedings of the 2011

International Conference on High Performance Computing and Simulation (HPCS 2011) Istanbul (Turkey) IEEE, July 2011, ISBN 978-1-61284-382-7 http://dx.doi.org/10.1109/HPCSim.2011.5999802,arXiv preprint arXiv:1105.2301. pp.1-9

[4] Yoginath, S. B., Perumalla, K. S., (2013) Empirical Evaluation of Conservative and Optimistic Discrete Event Execution on Cloud and VM platforms, In Proceedings of the 2013 ACM SIGSIM conference on Principles of advanced discrete simulation, pp. 201-210

[5] Fujimoto, R. M., (1990) Performance of Time Warp under Synthetic Workloads, In Proceedings of the SCS Multiconference on Distributed Simulation, San Diego, CA, USA, 17-19 January, 1990, pp. 23-28

[6] Fujimoto, R. M., (2000) Parallel and Distributed Simulation Systems, John Wiley & Sons, USA, ISBN: 0-471-18383-0

[7] Kunz, G.; Tenbusch, S., Gross, J., Wehrle, K., (2011) Predicting Runtime Performance Bounds of Expanded Parallel Discrete Event Simulations, In Modeling, Analysis & Simulation of Computer and Telecommunication Systems (MASCOTS), 2011 IEEE 19th International Symposium on IEEE, pp. 359-368

[8] Juhasz, Z., Turner, S., Kuntner, K., Gerzson, M., (2003) A Performance Analyser and Prediction Tool for Parallel Discrete Event Simulation, International Journal of Simulation, Vol. 4, No. 1, May 2003, pp. 7-22

[9] Muka, L., Lencse, G., (2008) Cooperating Modelling Methods for Performance Evaluation of Interconnected Infocommunication and Business Process Systems, In Proceedings of the 2008 European Simulation and Modelling Conference (ESM'2008), Le Havre, France, Oct. 27-29 EUROSIS-ETI, pp. 404-411

[10] Muka, L., Lencse, G., (2011) Method for Improving the Efficiency of Simulation of ICT and BP Systems by Using Fast and Detailed Models, Acta Technica Jaurinensis, Vol. 5, No. 1, pp. 31-42

[11] Muka, L., Benko, B. K., (2013) Meta-Level Performance Management of Simulation: The Problem Context Retrieval Approach, Periodica Polytechnica, Electrical Engineering and Computer Science, 55(1-2), pp. 53-64, DOI: 10.3311/pp.ee.2011-1-2.06

[12] Varga, A., Hornig, R., (2008) An Overview of the OMNeT++ Simulation Environment, In Proceedings of the 1st international conference on Simulation tools and techniques for communications, networks and systems & workshops, ICST (Institute for Computer Sciences, Social-Informatics and Telecommunications Engineering), pp. 60-69

[13] Komorowski, J., Øhrn, A., Skowron, A., (2002) The ROSETTA Rough Set Software System, In Handbook of Data Mining and Knowledge Discovery,

W. Klösgen and J. Zytkow (eds.), Oxford University Press, ch. 2-3, ISBN 0-19-511831-6

[14] Varga, A., Sekercioglu, Y. A., Egan, G. K. (2003) A Practical Efficiency Criterion for the Null Message Algorithm, Proceedings of the European Simulation Symposium (ESS 2003), Oct. 26-29, 2003, Delft, The Netherlands, SCS International, pp. 81-92

[15] Lencse, G., Varga, A., (2010) Performance Prediction of Conservative Parallel Discrete Event Simulation, Proceedings of the 2010 Industrial Simulation Conference (ISC'2010), Budapest, Hungary, 7-9, June, 2010, EUROSIS-ETI, pp. 214-219

[16] Lencse, G., Derka I., Muka, L., (2013) Towards the Efficient Simulation of Telecommunication Systems in Heterogeneous Execution Environments", In proceedings of: TSP2013, Edited by Norbert Herencsar, Karol Molnar, the 36th International Conference on Telecommunications and Signal Processing, Rome, Italy, pp. 304-310

[17] Lencse, G., Derka, I., (2013) Testing the Speed-up of Parallel Discrete Event Simulation in Heterogeneous Execution Environments, In proceeding of: ISC'2013, Edited by Veronique Limere and El-Houssaine Aghezzaf, ISBN 978-90-77381-76-2, 11th Annual Industrial Simulation Conference, Ghent University, Ghent, Belgium, pp. 101-107

[18] Lencse, G., (1998) Efficient Parallel Simulation with the Statistical Synchronization Method, Proceedings of the Communication Networks and Distributed Systems Modeling and Simulation (CNDS'98), San Diego, CA. Jan. 11-14, SCS International, pp. 3-8

[19] Lencse, G., (2002) Parallel Simulation with OMNeT++ using the Statistical Synchronization Method, Proceedings of the 2nd International OMNeT++ Workshop, Jan. 8-9, Technical University Berlin, Berlin, Germany, pp. 24-32

[20] Lencse, G., (2009) An Efficient Statistical Synchronization Method for Parallel Simulation, Journal on Information Technologies and Communications, (ISSN 0866-7039) Volume E-1, 1(5), pp. 15-23

[21] Preisler, T., Dethlefs, T., Renz, W., (2015) Simulation as a Service: A Design Approach for Large-Scale Energy Network Simulations, In Computer Science and Information Systems (FedCSIS), 2015 Federated Conference on IEEE, pp. 1765-1772

[22] Krishnaswamy, S., Zaslavsky A., Loke, S. W., (2002) Predicting Run Times of Applications Using Rough Sets, In Ninth International Conference on Information Processing and Management of Uncertainty in Knowledge-Based Systems (IPMU 2002), pp. 455-462

[23] Song, C., Guan, X., Zhao, Q., Ho, Y. C., (2005) Machine Learning Approach for Determining Feasible Plans of a Remanufacturing System,

Automation Science and Engineering, IEEE Transactions on, 2(3), pp. 262-275

[24] Muka, L., Derka, I., (2013) Improving Performance Prediction of Parallel and Distributed Discrete Event Simulation: A Rough Sets-based Approach, In proceeding of: ISC'2013, Edited by Veronique Limere and El-Houssaine Aghezzaf, ISBN 978-90-77381-76-2, 11th Annual Industrial Simulation Conference, Ghent University, Ghent, Belgium, pp. 95-100

[25] Pawlak, Z.; (1982) Rough sets, International Journal of Parallel Programming, 11(5), pp. 341-356

[26] Pawlak, Z., Skowron, A., (2007) Rudiments of Rough Sets, Information sciences, 177.1, pp. 3-27

[27] Zhang, J., Li, T., Ruan, D., Gao, Z., Zhao, C., (2012) A Parallel Method for Computing Rough Set Approximations, Information Sciences,194.2, pp. 209-223

[28] Bazan, J. G., Szczuka, M, (2005) The Rough Set Exploration System, In Transactions on Rough Sets III, Springer Berlin Heidelberg, pp. 37-56

[29] Suraj, Z., (2004) An Introduction to Rough Set Theory and Its Applications, ICENCO, Cairo, Egypt, pp. 1-39

[30] Gregory, F., (1993) Cause, Effect, Efficiency and Soft Systems Models, Journal of the Operational Research Society, Vol. 44 (4), pp. 333-344

[31] Checkland, P., (2000) Soft Systems Methodology: a Thirty Year Retrospective, Systems Research and Behavioral Science,17, S11-S58

[32] Muka, L., Derka, I., (2014) Simulation Performance Prediction in Clouds, Proceedings of 9th International Symposium on Applied Informatics and Related Areas (AIS2014), Székesfehérvár, Hungary, November 12, 2014, pp. 142-147, ISBN: 978-615-5460-21-010

Derivation and Application of a New Equation for Design and Analysis of Triple Spool Mixed Turbofan Jet Engines with Verification

Foroozan Zare, Árpád Veress

Department of Aeronautics, Naval Architecture and Railway Vehicle
Budapest University of Technology and Economics
Műegyetem rkp. 3, H-1111 Budapest, Hungary
e-mail: fzare@vrht.bme.hu; averess@vrht.bme.hu

Abstract*: The development of an improved mathematical model is reported, herein, for modeling the thermo-dynamic processes of triple spool mixed turbofan jet engines with an afterburner, at start conditions with special care for the verification. The T-s diagram and the main characteristics of the engines are determined by a concentrated parameter-distribution type method, implemented in the MATLAB environment. The governing equations are based on mass, energy balance and the real thermo-dynamic processes. A non-linear constraint optimization method is used, for identifying the unknown parameters. Temperature and component mass fraction dependent gas properties are calculated by iteration cycles in case of functional dependencies. A new and more accurate equation is derived and applied for determining the critical pressure at converging nozzle flow with consideration of the local material properties. The thermo-dynamic analyses are completed for NK-32 and NK-25 turbo jet engines. The plausibility of the method and the verification the new equation is provided.*

Keywords: triple spool turbojet engine, thermodynamics, mathematical model, verification

Nomenclature

Variables(Latin)

A_9	Outlet area of the engine (m^2)
C_f	Specific heat of the fuel (J/kg/K)
C_p	Specific heat (J/kg/K)
$\bar{C}_p$	Mean (between T_i and T_{i+1}) specific heat (J/kg/K)
d_9	Outlet diameter of the engine (m)
D	Inlet diameter of the engine (m)
f	Fuel to air ratio (kg/kg)

L	Length of the engine (m)
L_0	Theoretical air mass required to burn 1 kg fuel at stoichiometry condition (kg/kg)
$\dot{m}$	Mass flow rate (kg/s)
$\dot{m}_{air}$	Air mass flow rate enters in the engine (kg/s)
$\dot{m}_{tech}$	Bleed air mass flow rate due to the technological reason (kg/s)
P	Pressure (Pa)
Q_R	Lower heating value of the fuel (J/kg)
R	Total pressure recovery factor (-)
R	Specific gas constant (J/kg/K)
T	Temperature (K), thrust (kN)
$TSFC$	Thrust Specific Fuel Consumption (kg/(kN h))
V	Velocity (m/s)

Variables(Greek)

β	By-pass ratio (-)
γ	Ratio of specific heats (-)
$\bar{\gamma}$	Ratio of mean specific heats (-)
δ_{bc}	Air income ratio due to the turbine blade cooling (-)
γ_{gas}	Ratio of specific heats for gas (1.33) (-)
δ_{tech}	Bleed air ratio for technological reasons (-)
ζ	Power reduction rate for the auxiliary systems (-)
η	Efficiency (-)
π	Total pressure ratio (-)

Subscripts

0	Total
0-9	Engine cross sections
1, 2, 3	Number of turbine and compressor spool
A	Afterburner
A	Ambient
Al	Afterburner liner
C	Compressor
C	Critical
Cc	Combustion chamber
B	Burning

Bc	Blade cooling
D	Diffuser
F	Fuel, fan
Hp	High pressure
Ip	Intermediate pressure
Lp	Low pressure
M	Mechanical
mix	Mass flow weighted parameter for air-gas mixture
N	Nozzle
S	Isentropic
St	Stoichiometric condition
T	Turbine
tech	(Mass flow) re-movement for technological reason

1 Introduction

A significant number of leading technologies are established and transferred within the aeronautical sector. A wide range of R&D activities are in progress in fields, such as, the application of control theories [1, 2], feasibility study of a new system-solution [3], improvement of component characteristics [4], new approach for noise modeling [5] and diagnostics [6].

This is especially true for the propulsion systems of the aircraft, as it is going to be presented in the next paragraphs and chapters. Moreover, beside the aeronautical applications, the gas turbines are generally used in energy generation in the other contributions of transportation; they can be found in the energetics, oil and gas sectors of the industry. These types of engines have higher power-density ratios (~ 15-22 kW/kg) compared to piston engines (~ 0.7-1.5 kW/kg). The gas turbines are relatively light-weight structures and have a compact size, which makes their installation cost efficient. These engines are less sensitive for overloads; they have less solid cross sectional area against the upstream flow (less drag) and have less vibration due to the well balanced and rather axisymmetric rotating components. The gas turbines have high availability factor (80-99%) and their reliability can be over 99%. They have low emission (there is no lubricant in the combustion chamber and no soot during transient loads) they contain less moving parts and represent less sensitivity for the quality of the fuel used, compared to piston engines. Additionally, there is no need for liquid-based cooling system, but the maximum allowable temperature (e.g. ~ 1450°C) at the turbine inlet section must be limited due to metallurgical factors.

Besides, the technical characteristics of the gas turbines today, a certain amount of potential is available for improving their efficiencies, power and emissions. Although the experiences and the know-how of the gas turbine manufacturers increasing continuously, the different mathematical models with using of optimum choice and form of the most dominant processes can significantly contribute to decrease cost, time and capacity in the early phase of gas turbine design and developments. There are many scientific publications are subjected to the thermodynamic-based simulation approaches, which confirms also the need for creating more and more accurate calculation methods. Guha [7] determined the optimum pressure ratio of fan both in analytical and numerical way for separate stream and mixed stream bypass engines. It has been presented that the optimum fan pressure ratio depends on the thrust and it is a weak function of the bypass ratio. Two simple, explicit relations have been derived for determining the optimum fan pressure ratio in bypass engines. The results of the analytical equations are compared with the output of the numerical optimization. Silva and his co-workers [8] shown an evolutionary approach called the StudGA which is an optimization design method. The purpose of his works is to optimize the performance of the gas turbine in terms of minimizing fuel consumption at nominal thrust output, and simultaneously to maximize the thrust of the same fuel consumption as well as to decrease turbine blade temperature.

Recently, three spool mixed turbofan engines are frequently used in commercial and military applications due to their high power density and efficiency and so low normalized range factor and emission at relatively high flight speed and at wide operational range. Hence, the NK-32 (see Figure 1) and NK-25 turbo jet engines are considered for testing and verifying the results of the presently applied mathematical model. The Kuznetsov NK-32 is an afterburning 3-spool low bypass turbofan jet engine, which powers the Tupolev Tu-160 supersonic bomber, and was fitted to the later model Tupolev Tu-144LL supersonic transporter. It is the largest and most powerful engine ever fitted on a combat aircraft. It produces 245 kN of thrust in maximum afterburner [13]. The Kuznetsov NK-25 is a turbofan aircraft engine used in the Tupolev Tu-22M strategic bomber. It can equal the NK-321 engine as one of the most powerful supersonic engines in service today. It is rated at 245 kN thrust. It was superior to many other engines because of its improved fuel consumption [14].

A concentrated parameter distribution-type method has been developed in the present paper to determine the thermo-dynamic cycles of three spool mixed turbofan engines. Mass and energy balance with real thermo-dynamic processes are used in the computational procedure. The unknown input parameters are determined by a constraint nonlinear optimization. The goal function of the optimization is to minimize the difference between the calculated and available thrust and thrust specific fuel consumption if they are given in the datasheet of the engine. Concerning the material properties, iteration cycles are implemented to evaluate the temperature and component mass fraction dependent gas parameters

as specific heat at constant pressure and ratio of specific heats. A new equation has been derived for determining the critical pressure at converging nozzle flow with considering real thermodynamic conditions. The verifications of the results are carried out by considering available technical specifications, followed by the parameter identifications for the unknown parameters.

Figure 1
NK-32 turbofan jet engine [10]

2 Thermo-Dynamic Model for the Triple Spool Turbofan Engine

Description of the applied engines, assumptions and the modelling approach for the gas turbine has been discussed in the present chapter.

2.1 Introduction and General Remarks

A layout with the considered cross sections of a typical triple spool turbojet engine with afterburner is presented in Figure 2. The environmental parameters as pressure and temperature at static sea level conditions belong to section "0" are obtained by ISA (International Standard Atmosphere) and valid at start conditions:

- Ambient static pressure: p_a=101325Pa
- Ambient static temperature: T_a=288K

The ambient air enters into the engine at section "1". The operational fluid suffers from pressure drop in the inlet diffuser, which is between port "1" and "2". The compressed air is generated from cross section "2" to "3". The compressor unit

consists of three main segments as low, medium and high pressure components. The low pressure compressor unit operates as fan module also and the by-passed air leaves the downstream section of the last fan stage is not directly exhausted, but it flows in a duct around the engine core and it is mixed with the hot gases leaving the turbine at section "6". The combustion chamber is located between port "3" and "4", where the heat is generated by adding fuel to the compressed air at stoichiometric condition and at burning activation temperature. The flow stream with high total enthalpy expands and provides energy to the high, medium and low pressure turbines, which is transmitted to the high, medium and low pressure compressor spool respectively. The afterburner for increasing thrust is located section "6" and "7". The exhaust gases with unburned oxygen leaves the engine across the nozzle ("7"-"9") with producing thrust.

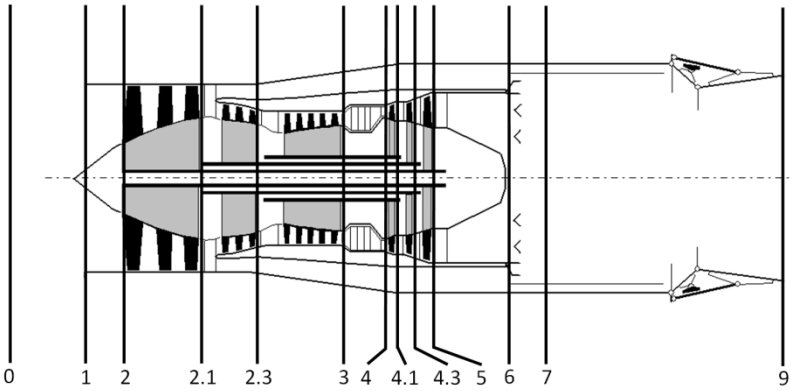

Figure 2

The layout of the mixed triple spool turbofan engine with afterburner [12]

Regarding the present investigations, real engine specifications are considered for plausibility. However, based on the available literature [9], there are known and unknown data that can be distinguished. The known parameters are the incoming air mass flow rate, pressure ratio of the compressor, turbine inlet total temperature and the length and the diameter of the engine, which are also considered as input parameters of the analyses. The unknown parameters are; efficiencies (mechanical, isentropic of compressor and turbine, burning and exhaust nozzle), losses (total pressure recovery of inlet diffuser, combustion chamber and afterburner or turbine exhaust pipe), power reduction rates of the auxiliary systems, total pressure ratio of the fan and intermediate pressure compressor, bleed air ratios for technological reasons, air income ratios due to blade cooling and total temperature at the afterburner. In order to determine these unknown parameters, constrained nonlinear optimization method is applied with the goal function to minimize the deviations between the calculated and given thrust and thrust specific fuel consumption.

Beside the unvarying material properties, such as, specific gas constants, it is important to take the local temperature and mass fraction conditions into consideration in determining other parameters, such as, the specific heat at constant pressure and the ratio of the specific heats. These variables can be changed not only at each cross section of the engine, but also at different operational conditions belongs to different compressor pressure ratio. Equation (1) and (3) shows the expressions how they are determined as the mean value through the considered process. Equation (2) and (4) presents their standalone value at given temperature and fuel to air mass flow ratio. Iteration processes are applied if the temperature and/or fuel to air ratio is the variable of the unknown parameter so as to gain the balance between the temperature and mass fraction dependent material properties and the determined unknown thermo-dynamic parameter.

$$\bar{C}_{pmix}(T_i, T_{i+1}, f) = \frac{1000 \sum_{j=0}^{n} \frac{a_j + f c_j}{(j+1)(f+1)} \left[\left(\frac{T_{i+1}}{1000}\right)^{j+1} - \left(\frac{T_i}{1000}\right)^{j+1} \right]}{T_{i+1} - T_i} \quad (1)$$

$$C_{pmix}(T, f) = \sum_{j=0}^{n} \frac{a_j + f c_j}{f+1} \left(\frac{T}{1000}\right)^{j} \quad (2)$$

$$\bar{\gamma}_{mix} = \frac{\bar{C}_{pmix}(T_i, T_{i+1}, f)}{\bar{C}_{pmix}(T_i, T_{i+1}, f) - R_{mix}} \quad (3)$$

$$\gamma_{mix} = \frac{C_{pmix}(T, f)}{C_{pmix}(T, f) - R_{mix}} \quad (4)$$

The polynomial constants for air and kerosene fuel are a_j and c_j according to [11]. The values of the polynomial constants for the used gases are shown in Table 1.

Table 1
The used Polynomial constants for determining the material properties of gases [11]

a_j	Value	c_j	Value
a_0	1043.797	c_0	614.786
a_1	-330.6087	c_1	6787.993
a_2	666.7593	c_2	-10128.91
a_3	233.4525	c_3	9375.566
a_4	-1055.395	c_4	-4010.937
a_5	819.7499	c_5	257.6096
a_6	-270.54	c_6	310.53
a_7	33.60668	c_7	-67.426468

2.2 Mathematical Model of the Triple Spool Turbojet Engine

The used physical and mathematical approaches have been introduced in the present subchapter.

The engine operates at sea level start condition in the present case. Total pressure recovery has been considered in the inlet diffuser of the engine. The isentropic efficiencies and pressure ratios are used at fan, intermediate and high pressure compressor for calculating the stagnation temperatures and pressures at the outlets of the units. Total pressure recovery has been considered due to the real flow modeling for determining the total pressure at the outlet of the combustion chamber. Stagnation enthalpy balance of the combustion chamber is used for determining the mass flow rate of the fuel, meanwhile the expected turbine inlet total temperature is considered. Equation (5) includes five terms as 1: stagnation enthalpy of the incoming pure air into the combustion chamber, 2: stagnation enthalpy of the fuel, 3: heat generation by the combustion, 4: stagnation enthalpy of the hot gas at the stoichiometric burning condition, which leaves the combustion chamber, 5: stagnation enthalpy of the pure air, that is found at the outlet section of the combustion chamber.

$$\overbrace{\frac{\dot{m}_{air}}{1+\beta}(1-\delta_{tech})C_{pmix}(T_{03},f=0)T_{03}}^{1}+\overbrace{\dot{m}_{f_{cc}}C_fT_{0,f_{cc}}}^{2}+\overbrace{\eta_bQ_R\dot{m}_{f_{cc}}}^{3}=\overbrace{\underbrace{(\dot{m}_{air,st,cc}+\dot{m}_{f_{cc}})C_{pmix}(T_{04},f_{st,cc})T_{04}}_{4}+\underbrace{(\frac{\dot{m}_{air}}{1+\beta}(1-\delta_{tech})-\dot{m}_{air,st,cc})C_{pmix}(T_{04},f=0)T_{04}}_{5}}^{} \quad (5)$$

$\delta_{tech}=\dot{m}_{tech}/\left(\frac{\dot{m}_{air}}{1+\beta}\right)$ in equation (5) represents the certain amount of mass flow rate re-movements in the high pressure compressor due to the technological reason. Q_R = 42MJ/kg is the lower heating value of the used fluid. $\dot{m}_{air,st,cc}$ (see (6)) is the air mass flow rate, which is involved in the burning process at stoichiometric condition and L_0 =14.72kg/kg. The definition of the fuel to air ratios in the combustion chamber is found in (7).

$$\dot{m}_{air,st,cc}=\dot{m}_{fcc}L_0 \quad (6)$$

$$f_{cc}=\frac{\dot{m}_{fcc}(1+\beta)}{\dot{m}_{air}(1-\delta_{tech})},\ f_{st,cc}=\frac{\dot{m}_{fcc}}{\dot{m}_{air,st,cc}} \quad (7)$$

Iteration cycle is applied for (5) in order to elaborate the coherent values of the fuel to air ratio and the specific heat at constant pressure.

Power equilibrium of the high pressure compressor and turbine is used to determine the total temperature at the outlet section of the high pressure turbine; $T_{04.1}$:

$$\frac{\dot{m}_{air}}{1+\beta}\bar{C}_{pmix}(T_{02.3},T_{03},f=0)(T_{03}-T_{02.3})=$$
$$\eta_m\dot{m}_{4-4.1}(1-\zeta)\bar{C}_{pmix}(T_{04},T_{04.1},f_{hp,T})(T_{04}-T_{04.1}) \quad (8)$$

The mas flow rate of the operational fluid in the high pressure turbine is shown in (9).

$$\dot{m}_{4-4.1} = \frac{\dot{m}_{air}}{1+\beta}(1-\delta_{tech})(1+f_{cc})(1+\delta_{bc}) \tag{9}$$

δ_{bc} represents the incoming air mass flow rate at high pressure turbine for blade cooling (see (10)).

$$\delta_{bc} = \dot{m}_{bc}(1+\beta)/\left(\dot{m}_{air}(1-\delta_{tech})(1+f_{cc})\right) \tag{10}$$

The power balances are used also for the low and intermediate pressure units for determining the exit temperature of the low and intermediate pressure turbines. Iteration cycles are applied also for updating the specific heat at constant pressure in the turbine segments.

The total pressure recovery of the engine section 5-6 (see Figure 2.) is included in the liner location corresponds to 6-7, which approximation has negligible effect for the output of the analyses.

The by-passed and core flow are mixed at section 6. Mass flow weighted averaging procedure is applied for determining the total pressure and energy balance is considered for having the total temperature of the gas mixture.

The afterburner is located between cross section 6. and 7. Total enthalpy balance has been considered for this segment in order to calculate the fuel mass flow rate enters into the afterburner as it is shown in (11).

$$\dot{m}_{air,6}\, C_{pmix}(T_{06}, f=0)T_{06} + \dot{m}_{f,A}C_f T_{0,fA} + \eta_b Q_R \dot{m}_{f_A} + \left(\dot{m}_{air,st,cc} + \dot{m}_{f_{cc}}\right) C_{pmix}\left(T_{06}, f_{st,cc}\right)T_{0,6} = \left(\dot{m}_{air,st,cc} + \dot{m}_{f_{cc}}\right) C_{pmix}\left(T_{07}, f_{st,cc}\right)T_{07} + \left(\dot{m}_{air,st,A} + \dot{m}_{f_A}\right) C_{pmix}\left(T_{07}, f_{st,A}\right)T_{07} + \left(\dot{m}_{air,6} - \dot{m}_{air,st,A}\right)C_{pmix}(T_{07}, f=0)T_{07} \tag{11}$$

The left side of equation (11) shows the incoming total enthalpy into the system and the right hand side represents the leaving one. The first term of equation (11) is the stagnation enthalpy of pure air, which is available at section 6. The second and third term is the total enthalpy of the fuel entering into afterburner and heat generated by the combustion respectively. The last term in the left hand side is the total enthalpy of the incoming hot gases, which are already burnt previously in the combustion chamber. The total enthalpy of the hot gases of the combustion chamber and the afterburner are represented by the first two terms in the right side of the (11). The last term is the total enthalpy of the pure air, which leaves the system. Iterative calculation procedure is used here also to determine the fuel to air ratio of the afterburner at stoichiometric condition $\left(f_{st,A} = \dot{m}_{f_A}/\dot{m}_{air,st,A}\right)$ and the specific heat at constant pressure, which are corresponds to each other by means of functional dependencies.

Expansion processes occur in the exhaust nozzle shown in Figure 3. In order to clarify whether the supposed converging nozzle is chocked or is not, temperature

and component dependent material properties, inlet conditions of the nozzle and its isentropic efficiency are considered. If the calculated critical pressure is higher than ambient pressure, the nozzle flow is considered to be choked, which means that the exit pressure of the nozzle is equal to the critical pressure: p_c. If the ambient pressure is higher than the critical pressure, then the nozzle flow is unchocked; therefore, the exhaust pressure of the exit is equal to the ambient pressure. After having this information and determining the pressure, the temperature and the velocity at the exit of the exhaust nozzle can be calculated.

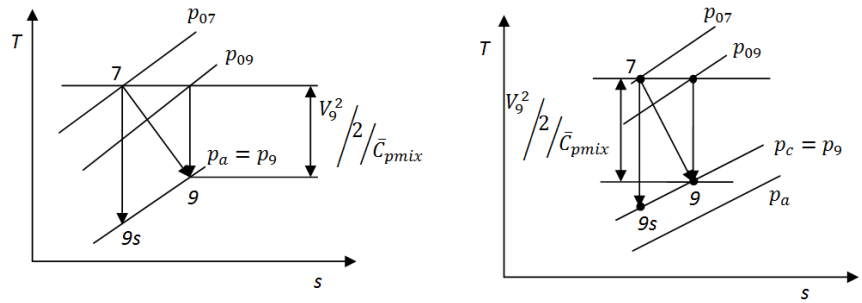

Figure 3
Nozzle flow with losses for unchoked (left side) and for choked (right side) flow conditions

A new analytical equation has been derived for determining the critical pressure at the exhaust port of the nozzle (see (18)), in which, beside the dependences of temperature variation and fuel to air ratio in the specific heat at constant pressure, the ratio of the specific heats are also considered. The critical static pressure at the outlet section of the exhaust system is coupled with the outlet static temperature; hence, iteration cycling is used for determining these variables together with the material properties in case of chocked conditions. The fuel to air ratio at the afterburner is also included in the overall fuel to air ratio:

$$f = \left(\dot{m}_{f_{cc}} + \dot{m}_{f_A}\right)/(\dot{m}_{air} - \dot{m}_{tech} + \dot{m}_{bc}) \tag{12}$$

The derivation of the new equation for the critical pressure at the exhaust nozzle is presented in the followings. First the total enthalpy and then total temperature at section 9 is introduced as it is shown in equation (13) and (14).

$$h_{09} = h_9 + \frac{V_9^2}{2} \Rightarrow C_{pmix}(T_{09}, f)T_{09} = C_{pmix}(T_9, f)\,T_9 + \frac{V_9^2}{2} \Rightarrow T_{09} = T_9 \frac{C_{pmix}(T_9,f)}{C_{pmix}(T_{09},f)} + \frac{V_9^2}{2C_{pmix}(T_{09},f)} \tag{13}$$

$$T_{09} = T_9 \frac{C_{pmix}(T_9,f)}{C_{pmix}(T_{09},f)} + \frac{1}{C_{pmix}(T_{09},f)} \frac{V_9^2}{2} \frac{a_9^2}{a_9^2} \Rightarrow T_{09} = T_9 \frac{C_{pmix}(T_9,f)}{C_{pmix}(T_{09},f)} + \frac{1}{C_{pmix}(T_{09},f)} M_9^2 \frac{\gamma_{mix}(T_9,f)R_{mix}T_9}{2} \tag{14}$$

The critical condition corresponds to M_9=1 and $T_9 = T_c$, so Equation (14) can be reformulated as follows:

$$\frac{T_{09}}{T_c} = \frac{C_{pmix}(T_c,f)}{C_{pmix}(T_{09},f)} + \frac{\gamma_{mix}(T_c,f)R_{mix}}{2C_{pmix}(T_{09},f)} = \frac{2C_{pmix}(T_c,f)+\gamma_{mix}(T_c,f)R_{mix}}{2C_{pmix}(T_{09},f)} \quad (15)$$

The nozzle efficiency and the isentropic static temperature at point 9 is given by equation (16).

$$\eta_n = \frac{C_{pmix}(T_{09},f)T_{09} - C_{pmix}(T_c,f)T_c}{C_{pmix}(T_{09},f)T_{09} - C_{pmix}(T_{9s},f)T_{9s}} \Rightarrow T_{9s} = \frac{C_{pmix}(T_{09},f)}{C_{pmix}(T_{9s},f)}T_{09} - \frac{1}{\eta_n}\frac{C_{pmix}(T_{09},f)T_{09} - C_{pmix}(T_c,f)T_c}{C_{pmix}(T_{9s},f)} \quad (16)$$

The thermodynamic process between point 7 and 9s is isentropic:

$$\frac{p_C}{p_{07}} = \left(\frac{T_{9s}}{T_{09}}\right)^{\frac{\bar{\gamma}_{mix}(T_{09},T_{9s},f)}{\bar{\gamma}_{mix}(T_{09},T_{9s},f)^{-1}}} \quad (17)$$

Equation (18) is appeared after inserting equation (16) and then (15) in (17) $(T_{09} = T_{07})$.

$$p_c = p_{07}\left[\left(\frac{C_{pmix}(T_{09},f)}{C_{pmix}(T_{9s},f)}\right)\left(1 - \frac{1}{\eta_n}\left(1 - \frac{2C_{pmix}(T_c,f)}{(2C_{pmix}(T_c,f)+\gamma_{mix}(T_c,f)R_{mix})}\right)\right)\right]^{\frac{\bar{\gamma}_{mix}(T_{09},T_{9s},f)}{\bar{\gamma}_{mix}(T_{09},T_{9s},f)^{-1}}} \quad (18)$$

$$\gamma_{mix}(T_9,f) = \frac{C_{pmix}(T_9,f)}{C_{pmix}(T_9,f) - R_{mix}} \quad (19)$$

$$\bar{\gamma}_{mix}(T_{09},T_{9s},f) = \frac{\bar{C}_{pmix}(T_{09},T_{9s},f)}{\bar{C}_{pmix}(T_{09},T_{9s},f) - R_{mix}} \quad (20)$$

The output parameters of the analyses are the thrust and thrust specific fuel consumption, which are shown in equation (21) and (22) respectively.

$$T = [\dot{m}_9 V_9 - \dot{m}_{air} V_0] + A_9(p_9 - p_0) \quad (21)$$

$$TSFC = \frac{\dot{m}_{f_{cc}} + \dot{m}_{f_A}}{T} \quad (22)$$

The mass flow rate leaves the engine is found in equation (23).

$$\dot{m}_9 = \frac{\dot{m}_{air}}{1+\beta}[(1 - \delta_{tech})(1 + f_{cc})(1 + \delta_{bc}) + \beta] \quad (23)$$

3 Results and Discussion

NK-32 and NK-25 turbofan engines are used as two gas turbines to analyse and verify the simulation method. The input parameters of the two selected engines are presented in Table 2. However, as it was mentioned before, there are also several unavailable parameters, which are determined by parameter identifications.

The missing efficiencies (mechanical, isentropic of compressor and turbine, burning and exhaust nozzle), losses (total pressure recovery factor of inlet diffuser, combustion chamber and afterburner or turbine exhaust pipe), total pressure ratio of the fan and intermediate pressure compressor, power reduction rates of the auxiliary systems, bleed air ratios for technological reasons, air income ratio due to blade cooling and total temperature of the afterburner are identified by nonlinear constrained optimization. The goal function to be minimized is the difference between the calculated and given thrust and thrust specific fuel consumption by the engine manufacturer. Tables 3, 4 and 5 show the results of the optimizations. The parameters are in the reasonable range therefore they can be accepted.

Table 2
Operational data of the NK-32 and NK-25 turbofan engines from the available specifications [9, 13]

Type of engine	The main characteristics of the engine(at start positions)				
	T_{04} (K)	π_C	β	$\dot{m}_{air}$ (kg/s)	L/D (m/m)
NK-32	1630	28.4	1.4	290	7.45/1.79
NK-25	1600	26	1.44	280.9	7.3/1.442

The thrust and thrust specific fuel consumption – belongs to the parameters found in Tables 2, 3, 4 and 5 – are shown in Table 6. The relative maximal deviation between the given and the calculated data during the parameter fitting is 0.122% in case of thrust and 0.195% at the thrust specific fuel consumption. It means, together, with the plausible parameter identifications, the analysis is suitable for modeling the thermo-dynamic processes of the three spool turbojet engine.

Concerning the verification of the analyses it can be concluded, that although the both engines have the same thrust, the fuel consumption of NK-32 engine is higher due to the lower total pressure recovery factor (higher pressure loss) in the combustion chamber (r_{cc}), afterburner liner (r_{al}) and intake duct (r_d). Moreover, the NK-32 has lower mechanical, nozzle and burning efficiency beside lower fan and compressor segments isentropic efficiencies in comparing with NK-25.

Although the simulation parameters and the results are in acceptable agreement with the available data and with the expectations, more analyses will be necessary for satisfying the accuracy of the method over wider range of applications, including different engine types, operational conditions and more measured data.

Table 3
Identified efficiencies of the NK-32 and NK-25 turbofan engines

	Efficiencies of the cycles						
Type of Engine	η_m	η_n	η_b	$\eta_{hp,T,s}$ $\eta_{ip,T,s}$ $\eta_{lp,T,s}$	$\eta_{f,s}$	$\eta_{hp,C,s}$	$\eta_{\mathrm{ip,C,s}}$
NK-32	0.99	0.94	0.94	0.89	0.84	0.83	0.84
NK-25	0.992	0.95	0.97	0.89	0.86	0.87	0.87

Table 4
Identified total pressure recovery factors of the 2 investigated turbofan engines

	Total pressure recovery factors of comb. chamber (r_{cc}), afterburner liner (r_{al}) and intake duct (r_d)		
Type of Engine	r_{cc}	r_{al}	r_d
NK-32	0.95	0.9	0.91
NK-25	0.96	0.94	0.94

Table 5
Identified parameters of the 2 investigated turbofan engines

	Total pressure ratio of the fan (π_f) and intermediate pressure compressor ($\pi_{ip,C}$), bleed air ratio for technological reasons (δ_{tech}), air income ratio due to blade cooling (δ_{bc}), power reduction rates for the auxiliary systems (ξ) and total temperature of the afterburner (T_{07})					
Type of Engine	π_f	$\pi_{ip,C}$	δ_{tech}	δ_{bc}	ξ	T_{07} (K)
NK-32	2	3	0.16	0.116	0.005	1800
NK-25	2.19	3	0.18	0.0952	0.005	1780

Table 6
Comparisons of the available data with the outputs of the parameter fitting

Type of Engine	Available data (start position)		Outputs of the parameter fitting (start position)	
	T (kN)	*TSFC* (kg/(kN h))	*T* (kN)	*TSFC* (kg/(kN h))
NK-32	245	-	245.1	229.4
NK-25	245	205.3	245.3	205.7

The thermo-dynamic cycles of the engine processes are found in Figure 4. The red curve-sections (or lighter and thinner in grayscale) represent the constant pressures in the T-s diagrams (total from points 0-7 and static at 9). The processes between the engine states denoted, by numbers, are plotted by thicker lines. This visualization effect is the reason of the constant pressure line goes below the process line in case of pressure decrement just after section "3".

The analyses of the NK-32 and NK-25 engines are also completed by using the conventional equation (24) for determining the critical pressure at the exit of the converging nozzle in case of the same thermo-dynamic conditions.

$$p_c = p_{07}\left(1 - \frac{1}{\eta_n}\left(\frac{\gamma_{gas}-1}{\gamma_{gas}+1}\right)\right)^{\frac{\gamma_{gas}}{\gamma_{gas}-1}} \tag{24}$$

The effect of the fuel to air ratio and temperature are not considered in the ratio of specific heat in (24), the flow is considered to be pure gas with γ_{gas}=1.33. The results of the calculations are shown in Table 7. The average deviation between the resulted and the available thrust and thrust specific fuel consumption is

0.119% by using the new equation (18) and 3.13% at the conventional equation (24).

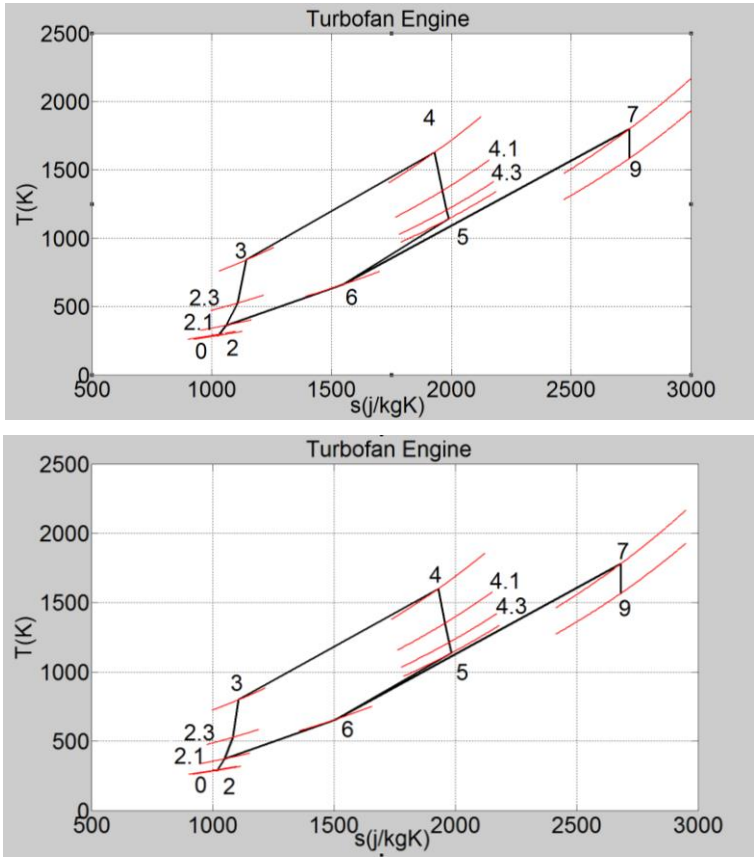

Figure 4

Thermo-dynamic cycle of the NK-32 (top) and NK-25 (bottom) turbofan engine with afterburner (the red curve sections (the lighter thinner ones in grayscale) in the T-s diagrams are the constant pressure curves (total from 0-7 and static at 9) belong to the shown numbers of the engine cross sections)

Table 7

Comparison the effect of the conventional and the new equation on the thrust and the thrust specific fuel consumption in case of NK-32 and NK-25 turbofan engines

Type of Engine	Relative difference (new equation)		Relative difference (conventional equation)	
	T (kN)	*TSFC* (kg/(kNh))	*T* (kN)	*TSFC* (kg/(kNh))
NK-32	0.04%	-	3.27%	-
NK-25	0.122%	0.195%	2.85%	3.27%

Conclusions

A thermo-dynamic model has been developed and implemented in the MATLAB environment, for determining the main characteristics of the triple spool turbojet engines with afterburner. The mass, energy balance and the real thermo-dynamic process equations are used in the concentrated parameter distributions type model, in which the mechanical, isentropic and burning efficiencies, pressure losses and the bleed air ratio, for technological reasons, air ratio for blade cooling, fan and intermediate compressor pressure ratios, the afterburner temperature and power reduction rate of the auxiliary systems are considered. Nonlinear constraint optimization is applied for determining the mentioned data by means of fitting the calculated the thrust and thrust specific fuel consumption – if it was available – to the known parameters, which are given in the specification. Ambient conditions, incoming air mass flow rate, pressure ratio of the compressor, turbine inlet total temperature, the length and diameter of the engine are the input parameters of the analyses. The material properties, such as, specific heat and the ratio of specific heat depends on the temperature and component mass fraction and so they are determined by iteration cycles, in case of functional dependencies.

The calculated thrust and thrust specific fuel consumption of the NK-32 and NK-25 engines by parameter fitting and the available data are compared with each other at start conditions. The results show that the relative maximum deviation between the given and the calculated parameters is 0.122% in case of thrust and 0.195% at the thrust specific fuel consumption, meanwhile the identified parameters are within the plausible range.

A new analytical equation has been derived for determining the critical pressure at the exit of the converging nozzle, in which, beside, the dependences of temperature variation and fuel to air ratio in the specific heat at constant pressure, the ratio of the specific heats is also included. The new equation provides 3.01% (delta) improvements with respect to the conventional formula, for the case of averaged deviation between the resulted and the available thrust and thrust specific fuel consumption for the investigated engine types at the same condition and parameters.

References

[1] Bréda R., Lazar T., Andoga R. and Madarász L.: Robust Controller in the Structure of Lateral Control of Maneuvering Aircraft, Acta Polytechnica Hungarica, pp. 101-124, Vol. 10, No. 5, 2013

[2] Gáti B., and Drouin A.: Open Source Autopilot for Academic Research – The Paparazzi System, Proceedings of the American Control Conference, Washington DC: AACC International, 1-6. ISBN: 978-1-4799-0175-3, 2013

[3] Voskuilj M., Rohács D., Rohács J. and Schousttra R. J.: Preliminary Evaluation of the Environmental Impact related to Aircraft Take-off and

Landings supported with Ground Based (MAGLEV) Power, Proceedings of the 4th Annual International Air Transport and Operations Symposium (ATOS), Toulouse, French, 10.07.2013-12.07. 2013

[4] Beneda K. and Rohács J.: Dynamic Model of Variable Inducer Shroud Bleed for Centrifugal Compressor Surge Suppression, International Review of Aerospace Engineering 6, 163-173, Paper online, 2013

[5] Bera J. and Pokorádi L.: Monte-Carlo Simulation of Helicopter Noise, Acta Polytechnica Hungarica, 12:(2) pp. 21-32, 2015

[6] Andoga R., Főző L., Madarász L. and Karol T.: A Digital Diagnostic System for a Small Turbojet Engine, Acta Polytechnica Hungarica, pp. 45-58, Vol. 10, No. 4, 2013

[7] Abhijit G.: Optimum Fan Pressure Ratio for Bypass Engines with Separate or Mixed Exhaust Streams, Propulsion and power J, Vol. 17, No. 5, 2001, 1117-1122

[8] Silva V. V. R., Khatib W. and Fleming P. J.: Performance Optimization of Gas Turbine Engine, Artificial Intelligence, Vol. 18, No. 5,575-583, Aug. 2005

[9] Кулагин В. В.: Теория расчёт и проектирование авиационных двигателей и энергетических установок. Книга 1, 2, Moscow, 2005

[10] http://www.uk-odk.ru/img/content/products/NK-32_big.png, 15.06.2014

[11] Sánta I.: Gázturbinás Repülőgép Hajtóművek, BME Repülőgépek és Hajók Tanszék, tanszéki jegyzet (Lecture Notes on Jet Engines at BME University), 2008

[12] Kurzke J.: http://www.gasturb.de/, 03.03.2014

[13] https://en.wikipedia.org/wiki/Kuznetsov_NK-32, 01.05.2016

[14] https://en.wikipedia.org/wiki/Kuznetsov_NK-25, 01.05.2016

Numerical Estimation Method of Orthotropic Material Properties of a Roving for Reinforcement of Composite Materials

Gergely Bojtár[1], Béla M. Csizmadia[2], János Égert[1]

[1] Széchenyi István University, Department of Applied Mechanics,
9026 Győr, Egyetem tér 1, Hungary, bojtar@sze.hu, egert@sze.hu
[2] Szent István University, Institute of Mechanics and Machinery,
2103 Gödöllő, Páter K. u. 1, Hungary, csizmadia.bela@gek.szie.hu

Abstract: Knowledge of the material properties is important at machine design from composite materials. This information cannot be found in related literature and is not standard, therefore, it was necessary to determine, by measurements and by basic experiments of the mechanics of materials. This paper presents a new 3D finite element (FE) model-cell for the modeling of the material properties of a roving. By this numerical modeling method, one can determine the orthotropic and macroscopic material properties of a roving. This model-cell, models numerically, a roving, which consists of multiples of thousands of fibers that are embedded in a matrix material, as a homogenized orthotropic material. The numerical results of the material properties of the roving, can be applied to the definition of the macroscopic material properties of fiber reinforced composite laminates.

Keywords: roving; orthotropic material properties; fiber reinforced composite; finite element method; model-cell

1 Introduction

Fiber reinforced composite is a plastic material which is reinforced by glass, carbon, aramid, etc., fibers or roving's. Textile composite plates are layer structured and each layer contains a textile which is impregnated by some sort of plastic. The fibers in the textile are ordered usually in roving's. In a roving there are many thousand straight fibers laying parallel to each other or running in a twisted form and also between the fibers there is plastic material [2]. The diameter of the fibers can be measured in μm-, the thickness of a textile and a composite layer can be measured in tenth of mm-s. The plastic in the composite, the so called matrix, is the carrier or embedding material for the fibers, which can be e.g. a thermo-softening or thermosetting polymer.

For dimensioning or stress checking of a composite structure one needs the material properties of the composite plate. This can be defined by measurements and this is the usual way nowadays [1]. By knowing the textile and the matrix, which was chosen based on an earlier experience, test specimens are produced and the material properties are determined by measurement. There are numerical methods as well for the calculation of material properties of the composite plate, assuming that we know the material properties of the layers [3]. However, the material properties of the layers are unknown in general either. For their definition there is a finite element computation method for building up the material properties of composite layer from the material properties of the textile and the matrix. These numerical methods deliver an approach for the properties of layers, but these calculations are not accurate enough [7, 11, 12]. Failures and uncertainties occur at requirements of the boundary conditions.

The ultimate goal of this research is to determine or at least to estimate numerically, the macroscopic material properties of a textile composite layer with a known geometry and material with a finite element (FE) model-cell. Then, this numerical result is compared to the results of the measurement. But before we would be able to solve this problem, which will be presented in another following article, first we need to understand the behavior of the materials building up the composite layer. The matrix can be described as a homogenous isotropic material, therefore its material properties can be determined safely, by measurement, regardless of the actual composite. The orthotropic material properties resulting from the material structures of the fibers that build up the roving can be assumed known from factory catalogues or literature. These are not modeled separately but we consider the roving itself as a "fiber" in the layer model-cell. The roving can be very multifarious and, as we mentioned earlier, impregnated by matrix material. This means that one roving should be considered as a structure and on a macroscopic level its linear elastic orthotropic material properties should be determined by a computational method. This is our aim with the present paper.

The constitutive equation of linear elastic orthotropic material can be described by [2] to (1) relationship:

$$\begin{bmatrix} \bar{\varepsilon}_{r1} \\ \bar{\varepsilon}_{r2} \\ \bar{\varepsilon}_{r3} \\ \bar{\gamma}_{r12} \\ \bar{\gamma}_{r23} \\ \bar{\gamma}_{r13} \end{bmatrix} = \begin{bmatrix} \frac{1}{E_{r1}} & -\frac{\nu_{r21}}{E_{r2}} & -\frac{\nu_{r31}}{E_{r3}} & 0 & 0 & 0 \\ -\frac{\nu_{r12}}{E_{r1}} & \frac{1}{E_{r2}} & -\frac{\nu_{r32}}{E_{r3}} & 0 & 0 & 0 \\ -\frac{\nu_{r13}}{E_{r1}} & -\frac{\nu_{r23}}{E_{r2}} & \frac{1}{E_{r3}} & 0 & 0 & 0 \\ 0 & 0 & 0 & \frac{1}{G_{r12}} & 0 & 0 \\ 0 & 0 & 0 & 0 & \frac{1}{G_{r23}} & 0 \\ 0 & 0 & 0 & 0 & 0 & \frac{1}{G_{r13}} \end{bmatrix} \begin{bmatrix} \bar{\sigma}_{r1} \\ \bar{\sigma}_{r2} \\ \bar{\sigma}_{r3} \\ \bar{\tau}_{r12} \\ \bar{\tau}_{r23} \\ \bar{\tau}_{r13} \end{bmatrix}. \tag{1}$$

The matrix of material properties in (1) is symmetric, therefore the relationships between Young's modulus and Poisson's ratio look as follows [2]:

$$\frac{\nu_{r12}}{E_{r1}} = \frac{\nu_{r21}}{E_{r2}}, \quad \frac{\nu_{r13}}{E_{r1}} = \frac{\nu_{r31}}{E_{r2}}, \quad \frac{\nu_{r23}}{E_{r2}} = \frac{\nu_{r32}}{E_{r3}}. \tag{2}$$

Considering formula (2) the matrix of material properties in equation (1) has nine independent material constants:

$$E_{r1},\ E_{r2},\ E_{r3},\ \nu_{r12},\ \nu_{r23},\ \nu_{r13},\ G_{r12},\ G_{r23},\ G_{r13}.$$

For the roving model-cell with Volume V, the average strain and stress can be introduced and defined as follows [7], [8], [11]:

$$\bar{\varepsilon}_{rij} = \frac{1}{V}\int_{(V)} \varepsilon_{rij}\, dV, \tag{3}$$

$$\bar{\sigma}_{rij} = \frac{1}{V}\int_{(V)} \sigma_{rij}\, dV. \tag{4}$$

2 The Roving Model-Cell

The aim of creation of the roving model-cell is to be able to model the roving as a homogeneous material. This can be reached by considering average strains and stresses according to (3) and (4). The complete roving can be modeled as homogeneous population of such model-cells.

2.1 The Geometry and Finite Element Mesh of the Roving Model-Cell

The reinforcing fibers in the roving are not regularly positioned in the matrix. In Figure 1 we can see the microscopic structure of a carbon/epoxy composite roving, where the diameter of a fiber is $7\ \mu m$ [9].

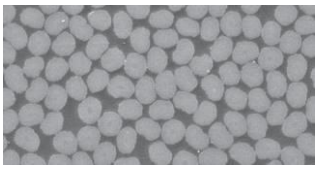

Figure 1
The real position of the fibers in the roving, in the matrix

It is also necessary to model the position of the fibers in the matrix [6]. At the modeling is assumed that the reinforcing fibers are positioned in the model-cell in a regular hexagonal shape (Figure 2). This is a good geometrical approach (Figure 3) to the real case illustrated in Figure 1.

In order to have more simple boundary conditions we configure the side surfaces of the model-cell parallel to the planes of the principal material-directions [5]. At a hexagonal shape there are two possible roving model-cell configurations (Figure 3). For our further examination, we chose the geometry on the right side. The ratio of two sides of these model-cells is:

$$\frac{a}{b} = \frac{1}{\sqrt{3}} . \tag{5}$$

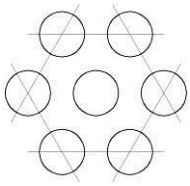

Figure 2
Regular hexagonal shape

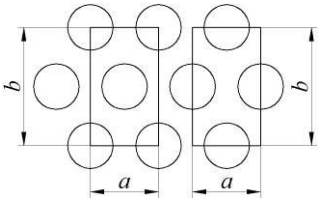

Figure 3
Geometry of possible roving model-cells

The usual ideal cross-section of an untwisted, straight roving is a rectangle ending up in a semicircle, an ellipse or a lens shape (Figure 4) [11]. The cross-section area of the roving is A_r, where n_f number of fiber is located with diameter d_f. This area is provided by the geometry of the roving.

a) Rectangular shape ending up in a semicircle

b) Ellipse shape

c) Lens shape

Figure 4
The usual cross-sections of an untwisted straight roving

The volume ratio of the fibers in the roving can be calculated from the cross-section area of the fibers and from the whole area of the roving:

$$\varphi_{fr} = \frac{A_{fr}}{A_r} = \frac{d_f^2 \pi}{4 A_r} n_f . \tag{6}$$

It is necessary to determine this in order to have the same ratio in the roving model-cell.

The dimensions of the roving model-cell are 10^3 times larger that of the dimensions of the real roving. The units used at the real roving and the roving model-cell are summarized in Table 1. In order to have stresses in the model-cell that are identical to the stresses in the real roving it is necessary to apply force on the model-cell which is 10^6 times higher that of the real force (Table 1).

Table 1
Units in reality and in the roving model-cell

	Real roving	Roving model-cell
Length: l	μm	$\text{mm}=\mu\text{m}\cdot 10^3$
Area: A	μm^2	$\text{mm}^2=\mu\text{m}^2\cdot 10^6$
Force: F	μN	$\text{N}=\mu\text{N}\cdot 10^6$
Stresses: σ_i, τ_{ij}	$\frac{\mu\text{N}}{\mu\text{m}^2}=\frac{10^{-6}\ \text{N}}{10^{-6}\ \text{mm}^2}=\text{MPa}$	$\frac{\text{N}}{\text{mm}^2}=\text{MPa}$

The roving model-cell (Figure 3) includes altogether two fibers. Considering the volume ratio (6) and the side ratio (5) the a and b side length of the roving model-cell can be calculated for the creation of the model-cell of the given roving:

$$a=\sqrt{\frac{d_f^2\pi}{2\sqrt{3}\varphi_{fr}}}, \qquad b=\sqrt{3}a\,. \tag{7}$$

Figure 5 shows also the identification signs of the six side-surfaces of the cell. The dimension of the side-areas is clear.

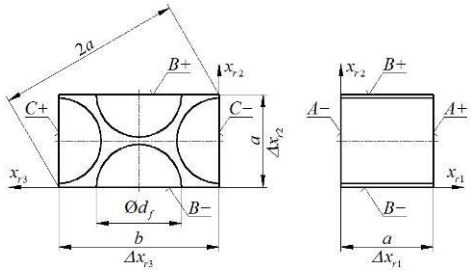

Figure 5
Dimensions of the roving model-cell used for the numerical modeling

A next paper will show a textile layer composite model-cell as well. The results of this model-cell will be checked by experiments. Roving with cross section shown in Figure 6 are applied in this model-cell of the textile layer (see also: Section 2.5).

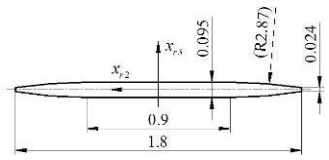

Figure 6
The cross section of the applied roving in the textile layer model-cell

The dimensions of the applied roving in the examined textile material:

$$d_f = 7\ \mu\text{m},\quad n_f = 3000\ \text{db},\quad \varphi_{fr} = 0.7667\,.$$

The dimensions of the examined roving model-cell according to the Table 1:

$$d_f = 7\ \text{mm},\quad a = 7.613\ \text{mm},\quad b = 13.186\ \text{mm},\quad \varphi_{fr} = 0.7667\,,$$

$$A_{A+} = A_{A-} = A_{B+} = A_{B-} = 100.385\ \text{mm}^2,\quad A_{C+} = A_{C-} = 57.958\ \text{mm}^2\,.$$

The finite element computations were carried out with the NX I-deas 6.1 program system. The material coordinate system of the roving is $x_{r1}x_{r2}x_{r3}$, where x_{r1} is the direction parallel to the single fibers (Figure 5). Due to the periodicity we need to apply the so called periodical boundary conditions for the roving model-cell. Therefore we need to generate the finite element mesh in the way that, on the opposite surfaces there should be nodes at the same coordinates and so node-pairs shall be created in the model-cell. A mesh consisting of quadratic hexahedron elements was generated for the examined roving model-cell (Figure 8). The geometry of the model-cell was split into, consisting of five larger volume sections (Figure 8), into further 80 sections in order to be able to create a regular net (Figure 7). In Figure 8 the finite element mesh of the roving model-cell is seen, which consists of 34 994 hexahedron elements and 149 521 nodes.

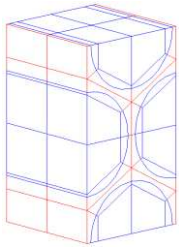

Figure 7
Volume sections of the roving model-cell

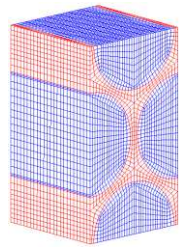

Figure 8
Finite element mesh of the roving model-cell

Due to the regular hexagonal order of the reinforcing fibers the material properties are identical in x_{r2}, x_{r3} direction and in $x_{r1}x_{r2}$, $x_{r1}x_{r3}$ planes:

$$E_{r2} = E_{r3},\quad \nu_{r12} = \nu_{r13},\quad G_{r12} = G_{r13}\,. \tag{8}$$

2.2 The Loading of the Roving Model-Cell

In consideration of the relationships (8) it is enough to model two axial tensions and two plane shears with the roving model-cell.

To ensure the periodicity we prescribed a kinematic loading is prescribed, i.e. a node displacement field for the roving model cell. The nodes at the vertex points of the model-cell and at the center points of the side surfaces are identified with node numbers (Figure 9).

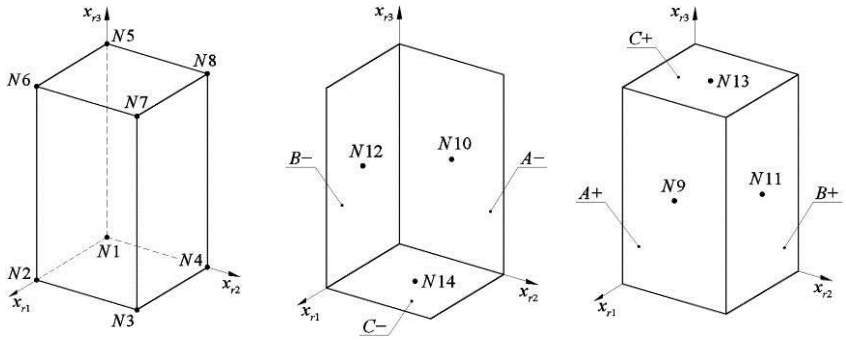

Figure 9

Notation of the nodes at the eight vertexes and at the six center points of the sides of the model-cell

The node displacement vector for the roving model-cell in the $x_{r1}x_{r2}x_{r3}$ coordinate system:

$$\vec{u} = u\vec{e}_{r1} + v\vec{e}_{r2} + w\vec{e}_{r3}. \tag{9}$$

For the roving model-cell (Figures 7 and 8) the following general boundary conditions can be applied [7]:

$$u_i^{j+}\left(x_1, x_2, x_3\right) - u_i^{j-}\left(x_1, x_2, x_3\right) = \Delta x_{rj}\bar{\varepsilon}_{rij} = c_i^j. \tag{10}$$

On the surface pair perpendicular to x_{rj} axis u_i^{j+}, u_i^{j-} are displacements in x_i direction the $x_1x_2x_3$ global coordinate system. The $j+$ index indicates the positive direction of x_{rj} axis whereas the $j-$ indicates the negative direction of x_{rj} (Figure 5). Δx_{rj} is the side length of the roving model-cell. c_i^j ($i = j = 1, 2, 3$) is the change in x_{rj} directions of distance (displacement difference) of the side surface pairs of the model cell, whereas $c_i^j = c_j^i$ ($i \neq j = 1, 2, 3$) is the displacement difference resulting from the shear of the side surfaces. The (10) boundary conditions ensure the periodicity and the continuity of the displacement field in the roving of composite material. Equation (10) provides the displacement differences between the proper nodes on both opposite surfaces. u_i^{j+}, u_i^{j-} displacements are

the functions of x_1, x_2, x_3 coordinates, therefore these surfaces not necessarily stay in plane during the deformation. c_i^j are prescribed displacement differences or computed by the finite element method.

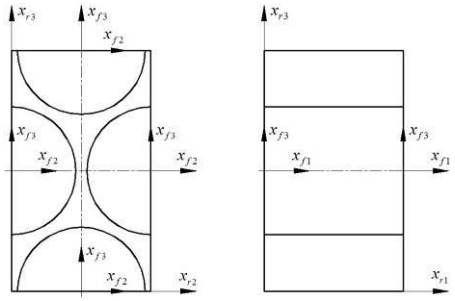

Figure 10
$x_{r1}x_{r2}x_{r3}$ material coordinate system of the roving model-cell and $x_{f1}x_{f2}x_{f3}$ material coordinate system of the reinforcing fibers

In Figure 10 the $x_{r1}x_{r2}x_{r3}$ material coordinate system of the roving model cell and the $x_{f1}x_{f2}x_{f3}$ material coordinate system of the reinforcing fibers are seen. At the fibers $x_{f1}x_{f2}$ and $x_{f1}x_{f3}$ are planes of symmetry. Due to the fact that the side surfaces of the roving model cell are identical to the surfaces of $x_{f1}x_{f2}$, $x_{f2}x_{f3}$ and $x_{f1}x_{f3}$ of the fibers, at the tensile-test, illustrated below, the side surfaces of the model cell remain plane and displace parallel with the surfaces of the main material directions. On the other hand there is no deformation at the shear test in the $x_{ri}x_{rj}$ surface, on the side surfaces perpendicular to x_{ri} axis in x_{rj} direction and on the side surfaces perpendicular to x_{rj} axis in x_{ri} direction.

As mentioned earlier, with the introduction of the roving model-cell, we can model the roving as a homogenous material, and we can also determine, by basic experiments of strength of materials (by tensile-compression tests and shear tests), the material properties. With the instruction of kinematic loading, we will give the displacement for whole side surfaces of model-cell instead of certain selected nodes. *From these kinematic loadings reaction forces occur on the side surfaces. We reduced the side surface reaction force to the center node of the side in a way that we prescribed the displacement to the central node and coupled all the nodes on the surface in the given direction. This prescription ensures that the side surface can displace as a rigid plane in the prescribed direction. Due to the fact that the side surfaces of the roving model-cell coincide to the surfaces of the material main directions of the fibers, the average of the model-cell appears on the side surfaces. The average stress is determined by the fraction of the reaction force appearing on the side surface and the area of the side surface:*

$$\bar{\sigma}_{rij} = \frac{1}{A_j} \int_{(A_j)} \sigma_{rij}\, dA = \frac{F_{ri}}{A_j}. \tag{11}$$

F_{ri} is a reaction force in x_{ri} direction and it is appearing on a side surface A_j area that is perpendicular to x_{rj} axis.

2.3 Tensile-Compression Test Simulation with the Roving Model-Cell

For computation of E_{r1} Young's modulus and ν_{r12}, ν_{r13} Poisson's ratios of the roving and for determination of E_{r2}, ν_{r21}, ν_{r23} we need to simulate a pure tension-compression on the roving model-cell in x_{r1} direction and x_{r2} direction respectively. For the calculation of E_{r3}, ν_{r31}, ν_{r32} we need to simulate a tension in x_{r3} direction. Since the reinforcing fibers are in a regular hexagonal order, the material properties are the same in x_{r2} and x_{r3} directions. Because of the numerical verification we also simulated a tension in x_{r3} direction but we will not give the details of that here, we will only show the test simulation in x_{r1} and x_{r2} directions.

In the strain matrix in (1) only three tensile strains are different from zero, the three coordinates of the axial tensions. ($\bar{\varepsilon}_{r1}$, $\bar{\varepsilon}_{r2}$, $\bar{\varepsilon}_{r3} \neq 0$). At tension (10) formula looks as follows:

$$c_i^j = \Delta x_{rj} \bar{\varepsilon}_{rj}, \qquad \bar{\varepsilon}_{rj} = \frac{c_i^j}{\Delta x_{rj}}, \qquad (i = j = 1,\ 2,\ 3). \tag{12}$$

The condition of parallelism at the tensile loading is ensured by coupling all the nodes on the side surface in direction perpendicular to the surface. These requirements are summarized by the (13) – (15) relationships. According to (13) equation we couple all nodes on $A+$ surface in x_{r1} direction. The independent node is $N2$ and that means the displacements of all nodes on $A+$ surface are identical with the displacement of $N2$ node in x_{r1} direction.

$$u_{A-} = u(0; x_{r2}; x_{r3}) = u_{N1}, \qquad u_{A+} = u(a; x_{r2}; x_{r3}) = u_{N2}, \tag{13}$$

$$v_{B-} = v(x_{r1}; 0; x_{r3}) = v_{N5}, \qquad v_{B+} = v(x_{r1}; a; x_{r3}) = v_{N8}, \tag{14}$$

$$w_{C-} = w(x_{r1}; x_{r2}; 0) = w_{N3}, \qquad w_{C+} = w(x_{r1}; x_{r2}; b) = w_{N7}. \tag{15}$$

In (13) – (15) relationships:

$$0 \le x_{r1} \le a, \qquad 0 \le x_{r2} \le a, \qquad 0 \le x_{r3} \le b. \tag{16}$$

At the x_{r1} and x_{r2} directional tensions we clamped the *A*–, *B*– and *C*– side surfaces at their central node in direction perpendicular to the surface:

$$u_{A-} = u_{N10} = 0\,, \qquad v_{B-} = v_{N12} = 0\,, \qquad w_{C-} = w_{N14} = 0\,. \tag{17}$$

The kinematic loading belonging to both axial tension tests of the roving model-cell is defined as follows: at the x_{rj} directional, axial tension we gave the $\bar{\varepsilon}_{rj}$ tensile strain of the model-cell, and we simulate by FEM the normal displacement of the side surface with x_{rj} normal direction to (12). We did not give the transversal contraction of the surface, we computed it numerically.

At x_{r1} directional tension $\bar{\varepsilon}_{r1}$ is given, from which the displacement of the *A*+ side surface is:

$$u_{A+} = u_{N9} = a\,\bar{\varepsilon}_{r1}\,. \tag{18}$$

At x_{r2} directional tension $\bar{\varepsilon}_{r2}$ is given, from which:

$$v_{B+} = v_{N11} = a\,\bar{\varepsilon}_{r2}\,. \tag{19}$$

At tension, in both loading case, we still need to ensure that the opposite nodes displace in same way in the plane on the side surface. The node pairs should be coupled on the opposite side surfaces, except the edges of the model-cell, as follows:

$$A-/A+: \quad v\left(0;x_{r2};x_{r3}\right) = v\left(a;x_{r2};x_{r3}\right), \quad w\left(0;x_{r2};x_{r3}\right) = w\left(a;x_{r2};x_{r3}\right), \tag{20}$$

$$B-/B+: \quad u\left(x_{r1};0;x_{r3}\right) = u\left(x_{r1};a;x_{r3}\right), \quad w\left(x_{r1};0;x_{r3}\right) = w\left(x_{r1};a;x_{r3}\right), \tag{21}$$

$$C-/C+: \quad u\left(x_{r1};x_{r2};0\right) = u\left(x_{r1};x_{r2};b\right), \quad v\left(x_{r1};x_{r2};0\right) = v\left(x_{r1};x_{r2};b\right). \tag{22}$$

In (20) – (22) and (24) – (26) relationships:

$$0 < x_{r1} < a\,, \qquad 0 < x_{r2} < a\,, \qquad 0 < x_{r3} < b\,. \tag{23}$$

We need to couple the node pairs at the opposite edges, except the corner points of the model-cell, according to (24) – (26) relationships:

For edges in x_{r1} direction:

$$u\left(x_{r1};0;0\right) = u\left(x_{r1};a;0\right) = u\left(x_{r1};a;b\right) = u\left(x_{r1};0;b\right), \tag{24}$$

For edges in x_{r2} direction:

$$v\left(0;x_{r2};0\right) = v\left(0;x_{r2};b\right) = v\left(a;x_{r2};b\right) = v\left(a;x_{r2};0\right), \tag{25}$$

For edges in x_{r3} direction:

$$w\left(0;0;x_{r3}\right) = w\left(a;0;x_{r3}\right) = w\left(a;a;x_{r3}\right) = w\left(0;a;x_{r3}\right) \tag{26}$$

Figure 11 shows the coupling of the nodes between the opposite side surfaces and the edges. *It is necessary to skip the edges at the opposite sides and the corners at the opposite edges so that the model-cell will not be overdetermined.*

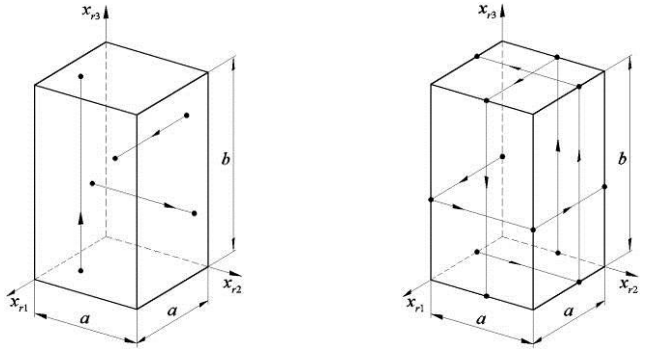

Figure 11
Coupling between the nodes

Table 2 summarizes the numerically determined reaction forces with the roving model-cell for both axial tensions as well as the displacement field (cross contraction) perpendicular to the direction of the tension.

Table 2
Properties defined by the finite element model-cell in case of both load-cases

	Reaction force on the side surfaces	Cross contraction
Tension in x_{r1} direction	$\vec{F}_{rA+} = -\vec{F}_{rA-}$, $\vec{F}_{rB-} = \vec{F}_{rC-} = \vec{0}$	v_{B+}, w_{C+}
Tension in x_{r2} direction	$\vec{F}_{rB+} = -\vec{F}_{rB-}$, $\vec{F}_{rA-} = \vec{F}_{rC-} = \vec{0}$	u_{A+}, w_{C+}

At x_{r1} directional tension we calculate the average $\bar{\sigma}_{r1}$ normal stress from the reaction force created on $A+$ side surface and from the area of the side surface according to (11), from which we can determine the Young's modulus in the usual way. Poisson's ratio can also be calculated in the usual way from the relevant data received from the calculated displacement field. We can also follow these methods for the cross directions of the roving model-cell.

Material properties determined above of a single roving cannot be measured directly. Therefore the validity of the proposed model-cell can only be verified directly by measurement on a composite specimen. For this we need to create the model-cell for a textile composite layer which we will discuss in our next paper. Applying this layer model-cell, using the results generated by the roving model-cell we can verify only together the validity and accuracy of both model-cells. We have given the geometrical and material properties of the composite specimen, used for the verification of model-cells in Section 2.5. Table 3 summarizes the results (for the two axial tensions) generated by numerical methods with these

data. The table consists of the kinematic loading, the reaction forces determined numerically, the cross contractions (displacements) and the average stresses and the material properties computed from those for both tensions. We publish these as application of the roving model-cell and use them at the evaluation of the measurements.

Table 3, Part 1

The given data and determined material properties for the applied roving model-cell

Tension in x_{r1} direction	
Kinematic loading	$\bar{\varepsilon}_{r1} = 2.5 \cdot 10^{-3}$, $u_{A+} = u_{N9} = 19.0325 \cdot 10^{-3}$ mm
Numerically determined quantities	$\vec{F}_{rA+} = \left(44479.2\vec{e}_{r1}\right)\text{N}$, $\vec{F}_{rA-} = \left(-44479.2\vec{e}_{r1}\right)\text{N}$
	$v_{B+} = -3.854 \cdot 10^{-3}$ mm, $w_{C+} = -6.675 \cdot 10^{-3}$ mm
Average stress	$\bar{\sigma}_{r1} = 443.09$ MPa
Material properties	$E_{r1} = 177236$ MPa, $\nu_{r12} = 0.202$, $\nu_{r13} = 0.202$

Table 3, Part 2

The given data and determined material properties for the applied roving model-cell

Tension in x_{r2} direction	
Kinematic loading	$\bar{\varepsilon}_{r2} = 2.5 \cdot 10^{-3}$, $v_{B+} = v_{N11} = 19.0325 \cdot 10^{-3}$ mm
Numerically determined quantities	$\vec{F}_{rB+} = \left(2597.9\vec{e}_{r2}\right)\text{N}$, $\vec{F}_{rB-} = \left(-2597.9\vec{e}_{r2}\right)\text{N}$
	$u_{A+} = -2.251 \cdot 10^{-4}$ mm, $w_{C+} = -14.189 \cdot 10^{-3}$ mm
Average stress	$\bar{\sigma}_{r2} = 25.88$ MPa
Material properties	$E_{r2} = 10352$ MPa, $\nu_{r21} = 0.012$, $\nu_{r23} = 0.430$

2.4 Shear Test Simulation with the Roving Model-Cell

According to (8): $G_{r12} = G_{r13}$. Because of numerical verification we modeled the shear test on both surfaces of roving model-cell, however, we will not discuss the details here. At the shear on $x_{ri}x_{rj}$ surface $\bar{\gamma}_{rij} \neq 0$ and the other strain coordinates are zeroes in the strain tensor. Also at the shear we prescribed the kinematic loading and here $\bar{\gamma}_{rij}$ is the average shearing strain. We simulated pure shear with the roving model-cell. From (10) follows for the pure shear:

$$c_i^j = \Delta x_{rj} \frac{1}{2} \bar{\gamma}_{rij}, \qquad c_j^i = \Delta x_{ri} \frac{1}{2} \bar{\gamma}_{rji} \qquad \left(i \neq j = 1,\ 2,\ 3\right). \tag{27}$$

For determination of the shear modulus G_{r12} of roving material we need to model pure shear on the $x_{r1}x_{r2}$ surface. The given shearing strain is:

$$\frac{1}{2}\overline{\gamma}_{r12} = \frac{1}{2}\overline{\gamma}_{r21}, \qquad \overline{\gamma}_{r12} = \frac{1}{2}\overline{\gamma}_{r12} + \frac{1}{2}\overline{\gamma}_{r21}. \tag{28}$$

The pure shear is simulated by a given displacement in x_{r2} direction on the side surfaces perpendicular to the x_{r1} axis and by a given displacement in x_{r1} direction on the side surfaces perpendicular to the x_{r2} axis of the roving model-cell. At the shear on $x_{r1}x_{r2}$ plane the *C*+ and *C*– side surfaces remain planes and do not displace in x_{r3} direction. We have given the above kinematic requirements (27) by using the given values for the nodes at the center points of the side surfaces, as follows:

$$v_{A-} = v_{N10} = 0, \qquad v_{A+} = v_{N9} = a\frac{1}{2}\overline{\gamma}_{r21}, \tag{29}$$

$$u_{B-} = u_{N12} = 0, \qquad u_{B+} = u_{N11} = a\frac{1}{2}\overline{\gamma}_{r12}, \tag{30}$$

$$w_{C-} = w_{N14} = 0, \qquad w_{C+} = w_{N13} = 0. \tag{31}$$

At the shear modeling we need to couple the nodes on the side surfaces as follows:

$$v_{A-} = v\left(0; x_{r2}; x_{r3}\right) = v_{N1}, \qquad v_{A+} = v\left(a; x_{r2}; x_{r3}\right) = v_{N2}, \tag{32}$$

$$u_{B-} = u\left(x_{r1}; 0; x_{r3}\right) = u_{N5}, \qquad u_{B+} = u\left(x_{r1}; a; x_{r3}\right) = u_{N8}, \tag{33}$$

$$w_{C-} = w\left(x_{r1}; x_{r2}; 0\right) = w_{N3}, \qquad w_{C+} = w\left(x_{r1}; x_{r2}; b\right) = w_{N7}. \tag{34}$$

In relation (32) – (34):

$$0 \le x_{r1} \le a, \qquad 0 \le x_{r2} \le a, \qquad 0 \le x_{r3} \le b. \tag{35}$$

The node pairs should be coupled at the opposite side surfaces, with exception of the edges of the model cell, according to (36) – (38):

$$A-/A+: \quad u\left(0; x_{r2}; x_{r3}\right) = u\left(a; x_{r2}; x_{r3}\right), \quad w\left(0; x_{r2}; x_{r3}\right) = w\left(a; x_{r2}; x_{r3}\right), \tag{36}$$

$$B-/B+: \quad v\left(x_{r1}; 0; x_{r3}\right) = v\left(x_{r1}; a; x_{r3}\right), \quad w\left(x_{r1}; 0; x_{r3}\right) = w\left(x_{r1}; a; x_{r3}\right), \tag{37}$$

$$C-/C+: \quad u\left(x_{r1}; x_{r2}; 0\right) = u\left(x_{r1}; x_{r2}; b\right), \quad v\left(x_{r1}; x_{r2}; 0\right) = v\left(x_{r1}; x_{r2}; b\right). \tag{38}$$

In relations (36) – (38) and (40) – (42):

$$0 < x_{r1} < a, \qquad 0 < x_{r2} < a, \qquad 0 < x_{r3} < b. \tag{39}$$

At the opposite edges, with exception of the corner points of the model cell, we need to couple the node pairs as follows:

For edges in x_{r1} direction:

$$v(x_{r1};0;0)=v(x_{r1};a;0)=v(x_{r1};a;b)=v(x_{r1};0;b), \tag{40}$$

For edges in x_{r2} direction:

$$u(0;x_{r2};0)=u(0;x_{r2};b)=u(a;x_{r2};b)=u(a;x_{r2};0), \tag{41}$$

For edges in x_{r3} direction:

$$w(0;0;x_{r3})=w(a;0;x_{r3})=w(a;a;x_{r3})=w(0;a;x_{r3}). \tag{42}$$

With the help of the roving model cell, the reaction forces for the $x_{r1}x_{r2}$ surface shear are numerically determined:

$$\vec{F}_{rA+}=-\vec{F}_{rA-},\ \vec{F}_{rB+}=-\vec{F}_{rB-},\ \vec{F}_{rC+}=\vec{F}_{rC-}=\vec{0}.$$

The average shear stresses on the side surfaces are:

$$\overline{\tau}_{r12}=\frac{F_{r1B+}}{A_{B+}},\qquad \overline{\tau}_{r21}=\frac{F_{r2A+}}{A_{A+}}. \tag{43}$$

Numerical verification opportunity of results is to check that the shear stresses should be the same on the side surfaces perpendicular to x_{r1}, x_{r2} axes (due to the duality of τ stresses):

$$\overline{\tau}_{r12}=\overline{\tau}_{r21}. \tag{44}$$

The shear stress distribution is never homogenous on the roving model-cell. Figure 12 shows the τ_{r12} stress distribution on the roving model-cell. The deformation is illustrated in a zoom of hundred times. The XYZ coordinate system in figure is identical to the $x_{r1}x_{r2}x_{r3}$ coordinate system.

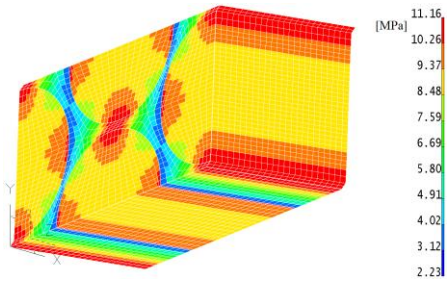

Figure 12
τ_{r12} stress distribution on the roving model-cell

The shear modulus on the $x_{r1}x_{r2}$ surface is:

$$G_{r12} = \frac{\overline{\tau}_{r12}}{\overline{\gamma}_{r12}}. \tag{45}$$

In order to determine the shear modulus G_{r23} of the roving material we need to model pure shear on the $x_{r2}x_{r3}$ surface:

$$\frac{1}{2}\overline{\gamma}_{r23} = \frac{1}{2}\overline{\gamma}_{r32}, \qquad \overline{\gamma}_{r23} = \frac{1}{2}\overline{\gamma}_{r23} + \frac{1}{2}\overline{\gamma}_{r32}. \tag{46}$$

At the shear on $x_{r2}x_{r3}$ plane the *A*+ and *A*– side surfaces remain planes and do not displace in x_{r1} direction. For simulation of pure shear with the roving model-cell we have given values for the nodes at the center points of the side surfaces, as follows:

$$w_{B-} = w_{N12} = 0, \qquad w_{B+} = w_{N11} = a\frac{1}{2}\overline{\gamma}_{r32}, \tag{47}$$

$$v_{C-} = v_{N14} = 0, \qquad v_{C+} = v_{N14} = b\frac{1}{2}\overline{\gamma}_{r23}, \tag{48}$$

$$u_{A-} = u_{N10} = 0, \qquad u_{A+} = u_{N9} = 0. \tag{49}$$

The nodes are coupled at the side surfaces with (50) – (52) relations.

$$w_{B-} = w\left(x_{r1};0;x_{r3}\right) = w_{N5}, \qquad w_{B+} = w\left(x_{r1};a;x_{r3}\right) = w_{N8}, \tag{50}$$

$$v_{C-} = v\left(x_{r1};x_{r2};0\right) = v_{N3}, \qquad v_{C+} = v\left(x_{r1};x_{r2};b\right) = v_{N7}, \tag{51}$$

$$u_{A-} = u\left(0;x_{r2};x_{r3}\right) = u_{N1}, \qquad u_{A+} = u\left(a;x_{r2};x_{r3}\right) = u_{N2}. \tag{52}$$

In (50) – (52) relations:

$$0 \le x_{r1} \le a, \qquad 0 \le x_{r2} \le a, \qquad 0 \le x_{r3} \le b. \tag{53}$$

According to the (54) – (56) requirements the nodes have equal displacements on the opposite side surfaces, with exception to the edges of the model-cell:

$$B-/B+: \quad u\left(x_{r1};0;x_{r3}\right) = u\left(x_{r1};a;x_{r3}\right), \quad v\left(x_{r1};0;x_{r3}\right) = v\left(x_{r1};a;x_{r3}\right), \tag{54}$$

$$C-/C+: \quad u\left(x_{r1};x_{r2};0\right) = u\left(x_{r1};x_{r2};b\right), \quad w\left(x_{r1};x_{r2};0\right) = w\left(x_{r1};x_{r2};b\right), \tag{55}$$

$$A-/A+: \quad v\left(0;x_{r2};x_{r3}\right) = v\left(a;x_{r2};x_{r3}\right), \quad w\left(0;x_{r2};x_{r3}\right) = w\left(a;x_{r2};x_{r3}\right). \tag{56}$$

In relations (54) – (56) and (58) – (60):

$$0 < x_{r1} < a, \qquad 0 < x_{r2} < a, \qquad 0 < x_{r3} < b. \tag{57}$$

For the node pairs at the opposite edges, except the corner points of the model-cell, we prescribe the relations as follows:

For edges in x_{r1} direction:

$$u(x_{r1};0;0)=u(x_{r1};a;0)=u(x_{r1};a;b)=u(x_{r1};0;b), \tag{58}$$

For edges in x_{r2} direction:

$$w(0;x_{r2};0)=w(0;x_{r2};b)=w(a;x_{r2};b)=w(a;x_{r2};0), \tag{59}$$

For edges in x_{r3} direction:

$$v(0;0;x_{r3})=v(a;0;x_{r3})=v(a;a;x_{r3})=v(0;a;x_{r3}). \tag{60}$$

With FE computation we got at the $x_{r2}x_{r3}$ surface shear the following reaction forces:

$$\vec{F}_{rB+}=-\vec{F}_{rB-},\ \vec{F}_{rC+}=-\vec{F}_{rC-},\ \vec{F}_{rA+}=\vec{F}_{rA-}=\vec{0}.$$

The average shear stresses on the side surfaces:

$$\overline{\tau}_{r23}=\frac{F_{r2C+}}{A_{C+}},\qquad \overline{\tau}_{r32}=\frac{F_{r3B+}}{A_{B+}}. \tag{61}$$

The duality of τ stresses should be valid on the side surfaces perpendicular to x_{r2}, x_{r3} axes:

$$\overline{\tau}_{r23}=\overline{\tau}_{r32}. \tag{62}$$

Shear modulus on $x_{r2}x_{r3}$ surface:

$$G_{r23}=\frac{\overline{\tau}_{r23}}{\overline{\gamma}_{r23}}. \tag{63}$$

Table 4 summarizes a numerical example for comparison with the further experiments, the results of computations received as results of simulation of the roving model-cell. The table contains the given kinematic loadings for both, shear cases, the computed reaction forces, the calculated average shear stresses and the shear moduli.

Table 4
The prescribed and defined properties at the examined roving model cell

Pure shear on $x_{r1}x_{r2}$ surface	
Kinematic loading	$\overline{\gamma}_{r12} = 2 \cdot 10^{-3}$, $\frac{1}{2}\overline{\gamma}_{r12} = \frac{1}{2}\overline{\gamma}_{r21} = 10^{-3}$
	$v_{A+} = v_{N9} = 7.613 \cdot 10^{-3}$ mm, $u_{B+} = u_{N11} = 7.613 \cdot 10^{-3}$ mm
Reaction forces	$\vec{F}_{rA+} = (825.9\vec{e}_{r2})$N, $\vec{F}_{rA-} = (-825.9\vec{e}_{r2})$N
	$\vec{F}_{rB+} = (825.9\vec{e}_{r1})$N, $\vec{F}_{rB-} = (-825.9\vec{e}_{r1})$N
Average stresses	$\overline{\tau}_{r12} = 8.23$ MPa, $\overline{\tau}_{r21} = 8.23$ MPa
Shear modulus	$G_{r12} = 4115$ MPa
Pure shear on $x_{r2}x_{r3}$ surface	
Kinematic loading	$\overline{\gamma}_{r23} = 2 \cdot 10^{-3}$, $\frac{1}{2}\overline{\gamma}_{r23} = \frac{1}{2}\overline{\gamma}_{r32} = 10^{-3}$
	$w_{B+} = w_{N11} = 7.613 \cdot 10^{-3}$ mm, $v_{C+} = v_{N14} = 13.186 \cdot 10^{-3}$ mm
Reaction forces	$\vec{F}_{rB+} = (726.45\vec{e}_{r3})$N, $\vec{F}_{rB-} = (-726.45\vec{e}_{r3})$N
	$\vec{F}_{rC+} = (419.419\vec{e}_{r2})$N, $\vec{F}_{rC-} = (-419.419\vec{e}_{r2})$N
Average stresses	$\overline{\tau}_{r23} = 7.24$ MPa, $\overline{\tau}_{r32} = 7.24$ MPa
Shear modulus	$G_{r23} = 3620$ MPa

2.5 Characteristic Data of the Textile Composite Layer used in the Experiment

The composite plate is reinforced with a SIGRATEX KDL 8003 type plain weave carbon fabric and the matrix is a polyester resin.

Figure 13
Plain weave fabric

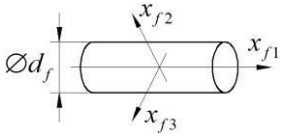

Figure 14
Material coordinate system of a carbon fiber

In Figure 13 the plain weave fabric before impregnation is seen. The fibers are ordered into flat, untwisted roving. The type of the roving is Torayca T300-3K.

3K means that the number of fibers is $n_f = 3000$ pieces and the diameter of a carbon fiber is $d_f = 7$ μm in the roving.

Material properties of the carbon fiber originate from literature [4], [10], in the $x_{f1}x_{f2}x_{f3}$ material coordinate system (Figure 14):

$E_{f1} = 230000$ MPa $\quad \nu_{f12} = \nu_{f13} = 0.166 \quad G_{f12} = G_{f13} = 6432$ MPa

$E_{f2} = E_{f3} = 15000$ MPa $\quad \nu_{f23} = 0.400 \quad G_{f23} = 5357$ MPa

The matrix is an AROPOL M105TB type polyester resin which is a linear-elastic, isotropic material. The Young's modulus E_m and the Poisson's ratio ν_m were measured according to standard [1], the shear modulus G_m was defined by the (64) relationship, valid for the isotropic materials:

$$E_m = 3677 \text{ MPa}, \quad \nu_m = 0.346, \quad G_m = \frac{E_m}{2(1+\nu_m)} = 1365.9 \text{ MPa}. \tag{64}$$

2.6 Material Properties Determined by the Roving Model-Cell

For the investigated roving material, considering the relationships (8), we determined the material properties with the finite element roving model-cell as follows:

$E_{r1} = 177236$ MPa, $\quad \nu_{r12} = \nu_{r13} = 0.202, \quad G_{r12} = G_{r13} = 4115$ MPa,

$E_{r2} = E_{r3} = 10352$ MPa, $\quad \nu_{r23} = 0.430, \quad G_{r23} = 3620$ MPa.

If the reinforcing fiber in the roving is transversely isotropic, the roving has the same material behavior because the fibers are ordered hexagonally in that. Transversely isotropic materials have a plane with isotropic behavior. The given carbon fibers are isotropic in the plane of their cross sections because G_{f23} shear modulus can be determined with formula (65) which is valid for the isotropic materials:

$$G_{f23} = \frac{E_{f2}}{2(1+\nu_{f23})} = \frac{15000}{2(1+0.4)} = 5357 \text{ MPa}. \tag{65}$$

The roving model-cell is also transversely isotropic because one can calculate the shear modulus $G_{r23} = 3620$ MPa determined with the model-cell, by (66) relationship:

$$G_{r23} = \frac{E_{r2}}{2(1+\nu_{r23})} = \frac{10352}{2(1+0.43)} = 3620 \text{ MPa}. \tag{66}$$

The roving model-cell delivers transversely isotropic results, so the material has only five independent material constants: E_{r1}, E_{r2}, ν_{r12}, ν_{r23}, G_{r12}.

Conclusions

This work presents a FE roving model-cell, for determination of macroscopic, orthotropic material properties of the reinforcing roving impregnated by the matrix material. It defines the structure of the finite element roving model-cell and gives the boundary conditions applied to the finite element computations. Using this roving model-cell, we determine the material properties for a roving, where the shape of the cross sections of the roving, the number of reinforcing fibers in the roving and the material properties of the fiber and the matrix are known. It computes the macroscopic material properties of an actual roving by numerical simulation for two axial tensile tests and for two pure shear tests.

Future work will summarize the numerical determination of the material properties of a textile composite layer. The macroscopic material properties of a textile composite layer will be determined by a finite element model-cell and we will compare them with experimental results. The applied roving of the textile composite layer is the same as dealt with in this current work. Here we have carried out a numerical verification with the roving model-cell. The experimental verification will take place, by the measurement data of the layer, in the future work.

References

[1] ASTM D638-10, Standard Test Method for Tensile Properties of Plastics, 2010

[2] Bunsell, A. R.; Renard, J.: Fundamentals of Fibre Reinforced Composite Materials, Series in Material Science and Engineering, Institute of Physics Publishing, 398 p., 2005

[3] Égert J., Pere B.: Finite Element Analysis, MSc Lecture notes, Universitas-Győr Non-profit Ltd., Győr, 218 p., 2011 (in Hungarian)

[4] Goda T.: Wear Mechanism of Composite-Steel Sliding Pairs, PhD Thesis, 2002, Budapest University of Technology and Economics, Faculty of Mechanical Engineering, Supervisor: Váradi K. (In Hungarian)

[5] Hallal, A., Fardoun, F., Younes, R., Hage Chehade, F.: Evaluation of Longitudinal and Transversal Young's Moduli for Unidirectional Composite Material with Long Fibers, Advanced Materials Research, Vol. 324, p. 189-192, 2011

[6] Jones, R. M.: Mechanics of Composite Materials, Second Edition, Taylor & Francis Group, 519 p., 1999

[7] Leijan H.: Determining Micro- and Macro- Geometry of Fabric and Fabric Reinforced Composites, Dissertation, 2013, Department of Mechanical and Nuclear Engineering College of Engineering, Kansas State University, Manhattan, Kansas, Advisor: Youqi W.

[8] Siva Bhaskara Rao Devireddy; Sandhyarani Biswas: Effect of Fiber Geometry and Representative Volume Element on Elastic and Thermal Properties

of Unidirectional Fiber-Reinforced Composites, Hindawi Publishing Corporation Journal of Composites, Article ID 629175, 12 pages, 2014

[9] Srinivasa, V., Shivakumar, V., Nayaka, V., Jagadeeshaiaih, S., Seethram, M., Shenoy, R., Nafidi, A.: Fracture Morphology of Carbon Fiber Reinforced Plastic Composite Laminates, Materials Research, Vol. 13, No. 3, pp. 417-424, 2010

[10] Torayca T300 factory data sheet catalogue (No. CFA-001) Toray Carbon Fibers America, Inc. (CFA), 2012

[11] Xia, Z., Zhang, Y., Ellyin, F.: A Unified Periodical Boundary Conditions for Representative Volume Elements of Composites and Applications, International Journal of Solids and Structures, Vol. 40, No. 8, p. 1907-1921, 2003

[12] Zhang., C.: Multi-Scale Characterization and Failure Modeling of Carbon/Epoxy Triaxially Braided Composite, Dissertation, 2013, The Graduate Faculty of The University of Akron, Advisor: Binienda, W. K

Highly Accurate Scheme for the Cauchy Problem of the Generalized Burgers-Huxley Equation

José António Tenreiro Machado[†], Afshin Babaei[‡], Behrouz Parsa Moghaddam[††,§]

[†]Department of Electrical Engineering, Institute of Engineering, Rua Dr. António Bernardino de Almeida, 431, Porto 4249-015, Portugal. E-mail: jtm@isep.ipp.pt.
[‡]Department of Mathematics, University of Mazandaran, Pasdaran Street, P.O. Box: 47416 95447, Babolsar, Iran. E-mail: babaei@umz.ac.ir.
[††]Department of Mathematics, Lahijan Branch, Islamic Azad University, Shaghayegh Street, P.O. Box: 1616, Lahijan, Iran. [§]Corresponding author. E-mail: parsa@liau.ac.ir.

Abstract: In this paper, a weighted algorithm, based on the reduced differential transform method, is introduced. The new approach is adopted in the approximate analytical solution of the Cauchy problem for the Burgers-Huxley equation. The proposed scheme considers the initial and boundary conditions simultaneously for obtaining a solution of the equation. Several examples are discussed demonstrating the performance of the algorithm.

Keywords: Weighted reduced differential transform method; Burgers-Huxley equation; Cauchy problem.

1 Introduction

Obtaining solutions for nonlinear equations plays an important role in the study of many nonlinear phenomena. In this perspective, during the last years, seeking the solution of nonlinear models has been an important topic in mathematical physics. One important nonlinear equation is the generalized Burgers-Huxley equation [1, 2, 3, 4, 5]

$$\frac{\partial u}{\partial t} = \kappa \frac{\partial^2 u}{\partial x^2} - \alpha u^{\delta} \frac{\partial u}{\partial x} + \beta u(1-u^{\delta})(\eta u^{\delta} - \gamma), \tag{1}$$

where κ, α, β and η are real constants, δ is a positive integer and $\gamma \in [0,1]$.
The equation (1) is a generalization of various well known nonlinear equations, such as the Burgers, Huxley, FitzHugh-Nagumo, Burgers-Huxley and Burgers-Fisher models [1, 2, 6, 7, 8]. These equations describe different phenomena in mathematical physics, biomathematics, chemistry and mechanics [9, 10, 11, 12, 13]. The Burgers equation characterizes the wave propagation in dissipative systems [1].

The reaction-diffusion FitzHugh-Nagumo equation is used for investigating the dynamical behavior near the bifurcation point for the Rayleigh-Benard convection of binary fluid mixtures [6]. The Huxley equation describes the dynamics of electric pulses propagation in nerve fibres [7]. The Burgers-Fisher equation has application in plasma physics, capillary-gravity waves, optics and chemical physics [9, 10, 11, 12, 13, 14].
The generalized Burgers-Huxley equation has been considered recently by researchers that developed some analytical and numerical methods for its solution. Schemes such as the adomian decomposition [14], homotopy perturbation [15], homotopy analysis [16], and reduced differential transform [17] were proposed to solve the initial value problem of the Burgers-Huxley equation. Moreover, some authors considered the initial boundary value problem of this equation and used spectral collocation [18], finite-difference [19, 20], Haar wavelet [21] and modified cubic B-spline differential quadrature [22] methods for its solution.
The generalized Burgers-Huxley equation (1) is considered with the conditions

$$u(x,0) = f(x), \tag{2}$$

and

$$u(0,t) = p(t), \qquad u_x(0,t) = q(t). \tag{3}$$

In this work, a weighted technique, according to the reduced differential transform method (RDTM), is introduced for solving (1)-(3).
The RDTM was adopted by researchers to obtain the analytical and approximate solutions for nonlinear problems [23, 24, 25]. Often, the differential transform method is considered according to the initial condition of the problem, but, here we use the initial and boundary conditions.
Bearing these ideas in mind, this paper is organized as follows. In Sections 2 and 3, the RDTM and a weighted algorithm are introduced, respectively. In Section 4, several prototype problems are solved in order to show the ability and efficiency of the new algorithm. Finally, in section 5 the main conclusions are outlined.

2 Reduced differential transform method

In this section, the fundamental definitions and operations of the RDTM are reviewed. Consider a function of $u(x,t)$ and suppose that the two-dimensional function $u(x,t)$ is separable as $u(x,t) = f(x)g(t)$. Based on the features of differential transform [23], we can represent this function as

$$u(x,t) = \sum_{k=0}^{\infty} F_i x^i \sum_{j=0}^{\infty} G_j t^j = \sum_{k=0}^{\infty} U_k(x) t^k = \sum_{k=0}^{\infty} V_k(t) x^k, \tag{4}$$

where $V_k(t)$ and $U_k(x)$ are called x-dimensional and t-dimensional spectrum functions of $u(x,t)$, respectively.

Definition 1. *Suppose that $u(x,t)$ is analytic and differentiated continuously with respect to t and x in their domains. Then*

Table 1
Some operations of the reduced differential transform.

Function Form	Transformed Form
$u(x,t)$	$U_k(x) = \frac{1}{k!}\left[\frac{\partial^k}{\partial t^k}u(x,t)\right]_{t=0}$
$u(x,t) = c \ \ (c \text{ is a constant})$	$U_k(x) = \delta(k) \ = \begin{cases} 1 & k=0 \\ 0 & k\neq 0 \end{cases}$
$u(x,t) = v(x,t) + w(x,t)$	$U_k(x) = V_k(x) + W_k(x)$
$u(x,t) = cv(x,t)$	$U_k(x) = cV_k(x) \ \ (c \text{ is a constant})$
$u(x,t) = x^m v(x,t)$	$U_k(x) = x^m V_k$
$u(x,t) = t^m v(x,t)$	$U_k(x) = V_{k-m}$
$u(x,t) = x^m t^n$	$U_k(x) = x^m \delta(k-n) \ = \begin{cases} x^m & k=n \\ 0 & k\neq n \end{cases}$
$u(x,t) = \frac{\partial^m}{\partial t^m}v(x,t)$	$U_k(x) = \frac{(k+m)!}{k!}V_{k+m}(x)$
$u(x,t) = \frac{\partial^m}{\partial x^m}v(x,t)$	$U_k(x) = \frac{\partial^m}{\partial x^m}V_k(x)$
$u(x,t) = v^2(x,t)$	$U_k(x) = \sum_{r=0}^{k-1} V(r)(x)V(k-r-1)(x)$
$u(x,t) = v^3(x,t)$	$U_k(x) = \sum_{s=0}^{k-1}\sum_{r=0}^{s} V(r)(x)V(k-s-1)(x)V(s-r)(x)$

- *The transformed function $U_k(x)$ is defined as*

$$U_k(x) = \frac{1}{k!}\left[\frac{\partial^k}{\partial t^k}u(x,t)\right]_{t=0}. \tag{5}$$

Its inverse differential transformation of $U_k(x)$ is

$$u(x,t) = \sum_{k=0}^{\infty} U_k(x)t^k. \tag{6}$$

- *The transformed function $V_k(t)$ is defined as*

$$V_k(t) = \frac{1}{k!}\left[\frac{\partial^k}{\partial t^k}u(x,t)\right]_{x=0}. \tag{7}$$

The inverse differential transformation of $V_k(t)$ is

$$u(x,t) = \sum_{k=0}^{\infty} V_k(t)x^k. \tag{8}$$

The main operations of the reduced differential transform, according to the variable t, that can be deduced from Eqs. (5) and (6) [24, 25] are listed in Table 1. These operations can be obtained in a similar way for the reduced differential transforms according to the variable x.

Let us illustrate the fundamental concepts in more detail. Suppose L is a linear operator and N is a nonlinear operator. Consider a general nonlinear differential equation as

$$L[u(x,t)] + N[u(x,t)] = \phi(x,t), \tag{9}$$

with the initial condition

$$u(x,0) = u_0(x), \tag{10}$$

where $\phi(x,t)$ is an inhomogeneous term. We assume that $L = \frac{\partial}{\partial t}$. According to the properties of RDTM in Table 1, we get

$$(k+1)U_{k+1}(x) = \Phi_k(x) - N[U_k(x)], \tag{11}$$

where $U_k(x)$, $NU_k(x)$ and $\Phi_k(x)$ are the transformations of $Lu(x,t)$, $Nu(x,t)$ and $\phi(x,t)$.
If we consider $U_0(x) = u_0(x)$ as the transformation of (10), then $u(x,t)$ can be written as

$$u(x,t) = \sum_{k=0}^{\infty} U_k(x)t^k, \tag{12}$$

Similarly, the recurrence relation (11) and the expressions of Table 1 may be introduced for $L = \frac{\partial^2}{\partial x^2}$ as well. In this case, considering $V_0(t) = p(t)$ and $V_1(t) = q(t)$, we get

$$u(x,t) = \sum_{k=0}^{\infty} V_k(t)x^k. \tag{13}$$

3 The weighted method

A weighted method according to the RDTM is now presented for the solution of (1)-(3). We formulate the algorithm in two steps. In the first step, we consider (1) and we denote $L = \frac{\partial}{\partial t}$. Applying the basic properties of the differential transformations and Table 1, and substituting $U_0(x) = f(x)$ as the differential transformation of (2), we get the approximate solution

$$\hat{u}_n(x,t) = \sum_{k=0}^{n} U_k(x)t^k. \tag{14}$$

In the second step, we seek the approximate solution of the Eq. (1) according to the conditions (3). Suppose that $L = \frac{\partial^2}{\partial x^2}$. Taking the differential transformation of (1) and applying the basic properties listed in Table 1 with respect to x, the approximate solution

$$\check{u}_n(x,t) = \sum_{k=0}^{n} V_k(t)x^k, \tag{15}$$

is obtained. From the boundary conditions (3), we have

$$V_0(t) = p(t), \tag{16}$$

and

$$V_1(t) = q(t). \tag{17}$$

The approximate solutions (14) and (15) are not solutions of the problem (1)-(3), because expression (14) is obtained according to the initial condition (2) while expression (15) is obtained according to the boundary conditions (3). Thus, to obtain an approximate solution of the generalized Burgers-Huxley equation (1) that satisfies the conditions (2) and (3) simultaneously, we consider a convex combination of (14) and (15) as

$$u_{approx[n]}(x,t) = c\hat{u}_n(x,t) + (1-c)\check{u}_n(x,t), \tag{18}$$

where $c \in [0,1]$. The limit of $u_{approx[n]}(x,t)$ is equal to $u(x,t)$ when n approaches infinity. For determining the value of the parameter c, we follow the scheme presented in [26] to minimize the discrepancy between $u_{approx[n]}(x,0)$, $u_{approx[n]}(0,t)$ and $\frac{\partial u_{approx[n]}}{\partial x}(0,t)$ with $f(x)$, $\varphi(t)$ and $\psi(t)$ in (2) and (3).

Theorem 1. *Suppose that $f(x) \in L^2[(0,L)]$, $\phi(t), \psi(t) \in L^2[(0,T)]$ and $\|.\|$ denotes the L^2-norm. Let*

$$c_1 = \|\hat{u}_n(0,t) - \phi(t)\|,$$
$$c_2 = \|\frac{\partial \hat{u}_n}{\partial x}(1,t) - \psi(t)\|,$$
$$c_3 = \|\check{u}_n(x,0) - f(x)\|.$$

Then the optimal value for c in (18) is

$$c = \frac{c_3^2}{c_1^2 + c_2^2 + c_3^2}, \qquad n \geq 0. \tag{19}$$

Proof. According to conditions (1)-(3), we define the following residual function on the domain $\{(x,t)|(x,t) \in [0,L] \times [0,T]\}$ as

$$F_n(x,t;c) = \|u_n(0,t) - \phi(t)\| + \|\frac{\partial u_n}{\partial x}(1,t) - \psi(t)\| + \|u_n(x,0) - f(x)\|. \tag{20}$$

Substituting (18) into (20), we have

$$\begin{aligned} F_n(x,t;c) &= \|c\hat{u}_n(0,t) + (1-c)\check{u}_n(0,t) - \phi(t)\|^2 \\ &+ \|c\frac{\partial \hat{u}_n}{\partial x}(1,t) + (1-c)\frac{\partial \check{u}_n}{\partial x}(1,t) - \psi(t)\|^2 \\ &+ \|c\hat{u}_n(x,0) + (1-c)\check{u}_n(x,0) - f(x)\|^2. \end{aligned}$$

From (14), (15) and (18), we get

$$\begin{aligned} F_n(x,t;c) &= \|c\hat{u}_n(0,t) + (1-c)\phi(t) - \phi(t)\|^2 + \|c\frac{\partial \hat{u}_n}{\partial x}(1,t) + (1-c)\psi(t) - \psi(t)\|^2 \\ &+ \|cf(x) + (1-c)\check{u}_n(x,0) - f(x)\|^2 \\ &= \|c\hat{u}_n(0,t) - c\phi(t)\|^2 + \|c\frac{\partial \hat{u}_n}{\partial x}(1,t) - c\psi(t)\|^2 \\ &+ \|(1-c)\check{u}_n(x,0) - (1-c)f(x)\|^2 = c^2c_1^2 + c^2c_2^2 + (1-c)^2c_3^2. \end{aligned}$$

The optimal value of c will minimize the residual function F_n. Thus, differentiating F_n with respect to c and setting the result equal to zero, yields

$$c = \frac{c_3^2}{c_1^2 + c_2^2 + c_3^2}, \qquad n \geq 0.$$

4 Applications

We analyze here the efficiency and applicability of the weighted reduced differential transform method (WRDTM). In this line of thought, we apply the WRDTM to Cauchy problems of some special cases of the generalized Burgers-Huxley equations in the areas of mathematical physics and mathematical biology. In the sequel we adopt n terms when evaluating the approximate solution $u_n(x,t)$.

Example 1. *Consider the following problem*

$$\frac{\partial u}{\partial t} = \frac{\partial^2 u}{\partial x^2} - \frac{\partial u}{\partial x}, \qquad x > 0, \;\; t > 0, \tag{21}$$

with initial condition:

$$u(x,0) = \lambda \left(1 - \tanh\left(\frac{\lambda x}{2}\right)\right), \tag{22}$$

and boundary conditions:

$$u(0,t) = \lambda \left(\tanh\left(\tfrac{\lambda^2 t}{2}\right) + 1\right), \qquad u_x(0,t) = -\tfrac{1}{2}\lambda^2 \operatorname{sech}^2\left(\tfrac{\lambda^2 t}{2}\right), \tag{23}$$

where $\lambda \in \mathscr{R}$ is an arbitrary parameter.

The problem (21)-(23) has the exact solution $u(x,t) = \lambda(1 - \tanh(\frac{1}{2}\lambda(x - \lambda t)))$. By using the properties of the differential transformation with respect to t, we can write

$$U_k(x) = \frac{1}{k}\left(\frac{\partial^2}{\partial x^2} U_{k-1}(x) - \sum_{r=0}^{k-1} \frac{dU_r(x)}{dx} U_{k-r-1}(x)\right). \tag{24}$$

Starting with $U_0(x) = \lambda\left(1 - \tanh\left(\frac{\lambda x}{2}\right)\right)$, from (24) we find

$$U_1(x) = \frac{1}{2}\lambda^3 \operatorname{sech}^2\left(\frac{\lambda x}{2}\right),$$

$$U_2(x) = 2\lambda^5 \sinh^4\left(\frac{\lambda x}{2}\right) \operatorname{csch}^3(\lambda x),$$

$$U_3(x) = \frac{1}{24}\lambda^7(\cosh(\lambda x) - 2)\operatorname{sech}^4\left(\frac{\lambda x}{2}\right),$$

$\cdots$.

The differential inverse transform of $U_k(x)$ gives:

$$\hat{u}_n(x,t) = \sum_{k=0}^{n} U_k(x) t^k. \tag{25}$$

Now, we take the differential transformation of the Eq. (21) with respect to x. We apply the properties of Table 1 yielding

$$V_k(t) = \frac{1}{k(k-1)}\left(\frac{\partial}{\partial t}V_{k-2}(t) - V_{k-2} + \sum_{r=0}^{k-2}(r+1)V_{r+1}(t)V_{k-2-r}(t)\right). \tag{26}$$

After substituting

$$V_0(t) = \lambda\left(\tanh\left(\frac{\lambda^2 t}{2}\right)+1\right),$$

and

$$V_1(t) = -\frac{1}{2}\lambda^2 \operatorname{sech}^2\left(\frac{\lambda^2 t}{2}\right),$$

as the transformation of the boundary conditions in (23) , into (26), we obtain the next terms as

$$\begin{aligned} V_2(t) &= -2\lambda^3 \sinh^4\left(\frac{\lambda^2 t}{2}\right)\operatorname{csch}^3\left(\lambda^2 t\right), \\ V_3(t) &= -\frac{1}{24}\lambda^4\left(\cosh\left(\lambda^2 t\right)-2\right)\operatorname{sech}^4\left(\frac{\lambda^2 t}{2}\right), \\ &\cdots. \end{aligned}$$

Using the differential inverse transform of $V_k(x)$, we obtain

$$\breve{u}_n(x,t) = \sum_{k=0}^{n} V_k(t)x^k. \tag{27}$$

Suppose that $\lambda = 0.7$ and $n = 12$. According to (25), (27) and Theorem 1 we get $c = 0.999877$.
The approximate solution will be obtained by means of the expression (18). Figure 1 shows the exact and the approximate solutions of the problem for several values of t. The absolute error function $e_{12}(x,t) = |u(x,t) - u_{approx[12]}(x,t)|$ on the domain $\{(x,t)|(x,t) \in [0,5]\times[0,5]\}$, is shown in Figure 2.

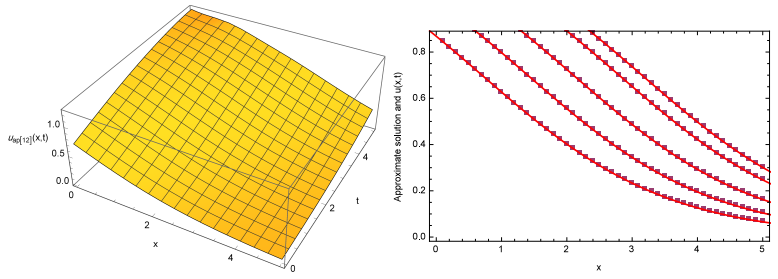

Figure 1
The exact and approximate solutions of example 1 with $n = 12$. Left: Plot of the approximate solution. Right: Exact solution (red line) and approximate solution (gray points) for various values of t.

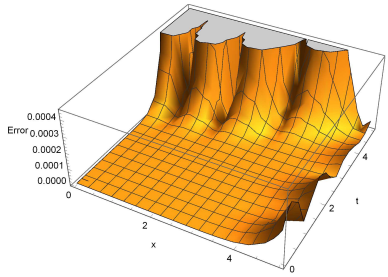

Figure 2
Absolute error for the approximate solution of example 1 with $n = 12$.

Example 2. *Consider the problem*

$$\frac{\partial u}{\partial t} = \frac{\partial^2 u}{\partial x^2} + u\frac{\partial u}{\partial x} + u(1-u)(u-1), \qquad x > 0, \;\; t > 0, \tag{28}$$

with initial condition:

$$u(x,0) = \frac{1}{2} - \frac{1}{2}\tanh\left(\frac{x}{4}\right), \tag{29}$$

and boundary conditions:

$$u(0,t) = \tfrac{1}{2} - \tfrac{1}{2}\tanh\left(\tfrac{3t}{8}\right), \qquad u_x(0,t) = -\tfrac{1}{8}\mathrm{sech}^2\left(\tfrac{3t}{8}\right). \tag{30}$$

The equation (28) is called Chaffee-Infante equation representing a reaction Duffing model discussed in mathematical physics. The exact solution of this problem is as follow:

$$u(x,t) = \frac{1}{2} - \frac{1}{2}\tanh\left(\frac{3t}{8} + \frac{x}{4}\right).$$

For applying the WRDTM we take the differential transform of (1) according to x and t, respectively, gives

$$\begin{aligned} U_k(x) = \tfrac{1}{k}\Bigg(& \tfrac{\partial^2}{\partial x^2}U_{k-1}(x) - U_{k-1}(x) + \sum_{r=0}^{k-1}\tfrac{\partial}{\partial x}U_r(x)U_{k-1-r}(x) \\ & + 2\sum_{r=0}^{k-1}U_r(x)U_{k-1-r}(x) - \sum_{s=0}^{k-1}\sum_{r=0}^{s}U_r(x)U_{s-r}(x)U_{k-1-s}(x)\Bigg), \end{aligned} \tag{31}$$

$$\begin{aligned} V_k(t) = \tfrac{1}{k(k-1)}\Bigg(& \tfrac{\partial}{\partial t}V_{k-2}(t) + V_{k-2}(t) - \sum_{r=0}^{k-2}(r+1)\tfrac{\partial}{\partial x}V_{r+1}(t)V_{k-2-r}(t) \\ & - 2\sum_{r=0}^{k-2}V_r(t)U_{k-2-r}(t) + \sum_{s=0}^{k-2}\sum_{r=0}^{s}V_r(t)V_{s-r}(t)V_{k-2-s}(t)\Bigg). \end{aligned} \tag{32}$$

For finding the solution of (28)-(30), we start the recursive relation (31) with $U_0(x) = \frac{1}{2} - \frac{1}{2}\tanh\left(\frac{x}{4}\right)$ and the recursive relation (32) with $V_0(t) = \frac{1}{2} - \frac{1}{2}\tanh(\frac{3t}{8})$ and $V_1(t) = -\frac{1}{8}\mathrm{sech}^2(\frac{3t}{8})$. By using the relations (14), (15) and (18), the approximate solution will be obtained. Suppose that $n = 15$. From Theorem 1 we get

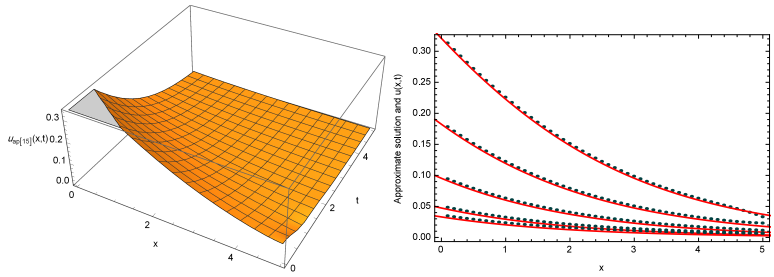

Figure 3
The exact and approximate solutions of example 2 with $n = 15$. Left: Plot of the approximate solution. Right: Exact solution (red line) and approximate solution (gray points) for various values of t.

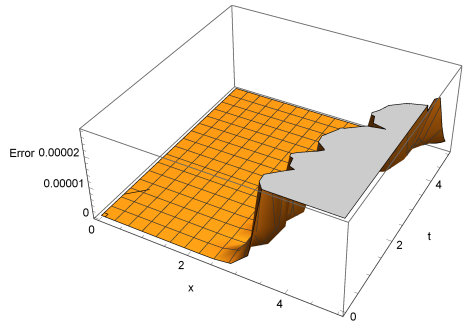

Figure 4
Absolute error for the approximate solution of example 2 with $n = 15$.

$c = 8.04462 \times 10^{-9}$. Figure 3 depicts the exact solution of (28)-(30) and its approximations in the domain $\{(x,t)|(x,t) \in [0,5] \times [0,5]\}$. The absolute error of the approximate solution, is shown in Figure 4.

Example 3. *Consider the equation (1) with* $\alpha = \beta = \eta = \kappa = 1$, $\gamma = -1$ *and* $\delta = 2$. *Also, in the conditions (2) and (3) assume that* $f(x) = \sqrt{\frac{1}{2} - \frac{1}{2}\tanh\left(\frac{x}{3}\right)}$, $p(t) = \sqrt{\frac{1}{2}\tanh\left(\frac{10t}{9}\right) + \frac{1}{2}}$ *and* $q(t) = -\dfrac{\operatorname{sech}^2\left(\frac{10t}{9}\right)}{12\sqrt{\frac{1}{2}\tanh(\frac{10t}{9}) + \frac{1}{2}}}$. *Under these assumptions, the exact solution of (1)-(3) is* $u(x,t) = \sqrt{\frac{1}{2}\tanh(\frac{10t}{9} - \frac{x}{3}) + \frac{1}{2}}$.
Taking the differential transform subject to x and t, we get the following recurrence relations

$$U_k(x) = \frac{1}{k}\left(\frac{\partial^2}{\partial x^2}U_{k-1}(x) + U_{k-1}(x) - \sum_{s=0}^{k-1}\sum_{r=0}^{s} U_r(x)U_{s-r}(x)U_{k-1-s}(x) - \sum_{s=0}^{k-1}\sum_{r=0}^{s}\frac{\partial}{\partial x}U_r(x)U_{s-r}(x)U_{k-1-s}(x)\right), \tag{33}$$

and

$$V_k(\mathrm{t}) = \frac{1}{k(k-1)}\left(\frac{\partial}{\partial t}V_{k-2}(t) - V_{k-2}(t) + \sum_{s=0}^{k-2}\sum_{r=0}^{s}(r+1)V_r(t)V_{s-r}(t)V_{k-2-s}(t) + \sum_{s=0}^{k-2}\sum_{r=0}^{s}V_r(t)V_{s-r}(t)V_{k-2-s}(t)\right). \tag{34}$$

Assuming that $n = 10$ and using (14), (15), (33) and (34), from (19) we get $c = 0.413211$. Substituting c in (18), yields an approximate solution. Figure 5 compares the approximate and the exact solution of the problem. The relative error function $r_{10}(x,t) = \frac{|u(x,t)-u_{approx[10]}(x,t)|}{|u(x,t)|}$ is shown in Figure 6.

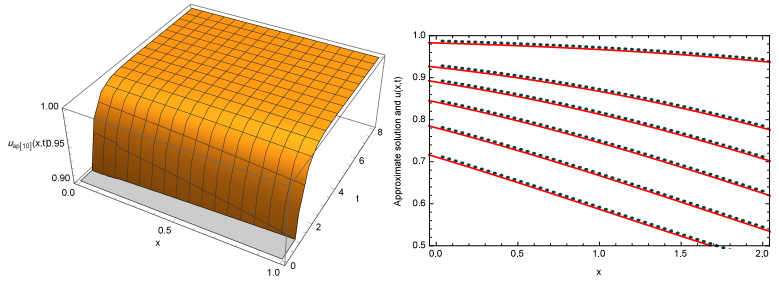

Figure 5
The approximate and exact solutions of example 3 with $n = 10$. Left: Plot of the approximate solution. Right: Exact solution (red line) and approximate solution (gray points) for various values of t.

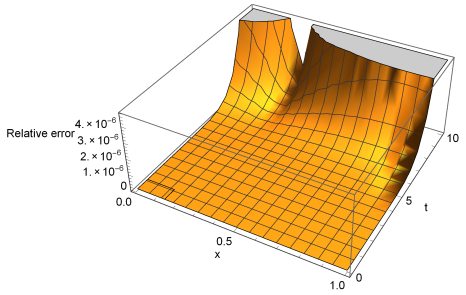

Figure 6
The relative errors for the approximate solution of example 3 with $n = 10$.

5 Conclusion

In this work a Cauchy problem of the generalized Burgers-Huxley equations was considered. Using the reduced differential transform method, a weighted algorithm to determine approximate-analytical solution was developed. To show the capability and reliability of the novel method, the solution of some special cases of the

generalized Burgers-Huxley equation were obtained. The results confirm that the WRDTM is an efficient technique to solve such Cauchy problems.

References

[1] G. B. Whitham, Linear and Nonlinear Waves, Wiley, New York, 1974.

[2] J. Satsuma, M. Ablowitz, B. Fuchssteiner, M. Kruskal, Topics in Soliton Theory and Exactly Solvable Nonlinear Equations, World Scientific, The Singapore City, 1987.

[3] D. Kotorová, Discrete duality finite volume scheme for the curvature-driven level set equation, Acta Polytechnica Hungarica 8 (3) (2011) 7–12.

[4] B. Laczik, P. Zentay, R. Horváth, A new approach for designing gear profiles using closed complex equations, Acta Polytechnica Hungarica 11 (6). doi:10.12700/aph.11.06.2014.06.10.

[5] E. Pap, D. Vivona, Basic equations of fluid dynamics treated by pseudo-analysis, Acta Polytechnica Hungarica 9 (2) (2012) 5–23.

[6] H. C. Rosu, O. Cornejo-Pérez, Super symmetric pairing of kinks for polynomial nonlinearities, Physical Review E 1 (4) (2005) 1–13. doi:http://dx.doi.org/10.1103/PhysRevE.71.046607.

[7] X. Y. Wang, Nerve propagation and wall in liquid crystals, Physics Letters A 112 (8) (1985) 402–406. doi:10.1016/0375–9601(85)90411–6.

[8] E. Pap, Pseudo-analysis approach to nonlinear partial differential equations, Acta Polytechnica Hungarica 5 (1) (2008) 31–45.

[9] E. Babolian, J. Saeidian, Analytic approximate solutions to Burgers, Fisher, Huxley equations and two combined forms of these equations, Communications in Nonlinear Science and Numerical Simulation 14 (5) (2009) 1984–1992. doi:10.1016/j.cnsns.2008.07.019.

[10] S. S. Ray, A new coupled fractional reduced differential transform method for the numerical solution of fractional predator-prey system, Computer Modeling in Engineering and Sciences 105 (3) (2015) 231–249.

[11] V. K. Srivastava, N. Mishra, S. Kumar, B. K. Singh, M. K. Awasthi, Reduced differential transform method for solving $(1+n)$–dimensional Burgers' equation, Egyptian Journal of Basic and Applied Sciences 1 (2) (2014) 115–119. doi:10.1016/j.ejbas.2014.05.001.

[12] Z. Odibat, S. Momani, A generalized differential transform method for linear partial differential equations of fractional order, Applied Mathematics Letters 21 (2) (2008) 194–199. doi:10.1016/j.aml.2007.02.022.

[13] X. J. Yang, J. A. T. Machado, H. M. Srivastava, A new numerical technique for solving the local fractional diffusion equation: Two-dimensional extended

differential transform approach, Applied Mathematics and Computation 274 (2016) 143–151. doi:10.1016/j.amc.2015.10.072.

[14] X. J. Yang, J. A. T. Machado, H. M. Srivastava, Nonlinear dynamics for local fractional Burgers' equation arising in fractal flow, Nonlinear Dynamics 84 (1) (2015) 3–7. doi:10.1007/s11071-015-2085-2.

[15] I. Hashim, M. S. M. Noorani, M. R. S. Al-Hadidi, Solving the generalized Burgers-Huxley equation using the adomian decomposition method, Math. Comput. Model 43 (11–12) (2006) 1404–1411. doi:10.1016/j.mcm.2005.08.017.

[16] A. Molabahrami, F. Khani, The homotopy analysis method to solve the Burgers-Huxley equation, Nonlinear Analysis: Real World Applications 10 (2) (2009) 589–600. doi:10.1016/j.nonrwa.2007.10.014.

[17] R. Abazari, M. Abazari, Numerical study of Burgers-Huxley equations via reduced differential transform method, Comp. Appl. Math. 32 (1) (2013) 1–17. doi:10.1007/s40314-013-0001-2.

[18] M. T. Darvishi, S. Kheybari, F. Khani, Spectral collocation method and Darvishi's preconditioning to solve the generalized Burgers-Huxley equation, Commun Nonlinear Sci Numer Simulat 13 (10) (2008) 2091–2103. doi:10.1016/j.cnsns.2007.05.023.

[19] J. E. Macías-Díaz, J. Ruiz-Ramírez, J. Villa, The numerical solution of a generalized Burgers-Huxley equation through a conditionally bounded and symmetry-preserving method, Computers and Mathematics with Applications 61 (11) (2011) 3330–3342. doi:10.1016/j.camwa.2011.04.022.

[20] B. P. Moghaddam, J. A. T. Machado, A Stable Three-Level Explicit Spline Finite Difference Scheme for a Class of Nonlinear Time Variable Order Fractional Partial Differential Equations, Computers and Mathematics with Applications, (2016). doi:10.1016/j.camwa.2016.07.010.

[21] I. Celik, Haar wavelet method for solving generalized Burgers-Huxley equation, Arab Journal of Mathematical Sciences 18 (1) (2012) 25–37. doi:10.1016/j.ajmsc.2011.08.003.

[22] B. K. Singh, G. Arora, M. K. Singh, A numerical scheme for the generalized Burgers-Huxley equation (2016). doi:10.1016/j.joems.2015.11.003.

[23] J. K. Zhou, Differential transform and its applications for electrical circuits, Huazhong University Press, Wuhan, China.

[24] Y. Keskin, G. Oturanc, Reduced differential transform method for partial differential equations, International Journal of Nonlinear Sciences and Numerical Simulation 10 (6) (2009) 741–749.

[25] A. Arikoglu, L. I. Ozkol, Solutions of integral and integro-differential equation systems by using differential transform method, Computer and Mathematics with Applications 56 (9) (2008) 2411–2417. doi:10.1016/j.camwa.2008.05.017.

[26] A. Shidfar, M. Garshasbi, A weighted algorithm based on adomian decomposition method for solving an special class of evolution equations, Commun. Nonlinear Sci. Numer. Simulat. 14 (4) (2009) 1146–1151. doi:10.1016/j.cnsns.2008.04.004.

Abrasive Wear and Abrasion Testing of PA 6 and PEEK Composites in Small-Scale Model System

László Zsidai, László Kátai

Szent István University, Faculty of Mechanical Engineering,
Institute for Mechanical Engineering Technology
Páter K. u. 1, H-2100 Gödöllő, Hungary
email: zsidai.laszlo@gek.szie.hu; katai.laszlo@gek.szie.hu

Abstract: Abrasion wear is one of the most common failure mechanisms of moving machine elements. Because of their mechanical and tribological ability, engineering polymer composites can be chosen to replace metal parts in certain applications (e.g. bearings). Increasingly newer polymer composites are appearing and data on their tribological behaviours are incomplete, it is not so easy to choose from this wide wide selection of choices (mechanical properties, price, etc.). In the present study two groups of polymer composites (PA 6 and PEEK with different mechanical properties and prices) are experimentally investigated by a unique small-scale abrasion tribotesting. The main objectives of our study were to compare the tribological properties of composites and to investigate the effect of different additives and mechanical properties. The tests were prepared using the pin on plane (band) model system and tested on different loads (11.5 N and 23 N), where the abrasion mating surface was emery cloth. We found among other things that the fillings have a favourable effect on PA opposite to PEEK. The short carbon fibres proved better for improving wear resistance as compared to short glass fibres. Our present work is connected to a research project, which aims to map the tribological features of different polymer composites.

Keywords: abrasion; PA 6; PEEK; friction; tribology

1 Introduction

Abrasion is the most common type of wear in industrial practice. It occurs when the micro-roughness of the harder counter body ploughs through the softness of the counter surface. Material is removed by micro cutting or micro cracking, and wear results by sharp and rigid particles or peaks of roughness. Wear gaps are created by the scratches of the surface. The particles that leave the gap are called the wear. Abrasive wear can occur in all places, where rigid particles can go between the sliding surfaces (e.g. in dusty work zone), where the surface

roughness is high, or the hardness of the sliding elements is very different, or if the machine works with abrasive material. Briscoe and Sinha [3] mentioned that cohesive wear results from surface and subsurface deformations, caused by the harder asperities of the counterface. Abrasion and fatigue wear processes are termed, 'cohesive wear'.

We can use machine elements (e.g. efficient seals) and optimal surface parameters to the reduce effects of abrasion wear, but unfortunately these are not always possible (e.g. in heavy dusty places, such as in agriculture, and in the mining industry). We may use tough or elastic materials or coatings with high strength to solve in these situations. The polymers and polymer composites can be chosen as sliding materials (because of their good deformation ability) in abrasive applications during the machine construction also as a counter measure. Regardless of the metals, where the cutting is the most important abrasion process, with polymers tearing-sheller effects are the most dominant. Polymer composites can also improve the tribological properties of the base polymers in an abrasion friction system. Several publications deal with the base mechanism of the abrasion wear [5, 6, 11] and its role in the machine industry applications [21] and the abrasion features of the polymers also [7, 9, 12, 24].

The abrasion friction test instruments are developed parallel to the former ones. Several standards (ASTM, DIN and ISO) deal with the abrasion tests of the polymers: ASTM D1242 is a standard test method to see the resistance of plastic materials to abrasion [8], ASTMD 3389 is for coated fabrics (rotary platform, double-head abrader), ASTM G 75 to determine the slurry abrasivity (miller number) and slurry abrasion response of materials (SAR Number) and ASTMG 132-96 for pin abrasion testing. DIN 52 347 is for testing of glass and plastics and DIN 53 516 is for testing of rubber and elastomers. ISO 4649 is for rubber, vulcanized or thermoplastic using a rotating cylindrical drum device and ISO 5470-1 for rubber- or plastics-coated fabrics and ISO 23794 is for rubber, vulcanized or thermoplastic [30]. These rigs are available in the technical market as a professional product [27]. Most of the previous model systems worked in sand slurry, liquid (cavitation ASTM G32-134), or gas (ASTM G76). Some examinations make it possible to do tests with reciprocating motion against plane or abrasion wheel in counterformal contact.

One of the capital novelties and key to our work is the unique model system, which developed the abrasion tribotest rig. The equipment makes it possible to obtain linear abrasion friction measurements of the different polymers on emery cloth using a pin-on-plate (band) test apparatus with one-way continuous motion in conformal contact (modeling most applications well, e.g. sliding bearings, V-belt, gears). No external lubricants were added to the tribological system.

The selected polymers were investigated with respect to friction and wear characteristics. The selection was based on a base polymer and different composites as applied by manufacturers and users. We selected two polymer

groups with special characteristics and significant differences between their mechanical properties and prices. Among many types of polyamides (PA), four PA were tested (PA 6 E reference, PA 6MO, PA 6G ELS, PA 6GLIDE). The relatively expensive PEEK (Poly-Ether-Ether-Ketone) was tested for base and composites PEEK PVX and PEEK GF30 that are widely used nowadays (e.g. medical implants, industrial sealings) were included in the experiments.

Many results can be found in the literature, that are connected to the mechanical and abrasion behaviours of the tested polymer groups. Polyamide 6 is a well known polymer [20, 22, 23, 37], therefore we will give a short overview of the tribological properties of PEEK composites mainly.

Several authors [2, 30] wrote that the friction coefficient of PEEK decreases with increasing temperature, it passes through an optimum point (around the glass-transition temperature at 143 °C) and then increases slightly. Shao et al. [36] and Wang et al. [29] found that micro and nanosized abrasive (SiO_2) fillers in PEEK provided lower wear rates and lower coefficients of friction than the unfilled polymer, and he reported also [28], that nanoparticles of ZrO_2 as the filler were effective in reducing the wear rate of PEEK.

The literature [25, 26, 32] shows a wide variety of different fillers available such as solid lubricants for reducing friction, reinforcing fibers for high mechanical strength or hard particles for abrasion resistance. In the literature we can see that the addition of carbon fibre (CF) to polymers resulted in increased hardness, tensile and flexural strength [13] and increased glass transition temperature [14]. Unlubricated sliding wear behaviour of short glass fibre (GF) and carbon fibre (CF) reinforced PEEK have been investigated by Voss et al. [10] and Friedrich et al. [18, 19]. They concluded that short carbon fibres proved better for improving wear resistance as compared to short glass fibres, but this trend can change under certain “pv limit” (contact pressure multiplicity sliding velocity) conditions.

To create a continuous transfer layer, solid lubricants, like graphite and PTFE are commonly used [1, 15]. More investigations describe that the 10-25 wt% of PTFE give an optimal wear resistance and minimum frictional coefficients for the PEEK composites PTFE [4, 31, 38, 39]. However, other studies point at important effects of the filling manner of PTFE, where the wear rates obtained from the inclusion of expanded PTFE filaments were better than conventional powder filled PTFE–PEEK composites. [16]

Friedrich and Alois K. Schlarb [17] refer to the tribological differences between PEEK and PA 6. They emphasize that for the low wear rate of PEEK makes a relative higher friction coefficient, but in case of the PA 6 both properties are low. For PEEK, the role of nanoparticles is to increase the load-bearing capacity of the material, and thus the actual contact area is reduced leading to lower frictional stress for the nanocomposite.

The main objectives of our investigations are:

- comparison of friction and wear behaviour of different PA and PEEK composites in connection with mechanical properties,
- presentation of a special abrasion test system, with one way motion and conformal contact,
- determination of optimal operational conditions of the selected polymers.

This article aims to be helpful in the selection of a proper polymer for a given operational condition.

2 Experimental Procedure

2.1 Apparatus

The experimental set-up as pictured in Fig. 1, is a unique building abrasion tribotester.

The detailed figure shows that continuous sliding friction is created by a polymer cylinder (1), which moves against a lower emery cloth (2) in conformal contact. The polymer specimen is fixed to the fixture (3) by nuts, preventing it from rolling during the test, and thus simple sliding is guaranteed. The continuous one-way motion of the emery cloth is provided by a controlled variable speed motor (4) through a twin roll power transmission (5) to produce the sliding motion. The abrasive emery cloth is tightened to a pair of rolling drums, and the friction contact is placed between these in the middle position. A metal plate is placed under the moving slide, therefore the contact abrasive surface will be a plane.

The machine is equipped with a manual loading system (6), which consists of a plate (7) and a vertical column (8), mechanically pulled down by loading weights (9). A head (load-cell) with strain gauges (10) is used to measure the friction force. The normal displacement of the cylindrical specimen towards the steel plate, as a result of the wear, is measured by a linear gauge (11). The vertical column and the linear gauge with supporting spindles are built in the console head (12).

The more detailed close-up of the equipment (upper-center) shows the manual load system and the special form of the measure head.

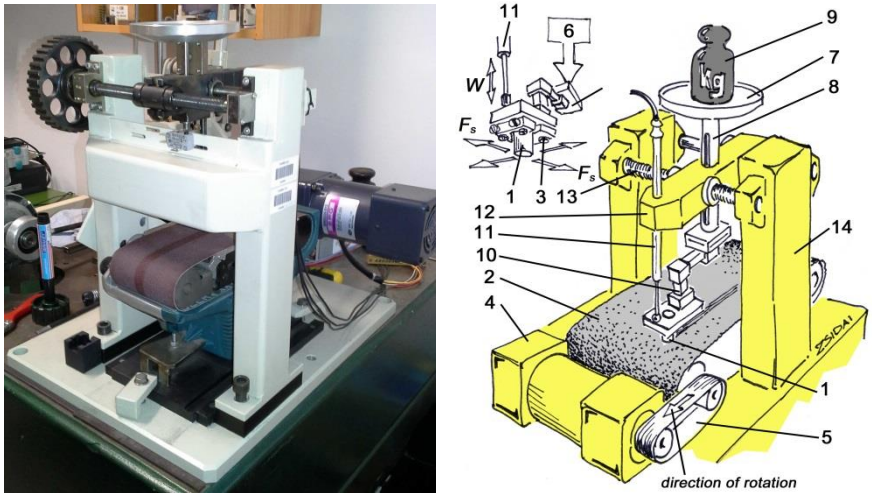

Figure 1
Abrasion testing equipment (photo and schematic view):

(1) polymer specimen; (2) emery cloth; (3) nuts and clamp; (4) electrical motor; (5) twin roll driving system; (6) manual loading system; (7) plate; (8) vertical column ; (9) weights; (10) load-cell; (11) linear gauge (for vertical displacement as a result of wear); (12) console head unit; (13) spindle for cross movement (it wasn't used for present tests)

2.2 Test Conditions

All experiments were performed in ambient temperate and humidity (25°C and 50%RH). The various conditions of the small-scale tests performed are gathered in Table 1.

Table 1
Parameters of tests

Parameters	**Values**
Type of the emery cloth	DEER XA167AA-100
Running time, t [s]	240
Normal load, F_N [N]	11.5 and 23
Length of emery cloth [mm]	610
Velocity, v [m/s]	0.05
Total sliding distance [m]	12
Humidity, RH [%]	50
Ambient temperature, T [°C]	25

Tests were conducted with normal load: 11.5 N and 23 N. The running time (240 s) of the tests were chosen in order to observe the wear value and the first (running in stage) period of the friction. For each test, the surface roughness of the emery cloths were determined by the type of abrasive DEER XA 167 AA-100. The tribological data described below result from an average of three runs with identical experimental parameters.

Materials and preparation of test specimens

The selection of the tested seven polymers and composites were made by cutting an 8mm diameter and a 10-15 mm length. The materials can be divided into two main composites groups. The experiments included one with a PA6, and the other with a PEEK base matrix.

Material of the mating plate

The counter plates are abrasive industrial emery cloth (type: DEER XA 167 AA-100), and it was chosen as a typical abrasion effect for the industry. The grain type of the grinder is Aluminium-Oxide and the bonding material is resin. [33]

Materials of the polymer cylinders

Table 2 gives an overview of the properties of the tested engineering plastics. Among these properties the E-modulus can be used to characterize the adhesion friction component, since it is correlated with the chain flexibility. The deformation ability is determined by tensile stress and strain, as their product is equivalent to the work of rupture and the material's toughness.

Table 2

Mechanical and physical properties of the tested polymers [34, 35]

Material code	**colour**	**density [g/cm^3]**	**Tensile strength at yield/ Modulus of Elasticity [MPa]$^{(1)}$**
PA 6E natural	black	1.14	80/3200
PA 6G ELS	black	1.15	90/3400
PA 6MO	black	1.16	80/3400
PA 6 Glide	green	1.13	76/3200
PEEK natural	beige	1.31	116/4200
PEEK PVX	black	1.44	84/5500
PEEK GF 30	yellow	1.53	105/6400

(1) Values referring to material in equilibrium with the standard atmosphere 23°C/50% RH

The list shows a short description of the tested polymers below. [34, 35]:

- The extruded type polyamide PA 6E were used as a reference material in the investigations. This polyamide has been a strategic engineering plastic for many years all over the world, thanks to the favourable performance/price

ratio. It offers a favourable combination of strength, toughness, mechanical damping ability and wear resistance. The product can be regarded as a polyamide type "for general use".

- The PA 6G ELS is the conductive version of magnesium catalysed cast polyamide 6.
- In comparison the PA 6MO (PA 6E+MoS_2) with the PA 6E material, it has a higher degree of strength and rigidity due to the molybdenum disulphide (MoS_2) content. Its heat and wear resistance is better, but its toughness and mechanical damping ability is worse. It can be readily machined with automatic cutting machines.
- PA 6 Glide is a hard semi-crystalline cast thermoplastic with a lubricant addition. It has good sliding properties, wear resistance, better tensile strength and machinability than PA 6E. Typical applications are (e.g. gears, rollers, cable rollers, universal material) wherever there are no special requirements.
- Natural, unfilled PEEK (polyetheretherketone) is a semi-crystalline advanced material that exhibits a unique combination of high mechanical properties, temperature resistance, and an excellent chemical resistance. The main properties are a high service temperature (permanently around 250 °C, briefly to 310 °C can be used), high mechanical strength, stiffness, excellent chemical, hydrolysis, wear resistance and good dimensional stability.
- PEEK PVX is a real bearing grade. It is filled with carbon fibres (CF), PTFE and graphite.
- PEEK GF30 composite contains 30% glass fibre (GF) reinforced for greater dimensional stability and higher strength properties.

The original forms, colours and dimensions of the small-scale specimens are included in Fig. 2. The polymer cylinder has a diameter of 8 mm and length of 10-15 mm.

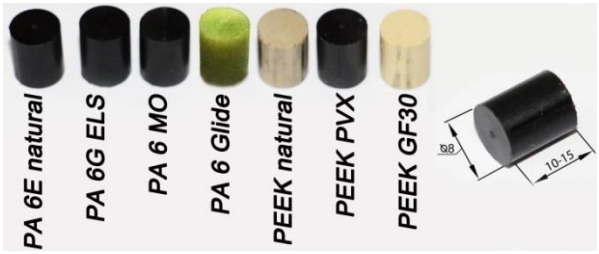

Figure 2
Original form and dimensions of the tested polymers and composites

The cylindrical specimens are in conformal connection with the abrasive (emery cloth). The components of composites are homogenously spread in the bulk of polymers.

3 Test Results And Discussion

3.1 General

Friction and wear results of the small-scale abrasion tests for both load categories (11.5N and 23N) are described in this section. For the correct interpretation of the graphs and tables mentioned below, the following annotations are emphasised:

Column charts: The dynamic and the maximum friction coefficients are represented in Figs. 3 and 5. For each material, the first column refers to maximum value of the friction and the second one refers to the dynamic friction coefficient. The white arrow marks the instable tendency (slowly growing, slowly decreasing). The wear is represented in Fig. 7. For each material the first column refers to the wear value of the lower load (11.5N) and the second one refers to the wear of the higher load (23N) tests. All values are averaged from three test runs with identical parameters.

Dynamic friction characteristics: The real friction curve as a function of sliding distance is shown in Fig. 4 and Fig. 6 for a given load and emery cloths. For example, for some polymer, only one typical curve of the three runs, is shown to reveal the differences in friction behaviour during the running-in stage and steady state regime. It has to be mentioned that the periodically repetitive more or less similar instabilities can be seen on the curves at the joint of the emery cloth bands.

3.2 Lower Load (11.5 N) Test Category

Figs. 3-4 show the dynamic and maximum friction coefficient of polymers tested under the lower 11.5 N loads.

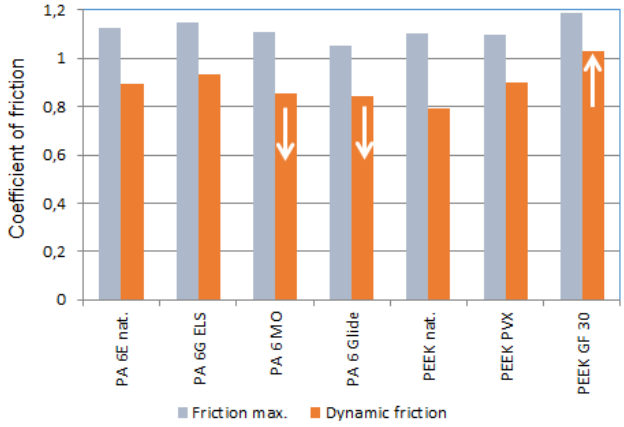

Figure 3
Dynamic friction coefficient (dark) and its maximum value (light) at lower 11.5 N load

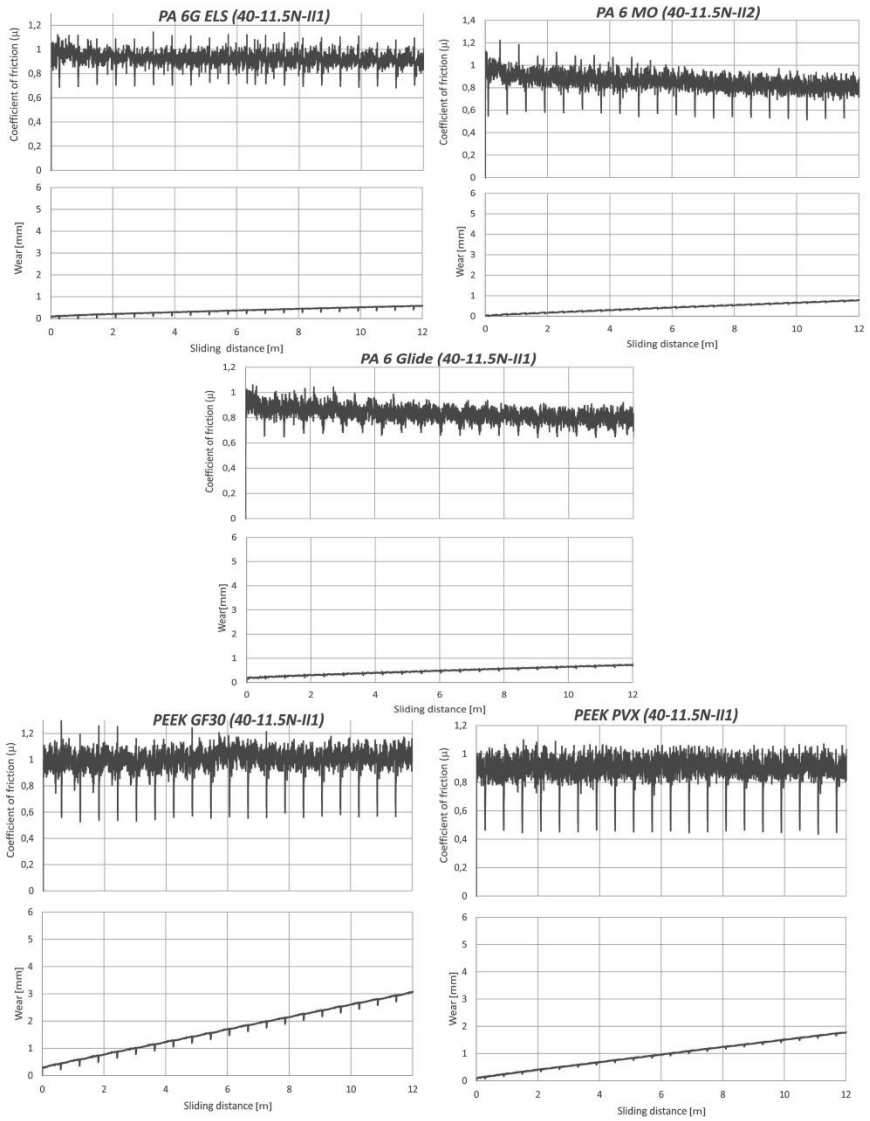

Figure 4
Dynamic friction and wear characteristics of tested composites against emery clothes at 11.5 N load

- From the view point of the dynamic friction, PEEK natural is most favourable and seems to have the lowest values over the total sliding time. However, the highest instability in the friction, which is shown by the maximum value of it's. PEEK PVX has a similar value of maximum friction but a higher dynamic value than natural PEEK. The highest frictions (maximum and dynamic) are represented by PEEK GF 30 on abrasive surfaces, this value is not constant but shows a slight increase during the running-time (Fig. 4).

- The friction behaviours are similar for PA 6E and PA 6G ELS, and they are very stable during the test (Fig. 4). Figure 4 shows the friction and wear curves of PA 6 MO and PA 6 Glide, these values are not constant but show a slight decrease during the running-time.
- The PA composites (mainly PA 6 Glide and PA MO) show a lower friction in opposite the PEEK composites. PA 6 Mo (Fig. 4) shows better sliding properties than PA 6E and PA 6G ELS. This behaviour is interesting because it is opposite to the effect of molybdenum addition (being tougher). The highest friction is presented by PA 6 ELS among all tested PA composites in lower load category.

3.3 Higher Load (23 N) Test Category

With the application of higher (23 N) load, the dynamic friction coefficients and maximum friction of the polymers are represented in Figs. 5-6.

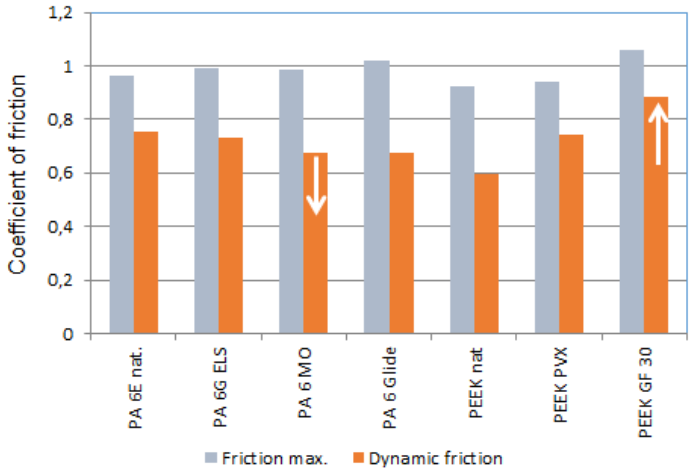

Figure 5
Dynamic friction coefficient (dark) and its maximum value (light) at higher 23 N load

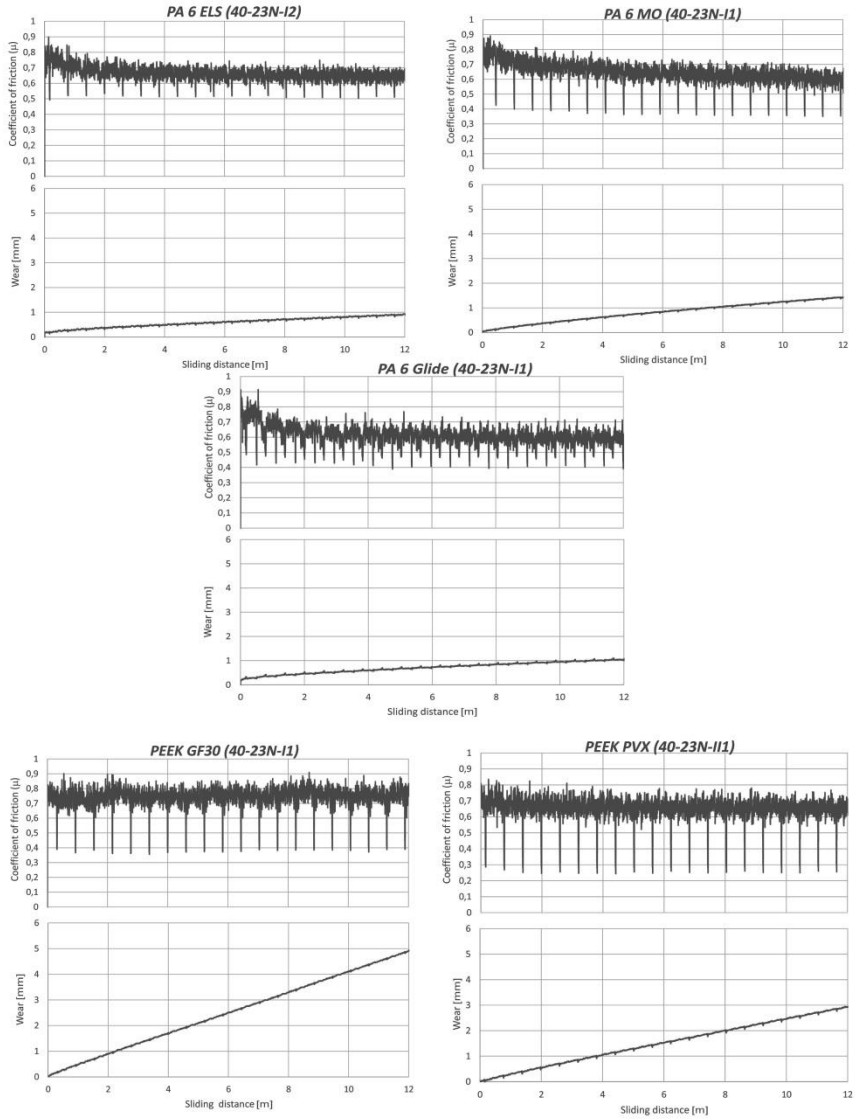

Figure 6

Dynamic friction and wear characteristics of tested composites against emery clothes at 23 N load

Comparing Fig. 3 and Fig. 5, it appears that globally under high loads the friction coefficient is lowered. We can see a similar difference and range among the friction behaviours of tested polymers at lower load categories.

- In accordance with the previous, the PEEK natural has the lowest friction coefficient under higher load (similar to lower load).

- In contrast to the results of the lower load category another range occurs between PA 6G ELS and PA 6E natural, in favour of PA 6G ELS.
- The friction of PA 6 Glide is more stable than when it was at a lower load. PA 6 Mo (Fig. 6) has similar favourable sliding properties as PA 6 Glide but shows a slight decrease during the running-time.
- PEEK GF30 shows the worst results in connection to friction coefficients and wear among the tested polymers.

3.4 Comparison of the Wear of Different Load Categories

It is clear that the effect of adhesion decreases with increasing load and increasing surface roughness. In our case the abrasion now becomes more important. The abrasion wear results of the tested polymers are shown in the Fig. 7 for both load categories. We can measure both the wear and deformation together, however - because of the small loads- this is negligible in the present study.

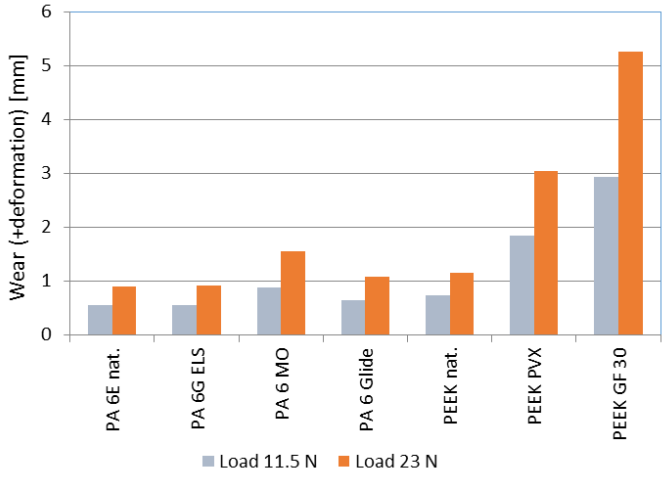

Figure 7
Wear values for different materials in 11.5 N and 23 N load categories

We can compare these results. It can be observed from the figure that the higher load increases proportionally (~1.6 times) in the wear of most of tested polymers.

- But in cases two of PA 6MO and PEEK GF 30 we can see bigger differences between the wear results. The wear is measured at a higher load, 1.77 times more than measured at a lower load. These polymers are a little bit more sensitive against the different loads.

- PA 6E natural has the lowest wear results close to PA 6G ELS. It can be observed from the wear result of these polymers, that they have increased deformation ability, due to the lower tensile stress and lower strain at break.
- The highest wear values are shown by PEEK PVX and mainly PEEK GF30, they are said to be more rigid because of their higher modulus of elasticity. So in our abrasion case the rigid behaviours can cause a higher value of wear.
- The polyamides show a better wear result among tested polymers in both categories, according to the low elasticity modulus of this polymer. The flexibility of the polymer chains is enhanced for soft materials (reflected by a low elasticity modulus), a better more effective transfer can occur.

Fig. 8 shows polymer films of all tested polymers (at first the PEEK, then PA 6) in the wear track, which are studied by a digital camera after the test. The forms and filling in the abrasive surface, show us the results of the wear behaviour of tested polymers.

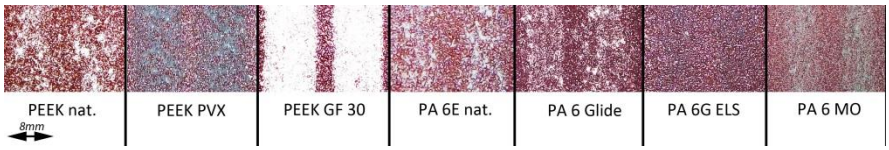

Figure 8
Different wear tracks on the emery cloth at 11.5 N load

- In the case of PEEK, natural non-continuous plastic layers cover the surface with several large and bitty wear particles.
- For both PEEK composites (PVX and GF30), the polymer films are thick and a more or less homogenous track (mainly GF30) is observed.
- The smallest and thinnest transfer layer is shown by polyamides; this great correlation makes them preferable for their wear properties.

According to generally accepted friction models, two mechanisms contribute to the friction force between a thermoplastic and steel: adhesion in the contact zone and deformation of the polymer [9, 11]. Their relative contribution depends on several conditions like load level, as well as, on the chemical, mechanical and geometrical properties. However, the surface roughness is the most important factor among them. The deformation ability of the polymers, basically determines the abrasion resistance of the tested polymers. Therefore, we have to see the mechanical properties of the polymers. The tensile strength at yield and modulus of elasticity were shown in Table 2, and the hardness (type: Shore D for rigid polymer tested by Zorn Stendal 8036 hardness tester) due to wear are illustrate in Fig. 9.

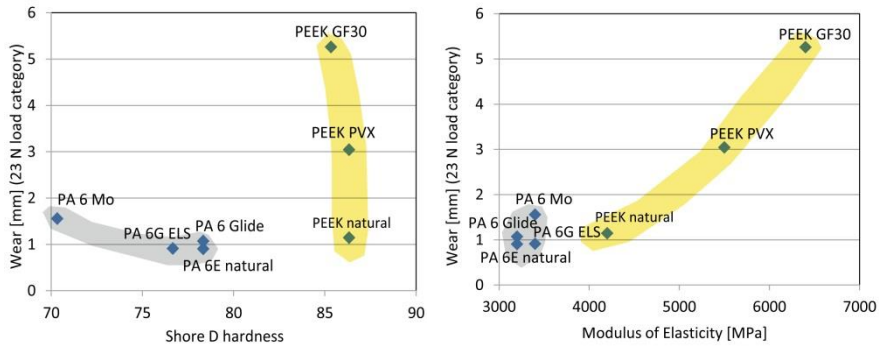

a) b)

Figure 9

The Shore D hardness (a) and the Modulus of Elasticity (b) of tested polymers are plotted against the measured wear (23 N load category)

From the trend lines, the following conclusions are drawn in the figures:

- We can see a correlation between the hardness and the wear in cases of polyamides (Fig. 9/a). Wear decreases with increasing Shore D hardness. However, the previous trend is not so clear in the case of PEEK because of similar hardness of PEEK composites, however the PEEK GF30 has the highest wear with a lower hardness among PEEKs.
- We can see the contrast with the previous ones, in a context between the modulus of elasticity and wear at PEEKs in Figure 9/b.
- In summary, on one hand the hardness of the polyamides have an influence on their wear, but on the other hand the PEEKs has the modulus of elasticity.

Conclusions

Based on the results of the unique experiments, the following conclusions can help and improve the further tribotesting of polymers, the selection of proper material and design. The experimental data suggests the following conclusions:

- There is a general trend from present investigations that the dynamic friction coefficient decreases with increasing normal load, and the wear is found to be ~1.6-1.8 times higher at double load.
- Among the investigated polymers and composites taken from the engineering practice the PA 6Glide and PEEK natural are most suitable sliding materials, because their friction is lowest and their wear resistance is higher.
- The effect of the internal lubrication in case of cast PA 6Glide composite is different from the effect of solid PTFE lubrication in PEEK PVX. In case of PA 6 the efficiency of the lubrication gives an excellent friction coefficient and

high wear resistance at both load categories. Opposite the PA 6Glide the addition of PTFE has a weak effect on the friction. The solid PTFE lubricant can't decrease the friction of the PEEK PVX (due to PEEK natural).

- The polyamides have a good abrasion wear resistance in connection with their increased deformation ability, but their friction coefficients do not differ significantly from the more „rigid" PEEKs.
- The addition fillings have a different effect on the PA and PEEK composites. While these fillings have a good effect for the friction coefficients of polyamides, in case of PEEK they have an unfavourable effect at both load categories. The former are true for the abrasion wear also where the PEEK composites suffer an essential higher abrasion in comparison with polyamide composites.
- Our abrasion investigations correlate with Voss et al. [10] and Friedrich et al [18, 19], that short carbon fibres proved better for improving wear resistance as compared to short glass fibres, in the given circumstances.
- We observed a difference between our results and the data presented previously [17]. Other data showed differences between the friction of PEEK (high) and PA6 (low), but the wear was similar. However, in our cases the frictions were more or less similar, but we found a major difference in the wear results (exceptions the natur PA and PEEK).
- The PA 6G ELS shows individual friction properties. The Mg-catalysed polymerization of this polymer has a more efficient effect on the friction at higher load, but it does not have any individual effect on the wear between both load categories.
- The presented photos of the wear gaps are in good correlation with the wear results (homogenous and thick gaps for the PEEK composites and thin ones for the polyamides).
- The Shore D hardness of the polymers has a different effect on the wear, while it seems a correlation between them at polyamides, but does not have any at PEEKs. The modulus of elasticity has an influence of the wear in cases of PEEKs rather.

For practical use we can mention by our results, that the polyamide composites are suitable as machine elements in normal abrasive applications, as they resist again abrasion wear. However, if there are any extreme demands, for example: high mechanical properties, temperature resistance and excellent chemical resistance etc., we can use PEEK composites also, but it is important to know the character of the filling. It is clear that the glass fibre (GF) has a bad effect on the friction and the wear at abrasive surface.

The small-scale abrasion tests with PA and PEEK polymers and composites with abrasive surface provided new information about their tribological behaviours. These results extend our tribological knowledge about polymers and show new possibilities for practical application.

Acknowledgement

The author (László Zsidai) would like to thank MTA (Hungarian Academy of Sciences) for supporting this work in the frame of the research fellowship BOLYAI (BO/00127/13/6).

Special thanks go to QuattroPlast for the delivery of material specimens.

References

[1] A. Häger, M. Davies: Advances in Composite Tribology, Elsevier, Amsterdam, 1993

[2] B. J. Briscoe: Interfacial Friction of Polymer Composites. General Fundamental Principles. In: Friedrich, K. (Ed.): Friction and Wear of Polymer Composites. Elsevier, Amsterdam (1986) pp. 25-59

[3] B. J. Briscoe and S. K, Sinha (Ed. by: G.M. Swallowe): 59-Wear, Mechanical properties and Testing Ok Polymers, Polymer Science and Technology Series, Volume 3 Springer-Science+Business Media, B. V. 1999

[4] D. Burris, W. Sawyer, A Low Friction and Ultra Low Wear Rate Peek/Ptfe Composite, Wear 261 (2006) pp. 410-418

[5] E. Rabinovicz: The Friction and Wear of Materials, John Wiley and Sons, New York, 1965

[6] F. P. Bowden, D. Tabor: The Friction and Lubrication of Solids, Clarendon Press, Oxford, 1950

[7] G. Kalácska, et al.: Műszaki műanyagok gépészeti alapjai (Mechanical Basics of Polymers), Minerva-sop Bt. Sopron, 1997

[8] G. M. Swallowe (Ed. by: G. M. Swallowe): 46-Standards for Polymer Testing, Mechanical Properties and Testing of Polymers, Polymer Science and Technology Series, Volume 3 Springer-Science+Business Media, B. V. 1999

[9] H. Uetz, J. Wiedemeyer: Tribologie der Polymere, Carl Hanser, Munich, 1985

[10] H. Voss and K. Friedrich: "On the Wear Behaviour of Short-Fibre-Reinforced-Peek," Wear, 116, 1, 1987. pp. 1-18

[11] I. M. Hutchings: Tribology, Friction and Wear of Engineering Materials, Arnold, London, 1992

[12] J. B. Ratner et al.: Connection between Wear Resistance of Plastics and other Mechanical Properties. Soviet Plastics, 1964. Vol. 12 (7) 37, 145 p.

[13] J. Hanchi and N. S. Eiss Jr.: "Dry Sliding Friction and Wear of Short-Fiber-Reinforced Poly-Etherether-Ketone (PEEK) at Elevated Temperatures," Wear, 203-204, 1997, pp. 380-386

[14] J. J. Rajesh, J. Bijwe and U. S. Tewari: "Influence of Fillers on Abrasive Wear of Short Glass Fibre Reinforced Polyamide Composites," Journal of Materials Science, 36, 2001, pp. 351-356

[15] J. J. Rajesh, J. Bijwe and U. S. Tewari: Abrasive Wear Performance of Various Polyamides, Wear, 2002. Volume 252, Issues 9-10, pp. 769-776

[16] J. R. Vail, B. A. Krick, K. R. Marchman, W. Gregory Sawyer: Polytetrafluoroethylene (PTFE) Fiber Reinforced Polyetheretherketone (PEEK) Composites, Wear, 2010. Volume 270, Issues 11-12, pp. 737-741

[17] K. Friedrich and A. K. Schlarb (Ed.: B. J. Briscoe): Tribology of Polymeric Nanocomposites. Tribology and Interface Engineering Series, 2008. No. 55

[18] K. Friedrich, J. Karger-Kocsis and Lu, Z.: "Effects of Steel Counterface Roughness and Temperature on Friction and Wear of PEEK-Composites under Dry Sliding Conditions," Wear, 148, 2, 1991, pp. 235-247

[19] K. Friedrich, Z. Lu and A. M. Häger: "Overview on Polymer Composites for Friction and Wear Application," Theoretical and Applied Fracture Mechanics, 19, 1, 1993, pp. 1-11

[20] L. C. Seabra, A. M. Baptista: Tribological Behaviour of Grade Polymers against Stainless Steel in Dry Sliding and with Sugar. Wear, 2002. Vol. 253 pp. 394-402

[21] L. Kátai, P.Gárdonyi, I. Szabó: Examination of Drive Misalignment and V-Belt Temperature Conditions, International journal of science, technics and innovations for the industry, 2015, Vol. 12, pp. 56-59

[22] L. Zsidai, G. Pistai, R. Keresztes: Abrasion testing of PA 6, POM and PET composites in small scale tribology model system, The 11th International Conference of The Carpathian Euro-Region Specialists in Industrial Systems CEurSIS 2016, 2-4 June, 2016, Baia Mare, Romania

[23] M Ando, J Sukumaran: Effect on Friction for Different Parameters in Roll-Slip of Polyamide-Steel Nonconformal Contacts, Tribology Transactions 2012. 55 (1) pp.109-116

[24] M. Kozma, G. Kalacska: Abrasive Wear of Polymers, in: Proceedings of the First Conference on Mechanical Engineering (Gepeszet'98), May 28-29, 1998, pp. 157-161

[25] N. Dyson, A. J. Kinloch, A. Okada: The Interlaminar Failure Behaviour of Carbon Fibre/Polyetheretherketone Composites. Composites 25, 1994. pp. 189-196

[26] P. Davies et al: Round-Robin Interlaminar Fracture Testing of Carbon-Fibre-reinforced Epoxy and PEEK Composites. Compos. Sci. Technol. 43, 1991, pp. 129-136

[27] Plint & Partners Ltd.: Delivery Programme Edition. England: Newburry, Berkshire, RG20 6NB, 2001

[28] Q. Wang, Q. Xue, H. Liu, W. Shen, J. Xu,: The Effect of Particle Size of Nanometer ZrO_2 on the Tribological Behaviour of PEEK, Wear 198 (1-2), 1996, pp. 216-219

[29] Q. Wang, Q. Xue, W. Shen: The Friction and Wear Properties of Nanometre SiO_2 filled Polyetheretherketone, Tribology International 30 (3), 1997. pp. 193-197

[30] W. Grellmann, S. Seidler: Polymer Testing, Carl Hanser Verlag, Münich, 2007

[31] W. Hufenbach, K. Kunze, J. Bijwe: Sliding Wear Behaviour of PEEK–PTFE blends, Journal of Synthetic Lubrication 20 (3), 2003. pp. 227-240

[32] W. I. Broughton: Shear. In: Hodgkinson, J.M. (Ed.): Mechanical Testing of Advanced Fibre Composites. Woodhead Publishing, Cambridge, 2000

[33] www.deerfos.com (28 .04. 2016) DEERFOS Products Information, 2008

[34] www.ensinger-online.com/modules/public/datapdf (28.4.2016)

[35] www.quattroplast.hu/files/file/B_kategoria.pdf (28.4.2016)

[36] X. Shao, Q.-J. Xue: Effect of Nanometer and Micrometer SiO(2) Particles on the Tribology Properties of Poly (phthalazine ether sulfone ketone) Composites, Materials and Mechanical Engineering (China) 28 (6), 2004, pp. 39-42

[37] Y. Yamaguchi: Tribology of Plastic Materials, Tribology Series 16, Elsevier, Amsterdam, 1990

[38] Z. Lu, K. Friedrich: High Temperature Polymer Composites for Applications as Sliding Elements, Materialwiss. Werkst. 28, 1997, pp. 116-123

[39] Z. P. Lu, K. Friedrich: On Sliding Friction and Wear of Peek and its Composites, Wear 181-183 (2), 1995, pp. 624-631

Continuous Periodic Fuzzy-Logic Systems and Smooth Trajectory Planning for Multi-Rotor Dynamic Modeling

Attila Nemes

Óbuda University, Doctoral School of Safety and Security Sciences
Bécsi út 96/b, H-1034 Budapest, Hungary
nemesa@stud.uni-obuda.hu

Abstract: Multi-rotors are popular unmanned aerial vehicles (UAVs) of versatile applicability. This paper presents a novel grey-box fuzzy-system identification method for multi-rotor UAV dynamic modelling by continuous, periodic, fuzzy-partitions based systems. The method is initiated by a linear, continuous, periodical transformation of fuzzy-system input data and a special parameterization of the antecedent part of fuzzy-systems that result in circularly connected fuzzy-partitions for antecedents. Fuzzy-rule consequents are designed so that the system output is continuous for the full input space of the naturally periodic angular orientation over the complete [0, 2π) interval, including the 2π-0 transition at complete rotations. The antecedent parameter representation method of fuzzy-rules ensures upholding of predefined linguistic value ordering and ensures that fuzzy-partitions remain intact throughout an unconstrained hybrid evolutionary and gradient descent based optimization process. The dynamic model is based on the Euler-Lagrange equations structure. State variables and their derivatives remain explicit, while their non-linear inertia multipliers are identified with fuzzy-systems. Christoffel symbols, partial derivatives of fuzzy-systems are used for Coriolis effects, gyroscopic and centrifugal terms modelling. Linear parameters of the model are evaluated by SVD-based least squares method. Non-linear parameters are subjected to a global multi-objective evolutionary optimization scheme and fine-tuned by gradient descent based local search. The training data is collected along specially designed trajectory of smooth high order derivatives.

Keywords: multi-rotor UAV; grey-box dynamic model; continuous periodic fuzzy-partition system; optimal smooth trajectory; hybrid multi-objective genetic algorithm

1 Introduction

Multi-rotors like quad- and hexa-rotors are popular representatives of unmanned aerial vehicles (UAVs) as they are relatively simple to build and easy to control, while being of versatile applicability, capable of vertical take-off and landing. Also, the multi-rotor architecture has simple mechanics, high relative payload capability and good maneuverability. The study of multi-rotor kinematics and

dynamics is based on the physics of aerial platforms - flying bodies, a good description can be found in [1]. The kinematics and general force and torque dynamics of any symmetric multi-rotor (quad-, hexa- or any other number of rotors) is equivalent.

High speed aerial platforms in open door environments are highly nonlinear systems subject to many nonlinear perturbations like (1) drag like effects: blade flapping, induced drag, translational drag, profile drag and parasitic drag, (2) ground effect, (3) in vertical descent: (i) vortex ring state, (ii) turbulent wake state, (iii) windmill brake state as described in [2]. Precision, robustness and adaptability of the applied dynamic model is the starting point to achieve precise and efficient autonomous control of the system [3].

Mathematical model design of complex real systems can readily take the so-called black-box common approach, which uses exclusively numerical system input-output data pairs for constructing the model. Without deeper understanding of the problem, these black box models can easily end up being clumsy and working only in some specific setups, without any guaranties for general precision or robustness. In contrast, to black-box there is white box (also called glass box or clear box) modelling, which uses extensive, state of the art physics and mathematics analysis, presuming to know all necessary information; still just to end up with only simplified models, as real complex nonlinear systems can in the end be only approximated. Grey-box modelling builds on both input-output data and also on essential expert knowledge; it efficiently incorporates them into the model structure used for system identification. Fuzzy-system modelling can be conducted as black-box modelling where all the system knowledge is mere input-output data. However, when expert knowledge is readily available, we should take advantage of it – fuzzy-grey-box modelling is a rational choice.

Angular orientations and induced torques for flying body systems are naturally continuous and periodic. It is our $[0, 2\pi)$ orientation representation that results in a discontinuity at full turn when returning to the origin. A proper dynamic model, be it fuzzy-system based or not, must not have a jump in the output when the input continuously changes between any two orientation angles. One possible solution is to transform the intuitive 3D Euler angles to quaternions, and perform the entire math in this transformed space. Quaternion solutions may be called elegant, by whoever likes them, but are surely not simple and intuitive. For a proper soft computing approach to flying body modeling new tools have to be designed.

2 Multi-Rotor Dynamic Model

The complete dynamics of an aircraft, taking into account aero-elastic effects, flexibility of wings, internal dynamics of engines, and the whole set of changing environmental variables is quite complex and somewhat unmanageable for the purpose of autonomous control engineering [7].

Multi-rotor UAV maneuvers are controlled by angular speeds of its motors. Each motor produces a thrust and a torque, whose combination generates the main trust, the yaw torque, the pitch torque, and the roll torque acting on the multi-rotor. Motors produce a force proportional to the square of the angular speed and the angular acceleration of the rotor; the acceleration term is commonly neglected as the speed transients are short thus exerting no significant effects. Motors of a multi-rotor can only turn in a fixed direction, so the produced force can be always presumed positive. Motors are set up so that opposites form pairs rotating in the same direction (clockwise/counter-clockwise), while their neighboring motors are rotating in the opposite direction (counter-clockwise/clockwise). This arrangement is chosen so that gyroscopic effects and aerodynamic torques are canceled in trimmed flight. The main trust is the sum of individual trusts of each motor. The pitch torque is a function of difference in forces produced on one pair of motors, while the roll torque is a function of difference in forces produced on the other pair of motors. The yaw torque is sum of all motor reaction torques due to shaft acceleration and blades drag. The motor torque is opposed by a general aerodynamic drag.

For a full dynamic model of a multi-rotor system both (i) the center of mass position vector of $\boldsymbol{\xi} = (x, y, z)$ in fixed frame coordinates and (ii) the orientation Euler angles: roll, pitch, yaw angles *(ϕ,θ,ψ)* around body axes *X, Y, Z* are considered. Using the Euler-Lagrange approach it can be shown how the translational forces $\boldsymbol{F}_{\xi}$, applied to the rotorcraft due to main trust, can be fully decoupled from the yaw, pitch and roll torques $\boldsymbol{\tau}$ as defined by equations (1-2).

$$m \cdot (\ddot{\boldsymbol{\xi}} + g \cdot [0\ 0\ 1]^T) = \boldsymbol{F}_{\xi} \tag{1}$$

where m is the multi-rotor mass and g is the gravitational constant, which is acting only along the third axes *z*.

$$\mathbb{J}(\boldsymbol{q}) \cdot \ddot{\boldsymbol{q}} + \mathbb{C}(\boldsymbol{q}, \dot{\boldsymbol{q}}) \cdot \dot{\boldsymbol{q}} = \boldsymbol{\tau} \tag{2}$$

where $\mathbb{J}$ is a 3x3 matrix, called the inertia matrix, $\mathbb{C}$ is also a 3x3 matrix that refers to Coriolis, gyroscopic and centrifugal terms, $\boldsymbol{q} = [\phi, \theta, \psi]$ is the state vector of Euler angles, its time derivatives are $d\boldsymbol{q}/dt = \dot{\boldsymbol{q}} = [\dot{\phi}, \dot{\theta}, \dot{\psi}]$ and $d\dot{\boldsymbol{q}}/dt = \ddot{\boldsymbol{q}} = [\ddot{\phi}, \ddot{\theta}, \ddot{\psi}]$. For the scope of this paper we shall address only equation (2) as the nonlinear complex part of the multi-rotor dynamic model to be identified.

Equation (2) can be analyzed as three resultant torques τ_i acting along the [ϕ, θ, ψ] axes for $i,j,k \in (\phi, \theta, \psi)$ as:

$$\sum_j (D_{ij}(\boldsymbol{q}) \cdot \ddot{q}_j) + \sum_j \sum_k \left(\dot{q}_j \cdot D_{ijk}(\boldsymbol{q}) \cdot \dot{q}_k\right) = \tau_i \tag{3}$$

The first component of equation (3) is the inertia matrix part expansion, the second is the Coriolis matrix term expansion, whose components are highly nonlinear functions containing $sin(\boldsymbol{q})$ and $cos(\boldsymbol{q})$ components, and also their products and sums defined by the rigid body system geometry as described in [8].

There are general relations that can be used for reducing the number of unknown inertia and Coriolis components: $\mathbb{J}$ is symmetric and $\mathbb{C}$ is defined by Christoffel-symbols of $\mathbb{J}$:

$$D_{ijk} = (\partial D_{ij}/\partial q_k + \partial D_{ik}/\partial q_j - \partial D_{jk}/\partial q_i)/2 \tag{4}$$

These properties results in further inherent relations as:

$$D_{ij} = D_{ji}, D_{ijk} = D_{ikj}, D_{kij} = -D_{jik}, D_{kjk} = 0,\ \forall i,k \geq j \tag{5}$$

It should be noted that direct measurement of any single D_{ijk} or D_{ij} component of equation (3) is not possible. Measurable data vector pairs are $[\ddot{\boldsymbol{q}}, \boldsymbol{\tau}]$ angular accelerations as system input and resultant torques proportional to rotation speed of motors as system output. Determining all D_{ijk} and D_{ij} non-linear functions is a considerable grey-box identification problem, but when achieved the model is usable in efficient robust and precise model based control implementations, as this model preserves all $\ddot{\boldsymbol{q}}, \dot{\boldsymbol{q}}$ in an explicit form.

3 Fuzzy-Logic Systems for Dynamic Modeling

Takagi-Sugeno-Kang (TSK) type Fuzzy-logic systems (FLSs) having *n* inputs and *1* output are defined in [9] as:

$$f(\boldsymbol{q}) = \sum_{l=1}^{M} \omega_l(\boldsymbol{q}) \cdot y_l(\boldsymbol{q}) \Big/ \sum_{l=1}^{M} \omega_l(\boldsymbol{q}) \tag{6}$$

where M is the number of rules, $\boldsymbol{q}$ is the vector of n input variables, y_l is the consequence, a scalar function of n input variables, defined by $(n+1)$ parameters c_{jl} as in equation (7) and ω_l is the antecedent, the premise part of a fuzzy-rule defined by $\mu_{F_l i}$ membership functions (MFs) of the i^{th} input variable in the l^{th} rule that defines the linguistic value MF_{li} as:

$$\omega_l(\boldsymbol{q}) = \prod_{i=1}^{n} \mu_{MF_l i}(q_i),\ y_l(\boldsymbol{q}) = \sum_{j=1}^{n} c_{jl} \cdot q_j + c_{0l} \tag{7}$$

Zadeh-formed MFs are μ_z, μ_s, μ_π the *z*-, the *s*-, and the π-functions, named after their shape, defined respectively with four parameters ($b_1 \leq b_2 \leq b_3 \leq b_4$) as:

$$\begin{aligned}
\mu_z(q, b_1, b_2) &= \begin{cases} 1 & q \leq b_1 \\ 1 - 2(q - b_1)/(b_2 - b_1) & b_1 < q \leq (b_2 - b_1)/2 \\ 2(q - b_1)/(b_2 - b_1) & (b_2 - b_1)/2 < q \leq b_2 \\ 0 & q > b_2 \end{cases} \\
\mu_s(q, b_1, b_2) &= 1 - \mu_z(q, b_1, b_2) \\
\mu_\pi(q, b_1, b_2, b_3, b_4) &= \begin{cases} \mu_s(q, b_1, b_2) & q \leq b_2 \\ 1 & b_2 < q \leq b_3 \\ \mu_z(q, b_3, b_4) & q > b_3 \end{cases}
\end{aligned} \tag{8}$$

A fuzzy-partition is a set of K μ_k MFs with $\boldsymbol{b}_k$ parameters, such that $\sum_{k=1}^{K} \mu_k(q, \boldsymbol{b}_k) = 1, \ \forall q$. Using fuzzy-partitions for antecedent membership functions of fuzzy-systems ensures that there cannot be a numerical input within the defined input range that will not result in firing at least one rule consequent of the fuzzy-model, which means that there is a defined output for all possible input states. Keeping specific properties of fuzzy-partitions imposes a set of hard constraints on membership function parameters as detailed in [11], but as a result the TSK model structure of equation (6) simplifies to:

$$f(\boldsymbol{q}) = \sum_{l=1}^{M} \omega_l(\boldsymbol{q}) \cdot y_l(\boldsymbol{q}) \tag{9}$$

Automatic fine tuning FLS parameters that satisfies all of above listed constraints is a significant problem. In [11] a Zadeh-formed MFs parametrization method is introduced that preserves all fuzzy-partition properties, and still simplifies $\boldsymbol{b}_k$ parameter tuning of equation (9) to an unconstrained optimization problem, where even gradient descent based optimization can be applied to.

As proposed in [11] fuzzy-partitions are formed from Zadeh-typed MFs by making equal the last two parameters of each preceding MF to the first two parameters of the succeeding MF: ($b_{k+1,1} = b_{k,3}, b_{k+1,2} = b_{k,4}$). The input space is normalized: (*min(q) =0, max(q)=1*). Plateaus are not allowed, so for every MF there will be only a single q input value for which the degree of membership will be 1: ($b_{k,2} = b_{k,3}, b_{1,1} = 0, b_{K,4} = 1$). The number of constrained variable b_i fuzzy-partition parameters is reduced to *(K-2)* for a fuzzy-partition of K Zadeh-formed MFs: ($b_0 = 0 < b_1 < b_2 < \cdots < b_{K-2} < b_{K-1} = 1$). As proposed in [11] for an unconstrained optimization of these b_i parameters, we use *(K-1)* pieces of rational, positive or zero parameters $a_i \in \mathbb{R}_0^+, i = 1,2, \dots, (K-1)$ like:

$$b_k = {\sum_{i=1}^{k} a_i} \Big/ {\sum_{j=1}^{K-1} a_j}, k = 1,2, \dots, K-2 \tag{10}$$

The result is a minimal number of independent $a_i \in \mathbb{R}_0^+$ nonlinear parameters, which fully define any fuzzy-partition of Zadeh-formed MFs. This is a very important result for optimization as over parameterized, constrained systems are hard to optimize. Substituting (10) to (8) then (9) we have obtained FLSs, which are capable of universal function approximation, they have a continuous output defined for the complete input space. Moreover, the number of its nonlinear parameters is minimal, and can be optimized without constraints; also, its linear parameters can be optimally calculated with an SVD-based least squares method. To avoid traps of local optimal solutions when looking for the a_i nonlinear parameters, a preliminary global search should be applied before fine tuning with a gradient descent method, as presented in [11].

4 Continuous Periodic Fuzzy-Logic Systems

The proposal of this paper is to transform equation (9) to form a continuous periodic FLS (cpFLS). Such cpFLSs are ready to be used for modeling systems which are inherently continuous and periodic, for example the orientation angle input based torque function of a multi-rotor dynamics in equation (2).

For physical systems in the Euclidian space orientation angles are naturally defined on the [0, 2π) interval. Any angular value α below *0* or above 2π is equivalent to a value $\beta=\alpha\pm 2k\pi$, where k is such an ordinary number that $\beta\in[0,2\pi)$. For orientation angles selection of the origin is arbitrary and transition between two orientation angles is smooth and continuous, without any jumps. As orientation angle of 2π is equivalent to angle 0 the transition from 2π-ε to 0+ε also has to be continuous.

For FLSs defined by equation (9) we can make the input space continuous and periodic over the *[0, 2π)* interval by applying a simple piecewise linear "seesaw" function transformation, whose output is in [-1,1] as defined by:

$$\hat{q} = \begin{cases} 2 * (\pi - q)/\pi, & 3 * \pi/2 < q > \pi/2 \\ 2 * (q - \pi)/\pi, & q > 3 * \pi/2 \\ 2 * (q)/\pi, & else \end{cases} \tag{11}$$

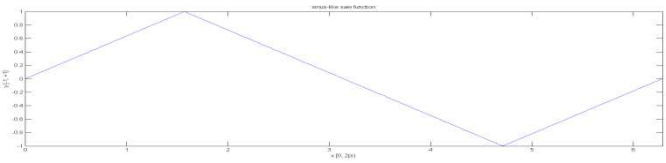

Figure 1
The piecewise linear "seesaw" function

With transformation (11) of the cpFLS input space we make sure that there is no discontinuity between angular cpFLS inputs of any two values, we simply force critical 2π-ε input values to become equal to $0+\varepsilon$ for all $\varepsilon < \pi/2$. This step is needed to ensure the output space $y_l(\boldsymbol{q})$ consequence part can become continuous over the $\boldsymbol{q} \in [0, 2\pi)$ input space even for full circle rotations. We also have to make the antecedent fuzzy-partition "circular" by combining the first μ_z and the last μ_s MF of the partition as defined in equation (8) into a single virtual μ_π MF to be substituted into equation (7), so that fuzzy-rules applied to the first z-MF equally apply to the last s-MF. We achieve this by making all the linear parameters of the last rule for each fuzzy-partition in equation (7) equivalent to the first rule of the same partition as $c_{jK_i} = c_{jK_1}$, where n is the number of cpFLS inputs, and each input is covered by a fuzzy partition of K_i MFs for $i=1..n$. By this procedure we have ensured to have a continuous periodic fuzzy-system (cpFLS) such that for $\forall \boldsymbol{q} \in \mathbb{R}^n, \forall k \in \mathbb{Z}$ and any arbitrary small $\boldsymbol{\varepsilon}$ there is a similarly small $\mu(\boldsymbol{\varepsilon})$ for which we have:

$$cpFLS(\boldsymbol{q} \pm 2k\pi) = cpFLS(\boldsymbol{q}),\ cpFLS(\boldsymbol{q} \pm \boldsymbol{\varepsilon}) = cpFLS(\boldsymbol{q}) \pm \mu(\boldsymbol{\varepsilon}) \quad (12)$$

Table 1 presents the linear parameter triplets for all 25 fuzzy-rule consequents $\boldsymbol{c_l} = (c_{0l}c_{1l}c_{2l})$, of equation (7) for a TSK FLS interpretation of a cpFLS with *n=2* inputs, where each antecedent is a Zadeh-formed fuzzy-partition of 5 MFs.

Table 1

TSK FLS interpretation of cpFLS linear parameter triplets for forming fuzzy-rule consequent

	μ_{z11}	$\mu_{\pi12}$	$\mu_{\pi13}$	$\mu_{\pi14}$	μ_{s15}
μ_{z21}	$\boldsymbol{c_1}$	$\boldsymbol{c_2}$	$\boldsymbol{c_3}$	$\boldsymbol{c_4}$	$\boldsymbol{c_1}$
$\mu_{\pi22}$	$\boldsymbol{c_5}$	$\boldsymbol{c_6}$	$\boldsymbol{c_7}$	$\boldsymbol{c_8}$	$\boldsymbol{c_5}$
$\mu_{\pi23}$	$\boldsymbol{c_9}$	$\boldsymbol{c_{10}}$	$\boldsymbol{c_{11}}$	$\boldsymbol{c_{12}}$	$\boldsymbol{c_9}$
$\mu_{\pi24}$	$\boldsymbol{c_{13}}$	$\boldsymbol{c_{14}}$	$\boldsymbol{c_{15}}$	$\boldsymbol{c_{16}}$	$\boldsymbol{c_{13}}$
μ_{s25}	$\boldsymbol{c_1}$	$\boldsymbol{c_2}$	$\boldsymbol{c_3}$	$\boldsymbol{c_4}$	$\boldsymbol{c_1}$

In the compact cpFLS interpretation form of the same fuzzy-system as in Table 1, we have to consider only linear parameter triplets for 16 unique fuzzy-rule consequents as presented in Table 2, where $\mu_{\pi ji}$ for *i>0* are equivalent to Table 1 MFs of the same index, and $\mu_{\pi j0}(q) = \mu_{zj1}(q) + \mu_{sj5}(q)$ for *j=1,2*. Triplets $\boldsymbol{c_l}$ in Table 2 are equivalent to triplets of matching index from Table 1.

Table 2

The compact cpFLS interpretation of the same fuzzy-system with $\mu_{\pi j0}(q) = \mu_{zj1}(q) + \mu_{sj5}(q)$

	$\mu_{\pi10}$	$\mu_{\pi12}$	$\mu_{\pi13}$	$\mu_{\pi14}$
$\mu_{\pi20}$	$\boldsymbol{c_1}$	$\boldsymbol{c_2}$	$\boldsymbol{c_3}$	$\boldsymbol{c_4}$
$\mu_{\pi22}$	$\boldsymbol{c_5}$	$\boldsymbol{c_6}$	$\boldsymbol{c_7}$	$\boldsymbol{c_8}$
$\mu_{\pi23}$	$\boldsymbol{c_9}$	$\boldsymbol{c_{10}}$	$\boldsymbol{c_{11}}$	$\boldsymbol{c_{12}}$
$\mu_{\pi24}$	$\boldsymbol{c_{13}}$	$\boldsymbol{c_{14}}$	$\boldsymbol{c_{15}}$	$\boldsymbol{c_{16}}$

5 Multi-Rotor Dynamic Model by cpFLSs

As proposed in [13] we identify D_{ij} components of the dynamic model in equation (3) as FLSs defined by equations (7) to (10), where the FLS general input variable $\boldsymbol{q}$ will be substituted for appropriate state variables of *(ϕ, θ, ψ)*. Instead of simple TSK FLSs we will use cpFLSs as defined in Chapter 5. Where the D_{ij} inertia matrix components are modeled by cpFLSs, forming the D_{ijk} components as Christoffel symbols is to be expressed by partial derivatives of equation (9) like:

$$\partial f(\boldsymbol{q})/\partial q_i = \sum_{l=1}^{M} (\partial \omega_l(\boldsymbol{q})/\partial q_i \cdot y_l(\boldsymbol{q}) + \omega_l(\boldsymbol{q}) \cdot \partial y_l(\boldsymbol{q})/\partial q_i) \quad (13)$$

The unknown 4 inertia matrix components of torques defined in equation (2), which have to be identified for a 3DOF rigid body rotational motion model, are:

$$D_{13}(\theta) = f_1(\theta), D_{22}(\phi) = f_2(\phi), D_{23}(\phi,\theta) = f_3(\phi,\theta), D_{33}(\phi,\theta) = f_4(\phi,\theta) \quad (14)$$

Based on the multi-rotor system structure and inertia matrix symmetry the remaining inertia components are known to be:

$$D_{11} = I_{xx}, D_{12} = 0, D_{21} = D_{12}, D_{31} = D_{13}, D_{32} = D_{23} \tag{15}$$

where I_{xx} is the constant multi-rotor body inertia around the *x* axis.

Based on equation (5) the following Coriolis term matrix D_{ijk} components can be calculated by equations (13):

$$\begin{aligned} &D_{122} = -\frac{1}{2}\frac{\delta D_{22}}{\delta \phi}, D_{123} = \frac{1}{2}\left(\frac{\delta D_{13}}{\delta \theta} - \frac{\delta D_{23}}{\delta \phi}\right), D_{322} = \frac{\delta D_{23}}{\delta \theta} \\ &D_{133} = -\frac{1}{2}\frac{\delta D_{33}}{\delta \phi}, D_{223} = -\frac{1}{2}\frac{\delta D_{33}}{\delta \theta}, D_{312} = \frac{1}{2}\left(\frac{\delta D_{23}}{\delta \phi} + \frac{\delta D_{13}}{\delta \theta}\right) \end{aligned} \tag{16}$$

The remaining D_{ijk} components are trivial identities as defined in equation (5). This way we can model the complete multi-rotor rotation dynamics as defined in equation (2) by only 1 linear constant and 4 cpFLSs, where 2 cpFLSs are functions of a single input, and 2 are functions of 2 inputs. We have for these fuzzy-systems 6 Zadeh-type fuzzy-partitions. Each partition consists of 1 μ_z-, 1 μ_s-, and 3 μ_π-type MFs as presented by equations (8) and (10), such a fuzzy-partition is defined by 3 nonlinear a_i parameters; 6 partitions totaling in 24 nonlinear parameters. These 4 cpFLSs consist of 2 times 4 rules for single input functions an 2 times 16 rules y_l as defined in equation (7) for two input functions. Each rule consequent y_l is defined by 2 (single input case) or 3 (two inputs case) c_{il} linear parameters, these 4 cpFLSs total in 112 linear parameters. The grand total for our model is 24 nonlinear and 113 linear parameters.

Linear parameters are best directly evaluated by a singular value decomposition based least squares method. We first substitute equations (7,8,9,11) to (14,15,16) and all to (2), then we express all the 113 linear $\boldsymbol{c} = (c_{il})$ parameters as:

$$(\mathbb{J}^*(\boldsymbol{q}) \cdot \ddot{\boldsymbol{q}} + \mathbb{C}^*(\boldsymbol{q}, \dot{\boldsymbol{q}}) \cdot \dot{\boldsymbol{q}}) \cdot \boldsymbol{c} = \mathbb{Q}(\boldsymbol{q}, \dot{\boldsymbol{q}}, \ddot{\boldsymbol{q}}) \cdot \boldsymbol{c} = \boldsymbol{\tau} \tag{17}$$

For SVD decomposition of $\mathbb{Q}(\boldsymbol{q}, \dot{\boldsymbol{q}}, \ddot{\boldsymbol{q}}) = U \cdot S \cdot V^T$ we obtain $\boldsymbol{c} = V \cdot S^{-1} \cdot U^T \cdot \boldsymbol{\tau}$.

6 Multi-Objective Genetic Algorithms

A genetic algorithm (GA) is constructed on bases of imitating natural biological processes and Darwinian evolution. GAs are widely used as powerful global search and optimization tools [10]. Real life optimization problems often have multiple objectives. To establish ranking of chromosomes for GAs the comparison of two objective vectors is required. A general multi-objective optimization problem consists of *n* number of scalar minimization objectives where every scalar objective function $f_i(\boldsymbol{x})$, $i=1..n$ is to be minimized simultaneously, where $\boldsymbol{x}$ is the vector of parameters.

A vector $\boldsymbol{x_1}$ Pareto-dominates $\boldsymbol{x_2}$, when no scalar component of $\boldsymbol{x_2}$ is less than the appropriate component of $\boldsymbol{x_1}$, and at least one component of $\boldsymbol{x_1}$ is strictly smaller than the appropriate component of $\boldsymbol{x_2}$. Since no metrics can be assigned to Pareto-dominance, in general there have been two different approaches to define a GA ranking method, which can be used for Pareto-dominance vector comparison, which have been widely used: (1) "Block-type" ranking is defined in [5] as: *Rank is equal to 1 + (number of individuals that dominate the i^{th} individual)* (2) "Slice-type" ranking is defined in [4] as: *Rank is equal to 1 + (number of turns when the non-dominated individuals are eliminated, needed for the i^{th} individual to become non-dominated)*.

Quantity-dominance, a not widely used method was proposed in [6]. It is defined as: *vector $\boldsymbol{x_1}$=[x_{1i}] Quantity-dominates vector $\boldsymbol{x_2}$=[x_{2i}] if $\boldsymbol{x_1}$ has more such x_{1i} components, which are better than the corresponding x_{2i} component of vector $\boldsymbol{x_2}$, and $\boldsymbol{x_1}$ has less such x_{1j} components, which are worse than the corresponding x_{2j} of vector $\boldsymbol{x_2}$*. A metrics can be defined as: *the measurement of the extent of Quantity-dominance is the difference between the number of better and the number of worse components*. For a measurement based ranking method the Rank of the i^{th} objective vector can be simply defined as: *the sum of Quantity-dominance distance metrics for every individual measured from the i^{th} vector*. This direct, efficient ranking method can be readily applied with Quantity-dominance based comparison.

Testing and comparison of existing GA variants, and also a proposal of new methods is scientifically sound only when performed on a number of carefully selected benchmark problems, tests repeated multiple times for statistically relevant data analysis, as it was done in [6] when proposing a new vector comparison for a new multi-objective GA type. The Quantity-dominance vector comparison method provides more information when comparing two vectors, compared to the classic Pareto-based comparison, thus the GA is faster, more efficient in its search. The MMNGA algorithm described in [6] is computationally less expensive and more efficient compared to classical Pareto-methods. The achieved quality of non-dominated individuals, which was analyzed on a number of GA hard problems in [6] is at least as good as for classical Pareto based ranking method GAs.

7 Optimal Trajectories of Limited, Smooth Derivatives

The roll and pitch of a multi-rotor can be calculated from state variables (x,y,z) and ψ as presented in [1] like:

$$\phi = asin\left(\frac{\dot{x}sin\psi - \dot{y}cos\psi}{\ddot{x}^2+\ddot{y}^2+(\ddot{z}+g)^2}\right), \theta = atan\left(\frac{\dot{x}cos\psi - \dot{y}sin\psi}{(\ddot{z}+g)}\right) \quad (18)$$

To have realistic, feasible torques along a trajectory, which are efficiently controllable without chattering, we need smooth torque changes. Having $\boldsymbol{\tau} = \boldsymbol{\tau}(\boldsymbol{q}, \dot{\boldsymbol{q}}, \ddot{\boldsymbol{q}})$ and $\boldsymbol{q} = \boldsymbol{q}(\psi, \dot{\boldsymbol{r}}, \ddot{\boldsymbol{r}})$ for smooth torque changes, we need smooth changes of the so called displacement crackle $\boldsymbol{c}(t) = d^5\boldsymbol{r}/dt^5$, the fifth time derivative of displacement $\boldsymbol{r}(x, y, z)$. A smooth displacement crackle function can be defined with a continuous displacement pop function $\boldsymbol{p}(t) = d^6\boldsymbol{r}/dt^6$.

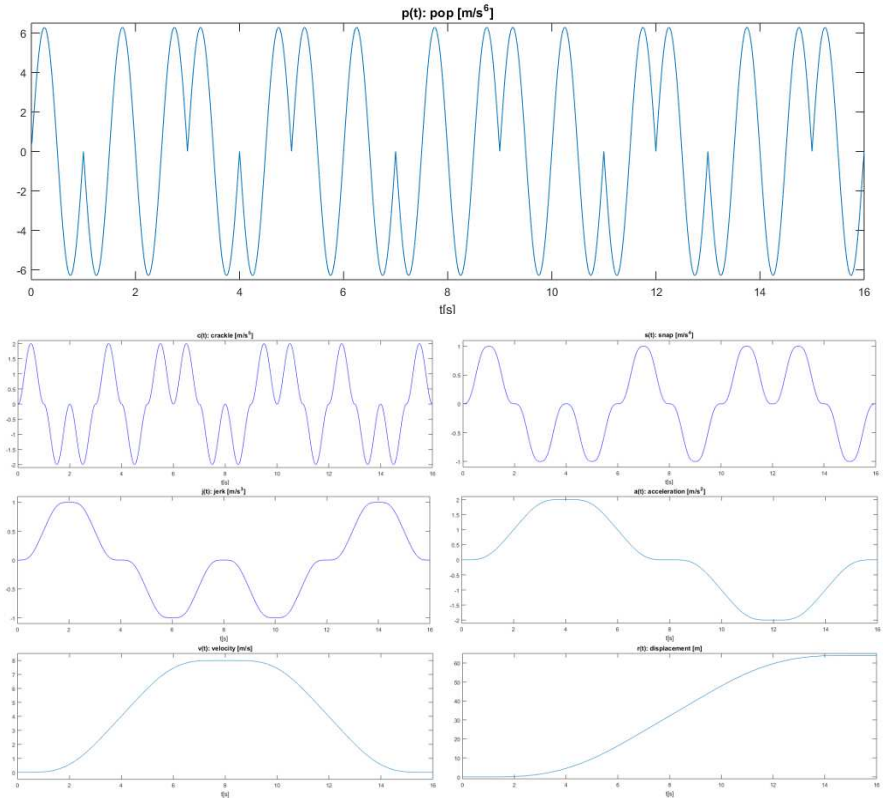

Figure 2

Trajectory pop *p(t)*, crackle *c(t)*, snap *s(t)*, jerk *j(t)*, acceleration *a(t)*, velocity *v(t)*, displacement *r(t)*

The proposal of this paper is to use a parameterised single sinus wave $\boldsymbol{p}(t) = \frac{2\pi}{P}\sin\left(\frac{2\pi}{P}t\right)$ as the base function for the displacement pop to reach the desired smooth crackle as $\boldsymbol{c}(t) = \int \boldsymbol{p}(t)dt = 1 - \cos\left(\frac{2\pi}{P}t\right)$. P is an arbitrary positive real value, which controls both the amplitude and the period of $\boldsymbol{p}(t)$, and by this the dynamics of the displacement. The integral of a full period $\boldsymbol{c}(t)$ for *t=1..P* is to be used for the ascending part of the jerk (jounce) function $\boldsymbol{j}^+(t) = \int \boldsymbol{c}(t)dt$, for simplicity we take 0 for the integral constant value. For $\boldsymbol{j}^-(t)$ descending part of jerk the **–c**(t) integral is taken. In case that the acceleration $\boldsymbol{a}(\boldsymbol{t}) = \int\left(\boldsymbol{j}^+(t) + \boldsymbol{j}^-(t+P)\right)dt$ does not reach the desired level, a constant $\boldsymbol{j_{max}}$ interval

is to be inserted between $\boldsymbol{j}^{+}$ and $\boldsymbol{j}^{-}$ intervals. The velocity is planned in an analogous manner, by integrating the rising acceleration and the falling deceleration interval, with optional inclusion of a constant acceleration interval to reach the desired maximum velocity without overshooting the reached acceleration limit. By keeping the velocity constant in the middle of the trajectory we ensure reaching the desired displacement without exceeding the speed limit.

Such a general basic 16 intervals smooth sinusoid pop function trajectory setup with $P=1$, and all its corresponding displacement derivatives are presented in Figure 2.

8 Training Data Set Reduction

By definition the condition number of a parameter data set, which defines a linear system of equations, is the ratio of its first, the highest and last, the smallest singular value. A very well-conditioned linear system of equations has a condition number of 10 to 20. The higher the condition number, the more uncertain the solution is, the more sensitive the solution is to small disturbances of system parameters.

When identifying a system, we have to design a sufficiently exciting trajectory, which will properly expose all singular values of the (linear) system. For a stable equation solution for linear parameters it is needed to have all singular values higher than one. For solving a linear system of equations it is recommended to use an SVD based decomposition method before calculating the inverse matrix as for equation (17), but calculating SVD decomposition for large matrices is very processor and memory demanding task, which increases exponentially with the data set size.

Data samples collected along sufficiently exciting trajectories tend to be oversized, thus redundant. In [13] it is shown for a robotic manipulator dynamic model identification, that by using only a reduced number of training data points the same quality of system identification can be reached as with the full set, given that the reduced set is representative enough of the full set, which is equivalent to having a similarly low condition number.

The proposal of this paper is to apply the following algorithm to determine an arbitrary quality / size balanced training data set for FLS based dynamic model identifications. The algorithm is:

0) start from the full trajectory data set:

   a) evaluate antecedents by equation (7), (8) and (10) using a uniform, equidistant fuzzy partition defined with $a_i=i/4$, $i=1,2,3$ for equation (10);

b) prepare evaluation of linear c_{ij} parameters, by substituting all nonlinear $\mathbb{Q}(\boldsymbol{q}, \dot{\boldsymbol{q}}, \ddot{\boldsymbol{q}})$ components of equation (17);

c) perform the SVD decomposition of $\mathbb{Q}(\boldsymbol{q}, \dot{\boldsymbol{q}}, \ddot{\boldsymbol{q}}) = \boldsymbol{U} \cdot \boldsymbol{S} \cdot \boldsymbol{V}^T$ and calculate $\boldsymbol{c} = \boldsymbol{V} \cdot \boldsymbol{S}^{-1} \cdot \boldsymbol{U}^T \cdot \boldsymbol{\tau}$;

d) calculate the reference condition number of the full set as:

$$cond(\mathbb{Q}_{full}(\boldsymbol{q}, \dot{\boldsymbol{q}}, \ddot{\boldsymbol{q}})) = max(diag(\boldsymbol{S}_{full})/min(diag(\boldsymbol{S}_{full})) \quad (19)$$

1) select the i^{th} trajectory point input data $\mathbb{Q}_i(\boldsymbol{q_i}, \dot{\boldsymbol{q}}_{\boldsymbol{i}}, \ddot{\boldsymbol{q}}_{\boldsymbol{i}})$ from the *FullTrainingSet*, which increases the $min(diag(\boldsymbol{S}_{red+i}))$ value of the reduced $[\mathbb{Q}_{red}(\boldsymbol{q}, \dot{\boldsymbol{q}}, \ddot{\boldsymbol{q}}) \cup \mathbb{Q}_i(\boldsymbol{q_i}, \dot{\boldsymbol{q}}_{\boldsymbol{i}}, \ddot{\boldsymbol{q}}_{\boldsymbol{i}})]$ the most, if no such point exists, then select the one that increases the $max(diag(\boldsymbol{S}_{red+i}))$ value of reduced set the most;

2) remove the selected i^{th} trajectory point from the *FullTrainingSet* and add it to the *ReducedTrainingSet*;

3) repeat steps 1 and 2, while the condition number of the *ReducedTrainingSet* is above the target value, and there remains any selectable points in the *FullTrainingSet* or the targeted maximum size of *ReducedTrainingSet* is not reached.

The target condition number of the *ReducedTrainingSet* cannot be set to lower than the reference condition number of the full *FullTrainingSet* data set. The target training data set size cannot be set to lower than the number of c_{ij} linear parameters of the system, as $\mathbb{Q}_{red}(\boldsymbol{q}, \dot{\boldsymbol{q}}, \ddot{\boldsymbol{q}})$ must not be rank deficient.

9 Simulation Setup

The proposed method is tested for a multi-rotor system simulation from [1] with parameters as in Table 3.

Table 3
Quad-rotor system dynamic parameters

parameter	value	unit
gravity constant, g	9.81	m/s2
mass, m	6	kg
torque lever, l	0.3	m
trust factor, k	121.5e-6	
drag factor, b	2.7e-6	
body inertia along axes X, I_{XX}	0.6	kgm2
body inertia along axes Y, I_{YY}	0.6	kgm2
body inertia along axes Z, I_{ZZ}	1.2	kgm2
simulation time, T	55	s

The training data set is collected from a simulation along a trajectory with defined sinusoid pop for (x,y,z) and ψ defined so that position changes simultaneously along a cube main diagonal, while performing a full circle rotation in jaw motion. Roll ϕ and pitch θ is calculated by equation (18). For the cpFLSs input variables ϕ and θ are converted to $[0, 2\pi)$ by eliminating unnecessary $2k\pi$ extensions, then transformed by the "seesaw" function of equation (11) and finally normalized to the $[0, 1]$ closed interval for cpFLS inputs.

Calculated roll and pitch motions are as presented in Figure 3. The simulated resultant torque training data set is presented in Figure 4.

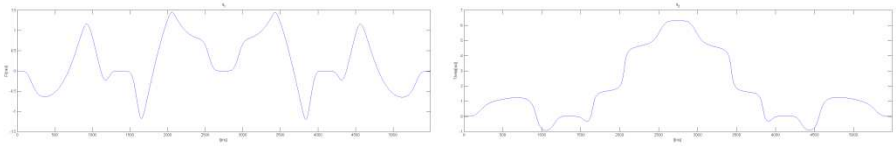

Figure 3
Smooth roll and pitch motions

The list of non-linear cpFLS parameters consists of six times four integer parameters for defining six fuzzy-partitions having five MFs each, where each partition consists of three classical π-type MFs and for the cpFLS setup one virtual π-type MF composed by one z-type MF at the beginning of the input interval and one s-type MF in the end of the input interval as in equation (8). These six fuzzy-partitions serve as antecedents for the four fuzzy-systems like in equation (9) and (12), used for identifying D_{ij}, ij=(*13, 22, 23, 33*) as defined in equations (3)-(5) and (14)-(16).

The unknown linear parameter D_{11} of the multi-rotor model as in equation (15), together with 112 linear parameters of the four TSK FLSs (2 FLSs with 5 MFs on one input, each rule with 2 *c* parameters, plus 2 FLSs with 5 MFs on both of the 2 inputs, each rule with 3 *c* parameters) of equations (7) substituted to (9) and (13) are determined by the SVD-based LS method as in equation (17).

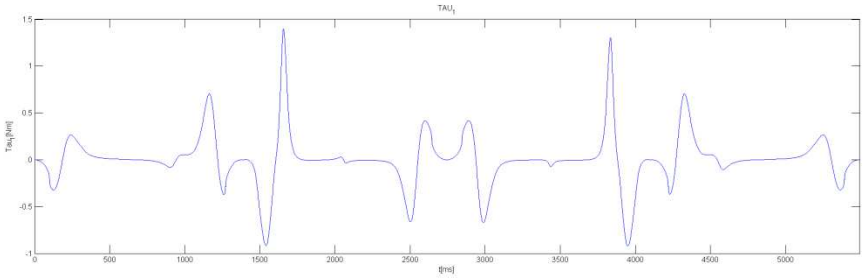

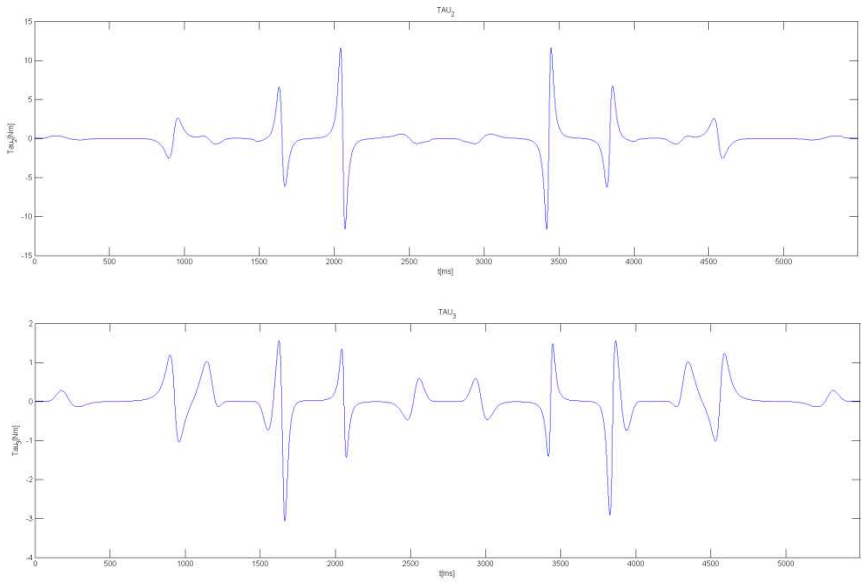

Figure 4
Smooth resultant torques

Concluded from equation (8),(10) six fuzzy-partitions (antecedent part of 2 FLSs with 1 input, plus 2 FLSs with 2 inputs are covered by 6 independent fuzzy-partitions) are represented by a vector of six times four parameters, which are optimized by a multi-objective hybrid genetic algorithm as detailed in [14]. Chromosomes are evaluated and subjected to a local gradient based search. Chromosome values are updated with the result of fine-tuning after each evaluation, so the GA does not waste time on local optimization; only global search capabilities of the GA are utilized.

The GA is set to work on a population of 200 chromosomes, divided into 5 subpopulations, with migration rate 0.2 taking place after each 5 completed generations. Chromosomes are comprised of 24 Gray-coded integers, each consisting of 16 bits. The initial population is set up in a completely random manner. Crossover rate, generation gap and insertion rate is set to 0.8, selection pressure is 1.5. In each generation 4% of individuals are subject to mutation, when 1% of the binary genotype is mutated.

Matrix of the linear equation $\mathbb{Q}(\boldsymbol{q}, \dot{\boldsymbol{q}}, \ddot{\boldsymbol{q}})$ from equation (17) is pre-processed, as FLSs like equation (9) and their partial derivatives like equation (13) are substituted as defined by equations (14)-(16). Unknown linear parameters are D_{11} and the 112 $\boldsymbol{c}$ parameters of fuzzy-rule consequents.

Evaluation of each individual is conducted as follows:

(a) Convert coded a_i values from the chromosome to b_k by equation (10).

(b) Evaluate all MFs, and antecedents which will comprise six fuzzy-partitions from each of six b_k quadruplets by equations (7) and (8). Also, evaluate antecedent derivatives of equation (13).

(c) Calculated the matrix coefficients of linear equations $\mathbb{Q}(\boldsymbol{q}, \dot{\boldsymbol{q}}, \ddot{\boldsymbol{q}})$ by values of triggered MFs and their partial derivatives.

(d) Linear components [D_{11}, $\boldsymbol{c}$] of equations (9) and (13) are calculated by SVD decomposition as in (17).

(e) Fine-tune a_i parameters, for example by the Matlab "lsqnonlin" function, while re-calculating steps (a)-(d) for each a_i tuning iteration.

(g) Re-insert optimized a_i parameters into the evaluated chromosome.

For the multi-objective rank assignment described in [6], the objective vector is created from:

(i) the mean square of the identified torque error,

(ii) the maximum absolute torque identification error and

(iii) the condition number of the matrix of the linear equation.

Stochastic universal sampling is used for selecting the next generation without explicit elitism. To speed up the GA processing, a database of evaluated chromosomes and their objective vectors is created, so only unique new individuals are evaluated in each generation.

10 Results

Results of this paper are: (i) a new fuzzy-logic system identification method is defined and validated on an example for a multi-rotor UAV torque dynamic model identification, typical torque identification error is <10%, presented in Figure 7; (ii) a new bounded, smooth, energy efficient and time optimal trajectory design method is defined and validated on an example for a multi-rotor UAV path planning, a single parameter controls the trajectory dynamics, as presented in Figure 2; (iii) a new training data set reduction algorithm is defined and validated, less than 20% of data points give more than 80% of contribution to the system condition number, a typical rate of condition number change for the most significant 25% of data points is presented in Figure 5.

The basic smooth trajectory parametrization curve used is with P=1, with dt=0.01[s] sampling time, which results in a time optimal trajectory with dynamic boundaries of maximum sinus pop=2π [m/s^6] wave of 1[s] period, maximum crackle=2[m/s^5], maximum snap=1[m/s^4], maximum jerk=1[m/s^3], maximum acceleration=2[m/s^2], maximum velocity=8[m/s], displacement=64[m], within

time=16[sec]. The integral of absolute jerk is 8[m/s^2], what is proportional to the expended energy (as mass and desired displacement we consider to be constant). This base trajectory curve is projected to the training path, which results in training data worth of ~55 seconds of flight time.

For uniformly distributed MFs in the fuzzy-partition of antecedents the $cond(\mathbb{Q}_{full}(\boldsymbol{q}, \dot{\boldsymbol{q}}, \ddot{\boldsymbol{q}}))$ condition number (Cond) of the *FullTrainingSet* and $cond(\mathbb{Q}_{red}(\boldsymbol{q}, \dot{\boldsymbol{q}}, \ddot{\boldsymbol{q}}))$ for the *ReducedTrainingSet* is in Table 4; the condition number change for the first 1170 points out of the total set of 5487 points is presented in Figure 3.

Table 4

Condition number change with changing the size of the reduced trading data set

	Full set	reduced to	reduced to	reduced to
training points	5487	2743	1170	685
% reduction to	100%	50%	25%	12.5%
Cond	56254	56805	59771	68934
% increase by	0%	+0.98%	+6.25%	+22.54%

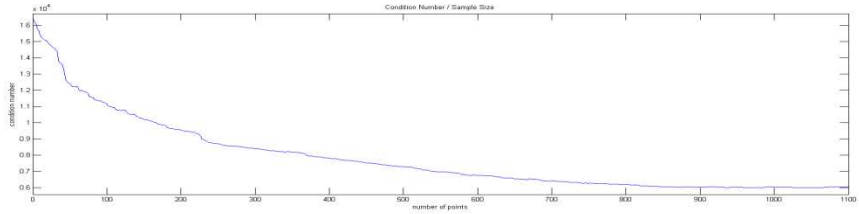

Figure 5

Condition number changes for the set reduction of 1170 points

Convergence of applied multi objective GAs of population size (Population#) 200, (or 75) is achieved in <200, (or <25) generation evaluations (Generation#), when the typical mean square error (MSE) is <1e-3, the typical maximum torque error (maxE) is <0.2 Nm, which means that the typical relative error is <10%. For fuzzy-partitions defined by non-dominated chromosomes the typical condition number (Cond) of $\mathbb{Q}(\boldsymbol{q}, \dot{\boldsymbol{q}}, \ddot{\boldsymbol{q}})$ the matrix of linear equations is ~4-5000. Averages of 10 simulations for each training data set size are presented in Table 5. For comparison to the new cpFLS model quality results of a simple FLS model, described in [14] are also presented. Results of a selected non dominated model are followed by the average values and the variance of 10 runs of each method and parametrization, as defined in the first 4 rows.

There is neither significant quality, nor identification performance degradation when using the new cpFLS compared to the simple FLS method described in [14]. While the most significant benefit of smooth output transitions for $(2k\pi-\varepsilon) - (0+\varepsilon)$ input space changes of continuous periodic FLSs cannot be achieved by a simple TSK FLS.

In average there is no significant difference in the identification quality for any of the reduced or the full data set. The only real, significant difference is the time required for evaluation, which is proportional to the increased speed of singular value decompositions of different sized samples. The 685 point sample set reduced to $1/8^{th}$ of the full set is significantly faster evaluated than any other larger set.

Further on the proposed GA setup method is robust enough to compensate for a significant reduction of the GA size parameters as well. The identification result is still very good when reducing the population size to 75 and generations evaluated to 25, which results in a (500*200)/ (75*25)≈5000% fold GA execution time gain.

Table 5
maximum error, means square error and condition number results of identification

FLS type	FLS[14]	cpFLS	cpFLS	cpFLS	cpFLS	cpFLS
Training points	5487	5487	2743	1170	685	685
Population #	500	500	500	500	500	75
Generation #	200	200	200	200	200	25
MSE selected	0,0007	0,0008	0,0009	0,0009	0,0008	0,0008
maxE selected	0,1531	0,1771	0,1786	0,1648	0,1952	0,2080
Cond selected	2707,1	5506,4	3399,4	4145,9	4262,2	3032,0
MSE mean	0,0008	0,0009	0,0010	0,0010	0,0012	0,0011
MSE variance	0,0001	0,0001	0,0001	0,0002	0,0003	0,0002
maxE mean	0,1845	0,1977	0,2912	0,2329	0,2968	0,2408
maxE variance	0,0324	0,0330	0,2568	0,0540	0,1020	0,0382
Cond mean	3815,5	7342,8	5651,6	6953,7	5368,1	5202,9
Cond variance	1701,2	8493,5	5259,3	5274,6	2434,5	2039,3

Numerical values representing a_i of equation (10) for the selected typical non-dominated chromosome are:

[3157 31387 59087 34526 61856 23999 31983 5100 21985 53525 13592 15164 41416 52669 17091 8246 27195 36846 42384 27934 32215 55957 57320 24610], which defines fuzzy-partition MF parameters by equation (10) as:

$\boldsymbol{b}_i$ $i=1,2,3$ for cpFLS modeling D_{13}: [0.024633, 0.26954, 0.7306].

$\boldsymbol{b}_i$ $i=1,2,3$ for cpFLS modeling D_{22}: [0.50315, 0.69836, 0.95851].

$\boldsymbol{b}_i$ $i=1,2,3$ for D_{23}: [0.21085, 0.72421, 0.85457, 0.34681, 0.78784, 0.93095].

$\boldsymbol{b}_i$ $i=1,2,3$ for D_{33}: [0.20241, 0.47664, 0.79209, 0.18939, 0.51835, 0.85532].

The graphical representation of a fuzzy-partition antecedent defined by this chromosome for D33 is shown by Figure 6:

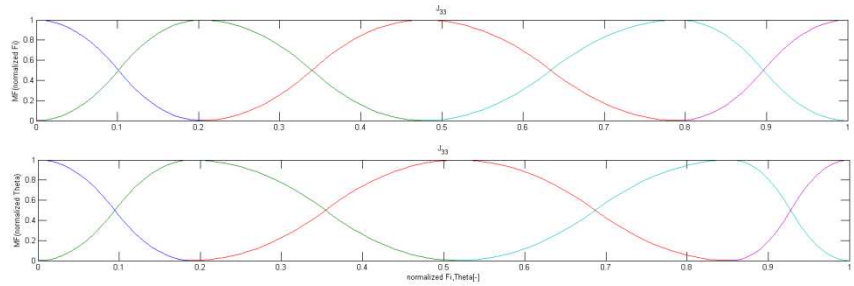

Figure 6
Antecedent fuzzy-partition for D_{33}

The torque identification error along the complete training data set for a cpFLS based quad-rotor model defined by the selected non-dominated chromosome is presented in Figure 7:

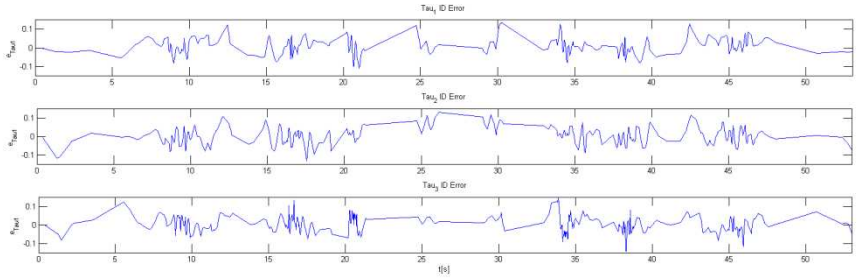

Figure 7
Torque identification error

11 Discussion

Simulation results of the proposed new multi-rotor dynamic model identification method by cpFLSs are promising. The quality of identification with the relative torque error being uniformly <10% is suitable for application in model based control algorithms.

The proposed trajectory design method results in real-life feasible smooth, limited torque transients, which is energy efficient for control signal design; while providing a flexible interface to arbitrary velocity, acceleration, jerk and snap limit enforcement. Dynamic transient properties and energy efficiency of the trajectory can be tuned with a single parameter, but the feasibility of torque transients must not be dismissed along this optimization. The resulting trajectory is always the time optimal solution, which complies with all defined limits.

The training data set reduction to 1/8th of the full set significantly increases the identification process speed, while the proposed reduction method ensures that the identification result quality does not deteriorates.

The typical condition number for used linear parameter evaluations is high for the used training data setup, which indicates that the system excitation with this trajectory is insufficient, so a more advanced training trajectory has to be planned with sufficient excitation along the complete input domain.

The new, more advanced training trajectory to be generated should take advantage of the smooth 2π - 0 transition, and it has to be designed so that both roll and pitch input parameters defined by equation are excited along the complete $[0, 2\pi)$ interval.

References

[1] R. Lozano, "*Unmanned Aerial Vehicles*," ISTE Ltd, London, 2010

[2] R. Stengel, "*FLIGHT DYNAMICS*," Princeton University Press, Cloth, 2004

[3] C. An, C. Atkeson, J. Hollerbach, "*Model-Based Control of a Robot Manipulator*," The MIT Press, Cambridge, 1988

[4] N. Srinivas, K. Deb, "Multiobjective Optimisation Using Nondominated Sorting in Genetic Algorithms," *Evolutionary Computation* Vol. 2, No. 3, pp. 221-248, 1994

[5] C. M. Fonseca, P. J. Fleming, "Multiobjective Optimisation and Multiple Constraint Handling with Evolutionary Algorithms I: A Unified Formulation," *University of Sheffield Technical Report* No. 564, Sheffield, UK, 1995

[6] A. Nemes, "New Genetic Algorithms for Multi-objective Optimisation," in proc. of the *1st International Symposium of Hungarian Researchers on Computational Intelligence (HUCI 2000)*, Budapest, 2000

[7] G. Carrillo, D. López, R. Lozano, C. Pégard, "Modeling the Multi-rotor Mini-Rotorcraft," *Quad Rotorcraft Control*, Springer, 2013

[8] M. Spong, M. Vidyasagar, "*Robot Dynamics and Control*," John Wiley and Sons, Inc. 1989

[9] L. Wang, "*Adaptive Fuzzy Systems and Control, Design and Stability Analysis*," PTR Prentice Hall, 1994

[10] H. Hellendron, D. Driankov, "*Fuzzy Model Identification, Selected approaches,*" Springer, 1997

[11] A. Nemes, "Function Identification by Unconstrained Tuning of Zadeh-type Fuzzy Partitions," in proc. of the *2nd International Symposium of*

Hungarian Researchers on Computational Intelligence (HUCI 2001), Budapest, 2001

[12] J. Jang, C. Sun, E. Mizutani, "*Neuro-Fuzzy and Soft Computing, A Computational Approach to learning and Machine Intelligence*," Prentice-Hall, 1997

[13] A. Nemes, B. Lantos "Training Data Reduction for Optimisation of Fuzzy Logic Systems for Dynamic Modeling of Robot Manipulators by Genetic Algorithms," in proc. of the *IEEE Instrumentation and Measurement Technology Conference (IMTC 2001)*, Vol. 3, pp. 1418-1423, 2001

[14] A. Nemes, "Genetic Fuzzy Identification Method for Qadrotor UAVs," *ANNALS of Faculty Engineering Hunedora*, Vol. 13, No. 3, 2015

[15] A. Rodic, G. Mester, "Sensor-based Navigation and Integrated Control of Ambient Intelligent Wheeled Robots with Tire-Ground Interaction Uncertainties," *Acta Polytechnica Hungarica*, Vol. 10, No. 3, pp. 113-133, 2013

[16] A. Rodic, G. Mester, "Virtual WRSN – Modeling and Simulation of Wireless Robot-Sensor Networked Systems," in proc. of the *8th IEEE International Symposium on Intelligent Systems and Informatics (SISY 2010)*, pp. 115-120, 2010

[17] G. Mester, "Introduction to Control of Mobile Robots," in proc. of the *YUINFO 2006*, pp. 1-4, 2006

[18] G. Mester, "Improving the Mobile Robot Control in Unknown Environments," in proc. of the *YUINFO 2007*, pp. 1-5, 2007

[19] G. Mester, "Adaptive Force and Position Control of Rigid Link Flexible-Joint SCARA Robots," in proc. of the *20th IEEE International Conference on Industrial Electronics, Control and Instrumentation (IECON'94)*, Vol. 3, pp. 1639-1644, 1994